



ELSEVIER

Contents lists available at ScienceDirect

## Progress in Materials Science

journal homepage: [www.elsevier.com/locate/pmatsci](http://www.elsevier.com/locate/pmatsci)

## The elastic properties, elastic models and elastic perspectives of metallic glasses

Wei Hua Wang\*

*Institute of Physics, Chinese Academy of Sciences, Beijing 100190, PR China*

## ARTICLE INFO

*Article history:*

Received 7 September 2010

Accepted 21 July 2011

Available online xxxx

## ABSTRACT

Bulk metallic glass (BMG) provides plentiful precise knowledge of fundamental parameters of elastic moduli, which offer a benchmark reference point for understanding and applications of the glassy materials. This paper comprehensively reviews the current state of the art of the study of elastic properties, the establishments of correlations between elastic moduli and properties/features, and the elastic models and elastic perspectives of metallic glasses. The goal is to show the key roles of elastic moduli in study, formation, and understanding of metallic glasses, and to present a comprehensive elastic perspectives on the major fundamental issues from processing to structure to properties in the rapidly moving field.

A plentiful of data and results involving in acoustic velocities, elastic constants and their response to aging, relaxation, applied press, pressure and temperature of the metallic glasses have been compiled. The thermodynamic and kinetic parameters, stability, mechanical and physical properties of various available metallic glasses especially BMGs have also been collected. A survey based on the plentiful experimental data reveals that the linear elastic constants have striking systematic correlations with the microstructural features, glass transition temperature, melting temperature, relaxation behavior, boson peak, strength, hardness, plastic yielding of the glass, and even rheological properties of the glass forming liquids. The elastic constants of BMGs also show a correlation with a weighted average of the elastic constants of the constituent elements. We show that the elastic moduli correlations can assist in selecting alloying components with suitable elastic moduli for controlling the elastic properties and glass-forming ability of

\* Address: Institute of Physics, Chinese Academy of Sciences, P.O. Box 603(42-1), Beijing 100190, PR China. Tel.: +86 10 82649198; fax: +86 10 82640223.

E-mail address: [whw@aphy.iphy.ac.cn](mailto:whw@aphy.iphy.ac.cn)

URL: <http://www.mmp.iphy.ac.cn>

the metallic glasses, and thus the results would enable the design, control and tuning of the formation and properties of metallic glasses.

We demonstrate that the glass transition, the primary and secondary relaxations, plastic deformation and yield can be attributed to the free volume increase induced flow, and the flow can be modeled as the activated hopping between the inherent states in the potential energy landscape. We then propose an extended elastic model to understand flow in metallic glass and glass-forming supercooled liquid, and the model presents a simple and quantitative mathematic expression for flow activation energy of various glasses. The elastic perspectives, which consider all metallic glasses exhibit universal behavior based on a small number of readily measurable parameters of elastic moduli, are presented for understanding the nature and diverse properties of the metallic glasses.

© 2011 Elsevier Ltd. All rights reserved.

## Contents

1.	Introduction . . . . .	00
2.	The brief description of the theory of elasticity . . . . .	00
2.1.	The characterization of elastic properties of solids . . . . .	00
2.2.	Physical origin for the elasticity . . . . .	00
2.2.1.	Basis for linear elasticity . . . . .	00
2.2.2.	Elastic properties and energy landscapes . . . . .	00
2.3.	Elastic properties in equilibrium liquids and supercooled liquids . . . . .	00
2.3.1.	Instantaneous elastic constants . . . . .	00
2.3.2.	Elastic properties in the equilibrium liquids and supercooled liquids . . . . .	00
2.4.	Correlations between elastic moduli and physical properties in crystalline materials . . . . .	00
3.	Experimental methods for determining elastic moduli of glasses . . . . .	00
3.1.	Ultrasonic methods . . . . .	00
3.1.1.	The theory for ultrasonic measurements . . . . .	00
3.1.2.	The ultrasonic experimental methods . . . . .	00
3.1.3.	The <i>in situ</i> measurement of ultrasonic wave velocities under high pressure . . . . .	00
3.1.4.	The measurement of ultrasonic wave velocities upon temperature . . . . .	00
3.2.	The information provided from ultrasonic study . . . . .	00
4.	Elastic moduli of metallic glasses . . . . .	00
5.	Pressure dependence of elastic properties of metallic glasses . . . . .	00
6.	Temperature dependence of elastic properties of metallic glasses . . . . .	00
6.1.	The elastic property of BMGs upon annealing temperatures . . . . .	00
6.2.	<i>In situ</i> measurement of temperature dependence of elastic moduli of BMGs . . . . .	00
6.2.1.	<i>In situ</i> measurement of temperature dependence of elastic moduli during glass transition . . . . .	00
6.2.2.	<i>In situ</i> measurement of temperature dependence of elastic moduli at low temperatures . . . . .	00
7.	Time dependence (structural relaxation) of elastic constants of metallic glasses . . . . .	00
8.	Correlations between elastic moduli and microstructure, glass formation, glass transition, fragility and melting . . . . .	00
8.1.	The correlations between elastic properties and microstructure of metallic glasses . . . . .	00
8.2.	Correlation between elastic constants of metallic glasses and elastic constants of their constituents . . . . .	00
8.3.	Correlation between elastic properties and glass formation . . . . .	00
8.4.	Correlation between elastic moduli and glass transition . . . . .	00
8.5.	Correlation between elastic moduli and melting . . . . .	00
8.6.	Correlation between elastic moduli and fragility . . . . .	00
8.7.	Correlation between elastic properties and boson peak . . . . .	00
8.8.	Other correlations . . . . .	00
9.	Correlations between elastic moduli and mechanical properties . . . . .	00

9.1.	Correlation between elastic moduli and strength . . . . .	00
9.2.	Correlation between elastic moduli and microhardness . . . . .	00
9.3.	Correlation between elastic moduli and toughness/plasticity . . . . .	00
9.4.	Correlation between elastic moduli and fracture . . . . .	00
10.	The summary for elastic correlations . . . . .	00
11.	Searching metallic glasses based on elastic moduli criterion . . . . .	00
12.	Elastic models of supercooled liquids and metallic glasses . . . . .	00
12.1.	Elastic models for glass-forming supercooled liquids . . . . .	00
12.2.	Elastic models for metallic glasses . . . . .	00
12.3.	Extended elastic model for flow in metallic glass-forming liquids and glasses . . . . .	00
13.	The elastic perspectives on metallic glasses . . . . .	00
14.	Summary and outlook . . . . .	00
	Acknowledgments . . . . .	00
	References . . . . .	00

## 1. Introduction

Glassy state, which is a universal property of supercooled liquids if they are cooled rapidly enough, is regarded as the fourth state of matter [1–5]. The mysterious glass transition phenomenon, which connects the liquid and glassy states, is related widely to daily life, industry, materials preparation, organism preservation and a lot of natural phenomena. However, the exact and comprehensive physical understanding of the glass transition and glass natures is considered to be one of the most challenging problems in condensed matter physics and material science. Due to the random disordered structure, the characterization of the glasses are very difficult, and this leads to problems for understanding the formation, deformation, fracture, nature, and the structure–properties relationship of the glasses [1–18].

Metallic glass, which is a newcomer in glassy family (discovered in 1959) and at the cutting edge of current metallic materials research, is of current interest and significance in condensed matter physics, materials science and engineering because of its unique structural features and outstanding mechanical, many novel, applicable physical and chemical properties [11,14]. Metallic glasses have also been the focus of research advancing our fundamental understanding of liquids and glasses and provide model systems for studying some long-standing fundamental issues and have potential engineering and functional applications. The recently developed bulk metallic glass (BMG) forming systems are complicated multicomponent alloys that vitrify with remarkable ease during conventional solidification. The BMGs represent a novel and exciting group of metallic materials with many favorable and applicable properties as compared to their crystalline counterparts. Their unique combinations of mechanical, physical, tribological and chemical properties are of current interest and importance [1–15]. It is known that the structure determines the properties of a crystalline material, while in the metallic glasses, due to the random atomic structure in long-range [16–18], the difficult for characterizing of the structural disordered glasses leads to problem for understanding the formation and the structure–properties relationship of the metallic glasses [1–18]. Therefore, the birth of the novel metallic glasses also presents a lot of unresolved issues, outstanding questions and challenges. The following is key questions that represent fundamental issues critical for metallic glasses. These issues include:

- (1) Where and why does metallic liquid end and glass begin? How could liquid suddenly stop moving while approaching glass transition temperature  $T_g$ ? How does structure connect to dynamics as they give rise to dynamical heterogeneity, fragility, aging and rejuvenation? So far, the understanding of these common phenomena in glass is still fragmentary. The fundamental studies on the rheology, dynamic, and nature of glasses is one of major drivers for research

**Nomenclature**

BMG	bulk metallic glass
MG	metallic glass
GFA	glass-forming ability
GFR	glass-forming composition range
EOS	equation of state
RT	room temperature
STZ	shear transformation zone
BP	boson peak
$\rho$	density of matter
$g(r)$	pair distribution function
$M$	mass per molar
$C_g$	atomic packing density
$\sigma$	stress
$\sigma_F$	fracture strength
$\sigma_y$	yield strength
$\varepsilon$	strain
$\tau$	shear stress
$\tau_y$	yield shear strength
$\gamma$	shear strain
$K_c$	fracture toughness
$G_c$	fracture energy
$H_v$	Vicker's hardness
$\mathbf{r}$	position vector before the deformation
$\mathbf{u}$	displacement vector
$V$	volume
$V_m$	average molar volume
$V_a$	atomic volume
$P$	pressure
$T$	temperature
$t$	time
$\eta$	viscosity
$\tau_R$	relaxation time
$\omega$	frequency
$K$	bulk modulus (or modulus of compression)
$\chi$	compressibility
$K_\infty$	instantaneous bulk modulus
$E$	Young's modulus
$Q^{-1}$	internal friction
$G$	shear modulus (modulus of rigidity)
$G_\infty$	instantaneous shear modulus
$G'$	storage modulus
$G''$	loss modulus
$\nu$	Poisson's ratio
$\gamma_G$	Grueneisen constant
$v_l$	longitudinal acoustic velocity
$v_s$	transverse acoustic velocity
$\Delta E$	activation energy
$\rho_E$	the flow activation energy density
$\alpha$	thermal expansion coefficient
$T_g$	glass transition temperature
$T_x$	crystallization temperature
$T_m$	melting temperature

$T_l$	liquidus temperature
$T_f$	fictive temperature
$T_K$	Kauzmann temperature
$T_0$	kinetic ideal glass transition temperature or VFT temperature
$T_c$	crossover temperature
$T_{g,r}$	reduced glass transition temperature ( $=T_g/T_l$ )
$\Delta T$	supercooled liquid temperature region, $\Delta T = T_x - T_g$
$C_p$ or $C_v$	specific heat
$\theta_D$	Debye temperature
$\theta_E$	effective Einstein temperature
$m$	fragility
$k_B$	Boltzmann constant
$N_A$	the Avogadro constant
$h$	Planck constant
DSC	differential scanning calorimeter
DTA	differential thermal analysis
XRD	X-ray diffraction
TEM	transmission electron microscope
SEM	scanning electron microscope
DMA	thermal mechanical analyzer

on the metallic glasses, which are regarded to have the simplest atomic structure in glass family. The study will further the understanding of above subjects on glass dating from ancient times [9].

- (2) What physical factors determine the glass-forming ability (GFA) in an alloy? What are the universal aspects of glass formation, and what accounts for these universal aspects? What factors suppress or affect crystal nucleation in multi-component alloy systems? The structural transform upon changes in thermodynamic and processing variables, and correlations of local atomic structures, electronic structures, and atomic motions with GFA still remain unclear. How can one predicts the composition with excellent GFA and search new metallic glass system and composition in smart way? Many empirical criteria correlating with thermodynamic parameters were proposed to predict the GFA of the metallic glass-forming alloys, while these criteria cannot predict the universal GFA, and are difficult to be applied to searching new metallic glass in practice. Despite the identification of a vast range of metallic glasses and applications, the development of methods and criterion for rationally designing metallic glasses with excellent GFA reaching or approaching that of oxide glasses and desirable physical and mechanical properties is still a challenge [8–10,17–20].
- (3) The metastable nature of the metallic glasses imposes a barrier to broad commercial and industry applications, and one of the main challenges is to avoid crystallization and aging during processing, annealing and applications. Hence, the understanding of the crystallization and aging processes is necessary to develop fabrication processes and to process and apply bulk metallic glasses. What is the nature of the crystallization and ageing mechanisms, and how do the effects of heterogeneities on the crystallization kinetics, and the thermodynamic and dynamic aspects of aging? What factors suppress or affect crystal nucleation and growth in glass alloy systems? All of the issues have to be deeply studied. The research on the crystallization of metallic glasses can uncover the nucleation and growth in supercooled liquid and find novel processing opportunities for the metallic glasses. The aging and crystallization studies are important both for applications and understanding of metallic glasses.
- (4) How to characterize and model the metallic glassy structure, and how do the atoms and clusters pack in metallic glasses with liquid-like metastable structure? What are the structural and electronic features and characteristics of metallic glasses? And how does the structure determine

the properties of glasses? How to characterize and model the structural heterogeneity or “defects”? And what is the relation between the static heterogeneity and dynamic heterogeneity? What is microstructure origin of structural relaxation and aging, physical and mechanical properties of metallic glasses? All of them are key topic in this field [16]. Many metallic liquids can be deeply supercooled without crystallizing and subsequently to form metallic glasses, while fundamental understandings of the atomic arrangements in supercooled metallic liquids are still lacking. To understand the structure of the supercooled liquid, one needs to identify different types of topological structural ordering, and monitor hierarchical structural ordering of supercooled liquids temporally and spatially, and uncover the correlations between atomic packing schemes and the dynamic slowing-down, liquid fragility, glass forming ability, etc. of the supercooled liquids. To reveal the details of atomic-level structural evolution and local atomic rearrangement in metallic liquids would advance the understanding of the structural underpinnings of the vitrification process of supercooled metallic liquids.

- (5) Compared with conventional crystalline metals and alloys, non-crystalline metallic glasses show higher strength and yet can still sustain plastic flow (permanent strains and shape changes). The plasticity of crystalline metals is well known to be carried by structural defects such as dislocations or grain boundaries. How does metallic glass respond to the application of mechanical stresses or other external applied energy both at and far below the glass transition? In contrast, the corresponding plastic flow mechanism in metallic glasses remains largely unresolved. Under imposed stresses, there should be preferential “flow defects” or “plastic units” generated which carries the plastic strain, and there must be structural origins responsible for the localized basic flow events. The locations of fertile and liquid-like sites, the initiation and percolation for the cooperative flow events under stresses or other external activations have not been identified based on specific local structural and dynamical properties, including the degree of local order and symmetry, atomic-site stresses and free volume content. How do we identify the “flow defects”? The atomic flow mechanisms (the triggering events and cooperative atomic shear/shuffling), the localized flow size (number of atoms involved) and the fertility or propensity of local atoms for flow, the evolution of the short-to-medium range order during the flow and in the flow state, and the percolating behavior of localized flow events leading to later shear banding still remain unclear. The flow barrier and its dependence on local structure and properties is a key issue for deformation in metallic glasses. The deformation events in metallic glasses involves in large range of length scale from atomic scale of free volumes, to nano-scale of plastic units (or shear transformation zone) and medium-range order change, to micrometer scale shear bands. How to characterize the changes of local structures in different length scales upon plastic deformation both at and far below the glass transition, the connection and correlation among these flow events in different length scales, the nature, operation and propagation of the shear bands, and how to overcome the shear band problem and make the metallic glasses ductile and tough, and the intrinsic mechanisms of the plastic deformation and record high strength in metallic glasses are still challenges [1,2,21–24].

With the development of more and more bulk metallic glass systems, the acoustic measurements are widely applied to study their acoustic and elastic properties and determine the elastic moduli as well as their composition, processing, cooling rate, temperature, pressure, aging time, creep and external stress dependences of the metallic glasses. Plentiful data on the elastic properties of the metallic glasses were accumulated and a lot of interesting experimental phenomena were observed. Combining with the plentiful elastic moduli data of non-metallic glasses, remarkable links among the elastic moduli and thermodynamic, kinetic, and property parameters are found. These elastic correlations should have common structural and physical origins, and the key challenge now is to understand these correlations and exploit such understanding to develop new glass systems and compositions that combine excellent glass-forming ability with desirable properties. The correlations with other properties and features of metallic glasses, and the elastic models provide insight into above long-standing issues of the glasses and are also useful for new metallic glasses design and searching. Some elastic models have been proposed based on the elastic data and correlations to understand the nature of the glasses. More and more evidences show that the elastic moduli, which can be easily measured

by experiments due to the macroscopically isotropic feature of the metallic glasses, are key parameters for developing, characterizing, toughening and understanding the metallic glasses, and they are the key physical quantity for controlling the main thermodynamic and kinetic, intrinsic static structural heterogeneity, mechanical and dynamic properties. Elastic model and elastic perspectives provide deep insight into above listed issues in the metallic glasses.

The purposes of this review paper are to comprehensively review and summarize the recent elastic properties studies of the metallic glasses and the established elastic moduli correlations and elastic models. Based on the elastic moduli data, the found correlations, the elastic models on supercooled liquid and glasses and other experimental observations, we try to understand, characterize and discuss the issues on the formation, glass transition, crystallization, stability, relaxation, structural and dynamic features, physical and mechanical properties and other found phenomena of the metallic glasses by using the elastic moduli as the key parameter. We propose an extended elastic model and elastic perspectives on above issues in metallic glasses and argue that the various metallic glasses exhibit universal behavior based on a small number of measurable parameters of elastic moduli. We show that a genuine understanding of these issues based on elastic properties, elastic model can assist in selecting alloying components for controlling the elastic properties and GFA of the metallic glasses, and thus can guide the new metallic glasses design and process, and should also make it possible to optimize properties of metallic glasses.

The paper consists of 14 parts. The first part is a brief introduction on the main issues in this field and on the purpose and the structure of the paper. The second part briefly introduces the general theory of elasticity for solid, the physical origin for the elasticity and its relationship with energy landscape, and describes how to characterize the elasticity of a solid especially the homogeneous and isotropic solid. The description of how to determine the elastic moduli in an isotropic solid is also presented. To describe the elasticity of supercooled liquid or liquid, the concept of instantaneous elastic moduli is introduced. The instantaneous elastic moduli are measured on short time scales or a high-frequency disturbance where the liquid does not have enough time to flow. Then, we briefly introduce the theory of elastic properties in the equilibrium liquids and supercooled liquids. These theories are basis for characterizing and understanding the elastic properties and elastic models of the metallic glass-forming liquids and glasses.

Part 3 describes the experimental measurements of the elastic moduli in metallic glasses and other non-metallic glasses with isotropic structure. In particular, the ultrasonic methods for the elastic moduli measurement in ambient conditions, under high pressure, under high or low temperature are systematically introduced. And the significance information on the metallic glasses one can get from the ultrasonic study is also summarized.

In part 4, the elastic moduli data compilation for available metallic glasses so far is presented. The elastic moduli of various metallic glasses are carefully analyzed, classified and characterized, and are compared with that of their crystalline counterparts and other typical non-metallic glasses. These data provide the basis for establishing the elastic correlation and elastic model.

In parts 5–7, the temperature, pressure and relaxation (or ageing) time dependences of elastic moduli of typical bulk metallic glasses are presented and are compared with that of their crystalline counterparts and other typical non-metallic glasses. These elastic moduli data demonstrate unique features of the metallic glasses under pressure and low or high temperatures, and show the influence of ageing effect on the physical and mechanical properties of metallic glasses. The studies also provide the information about equation of state, atomic configurations, excitations in the metallic glassy solids including the anharmonicity of the atomic vibrations, the density of electron states at the Fermi level and the shape of the Fermi surface, and the activation barriers for thermally activated relaxations.

After giving an overview of the basic experimental facts of the elastic property study, the paper in parts 8–9 attempts to correlate the elastic moduli of the metallic glasses to their microstructure, formation, glass-forming ability, stability, crystallization behavior, glass transition, thermodynamic and kinetic features, mechanical and physical properties, and reology of the glass-forming liquids. It is shown in these parts that the linear elastic moduli have correlations with the microstructure, glass transition temperature, relaxation, GFA, melting temperature, strength, hardness, plasticity and toughness, and even the fragility of the glass forming liquids. Meanwhile, the elastic constants of available BMGs show a rough correlation with a weighted average of the elastic constants for the

constituent elements. In part 10, we summarize various correlations in metallic glasses among elastic moduli and features and properties. The physical origins for these correlations are discussed.

Based on these found elastic correlations, in part 11, the plausible elastic moduli criterion is proposed for searching metallic glasses. It is demonstrated that the elastic correlations as well as the elastic criterion can assist in BMG design and exploration.

In part 12, the prevailing elastic models for supercooled liquids and glasses are introduced, and an extended elastic model for flow in metallic glasses is proposed. It is shown that the extended elastic model is in remarkable agreement with a variety of experimental observations and offers a simple scenario for explaining some correlations between elastic constants and properties and for understanding the nature of the metallic glasses.

In part 13, attempt is made to understand some puzzles and fundamental issues in metallic glasses based on their elastic properties, the elastic correlations and the elastic models. The roles of elastic moduli as the key parameters for developing, characterizing, toughening and understanding the metallic glasses and their forming liquids are emphasized. The elastic perspectives on the formation, GFA, the thermodynamic and kinetic aspects, intrinsic static structural and dynamic heterogeneities, mechanical and physical properties of the metallic glasses are suggested. The review paper ends with summary and outlook in part 14.

## 2. The brief description of the theory of elasticity

### 2.1. The characterization of elastic properties of solids

The mechanics of solids, regarded as continuous media, forms the content of the theory of elasticity. The macroscopic behavior of a solid is described by a continuum field theory, the theory of elasticity, which describes the way a solid deforms when external stresses are applied [25]. Under the action of applied stress, solid body exhibits shape and volume changes to some extent, and every point in the solid body is in general displaced. Let the position vector before the deformation be  $\mathbf{r}$ , and after the deformation has a value  $\mathbf{r}'$  with component  $x_i$ . The displacement of this point due to deformation then given by the displacement vector  $\mathbf{u} = \mathbf{r} - \mathbf{r}'$  or  $u_i = x'_i - x_i$ . If  $u_{ij}(x_1, x_2, x_3)$  is the  $j$ th component of the displacement at point  $(x_1, x_2, x_3)$ , the strain tensor for small deformations is

$$u_{ij} = \frac{1}{2} \left( \frac{\partial u_i}{\partial x_j} + \frac{\partial u_j}{\partial x_i} \right) \quad (2.1)$$

When a deformation happens, the body ceases to be in its original state of equilibrium, and the forces, which are called internal stresses, therefore arise which tend to return the body to its equilibrium state. If the deformation of the body is fairly small, it returns to its original undeformed state when the external forces cease to act. Such deformations are elastic. For large deformations, the removal of the external forces does not result in the fully recovery of the deformation. Such deformations are plastic [25]. For an isotropic solid, in elastic deformation case, the stress tensor in terms of the strain tensor can be expressed as [25]:

$$\sigma_{ij} = Ku_{ij}\delta_{ij} + 2G(u_{ij} - \delta_{ij}u_{ll}/3) \quad (2.2)$$

where  $K$  (in many text books, a different notation  $B$  is used) is bulk modulus, and  $G$  (in many text books, a different notation  $\mu$  is used) is shear modulus. The bulk modulus describes the strain response of a body to hydrostatic stress involving change in volume without change of shape. The shear modulus relates to strain response of a body to shear or torsional stress. It involves change of shape without change of volume.

For an isotropic solid, its elastic behavior is fully described by the longitudinal modulus ( $L = c_{11}$ ) and shear modulus ( $G = c_{44}$ ). Between the components of the related elastic stiffness tensor, the isotropic relation [26]:  $c_{11} = c_{12} + 2c_{44}$ . If in addition the atoms interact through a central potential, the Cauchy identity  $c_{12} = c_{44}$  may hold, and then, one obtains a reduction to only one independent elastic constant  $c_{11} = 3c_{44}$  (or  $L = 3G$ ). The Cauchy's identity, valid for an isotropic solid composed of molecular interacting with two-body central force, can also be stated as:

$$K = \frac{5}{3}G \quad (2.3)$$

which implies that  $L$  and  $K$  are equal to 0 when  $G = 0$ . For the Lennard Jones interaction potential, this identity changes to,  $L = a + bG$ , where  $a$  and  $b$  are constants. This leads to the relation,

$$K = a + (b - 1.333)G \quad (2.4)$$

which is known as the generalized Cauchy relation. Its parameters  $a$  and  $b$  remain constant with changing temperature and pressure, but are sensitive to small changes in the potential. This relation is valid for both liquids and glasses [25]. Recently, a generalized Cauchy relation was observed to hold in supercooled liquids and can be expressed as:  $c_{11}(T) = Bc_{44}(T) + A$ , where  $B$  and  $A$  are constants independent of  $T$  and  $P$  within their range involving the glass transition [26].

For minor deformation, the  $u_{ij}$  is a linear function of the  $\sigma_{ij}$ . That is, the deformation is proportional to the applied forces. This law is called Hooke's law, which is actually applicable to almost all elastic deformations in solids [25]. In simple case of homogenous deformations in which the strain tensor is constant throughout the volume of the body, the stress tensor is given in terms of the strain tensor by

$$\sigma_{ij} = \frac{E}{1+\nu} \left( u_{ij} + \frac{\nu}{1-2\nu} u_{ll} \delta_{ij} \right) \quad (2.5)$$

where  $E$  is the modulus of extension or Young's modulus. Young's modulus is named after Thomas Young (the 19th century British scientist). However, the concept was developed in 1727 by Leonhard Euler, and the first experiment that used the concept of Young's modulus was performed by the Italian scientist Giordano Riccati in 1782 [25]. Young's modulus, also known as the tensile modulus, is a measure of the stiffness of an isotropic elastic material. It is defined as the ratio of the uniaxial stress over the uniaxial strain in the elastic regime. This can be experimentally determined from the slope of a stress-strain curve created during tensile or compression tests conducted on a material. Young's modulus is also commonly, but incorrectly, called the elastic modulus or modulus of elasticity, because Young's modulus  $E$  is the best-known elastic constant, which is most commonly used in engineering design. There are other elastic moduli, such as the bulk modulus and the shear modulus. The  $E$  can be given in terms of  $G$  and  $K$  by:

$$E = 9KG/(3K + G) \quad (2.6)$$

The ratio of the transverse compression to the longitudinal extension is called Poisson's ratio,  $\nu$ , named after Siméon Poisson. Poisson's ratio is an important material property used in elastic analysis of material. When a material is compressed in one direction, it usually tends to expand in the other two directions perpendicular to the direction of compression. This phenomenon is called the Poisson effect. Poisson's ratio  $\nu$  is a measure of the Poisson effect. The  $\nu$  is the ratio of the fraction of expansion divided by the fraction of compression (for small values of these changes). In stretch case of a solid rather than the compression, the Poisson ratio will be the ratio of relative contraction to relative stretching, and will have the same value as compression case. The relation of Poisson's ratio with other elastic constants is (for isotropic solids):

$$\nu = \frac{1}{2}(3K - 2G)/(3K + G) \quad (2.7)$$

Since  $K$  and  $G$  are always positive, the Poisson's ratio can vary between  $-1$  (for  $K = 0$ ) and  $0.5$  (for  $G = 0$ ), that is  $-1 \leq \nu \leq 0.5$ . One might see Poisson's ratios larger than  $0.5$  reported in the literature, however, this implies that the material was stressed to cracking. Generally, "stiffer" materials will have lower Poisson's ratios than "softer" materials. While only in very rare cases, a material will actually shrink in the transverse direction when compressed (or expand when stretched) which will yield a negative value of the Poisson's ratio.

The  $G$  and  $K$  can also be given in terms of  $E$  and  $\nu$  by:

$$G = E/2(1 + \nu) \quad (2.8)$$

$$K = E/3(1 - 2\nu) \quad (2.9)$$

The quantity  $1/K$  is called coefficient of compression  $\chi$ :

$$\chi = \frac{1}{K} = -\frac{1}{V} \left( \frac{\partial V}{\partial P} \right)_T = -\frac{\partial(\ln V)}{\partial P} \Big|_T \quad (2.10)$$

The elastic properties of a solid body are temperature dependent. Deformations can occur accompanied by a change in temperature of the body either as a result of the deformation process itself or from external causes. Among the various types of deformations, isothermal and adiabatic deformations are of importance. In isothermal deformation, the temperature  $T$  of the body does not change, the  $K$ ,  $E$ ,  $G$ , and  $\nu$  therefore can be called isothermal moduli. If there is no exchange of heat between the various parts of the body, the deformation is called adiabatic, and the adiabatic moduli are labeled to be  $E_{ad}$ ,  $K_{ad}$ ,  $G_{ad}$ , and  $\nu_{ad}$ . The relations between adiabatic and isothermal moduli are [25]:

$$1/K_{ad} = 1/K - T\alpha^2/C_p \quad (2.11)$$

$$G_{ad} = G \quad (2.12)$$

$$E_{ad} = \frac{E}{1 - ET\alpha^2/9C_p} \quad (2.13)$$

$$\nu_{ad} = \frac{\nu + ET\alpha^2/9C_p}{1 - ET\alpha^2/9C_p} \quad (2.14)$$

where  $\alpha$  is the thermal expansion coefficient of the solid. This is the Debye–Grüneisen effect of thermal expansion on elastic constants for an isolated configurational state, in which  $T$  dependent elastic behavior arises from the anharmonicity of the vibrational parts of the motion of atoms [27–29]. For systems with positive thermal expansion the adiabatic  $K$  is higher than the isothermal  $K$ . The adiabatic and isothermal shear moduli are always identical. The time dependent elasticity is termed as *viscoelasticity* [25,30–32].

In isotropic solids, based on the Hooke's law:

- (1) Under the tensile or compressive state,  $E = \sigma/\varepsilon$ , where  $\varepsilon$  is strain. The  $E$  reflects the tensile or compression strain resistance of the materials.
- (2) Under the tensile or compressive state,  $G = \tau/\gamma$ , where  $\tau$  is shear stress, and  $\gamma$  is shear strain. The  $G$  reflects the tensile or compression shear strain resistance of the materials.
- (3) The  $K$  reflects the resistance to dilatation caused by the hydrostatic stress state:

$$K = -P/(-\Delta V/V) = E/3(1 - 2\nu) \quad (2.15)$$

- (4) The Poisson's ratio,  $\nu$  characterizes the relative value of the compressive and shear deformations of a solid. For most crystalline metals and alloys,  $\nu = 1/3$  [32].

For the isotropic solids or mediums, there are only two elastic constants are independent, and the four elastic constants correlate as [25,32]:

$$E = 3K(1 - 2\nu) \quad (2.16)$$

$$G = \frac{E}{2(\nu + 1)} \quad (2.17)$$

The metallic glasses are macroscopically isotropic in structure and homogeneous in physical and mechanical properties, and therefore, above equations can be applied to metallic glasses.

## 2.2. Physical origin for the elasticity

### 2.2.1. Basis for linear elasticity

The linear elastic behavior is macroscopic manifestation of atomic bonding. The elastic constants or elastic moduli are of fundamental importance for a material. The  $K$  is directly related to the external force required to compress or extend interatomic distances in opposition to the internal forces that seek to establish equilibrium interatomic distance. The  $G$  similarly represents a distortion or bending

of atomic bonds and does not vary in a direct manner with interatomic spacing as does  $K$ , and the  $E$  measures a combination of bond bending and extension/compression. The  $K$  (or  $E$ ) is fundamentally related to the curvature of the bonding energy-atomic volume curves, and the bonding energy [25,32].

Considering the variation of the internal potential energy of atoms with the interatomic spacing  $r$ , for the linear elasticity, the total potential energy,  $U$ , of the system of atoms can be expressed as [32]:

$$U = \frac{1}{2} \sum_{ij} z U_{ij} \quad (2.18)$$

where  $U_{ij}$  is the interaction potential energy between two near-neighbor atoms, and the sum is taken all the atoms in the solid. The coordination number  $z$  represents the number of interatomics each atom has, and the factor  $1/2$  is necessary to avoid duplicate counting of interactions. Eq. (2.18) assumes that interaction between second and third near neighbors is neglectable in determining system potential energy.

A valuable and commonly used interaction potential energy function between two near-neighbor atoms with a distance of  $r$  is known as the Lennard-Jone potential:

$$U_{ij} = -\frac{A}{r^n} + \frac{B}{r^m} \quad (2.19)$$

where  $A$ ,  $B$ ,  $n$ ,  $m$  are real positive constants which depend on the composition and structure of the body. The first term on the right-hand side represents the attraction term of the potential, and the second term represents the repulsive term. Research indicates that  $n < m$ , means that the repulsive part is more sensitive to  $r$ .

The interaction force  $F(r)$  of the atoms is:

$$F(r) = -\frac{dU(r)}{dr} = -\frac{nA}{r^{n+1}} + \frac{mB}{r^{m+1}} \quad (2.20)$$

The interatomic spacing for atoms in equilibrium state,  $r_0$ , that is:  $F = -\frac{dU}{dr}\Big|_{r=r_0} = 0$

$$r_0 = \left(\frac{mB}{nA}\right)^{1/(m-n)} \quad (2.21)$$

From this potential function the  $G$  and  $K$  can be given explicitly as known function of internal energy. The interatomic forces and the structure of a material determine its vibrational properties and hence its elastic constants. The adiabatic elastic constants are the second derivatives of the internal energy with respect to strain, and thus depend sensitively on the interatomic potentials. The temperature dependence is related to anharmonic interactions. The instantaneous elastic moduli of a solid or liquid are determined by the curvature of the potential energy minimum and the anharmonic force contributions [25].

### 2.2.2. Elastic properties and energy landscapes

Goldstein [33] proposed a paradigm for vibrational and configurational thermodynamics on collective motions of molecules systems. In his paradigm, the state point of an ultraviscous liquid explores a large number of minima in a multidimensional potential energy surface, known as an energy landscape [34,35]. The distribution of the energy minima in the landscape (also called the inherent states) is fixed by the interatomic potential function and volume. A liquid explores a host of configurations at high temperatures, each with a definite probability. This probability is higher for the deeper energy minimum corresponding to a more stable configuration. Any change in constituents or interaction of a liquid varies the energy landscape, and both the vibrational and configurational contributions to the properties of the system [34,35]. When a liquid is cooled, its state point shifts to a lower-energy minimum and becomes trapped in one of the deep energy minima. Goldstein [33] reasoned that deeper energy minima of lower energy are likely to have a higher curvature and would correspond to a higher lattice frequency. Dyre and Olsen [36] pointed out that curvature of the energy minimum would also determine the height of the potential energy barrier and hence the accessibility of another minimum to a liquid's state point at a given temperature. Hence, the curvature of the potential energy

minimum, which can be represented by the instantaneous elastic moduli of a material, would determine both the vibrational and configurational properties. Significant conceptual improvements to relate structure and energetics result from employing the concepts of potential energy landscapes (PEL) to glasses and liquids [34,35,37], or by considering the potential energy as a function of a generalized configurational parameter space. This allows for a natural interpretation of many materials properties including elastic properties, fragility [38] or relaxational dynamics [39]. The shape of a potential energy minimum related to the instantaneous elastic moduli determines accessibility to other minima at a given temperature, which in turn determines the configurational entropy of the glass. The concept of PEL is useful for understanding the elastic properties of metallic glasses and for understanding the correlations between elastic moduli and thermodynamic, kinetic, and other physical properties of metallic glasses. The flow induced both by temperature and stress in metallic glass and glass-forming liquids can be modeled as the activated hopping between the inherent states in the potential energy landscape. The elastic model for describing the flow is established based on the energy landscape theory.

### 2.3. Elastic properties in equilibrium liquids and supercooled liquids

#### 2.3.1. Instantaneous elastic constants

The elastic properties of a matter are frequency or time dependent. Even in liquids, the instantaneous elastic moduli (both shear and bulk moduli) can be measured on a short time scale or a high-frequency disturbance where the liquid does not have time to flow. When the probe frequency is larger than the relaxation frequency, the measured elastic longitudinal and shear moduli become so-called clamped properties [40]. The frequency-dependent elastic moduli can be related quite generally to frequency-dependent viscosity coefficients by [41]:

$$K_{\omega} = K + i\omega\eta_K(\omega) \quad (2.22)$$

$$G_{\omega} = i\omega\eta_G(\omega) \quad (2.23)$$

where  $\omega$  is frequency,  $\eta_K$ ,  $\eta_G$  are coefficients of shear and bulk viscosities, respectively. At zero frequency, the shear modulus vanishes for liquids, while the bulk modulus does not. At very high frequency ( $\omega \rightarrow \infty$ ),  $\lim_{\omega \rightarrow \infty} G(\omega) = G_{\infty}$ , even the liquids become solid like and  $G_{\infty} > 0$ . The high-frequency limits of the elastic moduli, which are regarded as instantaneous elastic constants, are determined by the high-frequency limits of the viscosity coefficients. The barrier transition for a “flow event” or a molecular rearrangement does take place on a very short time scale, so the height of the energy barrier could well be determined by liquid properties which can be probed on this time scale. During freezing or vitrification (polymerization) of glass-forming liquids, these clamped moduli behave in a strongly nonlinear fashion as a function of temperature or polymerization time. It has been shown that there exists a linear relation between  $c_{11}^{\infty}$  and  $c_{44}^{\infty}$  over a large temperature or polymerization time range [42]. The frequency range of the sound wave is 5–20 MHz, which is at least  $10^{10}$  times of the relaxation frequency of metallic glasses corresponding to its viscosity at their glass transition temperature. Therefore, the elastic moduli obtained by acoustic methods can be roughly regarded as instantaneous elastic constants.

#### 2.3.2. Elastic properties in the equilibrium liquids and supercooled liquids

The first kinetic theories for viscous flow in liquids are based on the presumption of homogeneous flow [43] in which the shear modulus is vanishing in similarity to gases [44]. Frenkel [40] is the first to point out the analogies to solids of a liquid in elastic properties, that is, a nonvanishing shear modulus at comparable atomic packing densities. When a mechanical force is suddenly applied to a liquid, the liquid responds elastically at first, just as if it were a solid. That means any liquid is solid-like when probed on a sufficiently short time scale. In other words, if the measurement time of elastic properties of a liquid is shorter than the relaxation time, the liquid, for practical purpose, is a solid, and its short-time elastic properties can be characterized by the instantaneous moduli of  $G_{\infty}$  and  $K_{\infty}$ .

The earliest suggestion that the liquid may response elastically to sudden disturbance appears to be Poisson in 1831. A mathematic expression for this idea was given by Maxwell in 1876 as [45]:

$$\eta = G_{\infty} \tau_R \quad (2.24)$$

The Maxwell expression indicates that the shear modulus of liquid can be measured on short time scales where the liquid does not have time to flow. Theoretical calculations for ideal monoatomic liquid metals, based on the assumption of spatial isotropy and two-body central interaction, shows that the high-frequency  $K_{\infty}$  and  $G_{\infty}$  can be expressed as [45,46]:

$$G_{\infty} = \rho k_B T + \frac{2\pi\rho^2}{15} \int_0^{\infty} \frac{d}{dr} \left[ r^4 \frac{dU}{dr} \right] g(r) dr \quad (2.25)$$

$$K_{\infty} = \frac{5}{3}G - \frac{4\pi\rho}{12} \int_0^{\infty} [r^3 U'(r)] g(r) dr = \frac{5}{3}G - \frac{\rho}{12} \langle rU'(r) \rangle \quad (2.26)$$

where  $\rho$  is atomic density,  $g(r)$ ,  $k_B$  are pair distribution function and the Boltzmann constant, respectively.  $U(r)$ : interaction pair potential. The pressure  $P$  is

$$P = \rho k_B T - \frac{2\pi\rho^2}{3} \int_0^{\infty} r^3 \frac{dU}{dr} g(r) dr \quad (2.27)$$

Consequently, the three quantities are related by the linear equation of generalized Cauchy relation [47]:

$$K_{\infty} = \frac{5}{3}G_{\infty} + 2(P - \rho k_B T) \quad (2.28)$$

In the absence of defects and anharmonicity, the Cauchy relation  $C_{11} = 3C_{44}$  (or equivalently  $K = 5/3G$ ) is expected to hold for an isotropic material. However, in simple mono-atomic liquids the high frequency elastic properties are expected to fit the generalized Cauchy relation:  $C_{11} = 3C_{44} + f(T, P)$  [41]. A generalized Cauchy relation was found to hold in supercooled liquids near and throughout the glass transition and also during the aging process of polymerizing liquids and metallic glasses [42,48], the generalized Cauchy relation is:

$$C_{11}(T) = BC_{44}(T) + A \quad (2.29)$$

In the case of aging  $T$  (temperature) is replaced by  $t$  (aging time) in the above equation.  $B$  and  $A$  are independent of  $T$  and  $P$  within their range involving the glass transition. It is found that  $B \approx 3$  for all very different glass-forming materials [44]. In some cases the degree of deviation from the Cauchy relation ( $K = 5/3G$ ) is related to the anharmonicity of the material. The high frequency elastic constants of the equilibrium liquid were recently estimated in few typical metallic glass-forming liquids [29], and a value of  $B = 2.87$  is obtained for the linear relation between  $C_{11}$  and  $C_{44}$ , which indicates an interesting agreement with the linear relation with  $B \approx 3$  obtained for very different glass-forming materials in Ref. [42]. However, more experimental evidences are needed to confirm or discard this hypothesis in metallic glasses forming liquids.

Krüger et al. [42,48] assumed a first order change of the elastic stiffness coefficients with temperature given by

$$C_{xx}(T) = C_{xx}(T_0)[1 - \alpha(1 + 2\gamma_x)(T - T_0)] \quad (2.30)$$

where  $\alpha$  is the volume expansion coefficient,  $C_{xx}$  is either  $C_{11}$  or  $C_{44}$ ,  $\gamma_x$  is either the longitudinal ( $\gamma_1$ ) or the shear ( $\gamma_4$ ) mode Grüneisen parameters of an equilibrium liquid, and  $T_0$  is a reference temperature. Using the above expression they obtained

$$A = 2C_{11}(T_g) \frac{\gamma_4 - \gamma_1}{1 + 2\gamma_4} \quad (2.31)$$

for the constant term in Eq. (2.29).

It is note that the elastic response of glasses is inherited from the infinite frequency response of the equilibrium liquid near the  $T_g$ . Different structural states of a glass can be described by a fictive temperature  $T_f$ , at which the elastic constants of the glass and the liquid have the same value. That is, the infinite frequency bulk and shear moduli of the liquid become frozen at  $T_f$ . Assuming  $K_{glass}$  and  $G_{glass}$  close to  $K_{\infty}^{liquid}(T_f)$  and  $G_{\infty-liquid}(T_f)$ , and then  $T_f$  controls the elastic properties of the glass. The lower

$T_f$  implies a reduction of the  $K/G$  ratio of the glass. If  $T_{f1} < T_{f2}$ , then  $K_{\infty}^{\text{liquid}}(T_{f1})/G_{\infty\text{-liquid}}(T_{f1}) < K_{\infty}^{\text{liquid}}(T_{f2})/G_{\infty\text{-liquid}}(T_{f2})$  [49]. The typical behavior of the elastic constants throughout the transition from liquid to glass is illustrated in Fig. 1a and b. The understanding the behavior of the elastic constants of the equilibrium liquid near  $T_g$  is of great value for understanding the nature of the super-cooled liquids and glasses.

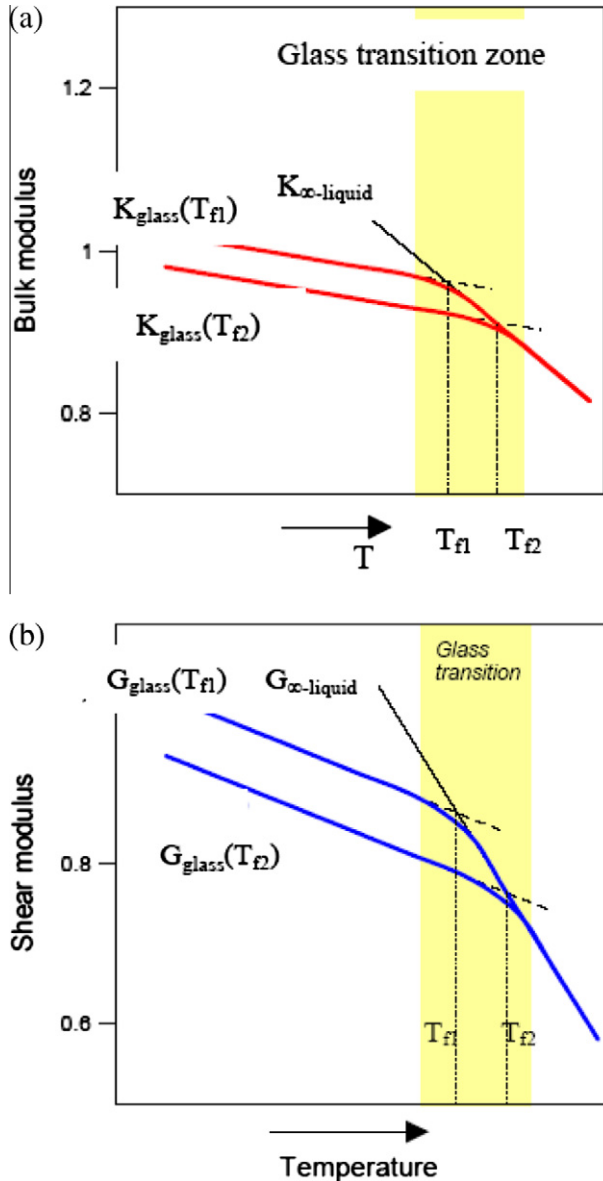


**Fig. 1.** Typical behavior of the elastic constants ( $G$  and  $K$ ) throughout the glass transition: (a) The relative change of  $K$ ; (b) the relative change of the  $G$ . The reference value is  $K$  or  $G$  and room temperature. The infinite frequency bulk and shear moduli of the liquid become frozen at  $T_f$ .

## 2.4. Correlations between elastic moduli and physical properties in crystalline materials

The elastic properties of a crystalline material correlate with many of its mechanical and physical qualities. Besides, the changes of the  $K$ ,  $G$ ,  $E$ , and  $\nu$  under pressure or temperature give information of the changes in the structure of a material. The shear stresses are associated with bond distortion, and  $K$  or  $E$  is fundamentally related to the curvature of the bonding energy-atomic volume curves, and the bonding energy. The bonding energy also correlates with the melting temperature  $T_m$  of crystalline materials; therefore,  $E$  has a relation with  $T_m$ :  $E \propto k_B T_m / M$ . The Debye temperature  $\theta_D$  and  $T_m$  are related to the vibration of atoms, therefore, the high value of  $\theta_D$  or  $T_m$  indicates strong atomic interaction, and then high value of elastic moduli of crystalline materials [50,51].

The temperature and density of a solid strongly affect its elastic moduli. The temperature dependent elastic modulus in some crystalline materials can be expressed as:

$$\beta = \frac{1}{E} \frac{dE}{dT} \quad (2.32)$$

The change of the vibrational properties with density is described by the Grüneisen parameter,  $\gamma_G$

$$\alpha = \frac{\gamma_G C_V}{3KV} \quad (2.33)$$

$\alpha$  is thermal expansion coefficient, and  $\gamma_G$  is a measure of the anharmonicity of a material. In some families of the periodic table of elements, the elastic modulus increases with the element number increasing (or atomic radius decrease) as:

$$E \propto k/a^m \quad (2.34)$$

where the  $k$  and  $m$  are constants. The mechanical properties of crystalline metallic alloys are known to correlate to the elastic properties. For example, in crystalline metals, the brittleness of alloys is known to correlate to the ratio of  $G/K$  or Poisson's ratio [52].

## 3. Experimental methods for determining elastic moduli of glasses

The elastic moduli of a matter are determined by its interatomic forces, the structure and its vibrational properties. And hence the values of the elastic constants  $K$ ,  $G$ , and  $E$  and Poisson's ratio  $\nu$  can be experimentally measured by many methods such as mechanical deformation or ultrasonic-wave propagation. For liquids, instantaneous elastic constants can be obtained from velocity measurements of high-frequency sound waves in order to avoid contributions of fast structural relaxations. In solids, basically, the methods for determining the elastic moduli are divided into static and dynamic methods. The static and dynamic methods can be regarded as isothermal and adiabatic measuring conditions, respectively. The basic theory for static method is to measure the stress-strain curve in the elastic deformation limit, and then calculate the elastic moduli based on the curves. While the experimental conditions such as loading as well as the loading rate significantly affect the measuring accuracy of the elastic moduli. The static method is also difficult to be applied to brittle materials such as glassy materials. The dynamic methods have relative high accuracy. According to the applied frequency range, the dynamic methods are classified as: acoustic method (the frequency is below  $10^4$  Hz) and ultrasonic method (the frequency is between  $10^4$  and  $10^8$  Hz). The dynamic methods are widely applied to study the elastic properties and determine the elastic moduli of glasses and glass-forming liquids. Therefore, in the following we focus on the introduction of one of the dynamic methods—the ultrasonic method and the related theory.

### 3.1. Ultrasonic methods

#### 3.1.1. The theory for ultrasonic measurements

The propagation velocity of the ultrasonic waves such as longitudinal and shear waves depends on the nature of the materials. However, in a given material, the propagation velocity of the ultrasonic

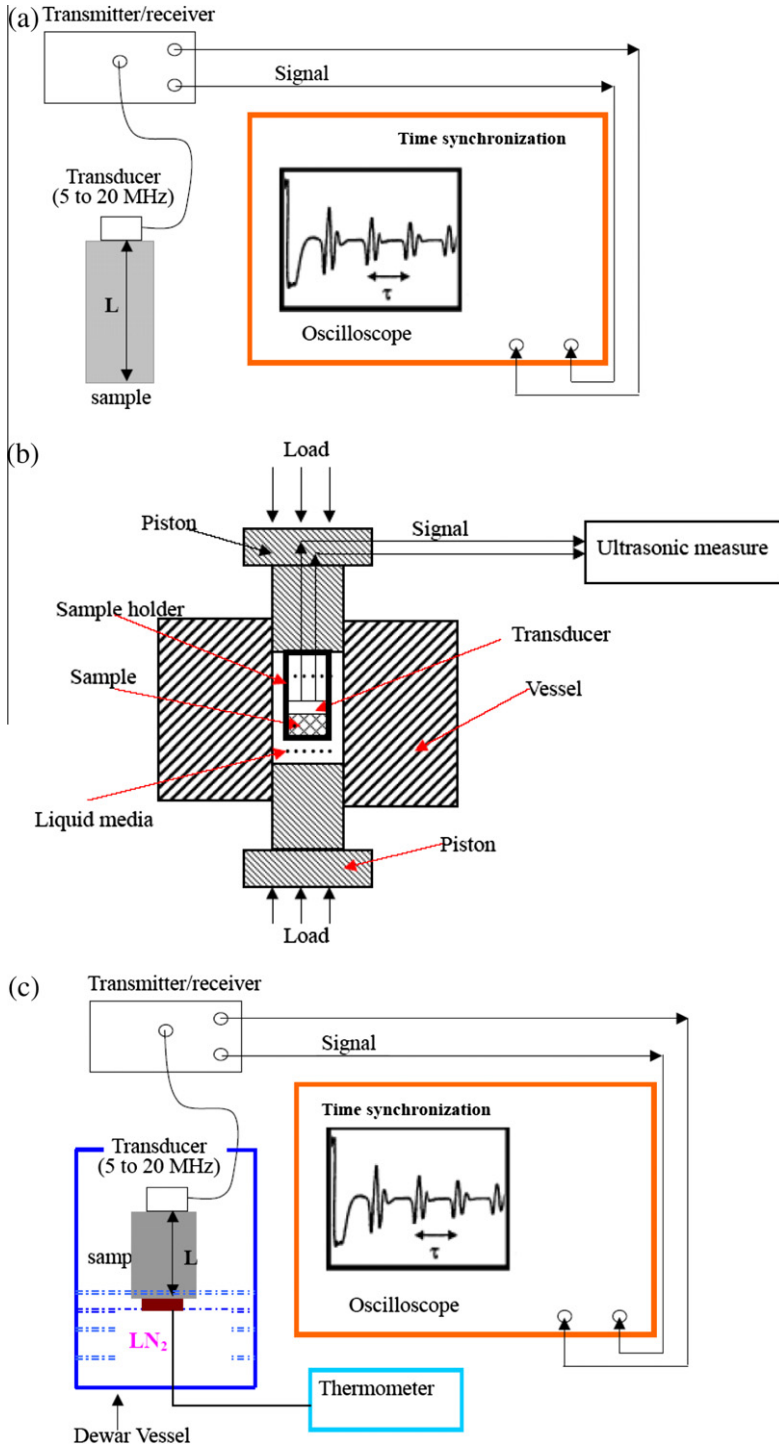


**Fig. 2.** The schematic illustrations for ultrasonic method. (a) The pulse echo overlap method; (b) the high-pressure sample assembly for ultrasonic wave velocities measurement; (c) the *in situ* low-temperature ultrasonic wave velocities measurements.

wave is independent of its frequency and the dimension of the material. In isotropic and homogeneous solids such as glassy materials, the one-dimensional acoustic wave equations are expressed as [50]:

$$\frac{d^2u}{dt^2} = \frac{Ld^2u}{\rho dx^2} \quad (\text{Longitudinal mode or compressional wave}) \quad (3.1)$$

$$\frac{d^2u}{dt^2} = \frac{Gd^2u}{\rho d^2x} \quad (\text{Shear mode or transverse mode}) \quad (3.2)$$

where  $u$  is displacement,  $L$  is longitudinal modulus. From above equations, one obtains:

$$G = \rho v_s^2 \quad (3.3)$$

$$L = \rho v_l^2 \quad (3.4)$$

where  $v_l$  and  $v_s$  are longitudinal and transverse sound velocities, respectively. It can be approximately generalized that the  $v_s$  is half of the  $v_l$  in homogenous metallic materials, that is  $v_l = 2v_s$ .

Based on Eqs. (2.6)–(2.9), the  $E$ ,  $K$ , and  $\nu$  of the isotropic solids such as glasses can be given in terms of  $v_l$ ,  $v_s$  and density as [50]:

$$K = \rho \left( v_l^2 - \frac{4}{3} v_s^2 \right) \quad (3.5)$$

$$\nu = \frac{v_l^2 - 2v_s^2}{2(v_l^2 - v_s^2)} \quad (3.6)$$

$$E = \rho v_s^2 \frac{3v_l^2 - 4v_s^2}{v_l^2 - v_s^2} \quad (3.7)$$

The Debye temperature  $\theta_D$  of the isotropic solids can also be derived from the acoustic velocities and density [50]. For the long wavelength like ultrasonic (its wavelength is much larger than the nearest atomic distance), the glassy solid can be considered as a classical elastic continuum which meets the Debye approximation [51]. Using acoustic data,  $\theta_D$  at room temperature can be represented as [51]:

$$\theta_D = \frac{h}{k_B} \left( \frac{4\pi}{9\Omega_0} \right)^{-1/3} \left( \frac{1}{v_l^3} + \frac{2}{v_s^3} \right)^{-1/3}$$

$$\text{or } \theta_D = \frac{h}{k_B} \left( \frac{4\pi}{9} \right)^{-1/3} \rho^{1/3} \left( \frac{1}{v_l^3} + \frac{2}{v_s^3} \right)^{-1/3} \quad (3.8)$$

where  $\Omega_0$  is the average atomic volume, and  $h$  is Planck constant.

The specific heat,  $C_v$ , then can be expressed as [51]:

$$C_v = 9Nk_B \left( \frac{T}{\theta_D} \right)^3 \int_0^{\theta_D/T} \frac{x^4 e^x}{(x^2 - 1)^2} dx \quad (3.9)$$

Therefore, from the ultrasonic wave velocities and density measurements, one can readily obtain the elastic moduli,  $C_v$ , and Debye temperature of the metallic glasses.

### 3.1.2. The ultrasonic experimental methods

The normally used ultrasonic methods are: phase comparison method (PC), pulse echo overlap method (PEO), phase position detection (PPD), resonant ultrasound spectroscopy method, ultrasonic echography methods (USE) and electron-magnetic acoustic resonance (EMAR). The pulse echo technique [52–63] and resonant ultrasound spectroscopy technique are widely used for measuring the velocities of longitudinal and transverse waves in glasses [64–69], hence we will focus on the introduction of the two techniques.

Fig. 2 schematically illustrates the PEO method. The instrument consists of three parts as shown in Fig. 2a: the pulse ultrasonic waves transmitter and receiver; the time synchronization; and the sample assembly including high frequency quartz transducers. The PEO technique is described in details by Papadakis [52], and here we only very briefly describe the method. The oscilloscope is

triggered at the carrier frequency of the synthesizer while the pulse generator used to drive the quartz crystal is triggered at a decade fraction of this frequency. Therefore, there is no actual overlap of the echo trains, and only an apparent overlap of the echoes on the oscilloscope when the repetition rate of the frequency synthesizer is of the same order as the reciprocal of the travel time in the sample or a multiple of this travel time. The careful adjustment of the frequency synthesizer allows the two chosen echoes to overlap accurately, and then yielding a precise measure of the travel time. The observations of the overlap of the pulses are aided by coincident intensification of the trace by strobe pulses to the oscilloscope [52]. From the obtained wave travel time and the length of the sample, the sound velocities are then to be determined.

The frequency range of the sound wave is 5–20 MHz, which is at least  $10^{10}$  times of the relaxation frequency of metallic glasses corresponding to its viscosity at their glass transition temperature [29]. The sensitivity for measurement of time of ultrasonic waves propagating through the sample for a MATEC 6600 ultrasonic system was 0.9 ns, which corresponds to a sensitivity of 5 cm/s in velocity [56]. The accuracy in measuring the velocities is approximately equal to 0.5% for shear waves and 1% for longitudinal waves. The excitation and detection of the ultrasonic pulses were provided by X- or Y-cut (for longitudinal and transverse waves, respectively) high frequency quartz transducers. The transducers were bonded to the specimen using honey or other glues (their effects on the ultrasonic velocity and attenuation have been already determined) for experiments. The density was measured using the Archimedes method with an accuracy of  $\sim 1.0\%$ . The elastic constants of  $E$ ,  $G$ ,  $K$ , and  $\nu$  were derived from the acoustic velocities and the density by Eqs. (3.3)–(3.9).

Another widely used ultrasonic technique in metallic glasses field is the resonant ultrasound spectroscopy (RUS). RUS is a technique developed by Migliori and his co-workers at Los Alamos National Laboratory for determining the complete elastic tensor of a solid by measuring its free-body resonance [64–69]. The mechanical resonances can be calculated for a sample with known dimensions, density, and elastic tensor. Fig. 3 shows the schematic illustration of the experimental set-up of the RUS. In the RUS experiment, the mechanical resonances of a freely vibrating solid of known shape are measured, and an iteration procedure is used to “match” the measured frequencies with the calculated spectrum. This allows determination of the full elastic tensor of the solid from a single frequency scan, which clearly indicates a main advantage of RUS. That is, there is no need for separate measurements to probe different moduli, and multiple sample remounts and temperature sweeps are avoided. Another advantage lies in the ability of RUS to work with small, mm-sized samples. The sample can be

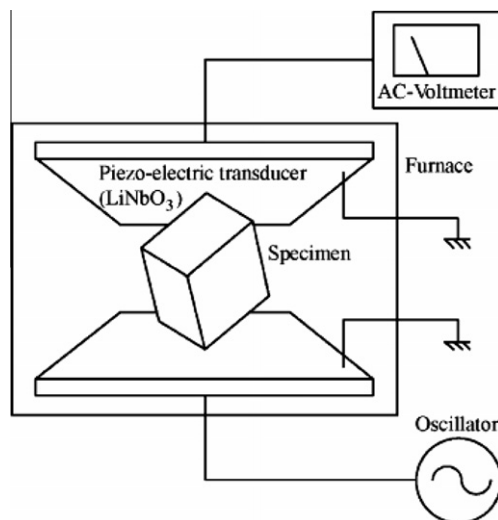


Fig. 3. Schematic illustration of the experimental set-up of the resonance ultrasound spectrometer [64–67].

**Table 1**

The acoustic data and elastic constants for various bulk metallic glasses, typical oxide glasses and other non-metallic glasses.

Glasses	$\rho$ (g/cm <sup>3</sup> )	$v_l$ (km/s)	$v_s$ (km/s)	$v_l/v_s$	$K$ (GPa)	$G$ (GPa)	$E$ (GPa)	$E/\rho$ (GPa cm <sup>3</sup> /g)	$\nu$	$K/G$	$\theta_D$ (K)	Refs.
Zr <sub>41</sub> Ti <sub>14</sub> Cu <sub>12.5</sub> Ni <sub>10</sub> Be <sub>22.5</sub>	6.125	5.174	2.472	2.09	114.1	37.4	101.2	16.53	0.352	3.05	326.8	[54,99]
Zr <sub>46.75</sub> Ti <sub>8.25</sub> Cu <sub>7.5</sub> Ni <sub>10</sub> Be <sub>27.5</sub>	6.014	5.182	2.487	2.08	111.9	37.2	100.5	16.70	0.350	3.01	327.1	[54]
Zr <sub>45.4</sub> Ti <sub>9.6</sub> Cu <sub>10.5</sub> Ni <sub>8.6</sub> Be <sub>26.25</sub>	6.048	5.163	2.473	2.09	111.9	37.0	99.9	16.52	0.350	3.02	325.6	[54]
Zr <sub>52.5</sub> Al <sub>10</sub> Ni <sub>10</sub> Cu <sub>15</sub> Be <sub>12.5</sub>	6.295	5.033	2.384	2.11	112.0	35.9	97.2	15.41	0.355	3.12	306.6	This work
Zr <sub>50</sub> Al <sub>10</sub> Ni <sub>10</sub> Cu <sub>15</sub> Be <sub>15</sub>	6.311	5.075	2.478	2.05	110.9	38.8	104.1	16.50	0.343	2.86	321.5	This work
Zr <sub>55</sub> Al <sub>10</sub> Ni <sub>10</sub> Cu <sub>15</sub> Be <sub>10</sub>	6.408	4.958	2.355	2.14	111.6	34.4	93.7	14.62	0.360	3.24	296.9	This work
Zr <sub>60</sub> Al <sub>10</sub> Ni <sub>10</sub> Cu <sub>15</sub> Be <sub>5</sub>	6.497	5.763	2.085	2.28	109.7	28.2	78.0	12.01	0.381	3.89	264.0	This work
(Zr <sub>46.75</sub> Ti <sub>8.25</sub> Cu <sub>7.5</sub> Ni <sub>10</sub> Be <sub>27.5</sub> ) <sub>98</sub> Al <sub>2</sub>	5.89				110.6	32.8	101.8	17.3	0.347	3.37		This work
(Zr <sub>46.75</sub> Ti <sub>8.25</sub> Cu <sub>7.5</sub> Ni <sub>10</sub> Be <sub>27.5</sub> ) <sub>95</sub> Al <sub>5</sub>	5.87				115.8	40.5	108.9	18.5	0.343	2.86		This work
(Zr <sub>46.75</sub> Ti <sub>8.25</sub> Cu <sub>7.5</sub> Ni <sub>10</sub> Be <sub>27.5</sub> ) <sub>92</sub> Al <sub>8</sub>	5.88				91.6	32.3	86.7	14.7	0.342	2.84		This work
(Zr <sub>46.75</sub> Ti <sub>8.25</sub> Cu <sub>7.5</sub> Ni <sub>10</sub> Be <sub>27.5</sub> ) <sub>90</sub> Al <sub>10</sub>	5.89				113.8	44.5	118.1	20.0	0.327	2.56		This work
(Zr <sub>46.75</sub> Ti <sub>8.25</sub> Cu <sub>7.5</sub> Ni <sub>10</sub> Be <sub>27.5</sub> ) <sub>88</sub> Al <sub>12</sub>	5.66				112.6	44.1	117.1	20.7	0.326	2.55		This work
(Zr <sub>46.75</sub> Ti <sub>8.25</sub> Cu <sub>7.5</sub> Ni <sub>10</sub> Be <sub>27.5</sub> ) <sub>85</sub> Al <sub>15</sub>	5.72				116.9	48.4	117.5	20.5	0.318	2.42		This work
Zr <sub>41</sub> Ti <sub>14</sub> Cu <sub>12.5</sub> Ni <sub>9</sub> Be <sub>22.5</sub> C <sub>1</sub>	6.161	5.097	2.534	2.01	107.3	39.5	105.7	17.15	0.336	2.71	335.7	[100]
Zr <sub>34</sub> Ti <sub>15</sub> Cu <sub>10</sub> Ni <sub>11</sub> Be <sub>28</sub> Y <sub>2</sub>	5.778	5.251	2.686	1.95	103.7	41.7	110.3	19.09	0.320	2.49	356.3	[101]
(Zr <sub>41</sub> Ti <sub>14</sub> Cu <sub>12.5</sub> Ni <sub>10</sub> Be <sub>22.5</sub> ) <sub>98</sub> Y <sub>2</sub>	5.860	5.263	2.619	2.01	108.7	40.2	107.3	18.31	0.340	2.71	339.2	[102]
Zr <sub>41</sub> Ti <sub>14</sub> Cu <sub>12.5</sub> Ni <sub>8</sub> Be <sub>22.5</sub> Fe <sub>2</sub>	6.083	5.135	2.436	2.11	112.3	36.1	97.8	16.08	0.355	3.11	321.5	This work
Zr <sub>41</sub> Ti <sub>14</sub> Cu <sub>12.5</sub> Ni <sub>8</sub> Be <sub>22.5</sub> Fe <sub>5</sub>	6.108	5.130	2.439	2.10	112.3	36.3	98.4	16.11	0.354	3.09	322.4	This work
Zr <sub>41</sub> Ti <sub>14</sub> Cu <sub>12.5</sub> Ni <sub>2</sub> Be <sub>22.5</sub> Fe <sub>8</sub>	5.938	4.942	2.427	2.04	98.4	35.0	93.8	15.79	0.341	2.81	317.4	This work
Zr <sub>41</sub> Ti <sub>14</sub> Cu <sub>12.5</sub> Be <sub>22.5</sub> Fe <sub>10</sub>	6.086	5.151	2.522	2.04	109.8	38.7	103.9	17.08	0.342	2.84	332.8	This work
Zr <sub>36</sub> Ti <sub>14</sub> Cu <sub>12.5</sub> Ni <sub>5</sub> Be <sub>20.5</sub> Fe <sub>12</sub>	6.520	4.933	2.283	2.16	113.4	34.0	92.7	14.21	0.364	3.34	310.2	This work
Zr <sub>53</sub> Ti <sub>5</sub> Cu <sub>20</sub> Ni <sub>12</sub> Al <sub>10</sub>	6.749	4.7774	2.155	2.22	112.3	31.3	86.0	12.74	0.37	3.58	276.0	[100]
(Zr <sub>58.9</sub> Ti <sub>5.6</sub> Cu <sub>22.2</sub> Ni <sub>13.3</sub> ) <sub>88</sub> Al <sub>12</sub>	6.696	4.825	2.232	2.16	111.4	33.4	91.0	13.59	0.36	3.34	286.2	[100]
(Zr <sub>59</sub> Ti <sub>6</sub> Cu <sub>22</sub> Ni <sub>13</sub> ) <sub>85.7</sub> Al <sub>14.3</sub>	6.608	4.890	2.269	2.15	112.7	34.0	92.7	14.03	0.363	3.31	291.1	[100]
Zr <sub>53</sub> Ti <sub>5</sub> Cu <sub>20</sub> Ni <sub>12</sub> Al <sub>15</sub>	6.572	4.893	2.268	2.16	112.3	33.8	92.1	14.02	0.36	3.32	290.5	[100]
(Zr <sub>58.9</sub> Ti <sub>5.6</sub> Cu <sub>22.2</sub> Ni <sub>13.3</sub> ) <sub>84</sub> Al <sub>16</sub>	6.553	4.946	2.319	2.13	113.3	35.3	95.8	14.62	0.36	3.21	297.9	[100]
Zr <sub>52.5</sub> Ti <sub>5</sub> Cu <sub>17.9</sub> Ni <sub>14.6</sub> Al <sub>10</sub>	6.730	4.833	2.191	2.20	114.1	32.3	88.6	13.16	0.37	3.53	280.7	[103]
Zr <sub>52.5</sub> Ti <sub>5</sub> Cu <sub>17.9</sub> Ni <sub>14.6</sub> Al <sub>10</sub> (+1%Carbon nanotube)	6.701	4.843	2.240	2.16	112.3	33.6	91.7	13.68	0.36	3.34	282.3	[100,162–164]
Zr <sub>40</sub> Mg <sub>0.5</sub> Ti <sub>15</sub> Cu <sub>1</sub> Ni <sub>11</sub> Be <sub>21.5</sub> Y <sub>1</sub>	6.048	5.081	2.396	2.12	109.9	34.7	94.2	15.58	0.357	3.16	315.3	This work
Zr <sub>48</sub> Nb <sub>8</sub> Cu <sub>14</sub> Ni <sub>12</sub> Be <sub>18</sub>	6.700	4.950	2.264	2.19	118.4	34.4	94.0	14.02	0.368	3.45	295.2	This work
Zr <sub>45</sub> Nb <sub>10</sub> Cu <sub>13</sub> Ni <sub>10</sub> Be <sub>22</sub>	6.523	5.050	2.361	2.14	117.9	36.4	98.9	15.16	0.360	3.24	308.2	This work
Zr <sub>45</sub> Nb <sub>8</sub> Cu <sub>13</sub> Ni <sub>4</sub> Be <sub>22</sub> Fe <sub>8</sub>	6.543	4.970	2.315	2.15	114.9	35.1	95.5	14.59	0.361	3.28	304.0	This work
Zr <sub>48</sub> Nb <sub>8</sub> Cu <sub>12</sub> Be <sub>24</sub> Fe <sub>8</sub>	6.436	4.994	2.338	2.14	113.6	35.2	95.7	14.87	0.360	3.23	305.4	[105]
Zr <sub>57</sub> Nb <sub>5</sub> Cu <sub>15.4</sub> Ni <sub>12.6</sub> Al <sub>10</sub>	6.690	4.740	2.186	2.17	107.7	32.0	87.3	13.05	0.365	3.37	274.8	This work
Zr <sub>60</sub> Nb <sub>3</sub> Cu <sub>14</sub> Ni <sub>13</sub> Al <sub>10</sub>	6.730	4.780	2.150	2.22	112.3	31.1	85.4	12.69	0.373	3.61	270.8	[106]
Zr <sub>55</sub> Nb <sub>9</sub> Cu <sub>15</sub> Ni <sub>11</sub> Al <sub>10</sub>	6.875	4.880	2.250	2.17	117.3	34.8	95.0	13.82	0.365	3.37	284.5	[106]
(Zr <sub>55</sub> Nb <sub>9</sub> Cu <sub>15</sub> Ni <sub>11</sub> Al <sub>10</sub> ) <sub>99</sub> B <sub>1</sub>	6.76	4.681	2.106	2.22	108.2	30.0	82.3	12.18	0.373	3.61	279.0	[106]

(continued on next page)

Table 1 (continued)

Glasses	$\rho$ (g/cm <sup>3</sup> )	$v_l$ (km/s)	$v_s$ (km/s)	$v_l/v_s$	$K$ (GPa)	$G$ (GPa)	$E$ (GPa)	$E/\rho$ (GPa cm <sup>3</sup> /g)	$\nu$	$K/G$	$\theta_D$ (K)	Refs.
Zr <sub>57</sub> Nb <sub>5</sub> Cu <sub>15.4</sub> Ni <sub>12.6</sub> Al <sub>10</sub>	6.758	4.755	2.157	2.20	110.9	31.5	86.2	12.75	0.370	3.53	272.3	This work
Zr <sub>52.7</sub> Nb <sub>5</sub> Cu <sub>17.9</sub> Ni <sub>14.6</sub> Al <sub>10</sub>	6.651	4.747	2.129	2.23	109.7	30.2	82.9	12.46	0.370	3.64	–	This work
Zr <sub>52.7</sub> Nb <sub>5</sub> Cu <sub>17.9</sub> Ni <sub>14.6</sub> Al <sub>10</sub> (+1% carbon fiber)	6.703	4.747	2.127	2.23	110.6	30.3	83.4	12.44	0.374	3.65	–	This work
Zr <sub>52.7</sub> Nb <sub>5</sub> Cu <sub>17.9</sub> Ni <sub>14.6</sub> Al <sub>10</sub> (+1.5% carbon fiber)	6.709	4.785	2.132	2.24	113.0	30.5	83.9	12.51	0.376	3.70	–	This work
Zr <sub>52.7</sub> Nb <sub>5</sub> Cu <sub>17.9</sub> Ni <sub>14.6</sub> Al <sub>10</sub> (+2% carbon fiber)	6.622	4.773	2.135	2.24	110.6	30.2	83.0	12.53	0.375	3.66	–	This work
Zr <sub>52.7</sub> Nb <sub>5</sub> Cu <sub>17.9</sub> Ni <sub>14.6</sub> Al <sub>10</sub> (+4% carbon fiber)	6.758	4.804	2.170	2.22	113.5	31.8	87.3	12.92	0.372	3.57	–	This work
(ZrNb) <sub>72.8</sub> (CuNiAl) <sub>27.2</sub>	6.675	4.604	1.990	2.31	106.2	26.4	73.2	10.97	0.385	4.02	–	This work
(ZrNb) <sub>73.4</sub> (CuNiAl) <sub>26.6</sub>	6.670	4.437	1.972	2.25	96.7	25.9	71.4	10.71	0.377	3.73	–	This work
(ZrNb) <sub>70.7</sub> (CuNiAl) <sub>29.3</sub>	6.643	4.633	2.038	2.27	105.8	27.6	76.1	11.46	0.380	3.84	–	This work
Zr <sub>58</sub> Ni <sub>26.6</sub> Al <sub>15.4</sub>	6.522	4.922	2.230	2.21	114.8	32.4	88.9	13.63	0.371	3.54	283.0	This work
Zr <sub>55.8</sub> Ni <sub>24.8</sub> Al <sub>19.4</sub>	6.328	5.029	2.339	2.15	113.9	34.6	94.3	14.90	0.362	3.29	296.2	This work
Zr <sub>53</sub> Ni <sub>23.5</sub> Al <sub>23.5</sub>	6.171	5.169	2.462	2.10	115.1	37.4	101.2	16.41	0.353	3.07	312.1	This work
Zr <sub>45.25</sub> Cu <sub>46.25</sub> Al <sub>7.5</sub> Sn <sub>1</sub>	–	–	–	–	118.0	37.5	97.3	–	–	–	–	666
(Zr <sub>55</sub> Al <sub>15</sub> Ni <sub>10</sub> Cu <sub>20</sub> ) <sub>98</sub> Y <sub>2</sub>	6.56	4.870	2.270	2.14	110.6	33.8	92.1	14.03	0.361	3.27	287.7	[107]
(Zr <sub>55</sub> Al <sub>15</sub> Ni <sub>10</sub> Cu <sub>20</sub> ) <sub>96</sub> Y <sub>4</sub>	6.44	4.774	2.212	2.16	104.8	31.5	85.9	13.34	0.363	3.32	278.3	[107]
Zr <sub>65</sub> Al <sub>10</sub> Ni <sub>10</sub> Cu <sub>15</sub>	6.271	5.050	2.393	2.11	112.0	35.9	97.3	15.52	0.355	3.12	292.9	[106]
Zr <sub>61.88</sub> Al <sub>10</sub> Ni <sub>10.12</sub> Cu <sub>18</sub>	6.649	4.704	2.092	2.25	108.3	29.1	80.1	12.05	0.377	3.72	262.9	[106]
Zr <sub>64.13</sub> Al <sub>10</sub> Ni <sub>10.12</sub> Cu <sub>15.75</sub>	6.604	4.679	2.076	2.254	106.6	28.5	78.4	11.87	0.377	3.75	259.6	[106]
Zr <sub>65.025</sub> Cu <sub>14.85</sub> Ni <sub>10.125</sub> Al <sub>10</sub>	6.585	4.648	2.078	2.24	104.4	28.4	78.2	11.87	0.375	3.67	259.2	[106]
Zr <sub>62.325</sub> Cu <sub>17.55</sub> Ni <sub>10.125</sub> Al <sub>10</sub>	6.678	4.702	2.100	2.24	108.4	29.5	81.0	12.13	0.375	3.68	264.1	[106]
Zr <sub>61.88</sub> Al <sub>10</sub> Ni <sub>10.12</sub> Cu <sub>18</sub>	6.664	4.693	2.096	2.24	107.7	29.3	80.5	12.08	0.375	3.68	263.5	[106]
Zr <sub>62.325</sub> Cu <sub>17.55</sub> Ni <sub>10.125</sub> Al <sub>10</sub>	6.685	4.706	2.113	2.23	108.3	29.9	82.0	12.27	0.373	3.63	266.0	[106]
Zr <sub>61</sub> Cu <sub>18.3</sub> Ni <sub>12.8</sub> Al <sub>7.9</sub>	6.824	4.527	2.057	2.20	101.4	28.9	79.1	11.59	0.370	3.50	260.2	This work
Zr <sub>61</sub> Cu <sub>17.8</sub> Ni <sub>12.8</sub> Al <sub>7.9</sub> Sn <sub>0.5</sub>	6.784	4.537	2.059	2.20	101.3	28.8	78.8	11.62	0.370	3.50	259.6	This work
Zr <sub>61</sub> Cu <sub>17.3</sub> Ni <sub>12.8</sub> Al <sub>7.9</sub> Sn <sub>1</sub>	6.801	4.539	2.035	2.23	102.6	28.2	77.4	11.38	0.374	3.64	256.7	This work
Zr <sub>61</sub> Cu <sub>16.8</sub> Ni <sub>12.8</sub> Al <sub>7.9</sub> Sn <sub>1.5</sub>	6.794	4.387	2.043	2.15	92.9	28.4	77.3	11.38	0.362	3.27	256.9	This work
Zr <sub>61</sub> Cu <sub>16.3</sub> Ni <sub>12.8</sub> Al <sub>7.9</sub> Sn <sub>2</sub>	6.779	4.542	2.105	2.16	99.8	30.1	81.9	12.08	0.363	3.32	264.2	This work
Zr <sub>61</sub> Cu <sub>15.8</sub> Ni <sub>12.8</sub> Al <sub>7.9</sub> Sn <sub>2.5</sub>	6.819	4.561	2.090	2.18	102.1	29.8	81.5	11.95	0.367	3.42	262.7	This work
Zr <sub>60.525</sub> Cu <sub>19.35</sub> Ni <sub>10.125</sub> Al <sub>10</sub>	6.701	4.712	2.110	2.23	109.0	29.8	82.0	12.24	0.374	3.65	266.2	[106]
Zr <sub>62</sub> Al <sub>10</sub> Ni <sub>12.6</sub> Cu <sub>15.4</sub>	6.615	4.723	2.090	2.26	109.0	28.9	79.7	12.04	0.378	3.77	262.3	[106]
Zr <sub>35</sub> Ti <sub>30</sub> Cu <sub>7.5</sub> Be <sub>27.5</sub>	5.329	5.172	2.545	2.03	96.5	34.5	92.5	17.36	0.340	2.79	–	This work
Zr <sub>33</sub> Ti <sub>30</sub> Cu <sub>7.5</sub> Be <sub>27.5</sub> Al <sub>2</sub>	5.260	5.270	2.640	2.00	97.2	36.7	97.7	18.57	0.332	2.65	–	This work
Zr <sub>30</sub> Ti <sub>30</sub> Cu <sub>7.5</sub> Be <sub>27.5</sub> Al <sub>5</sub>	5.134	5.429	2.782	1.95	98.3	39.7	105.1	20.50	0.322	2.48	–	This work
Zr <sub>25</sub> Ti <sub>30</sub> Cu <sub>7.5</sub> Be <sub>27.5</sub> Al <sub>10</sub>	4.926	5.700	2.980	1.91	101.7	43.7	114.8	23.30	0.312	2.33	–	This work
Zr <sub>50</sub> Cu <sub>25</sub> Be <sub>25</sub>	6.12	–	–	–	108.9	35.8	96.8	15.8	0.35	3.04	–	[59]
Zr <sub>50</sub> Cu <sub>43</sub> Ag <sub>7</sub>	–	–	–	–	124.7	32.8	90.5	–	0.379	3.80	–	[82]
Zr <sub>35</sub> Ti <sub>30</sub> Cu <sub>8.25</sub> Be <sub>26.75</sub>	5.4	–	–	–	113.7	31.8	86.9	16.1	0.370	3.57	–	[158]
Pd <sub>39</sub> Ni <sub>10</sub> Cu <sub>30</sub> P <sub>21</sub>	9.152	4.750	1.963	2.42	159.4	35.3	98.6	10.8	0.397	4.52	279.6	[113]
Pd <sub>40</sub> Ni <sub>10</sub> Cu <sub>30</sub> P <sub>20</sub>	9.259	4.874	1.959	2.49	172.6	35.5	99.8	10.77	0.404	4.86	279.4	This work

Table 1 (continued)

Glasses	$\rho$ (g/cm <sup>3</sup> )	$v_l$ (km/s)	$v_s$ (km/s)	$v_l/v_s$	$K$ (GPa)	$G$ (GPa)	$E$ (GPa)	$E/\rho$ (GPa cm <sup>3</sup> /g)	$\nu$	$K/G$	$\theta_D$ (K)	Refs.
Pd <sub>80</sub> P <sub>20</sub>	10.22	4.300	1.630	2.63	160.0	28.2	80.5	7.88	0.416	5.67	–	[111]
Pd <sub>64</sub> Ni <sub>16</sub> P <sub>20</sub>	10.08	4.560	1.790	2.55	172.0	32.8	93.5	9.26	0.410	5.24	–	[111]
Pd <sub>40</sub> Ni <sub>40</sub> P <sub>20</sub>	9.405	4.900	1.960	2.50	175.0	36.5	105.0	11.16	0.40	4.79	292	[111,112]
Pd <sub>16</sub> Ni <sub>64</sub> P <sub>20</sub>	8.750	5.017	2.080	2.41	169.8	37.9	105.8	12.09	0.396	4.48	–	[111]
Pd <sub>64</sub> Fe <sub>16</sub> P <sub>20</sub>	10.04	4.530	1.816	2.49	161.9	33.1	93.0	9.26	0.404	4.90	–	[111]
Pd <sub>56</sub> Fe <sub>24</sub> P <sub>20</sub>	9.90	4.572	1.860	2.45	161.2	34.3	96.0	9.70	0.401	4.90	–	[111]
Pd <sub>81</sub> Si <sub>19</sub>	10.61	4.627	1.775	2.61	182.6	33.4	94.5	8.91	0.414	5.46	246.3	This work
Pd <sub>77.5</sub> Si <sub>16.5</sub> Cu <sub>6</sub>	10.40	4.584	1.779	2.58	174.6	32.9	92.9	8.93	0.411	5.29	252.0	[111]
Pd <sub>79</sub> Ag <sub>3.5</sub> P <sub>6</sub> Si <sub>9.5</sub> Ge <sub>2</sub>	–	–	–	–	172.0	31.0	–	–	0.42	5.54	–	[671]
Pt <sub>60</sub> Ni <sub>15</sub> P <sub>25</sub>	15.71	3.965	1.467	2.67	201.9	33.8	96.1	6.12	0.421	5.94	205	[111]
Pt <sub>57.5</sub> Cu <sub>14.7</sub> Ni <sub>5.3</sub> P <sub>22.5</sub>	15.02	4.000	1.481	2.70	198.7	33.3	94.8	6.31	0.42	5.97	206	[113]
Pt <sub>74.7</sub> Cu <sub>1.5</sub> Ag <sub>6.3</sub> P <sub>18</sub> B <sub>4</sub> Si <sub>1.5</sub>	17.23	–	–	–	216.7	32.4	–	–	0.43	6.69	–	[113]
Au <sub>49</sub> Ag <sub>5.5</sub> Pd <sub>2.3</sub> Cu <sub>26.9</sub> Si <sub>16.3</sub>	–	–	–	–	132.3	26.5	74.4	–	0.406	5.00	–	[114]
Cu <sub>50</sub> Zr <sub>50</sub>	7.404	–	–	–	101.2	31.3	85.0	11.48	0.360	3.22	231	[108,154,155]
(Cu <sub>50</sub> Zr <sub>50</sub> ) <sub>96</sub> Al <sub>4</sub>	7.221	4.661	2.118	2.20	113.7	32.4	88.7	12.3	0.370	3.51	274.6	[115]
(Cu <sub>50</sub> Zr <sub>50</sub> ) <sub>94.5</sub> Al <sub>5.5</sub>	7.174	4.706	2.126	2.21	115.6	32.4	89.0	12.40	0.372	3.56	276.3	This work
(Cu <sub>50</sub> Zr <sub>50</sub> ) <sub>94</sub> Al <sub>6</sub>	7.129	4.722	2.179	2.17	113.8	33.8	92.4	12.96	0.365	3.36	282.4	[115]
(Cu <sub>50</sub> Zr <sub>50</sub> ) <sub>92</sub> Al <sub>8</sub>	7.076	4.787	2.202	2.17	116.4	34.3	93.7	13.24	0.366	3.39	286.0	[115]
(Cu <sub>50</sub> Zr <sub>50</sub> ) <sub>90</sub> Al <sub>10</sub>	7.204	4.855	2.246	2.16	121.4	36.3	99.1	13.76	0.364	3.34	294.8	This work
(Cu <sub>50</sub> Zr <sub>50</sub> ) <sub>92</sub> Al <sub>7</sub> Gd <sub>1</sub>	7.127	4.848	2.148	2.26	123.7	32.9	90.6	12.71	0.38	3.76	278.7	[115]
Cu <sub>45</sub> Zr <sub>45</sub> Al <sub>7</sub> Gd <sub>3</sub>	7.162	4.731	2.127	2.22	117.1	32.4	89.0	12.42	0.373	3.62	274.1	[115]
Cu <sub>50</sub> Zr <sub>45</sub> Al <sub>5</sub>	7.223	4.731	2.147	2.20	117.3	33.3	91.2	12.63	0.370	3.52	278.0	This work
Cu <sub>46</sub> Zr <sub>42</sub> Al <sub>7</sub> Y <sub>5</sub>	6.946	4.578	2.047	2.24	106.8	29.1	80.0	11.52	0.375	3.67	264.2	[115]
Cu <sub>46</sub> Zr <sub>44</sub> Al <sub>7</sub> Y <sub>3</sub>	7.026	4.694	2.135	2.20	112.1	32.0	87.7	14.80	0.37	3.50	276.12	This work
(Cu <sub>46</sub> Zr <sub>42</sub> Al <sub>7</sub> Y <sub>5</sub> ) <sub>96</sub> Cr <sub>4</sub>	7.001	4.719	2.110	2.24	114.3	31.2	85.7	12.24	0.375	3.66	274.1	This work
(Cu <sub>46</sub> Zr <sub>42</sub> Al <sub>7</sub> Y <sub>5</sub> ) <sub>96</sub> Nd <sub>4</sub>	7.053	4.597	2.209	2.08	103.2	34.4	92.9	13.17	0.350	3.00	283.3	This work
Cu <sub>60</sub> Zr <sub>20</sub> Hf <sub>10</sub> Ti <sub>10</sub>	8.315	4.620	2.108	2.19	128.2	36.9	101.1	12.16	0.369	3.47	282.0	[116]
Cu <sub>60</sub> Zr <sub>29</sub> Ti <sub>10</sub> Sn <sub>1</sub>	7.408	4.472	2.191	2.04	100.7	36.6	95.5	12.89	0.342	2.75	292.0	This work
Fe <sub>65.5</sub> Cr <sub>4</sub> Mo <sub>4</sub> Ga <sub>4</sub> P <sub>12</sub> C <sub>5</sub> B <sub>5.5</sub>	7.300	5.12	2.83	1.81	113.4	58.5	149.7	20.50	0.28	1.94	416.9	This work
Fe <sub>48</sub> Cr <sub>15</sub> Mo <sub>14</sub> C <sub>15</sub> B <sub>6</sub> Er <sub>2</sub>	7.897	6.228	3.296	1.89	191.9	85.8	224.0	28.36	0.305	2.24	488.5	This work
Fe <sub>60</sub> Cr <sub>10</sub> Mo <sub>9</sub> C <sub>13</sub> B <sub>6</sub> Er <sub>2</sub>	7.916	5.891	3.163	1.86	169.1	79.2	205.5	25.96	0.30	2.14	471.4	This work
Fe <sub>64</sub> Cr <sub>10</sub> Mo <sub>9</sub> C <sub>15</sub> Er <sub>2</sub>	7.994	5.964	3.321	1.80	166.8	88.2	224.9	28.13	0.275	1.89	489.61	This work
(Fe <sub>60</sub> Cr <sub>10</sub> Mo <sub>9</sub> C <sub>13</sub> B <sub>6</sub> Er <sub>2</sub> ) <sub>95</sub> Ni <sub>5</sub>	7.934	5.820	3.107	1.87	166.6	76.6	199.2	25.11	0.301	2.18	462.75	This work
(Fe <sub>60</sub> Cr <sub>10</sub> Mo <sub>9</sub> C <sub>13</sub> B <sub>6</sub> Er <sub>298</sub> ) In <sub>2</sub>	7.752	5.609	3.137	1.79	142.2	76.3	194.1	25.06	0.272	1.86	459.28	This work
(Fe <sub>60</sub> Cr <sub>10</sub> Mo <sub>9</sub> C <sub>13</sub> B <sub>6</sub> Er <sub>2</sub> ) <sub>98</sub> Be <sub>2</sub>	7.813	5.908	3.183	1.86	167.2	79.2	205.1	26.25	0.296	2.11	474.84	This work
(Fe <sub>60</sub> Cr <sub>10</sub> Mo <sub>9</sub> C <sub>13</sub> B <sub>6</sub> Er <sub>2</sub> ) <sub>95</sub> Be <sub>2</sub>	7.628	5.982	3.214	1.86	167.9	78.8	204.4	26.80	0.297	2.13	479.83	This work
(Fe <sub>60</sub> Cr <sub>10</sub> Mo <sub>9</sub> C <sub>13</sub> B <sub>6</sub> Er <sub>2</sub> ) <sub>98</sub> Pb <sub>2</sub>	7.977	5.891	3.159	1.86	170.7	79.6	206.7	25.91	0.298	2.14	463.23	This work
(Fe <sub>60</sub> Cr <sub>10</sub> Mo <sub>9</sub> C <sub>13</sub> B <sub>6</sub> Y <sub>2</sub> ) <sub>98</sub> V <sub>2</sub>	7.714	5.991	3.183	1.88	172.7	78.1	203.7	26.41	0.303	2.21	475.4	This work

(continued on next page)

Table 1 (continued)

Glasses	$\rho$ (g/cm <sup>3</sup> )	$v_l$ (km/s)	$v_s$ (km/s)	$v_l/v_s$	$K$ (GPa)	$G$ (GPa)	$E$ (GPa)	$E/\rho$ (GPa cm <sup>3</sup> /g)	$\nu$	$K/G$	$\theta_D$ (K)	Refs.
Fe <sub>41</sub> Co <sub>7</sub> Cr <sub>15</sub> Mo <sub>14</sub> C <sub>15</sub> B <sub>6</sub> Y <sub>2</sub>	7.904	6.208	3.262	1.90	192.5	84.1	220.2	27.86	0.309	2.29	487.9	This work
Fe <sub>68</sub> Cr <sub>3</sub> Mo <sub>10</sub> P <sub>6</sub> C <sub>10</sub> B <sub>3</sub>	–	–	–	–	172	67.7	180	–	0.326	2.54	–	[161]
Fe <sub>63</sub> Cr <sub>3</sub> Mo <sub>10</sub> P <sub>12</sub> C <sub>7</sub> B <sub>5</sub>	–	–	–	–	174	65.2	173	–	0.333	2.67	–	[161]
Fe <sub>70</sub> Mo <sub>5</sub> Ni <sub>5</sub> P <sub>12.5</sub> C <sub>5</sub> B <sub>2.5</sub>	–	–	–	–	150.1	57.31	–	–	–	–	–	[174]
Ni <sub>80</sub> P <sub>20</sub>	8.13	5.060	2.130	2.38	161.0	36.7	102.5	12.61	0.394	4.31	342	[111]
Co <sub>58</sub> Ta <sub>7</sub> B <sub>35</sub>	8.960	–	–	–	215.7	91.5	240.6	26.8	0.315	2.38	–	[672]
Co <sub>56</sub> Ta <sub>9</sub> B <sub>35</sub>	9.265	–	–	–	224.1	93.8	246.9	26.6	0.315	2.38	–	[672]
Ta <sub>42</sub> Ni <sub>36</sub> Co <sub>22</sub>	12.98	–	–	–	–	–	170.0	–	–	–	–	[673]
Ti <sub>40</sub> Zr <sub>25</sub> Ni <sub>3</sub> Cu <sub>12</sub> Be <sub>20</sub>	5.445	5.369	2.554	2.10	109.6	35.5	96.5	17.66	0.354	3.09	338.0	This work
Ti <sub>45</sub> Zr <sub>20</sub> Be <sub>35</sub>	4.59	–	–	–	111.4	35.7	96.8	21.0	0.36	3.12	–	[157]
Ti <sub>45</sub> Zr <sub>20</sub> Be <sub>30</sub> Cr <sub>5</sub>	4.76	–	–	–	114.5	39.2	105.6	22.2	0.35	2.92	–	[157]
Hf <sub>48</sub> Cu <sub>29.25</sub> Ni <sub>9.75</sub> Al <sub>13</sub>	11.0	–	–	–	128.9	43.1	116.4	–	0.349	–	–	[664]
Hf <sub>62</sub> Ni <sub>9.75</sub> Al <sub>13</sub>	11.1	–	–	–	128.8	41.3	112.0	–	0.355	–	–	[664]
Hf <sub>46</sub> Nb <sub>2</sub> Cu <sub>29.25</sub> Ni <sub>9.75</sub> Al <sub>13</sub>	11.8	–	–	–	130.3	43.1	116.5	–	0.351	–	–	[664]
Hf <sub>49</sub> Ta <sub>2</sub> Cu <sub>27.75</sub> Ni <sub>9.25</sub> Al <sub>12</sub>	11.3	–	–	–	127.6	42.4	114.6	–	0.350	–	–	[664]
Mg <sub>65</sub> Cu <sub>25</sub> Tb <sub>10</sub>	3.979	4.220	2.220	1.90	44.7	19.6	51.3	12.90	0.309	2.28	272.9	[117]
Mg <sub>60</sub> Cu <sub>25</sub> Gd <sub>15</sub>	4.220	4.164	2.171	1.92	46.6	19.9	52.2	12.38	0.313	2.34	261.0	[117]
Mg <sub>65</sub> Cu <sub>25</sub> Gd <sub>10</sub>	3.794	4.319	2.254	1.92	45.1	19.3	50.6	13.34	0.31	2.34	273.8	[117]
(Mg <sub>65</sub> Cu <sub>25</sub> Gd <sub>10</sub> ) <sub>99</sub> Ti <sub>1</sub>	3.940	4.341	2.245	1.93	47.8	19.9	52.3	13.28	0.317	2.41	275.7	This work
(Mg <sub>65</sub> Cu <sub>25</sub> Gd <sub>10</sub> ) <sub>97</sub> Ti <sub>3</sub>	3.811	4.272	2.238	1.91	44.1	19.1	50.0	13.13	0.311	2.31	271.6	This work
(Mg <sub>65</sub> Cu <sub>25</sub> Gd <sub>10</sub> ) <sub>95</sub> Ti <sub>5</sub>	3.936	4.250	2.245	1.89	44.6	19.8	51.8	13.17	0.306	2.25	275.2	This work
(Mg <sub>65</sub> Cu <sub>25</sub> Gd <sub>10</sub> ) <sub>99</sub> Sn <sub>1</sub>	3.881	4.269	2.235	1.91	44.9	19.4	50.8	13.10	0.311	2.32	271.5	This work
(Mg <sub>65</sub> Cu <sub>25</sub> Gd <sub>10</sub> ) <sub>97</sub> Sn <sub>3</sub>	4.027	4.225	2.220	1.90	45.42	19.9	52.0	12.90	0.309	2.29	270.4	This work
Mg <sub>58</sub> Cu <sub>27</sub> Y <sub>10</sub> Zn <sub>5</sub>	3.558	4.536	2.447	1.85	44.8	21.3	55.2	15.50	0.295	2.10	298.3	[120]
Mg <sub>60</sub> Cu <sub>25</sub> Gd <sub>10</sub> Zn <sub>5</sub>	4.062	4.274	2.254	1.90	46.7	20.6	54.0	13.28	0.307	2.26	275.47	[120]
Mg <sub>55</sub> Cu <sub>25</sub> Ag <sub>10</sub> Gd <sub>10</sub>	4.919	4.156	2.189	1.90	53.5	23.6	61.7	12.53	0.308	2.27	273.7	[120]
Mg <sub>58.5</sub> Cu <sub>30.5</sub> Y <sub>11</sub>	3.547	4.649	2.400	1.94	49.4	20.4	53.9	15.19	0.318	2.42	292.5	[121]
Mg <sub>57</sub> Cu <sub>31</sub> Y <sub>6.6</sub> Nd <sub>5.4</sub>	3.809	4.465	2.333	1.91	48.3	20.7	54.4	14.28	0.312	2.42	283.6	[121]
Mg <sub>57</sub> Cu <sub>34</sub> Nd <sub>9</sub>	4.1	–	–	–	50.7	20.5	54.2	–	0.322	–	–	[674]
Mg <sub>64</sub> Ni <sub>21</sub> Nd <sub>15</sub>	3.7	–	–	–	44.8	17.9	47.4	–	0.324	–	–	[674]
Ca <sub>50</sub> Mg <sub>20</sub> Cu <sub>30</sub>	–	–	–	–	29.0	12.6	33.2	–	0.311	–	–	[152]
Ca <sub>48</sub> Mg <sub>27</sub> Cu <sub>25</sub>	2.400	3.810	2.240	1.70	18.8	12.2	29.8	–	0.236	1.56	–	[152]
Ca <sub>65</sub> Mg <sub>8.54</sub> Li <sub>9.96</sub> Zn <sub>16.5</sub>	1.956	4.050	2.139	1.89	20.2	9.0	23.4	11.95	0.307	2.25	220.7	This work
Ca <sub>65</sub> Mg <sub>8.31</sub> Li <sub>9.69</sub> Zn <sub>17</sub>	1.983	3.915	2.127	1.84	18.5	9.0	23.2	11.69	0.291	2.05	219.6	This work
Ca <sub>55</sub> Mg <sub>25</sub> Cu <sub>20</sub>	2.221	–	–	–	22.6	10.81	27.98	12.60	0.294	2.09	–	This work
(CaCu) <sub>75</sub> Mg <sub>25</sub>	3.149	–	–	–	31.1	14.40	37.4	11.87	0.299	2.16	–	This work
(CaCu) <sub>70</sub> Mg <sub>30</sub>	3.069	–	–	–	33.3	14.48	37.9	12.36	0.310	2.30	–	This work
Sr <sub>60</sub> Mg <sub>18</sub> Zn <sub>22</sub>	3.04	2.862	1.592	1.80	14.6	7.71	19.7	6.48	0.276	1.89	156	[173]
Sr <sub>60</sub> Li <sub>5</sub> Mg <sub>15</sub> Zn <sub>20</sub>	2.990	2.918	1.531	1.91	16.1	7.02	18.4	6.14	0.310	2.29	151	[173]

Table 1 (continued)

Glasses	$\rho$ (g/cm <sup>3</sup> )	$v_l$ (km/s)	$v_s$ (km/s)	$v_l/v_s$	$K$ (GPa)	$G$ (GPa)	$E$ (GPa)	$E/\rho$ (GPa cm <sup>3</sup> /g)	$\nu$	$K/G$	$\theta_D$ (K)	Refs.
Sr <sub>50</sub> Mg <sub>20</sub> Zn <sub>20</sub> Cu <sub>10</sub>	3.26	2.983	1.658	1.80	17.1	8.97	22.9	7.02	0.276	1.91	169	[173]
Sr <sub>60</sub> Mg <sub>20</sub> Zn <sub>15</sub> Cu <sub>5</sub>	3.04	2.905	1.598	1.86	15.3	7.76	19.9	6.46	0.283	1.97	157	[173]
Sr <sub>40</sub> Yb <sub>20</sub> Mg <sub>20</sub> Zn <sub>15</sub> Cu <sub>5</sub>	3.95	2.668	1.413	1.89	17.6	7.88	20.6	5.22	0.305	2.23	142	[173]
Sr <sub>20</sub> Ca <sub>20</sub> Yb <sub>20</sub> Mg <sub>20</sub> Zn <sub>20</sub>	3.56	2.872	1.580	1.82	17.5	8.89	22.8	6.40	0.283	1.97	158	This work
Zn <sub>40</sub> Mg <sub>11</sub> Ca <sub>31</sub> Yb <sub>18</sub>	4.30						28.8		0.259			This work
Zn <sub>20</sub> Ca <sub>20</sub> Sr <sub>20</sub> Yb <sub>20</sub> Li <sub>11</sub> Mg <sub>9</sub>	3.60				12.0	6.3	16.0	4.44	0.280	1.90	336.8	[122]
Sc <sub>36</sub> Al <sub>24</sub> Co <sub>20</sub> Y <sub>20</sub>	4.214	5.351	2.770	1.93	77.6	32.3	85.2	20.21	0.317	2.40	188.3	[123–128]
Ce <sub>60</sub> Al <sub>15</sub> Ni <sub>15</sub> Cu <sub>10</sub>	6.669	3.037	1.676	1.81	36.6	18.7	48.0	7.19	0.281	1.95	145.6	[123–128]
Ce <sub>65</sub> Al <sub>10</sub> Ni <sub>10</sub> Cu <sub>10</sub> Nb <sub>5</sub>	6.759	2.589	1.312	1.97	29.8	11.6	30.9	4.57	0.327	2.56	145.0	[123–128]
Ce <sub>68</sub> Al <sub>10</sub> Cu <sub>20</sub> Nb <sub>2</sub>	6.738	2.601	1.315	1.98	30.1	11.7	31.0	4.59	0.328	2.58	146.1	[123–128]
Ce <sub>68</sub> Al <sub>10</sub> Cu <sub>20</sub> Co <sub>2</sub>	6.752	2.612	1.322	1.97	30.3	11.8	31.3	4.64	0.328	2.57	147.4	[123–128]
Ce <sub>68</sub> Al <sub>10</sub> Cu <sub>20</sub> Ni <sub>2</sub>	6.753	2.659	1.332	2.00	31.8	12.0	31.9	4.73	0.332	2.65	149.4	[123–128]
Ce <sub>68</sub> Al <sub>10</sub> Cu <sub>20</sub> Fe <sub>2</sub>	6.740	2.668	1.352	1.97	31.6	12.3	32.8	4.85	0.327	2.56	144.0	[123–128]
Ce <sub>70</sub> Al <sub>10</sub> Ni <sub>10</sub> Cu <sub>10</sub>	6.670	2.521	1.315	1.92	27.0	11.5	30.3	4.54	0.313	2.34	142.2	[123–128]
Ce <sub>70</sub> Al <sub>10</sub> Cu <sub>20</sub>	6.699	2.568	1.296	1.98	29.2	11.3	29.9	4.46	0.329	2.59	166.7	[123–128]
Ce <sub>60</sub> Al <sub>20</sub> Cu <sub>20</sub>	6.431	2.857	1.490	1.92	33.5	14.3	37.5	5.83	0.313	2.34	158.9	This work
(Ce <sub>0.72</sub> Cu <sub>0.28</sub> ) <sub>90</sub> Al <sub>10</sub>	6.70	2.801	1.431	1.96	34.3	17.7	36.3	5.42	0.323	2.50	143.6	[123–128]
(M) <sub>67.5</sub> Al <sub>10</sub> Cu <sub>22.5</sub> M = La,Pr,Nd	6.564	2.743	1.322	2.07	34.1	11.5	30.9	4.71	0.349	2.97	144.1	[123–128]
Ce <sub>69.8</sub> Al <sub>10</sub> Cu <sub>20</sub> Co <sub>0.2</sub>	6.733	2.631	1.309	2.01	31.2	11.5	30.8	4.58	0.335	2.71	144.8	[123–128]
Ce <sub>69.5</sub> Al <sub>10</sub> Cu <sub>20</sub> Co <sub>0.5</sub>	6.744	2.634	1.314	2.01	31.3	11.6	31.1	4.61	0.334	2.68	145.1	[123–128]
Ce <sub>69</sub> Al <sub>10</sub> Cu <sub>20</sub> Co <sub>1</sub>	6.753	2.629	1.315	2.00	31.07	11.68	31.3	4.63	0.333	2.66	161.5	This work
(Ce <sub>0.72</sub> Cu <sub>0.28</sub> ) <sub>85</sub> Al <sub>10</sub> Fe <sub>5</sub>	6.747	2.836	1.463	1.97	35.7	13.9	36.9	5.47	0.328	2.57	165.6	This work
(Ce <sub>0.72</sub> Cu <sub>0.28</sub> ) <sub>75</sub> Al <sub>10</sub> Fe <sub>15</sub>	6.870	2.818	1.434	1.97	35.7	14.1	37.4	5.44	0.325	2.53	188.2	This work
Pr <sub>55</sub> Al <sub>25</sub> Co <sub>20</sub>	6.373	3.233	1.650	1.96	43.46	17.36	45.96	7.21	0.324	2.50	194.9	[155,156]
Nd <sub>60</sub> Al <sub>10</sub> Fe <sub>20</sub> Co <sub>10</sub>	7.052	3.242	1.714	1.89	46.53	20.70	54.09	7.67	0.306	2.25	159.0	[396]
Nd <sub>60</sub> Al <sub>10</sub> Ni <sub>10</sub> Cu <sub>20</sub>	6.689				42.8	13.5	36.5	5.46	0.358	3.17	188.9	[129]
Pr <sub>55</sub> Al <sub>12</sub> Fe <sub>30</sub> Cu <sub>3</sub>	6.615	3.150	1.659	1.90	41.38	18.20	47.61	7.20	0.31	2.27	160.2	[130,131]
Pr <sub>60</sub> Cu <sub>20</sub> Ni <sub>10</sub> Al <sub>10</sub>	6.900	3.030	1.406	2.15	45.18	13.64	37.17	5.39	0.36	3.31	165.4	[130,131]
Pr <sub>60</sub> Cu <sub>17</sub> Ni <sub>8</sub> Al <sub>15</sub>	6.548	3.105	1.470	2.11	44.26	14.15	38.36	5.86	0.356	3.13	179.95	[130,131]
Pr <sub>55</sub> Cu <sub>17</sub> Ni <sub>8</sub> Al <sub>20</sub>	6.426	3.152	1.585	2.22	42.32	16.14	42.97	6.69	0.331	2.62	186.6	[130,131]
Pr <sub>55</sub> Cu <sub>14.3</sub> Ni <sub>5.7</sub> Al <sub>25</sub>	6.355	3.346	1.647	2.16	48.16	17.24	46.20	7.27	0.340	2.79	162.2	[132]
Pr <sub>60</sub> Al <sub>10</sub> Ni <sub>10</sub> Cu <sub>18</sub> Fe <sub>2</sub>	6.834	3.008	1.429	2.10	43.22	13.96	37.80	5.53	0.354	3.10	163.0	[132]
Pr <sub>60</sub> Al <sub>10</sub> Ni <sub>10</sub> Cu <sub>16</sub> Fe <sub>4</sub>	6.833	2.996	1.436	2.09	42.56	14.09	38.06	5.57	0.351	3.02	164.4	[132]
Pr <sub>60</sub> Al <sub>10</sub> Ni <sub>10</sub> Cu <sub>14</sub> Fe <sub>6</sub>	6.804	3.025	1.449	2.09	43.21	14.29	38.61	5.67	0.351	3.02	177.8	[132]
Pr <sub>60</sub> Al <sub>10</sub> Ni <sub>10</sub> Cu <sub>12</sub> Fe <sub>8</sub>	6.814	3.206	1.568	1.93	47.71	16.75	44.98	6.60	0.343	2.85	180.0	[132]
Pr <sub>60</sub> Al <sub>10</sub> Ni <sub>10</sub> Cu <sub>10</sub> Fe <sub>10</sub>	6.807	3.196	1.589	2.01	46.63	17.18	45.91	6.74	0.336	2.71	183.7	[132]
Pr <sub>60</sub> Al <sub>10</sub> Ni <sub>10</sub> Cu <sub>5</sub> Fe <sub>15</sub>	6.788	3.191	1.623	1.97	45.29	17.88	47.40	6.98	0.326	2.53	187.5	[132]
Pr <sub>60</sub> Al <sub>10</sub> Ni <sub>10</sub> Cu <sub>2</sub> Fe <sub>18</sub>	6.800	3.149	1.658	1.90	42.51	18.69	48.89	7.19	0.308	2.27	189.7	[132]

(continued on next page)

Table 1 (continued)

Glasses	$\rho$ (g/cm <sup>3</sup> )	$v_l$ (km/s)	$v_s$ (km/s)	$v_l/v_s$	K (GPa)	G (GPa)	E (GPa)	$E/\rho$ (GPa cm <sup>3</sup> /g)	$\nu$	K/G	$\theta_D$ (K)	Refs.
Pr <sub>60</sub> Al <sub>10</sub> Ni <sub>10</sub> Fe <sub>20</sub>	6.800	3.143	1.679	1.87	41.63	19.16	49.84	7.33	0.300	2.17	221.4	[132–138]
Gd <sub>36</sub> Y <sub>20</sub> Al <sub>24</sub> Co <sub>20</sub>	6.402	3.720	1.917	1.94	57.22	23.53	62.07	9.69	0.319	2.43	217.9	[132–138]
Gd <sub>40</sub> Y <sub>16</sub> Al <sub>24</sub> Co <sub>20</sub>	6.656	3.664	1.880	1.95	57.99	23.52	62.17	9.34	0.321	2.47	208.1	[132–138]
Gd <sub>51</sub> Al <sub>24</sub> Co <sub>20</sub> Zr <sub>4</sub> Nb <sub>1</sub>	7.314	3.529	1.783	1.98	60.08	23.25	61.79	8.45	0.329	2.58	203.0	[132–138]
Tb <sub>55</sub> Al <sub>25</sub> Co <sub>20</sub>	7.488	3.281	1.747	1.87	50.2	22.8	59.5	7.95	0.302	2.20	222.0	[132–138]
Tb <sub>36</sub> Y <sub>20</sub> Al <sub>24</sub> Co <sub>20</sub>	6.630	3.734	1.902	1.96	60.46	23.98	63.55	9.58	0.325	2.52	213.3	[132–138]
Sm <sub>40</sub> Y <sub>15</sub> Al <sub>25</sub> Co <sub>20</sub>	6.276	3.645	1.853	1.97	54.65	21.55	57.14	9.10	0.326	2.54	214.8	[132–138]
Er <sub>55</sub> Al <sub>25</sub> Co <sub>20</sub>	8.157	3.445	1.822	1.89	60.70	27.08	70.72	8.67	0.306	2.24	229.0	[139]
Er <sub>36</sub> Y <sub>20</sub> Al <sub>24</sub> Co <sub>20</sub>	6.982	3.769	1.951	1.93	63.75	26.58	70.00	10.03	0.317	2.40	218.4	[139]
Er <sub>50</sub> Y <sub>6</sub> Al <sub>24</sub> Co <sub>20</sub>	7.831	3.592	1.856	1.93	65.07	26.98	71.10	9.08	0.318	2.41	226.5	[140–142]
Ho <sub>39</sub> Al <sub>25</sub> Co <sub>20</sub> Y <sub>16</sub>	7.024	3.745	1.931	1.94	63.59	26.19	69.09	9.84	0.319	2.43	226.5	[140–142]
Ho <sub>30</sub> Al <sub>24</sub> Co <sub>20</sub> Y <sub>26</sub>	6.494	3.874	1.996	1.94	62.96	25.87	68.27	10.51	0.319	2.43	233.2	[140–142]
Ho <sub>40</sub> Al <sub>22</sub> Co <sub>22</sub> Y <sub>16</sub>	7.112	3.644	1.885	1.93	60.74	25.27	66.58	9.36	0.317	2.40	220.5	[140–142]
Ho <sub>55</sub> Al <sub>25</sub> Co <sub>20</sub>	7.888	3.428	1.795	1.91	58.78	25.43	66.67	8.45	0.311	2.31	210.2	[140–142]
Dy <sub>55</sub> Al <sub>25</sub> Co <sub>20</sub>	7.560	3.325	1.764	1.88	52.22	23.53	61.36	8.12	0.304	2.22	204.3	[133–138]
Dy <sub>46</sub> Y <sub>10</sub> Al <sub>24</sub> Co <sub>18</sub> Fe <sub>2</sub>	7.211	3.552	1.839	1.93	58.46	24.39	64.23	8.91	0.317	2.40	214.1	[133–138]
La <sub>55</sub> Al <sub>25</sub> Co <sub>20</sub>	5.802	3.213	1.630	1.97	39.35	15.41	40.91	7.05	0.327	2.55	180.9	[133–138]
La <sub>60</sub> Al <sub>20</sub> Co <sub>20</sub>	6.267	3.056	1.521	2.01	39.17	14.51	38.74	6.18	0.335	2.70	170.2	[133–138]
La <sub>66</sub> Al <sub>14</sub> Cu <sub>10</sub> Ni <sub>10</sub>	6.038	2.958	1.492	1.98	34.91	13.44	35.72	5.92	0.33	2.60	160.9	This work
La <sub>55</sub> Al <sub>25</sub> Cu <sub>10</sub> Ni <sub>5</sub> Co <sub>5</sub>	5.907	3.320	1.621	2.05	44.41	15.52	41.71	7.06	0.343	2.86	181.1	This work
La <sub>57.6</sub> Al <sub>17.5</sub> (Cu,Ni) <sub>24.9</sub>	6.004	3.158	1.523	2.07	41.31	13.93	37.56	6.26	0.348	2.97	168.6	This work
La <sub>64</sub> Al <sub>14</sub> (Cu = Ni) <sub>22</sub>	6.105	3.022	1.430	2.11	39.11	12.48	33.85	5.54	0.356	3.13	156.2	This work
La <sub>68</sub> Al <sub>10</sub> Cu <sub>20</sub> Co <sub>2</sub>	6.210	2.971	1.391	2.14	38.77	12.02	32.68	5.26	0.360	3.23	150.5	This work
Tm <sub>39</sub> Y <sub>16</sub> Al <sub>25</sub> Co <sub>20</sub>	7.301	3.806	2.018	1.89	66.1	29.73	77.5	10.62	0.304	2.22	238.1	[118]
Tm <sub>55</sub> Al <sub>25</sub> Co <sub>20</sub>	8.274	3.457	1.827	1.89	62.0	25.6	72.2	7.49	0.306	2.42	216.0	[118]
Tm <sub>45</sub> Y <sub>10</sub> Al <sub>25</sub> Co <sub>20</sub>	7.662	3.589	1.888	1.90	62.3	27.3	71.5	9.33	0.309	2.28	223	[118]
Tm <sub>27.5</sub> Y <sub>27.5</sub> Al <sub>25</sub> Co <sub>20</sub>	6.476	3.856	1.996	1.93	61.9	25.8	68.0	10.5	0.317	2.40	234	[118]
Tm <sub>40</sub> Zr <sub>15</sub> Al <sub>25</sub> Co <sub>20</sub>	7.695	3.702	1.907	1.94	68.1	28.0	73.8	9.59	0.319	2.43	228	[118]
Tm <sub>40</sub> Y <sub>15</sub> Al <sub>25</sub> Co <sub>10</sub> Ni <sub>10</sub>	8.032	3.687	1.945	1.89	68.7	30.4	79.4	9.89	0.307	2.26	236	[118]
Lu <sub>39</sub> Y <sub>16</sub> Al <sub>25</sub> Co <sub>20</sub>	7.593	3.828	1.987	1.92	71.3	30.0	78.9	10.39	0.316	2.37	236	[119]
Lu <sub>55</sub> Al <sub>25</sub> Co <sub>20</sub>	8.694	3.556	1.875	1.90	69.2	30.6	80.0	9.21	0.307	2.26	223	[119]
Lu <sub>45</sub> Y <sub>10</sub> Al <sub>25</sub> Co <sub>20</sub>	8.014	3.747	1.970	1.90	70.2	31.1	79.1	9.87	0.309	2.26	231	[119]
Yb <sub>62.5</sub> Zn <sub>15</sub> Mg <sub>17.5</sub> Cu <sub>5</sub>	6.516	2.272	1.263	1.80	19.78	10.4	26.54	4.07	0.276	1.90	132.1	[63]
(Ce <sub>10</sub> La <sub>90</sub> ) <sub>68</sub> Al <sub>10</sub> Cu <sub>20</sub> Co <sub>2</sub>	6.303	2.836	1.332	2.13	35.77	11.18	30.38	4.82	0.358	3.20	144.8	[143]
(Ce <sub>20</sub> La <sub>80</sub> ) <sub>68</sub> Al <sub>10</sub> Cu <sub>20</sub> Co <sub>2</sub>	6.334	2.815	1.337	2.10	35.07	11.33	30.7	4.84	0.354	3.10	145.5	[143]
(Ce <sub>30</sub> La <sub>70</sub> ) <sub>68</sub> Al <sub>10</sub> Cu <sub>20</sub> Co <sub>2</sub>	6.418	2.812	1.345	2.09	35.3	11.61	31.4	4.89	0.352	3.04	146.9	[143]
(Ce <sub>40</sub> La <sub>60</sub> ) <sub>68</sub> Al <sub>10</sub> Cu <sub>20</sub> Co <sub>2</sub>	6.447	2.766	1.320	2.10	34.4	11.2	30.4	4.71	0.353	3.06	144.4	[143]
(Ce <sub>50</sub> La <sub>50</sub> ) <sub>68</sub> Al <sub>10</sub> Cu <sub>20</sub> Co <sub>2</sub>	6.492	2.769	1.337	2.07	34.3	11.6	31.3	4.82	0.348	2.96	146.5	[143]
(Ce <sub>70</sub> La <sub>30</sub> ) <sub>68</sub> Al <sub>10</sub> Cu <sub>20</sub> Co <sub>2</sub>	6.653	2.707	1.335	2.03	32.9	11.9	31.8	4.77	0.339	2.78	147.2	[143]

Table 1 (continued)

Glasses	$\rho$ (g/cm <sup>3</sup> )	$v_l$ (km/s)	$v_s$ (km/s)	$v_l/v_s$	$K$ (GPa)	$G$ (GPa)	$E$ (GPa)	$E/\rho$ (GPa cm <sup>3</sup> /g)	$\nu$	$K/G$	$\theta_D$ (K)	Refs.
(Ce <sub>80</sub> La <sub>20</sub> ) <sub>68</sub> Al <sub>10</sub> Cu <sub>20</sub> Co <sub>2</sub>	6.694	2.659	1.319	2.02	31.79	11.6	31.1	4.65	0.337	2.73	145.6	[143]
Fused quartz	2.203	5.954	3.767	1.58	36.4	31.26	72.9	33.10	0.166	1.16	496	[64,144]
Amorphous carbon	1.557	3.880	2.407	1.61	11.4	9.02	21.4	13.76	0.187	1.26	338	[64,144]
Microcrystal glass	2.556	6.492	3.667	1.77	61.9	34.36	87.0	3.40	0.266	1.80	–	[64,144]
Breakaway glass	1.053	2.353	1.164	2.02	3.9	1.4	3.82	3.63	0.338	2.75	–	[64,144]
Water-white glass	2.479	5.836	3.423	1.70	45.7	29.1	71.9	29.01	0.238	1.57	–	[64,144]
Window glass	2.421	5.593	3.385	1.65	38.8	27.7	67.2	27.8	0.211	1.40	–	[64,144]
Float glass	2.518	5.850	3.470	1.69	45.8	30.3	74.5	29.6	0.228	1.51	320	[64,144]
Ti-glass	2.196	5.745	3.615	1.59	34.2	28.7	67.3	30.6	0.172	1.19	330	[64,144]
Borosilicate glass	2.32	5.64	3.28	1.72	40.5	24.9	61.9	26.7	0.24	1.60	–	[64,144]
SiO <sub>2</sub> Glass	2.20	6.48	3.988	1.63	45.7	35.0	83.6	38.0	0.195	1.31	530.4	[145]
B <sub>2</sub> O <sub>3</sub> glass	1.792	3.6	1.933	1.86	14.2	6.7	17.4	9.7	0.297	2.14	279.1	[145]
Glassy sulfur (at 0 °C)	1.940				7.9	2.1	5.8	3.0	0.379	3.81		[160]
Se <sub>70</sub> Ge <sub>30</sub>	4.277	2.16	1.2	1.8	11.7	6.2	15.7	3.7	0.277	1.90	128	[146,159]
Amorphous Se	4.3	1.840	0.905	2.04	9.9	3.5	9.4	2.2	0.343	2.85	96.4	[160]

heat-treated during the ultrasound spectroscopy measurements, which is very useful for study the elastic moduli changes during phase transition and glass transition upon temperature in glasses [69].

The typical various glassy specimens including bulk metallic glasses, oxide glasses (Table 1 lists all available relevant data on typical metallic glasses, BMGs based on different elements with representative compositions and other typical non-metallic glasses) were cut to a length of  $\sim 10$  mm, and its ends were carefully polished flat and parallel, and normal to the longitudinal axis. The diameter of the specimen normally should larger than 3 mm for a pulse echo overlap method. The BMGs were prepared by water quenching or Cu mold cast methods and the details for the BMGs preparation can refer to as Ref. [54,58]. The amorphous nature as well as the homogeneity of these glasses was ascertained by X-ray diffraction (XRD), differential scanning calorimeter (DSC), transmission electron microscopy (TEM), and high resolution TEM. The onset glass transition temperature,  $T_g$ , the onset temperature of the first crystallization event  $T_x$  and liquidus temperature  $T_l$  of the BMGs were determined by DSC and differential thermal analysis (DTA). The mechanical and physical properties such as fracture yield strength  $\sigma$ , microhardness  $H_v$ , and fracture toughness  $K_{Ic}$  for various BMGs and other non-metallic glasses were directly taken from literature sources or experimentally measured. The details for the properties measurements one can refer to as Refs. [54,58].

### 3.1.3. The *in situ* measurement of ultrasonic wave velocities under high pressure

Fig. 2b illustrates high-pressure glass sample assembly for PEO ultrasonic measurement. The transducers were bonded to the specimen's end using dow resin for high pressure experiments. The dow resin is generally used bonding material for ultrasonic measurements under pressure due to its effects on the ultrasonic velocity and attenuation under pressure had been already determined, and can be ruled out. Another reason to use dow resin is that its bond quality can be kept unchanged under pressure up to 2 GPa [60,70]. This system is capable of resolution of the velocity changes to 1 part in  $10^5$  and particularly well suitable for determination of pressure-induced changes in ultrasonic velocities [70]. The ultrasonic velocities measurements under high pressure were also calibrated by the known materials of Fe, Bi, and oxide glasses [60,70]. The sample with bonded transducer was immersed in the oil in the high pressure experiment. The high pressure was performed using a piston–cylinder high-pressure apparatus, and electric insulation oil was used for the pressure transmitting media, for which hydrostaticity has already been determined. The high-pressure measurements were performed for several pressure load–unload cycles to examine the reproducibility and minimize error. Pressure induced changes in the sample dimensions were accounted for by using the Cook's methods [71].

### 3.1.4. The measurement of ultrasonic wave velocities upon temperature

To study the relaxation, aging, nucleation and growth, and crystallization of the metallic glassy materials, the glassy sample was isothermally annealed at various times and cooled down to room temperature for the density and acoustic measurements. The samples annealing was kept in a pure argon atmosphere for a prechosen temperature and period. After a certain time, the sample was removed from this container and allowed to cool to room temperature for acoustic measurements. The sample was returned for further annealing at a given temperature for an additional period of time, and taken out again to cool down to room temperature, and acoustic measurements were repeated.

The *in situ* acoustic velocities for the BMGs and other glasses (such as breakaway glass, amorphous sulfur) with low  $T_g$  were measured in a  $N_2$  flushed atmosphere using PEO method. Since the used high frequency of 10 MHz is  $10^{10}$  times the relaxation rate of  $\sim 1$  mHz for the glasses in the measuring temperature range, the measured elastic constants are taken as the instantaneous elastic moduli. Quartz transducers were bonded to the glass specimens using a mixed commercial resin. The insignificant temperature effects on the quartz transducers and the bonding resin in the measuring  $T$ -range were determined by using standard samples (such as pure Cu) and ruled out to minimize their influence on the ultrasonic velocities measurements. For BMGs (such as Ce-based BMGs), the density variation with increasing  $T$  was calibrated by the thermal expansion efficient of the alloy. Fig. 2c schematically illustrates the *in situ* low-temperature measurements of acoustic velocities using PEO method. The temperature of this method could reach liquid helium. The method can obtain temperature dependence of the elastic moduli for the glassy materials. RUS technique can be applied to *in situ* study

the temperature dependence of elastic moduli at high temperature [69], which is useful method to monitor the elastic moduli change during glass transition or crystallization.

### 3.2. The information provided from ultrasonic study

Comparing with other elastic moduli measuremental methods, the ultrasonic measurements can conveniently obtain the longitudinal and shear acoustic velocities in the glassy materials. Because of the homogeneous feature of the glassy materials, the elastic moduli as well as the Debye temperature and specific heat can be easily determined by using of Eqs. (3.3)–(3.9). The elastic constants of glassy solids are interesting from both a technological and a scientific viewpoint. From the technological perspective, knowledge of the elastic constants is necessary to design structural components. From the scientific perspective, the magnitude of the elastic constants provides information about the strength of the interatomic forces and nature of the glasses.

Since acoustic property is particularly sensitive to the microstructure as well as its change, the studies of the acoustic and elastic properties of glasses can provide important information about their structural and vibrational characteristics which are quite difficult for other methods to accessible [72–74]. With the development of various new glassy materials especially the development of the bulk metallic glasses, the study on the elastic properties using ultrasonic methods will yield a wealth of experimental elastic data previously inaccessible. The availability of various glass samples, with marked differences in mechanical and physical properties, thermodynamic and kinetic features and GFA, make it possible to establish some correlations among the properties and elastic constants, and to contrast the differences and find the commonness among different glasses [56]. The Elastic moduli data are basis for establish the elastic model for understand the glass and elastic criterion for exploring new metallic glasses with controllable properties. The *in situ* ultrasonic measurements performed under high pressure and at different temperatures can investigate the pressure and temperature dependence of the structural and elastic properties of the glasses, which provide critical information on the microstructural characteristics and static heterogeneity, relaxation and phase evolution as well as the elastic and thermal properties during the glass transition of the glasses.

The anharmonicity in a solid gives rise to attenuation via the so called Akkieser effect [75]. The strong interatomic interaction (measured by Grueneisen parameter  $\gamma$ ) in a solid results in the larger anharmonicity. So the attenuation is associated with bonding configuration of the glasses. The ultrasonic attenuation study could obtain information about the microstructural characteristics and the origin for the glass formation.

The computer simulation can be used to determine the elastic constants of glasses [76], and the calculated results can be confirmed by the ultrasonic study. The elastic moduli are of fundamental importance for various glasses which have in common the short-range order but lack of long-range order in the atomic structure [77]. The adiabatic elastic constants are the second derivatives of the internal energy with respect to strain, and their temperature dependence is related to anharmonic interactions. Therefore, the elastic constants provide insight into the nature of the bonding of the glasses. Furthermore, the elastic moduli do not solely depend on the interatomic bonding energy but also depend on the coordination, on the polymerization degree (reticulation), on the atomic packing density and on the molecular organization, including the possible formation of ring, chain or layer units. Therefore, beside the essential role of elastic properties for glassy materials selection in mechanical design [78], the macroscopical elastic moduli provide an important way to get insight into the microstructure of glass, glass transition, and glass formation [79–86]. The importance of elastic moduli of glasses is obvious because they are attractive for the prediction of glass physical and mechanical properties from changes in the composition [56,87].

## 4. Elastic moduli of metallic glasses

Metallic glass is one of the simplest glasses with atoms or atomic clusters as its structural units which interact through metallic bonding. And the structure of the metallic glasses is close to dense random packing of spheres [88–92]. Metallic glassy alloys are normally regarded as elastically isotro-

pic with a well-defined dispersion relation, so that when the ultrasonic waves propagate through the glassy sample, the metallic glass behaves as an elastic continuum at temperatures far below their  $T_g$  [54]. However, metallic supercooled liquids are normally quite unstable with respect to crystallization. For many years, the very high cooling rate (larger than  $10^5 \text{ K s}^{-1}$ ) necessary to obtain the metallic glasses limits their geometry to be very thin ribbons or wires or powders [54]. This makes the studies of the intrinsic nature of the glass and glass transition, and the measurements of many physical and mechanical properties very difficult and the understanding of the glassy metallic state has been impeded [88]. The acoustic and elastic properties as well as the vibrational features in the metallic glasses are poorly understood resulting from the inability to prepare bulky metallic glassy specimens. Through careful selection of composition according to some empirical rules (for example, the confusion rule), for some alloys the stability of their supercooled liquid state can be very high (for example, the Vit alloy system and Pd-based alloy, their stability even approach that of conventional oxide glasses) [54,91–93]. At such compositions, bulk metallic glasses with a larger 3-dimension size can be cast at low cooling rates ( $<10 \text{ K s}^{-1}$ ) by the conventional copper mold casting process at a low cooling rate [54]. The preparation of metallic glasses in bulk form makes the accurate study of their elastic properties using ultrasonic techniques possible. The availability of these new glassy alloys with exceptional stable supercooled liquid state (the stable supercooled liquid temperature region of Zr-based glass-forming alloy could as large as  $150 \text{ K}$  [54]) also offers a wide experimental temperature and time windows for measuring accurately the acoustic and elastic properties and investigating the dynamical relaxation characteristics in metallic undercooled liquids, which are intimately linked to a very basic property of the corresponding glasses. The studies of the acoustic, elastic and thermal properties of metallic glasses can also provide important information about the vibrational characteristics [94,95].

With the recent development of a variety of metallic glasses which readily form bulk glass, significant amounts of data on their elastic and acoustic properties have indeed been obtained [54–58,82,87,99–146]. It is noted that the obtained elastic data of these BMGs are in good agreement with that measured using different methods [96–98]. Table 1 lists the density, acoustic data, elastic constants and Debye temperature for various metallic glasses and typical oxide glasses and other non-metallic glasses at ambient conditions. As an example, the values of density  $\rho$ , longitudinal velocity  $v_l$ , and transverse velocity  $v_s$  of a typical as-prepared  $\text{Zr}_{41}\text{Ti}_{14}\text{Cu}_{12.5}\text{Ni}_{10}\text{Be}_{22.5}$  BMG (Vit1) at ambient condition are  $6.125 \text{ g/cm}^3$ ,  $5.17 \text{ km/s}$  and  $2.47 \text{ km/s}$ , respectively. The elastic moduli of  $E$ ,  $G$ ,  $K$ , and  $\nu$ , and Debye temperature,  $\theta_D$  of Vit1 calculated from the acoustic data are  $101.2 \text{ GPa}$ ,  $37.4 \text{ GPa}$ ,  $114.1 \text{ GPa}$ ,  $0.35$ , and  $326.8 \text{ K}$ , respectively [54]. The obtained elastic constants are in good agreement with that of the BMG measured using other methods such as mechanical deformation method [96]. The studied metallic glass systems cover almost all the known bulk metallic glasses available including Zr-, Pd-, Pt-, Au-, CuZr-, Cu-, Fe-, Mg-, Ni-, Ti-, Hf-, W-, Ta-, Ca-, Sr-, CaLi-, CaYb-, Zn-, Sc-, Y-, La-, Nd-, Ce-, Ho-, Sm-, Er-, Gd-, Tb-, Dy-, Tm-, Lu-, Yb- and Pr-based BMG materials and hundreds of compositions [54–58,82,87,99–171]. These BMGs involve in most all transition metals, rare earth metals, rare metals and alkaline-earth metals. Due to the excellent GFA, these bulk forming alloys have wide glass forming range. These BMGs also have markedly different physical, chemical and mechanical properties. In the following we will show that these BMGs do show markedly different characteristics in elastic properties compared to their crystalline counterparts and other non-metallic glasses, and the different metallic glasses have different features in elastic properties.

From Table 1, one can see that the ratio of  $v_l/v_s$  for various BMGs arranges from 1.80 to 2.50, and the average values is around 2.00, which is obviously larger than that of the non-metallic glasses such as oxide glasses ( $v_l/v_s = 1.6\text{--}2.0$ ). Fig. 4 exhibits the variations of the ultrasonic velocities in BMGs with different compositions. It shows that the ratio of ultrasonic shear wave velocity to longitudinal velocity is independent of the composition and varies linearly with the longitudinal velocity, and they fit a linear equation:

$$v_s = a v_l + b \quad (4.1)$$

where  $a$  and  $b$  are constants. The values of  $a$  and  $b$  are fitted to be  $a = 0.84$  and  $b = -1.844$  for Zr- and Cu-based BMGs;  $a = 0.555$  and  $b = -0.2$  for rare earth-, Fe-, Mg-based BMGs, and  $a = 0.556$  and  $b = -0.6$  for Pd- and Pt-based BMGs, respectively. This analysis indicates that, though acoustic velocities in BMGs are dependent on their components and composition, yet the variation of the velocities is

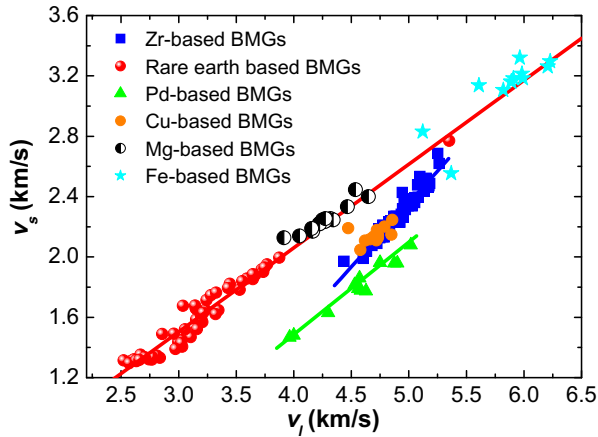


**Fig. 4.** Variations of shear velocity  $v_s$  and longitudinal velocity  $v_l$  of various BMGs. The solid lines correspond to the fit of  $v_s = av_l + b$ , where  $a$  and  $b$  are constant.

related to each other. Similar results have been found in various non-metallic glasses such as silicate glasses, tellurite glasses, borate glasses and phosphate glasses [146,172].

Elastic moduli give a global and often macroscopic view of a material stiffness, and reflect both the interatomic bonding energies and the connectivity. Since very different materials with all kinds of interatomic bonding can be formed in glasses, the glassy materials have markedly different elastic properties depending much on the glass composition and microstructural features. As shown in Table 1, the most frequently measured elastic modulus, the Young's modulus  $E$ , of various glassy materials extends from 5 to 365 GPa [56,172]. Fig. 5a shows a comparison of elastic moduli ( $K$  and  $E$ ) for various known BMGs. Fig. 5b shows the  $E$  at room temperature and glass transition temperature  $T_g$  of various glasses [172]. The figures show that the glasses with networks structure consisting primarily of chains, layers units or a highly cross-linked network resulting in a low packing density (such as  $\text{SiO}_2$  glasses, chalcogenides, low Si-content silicate glasses) correspond to low values of  $E$  and  $G$  [172]. The typical BMGs have Young's modulus between 25 GPa and 250 GPa, and shear modulus  $G$  between 9 GPa (CaLi-based BMGs) and 88 GPa (Fe-based BMGs). Up to now, the Ce-, Sr-, and CaLi-based BMGs have the lowest elastic moduli values among known BMGs (e.g. Young's modulus  $E \leq 30$  GPa) and are comparable to those of oxides fused quartz and close to those of polymers [123–128,173,174]; and Co-based glassy alloy exhibits ultrahigh fracture strength of 5.2 MPa, high Young's modulus of 268 GPa [175]. The maximum values of elastic moduli are observed in tungsten based metallic glasses ( $\text{W}_{46}\text{Ru}_{37}\text{B}_{17}$  metallic glass has an  $E$  of 365 GPa [176]). From Fig. 5b, one can see that the high performance bulk metallic glasses have higher  $E$  and  $K$  among the glassy materials. Fig. 6 shows the ratio of Young's modulus and density of various BMGs and the comparison with other materials. One can see that the BMGs have relative larger  $E/\rho$  compared with oxide glasses and close to the superhard materials.

For isotropic materials including glassy materials only two of these elastic constants are independent and other constants can be calculated using the relations given by the theory of elasticity. The best-known Young's modulus  $E$  is most commonly used in engineering design. Therefore, the efforts have been made to find the relationship between  $E$  with other elastic modulus such as  $G$ ,  $K$  and  $\nu$ . The relationships are useful and effective in the sense that they reduce the number of independent isotropic macroscopic elastic constants. Using Young's modulus which is the simplest elastic constant to measure experimentally, all other elastic constants can be evaluated easily. For polycrystalline metallic materials, a rough proportionality between  $E$  and  $G$  exists in the relation:  $E/G \approx 8/3 = 2.67$ ; and the  $E/G$  of porous ceramics is about 2.56. Fig. 7 plots experimental values of  $E$  vs.  $G$  of various BMGs (more than 200 data points listed in Table 1, and the Young's modulus ranges from 12 to 250 GPa) and some

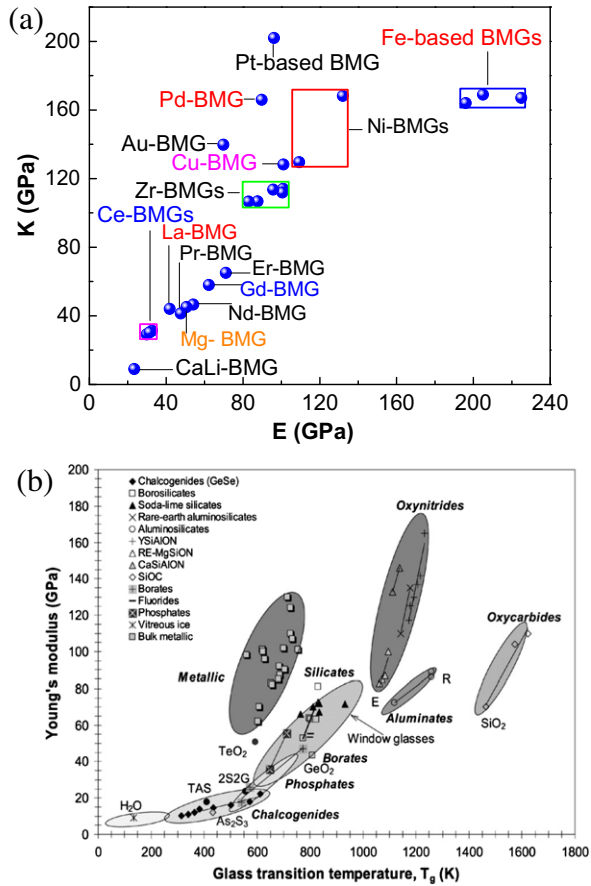
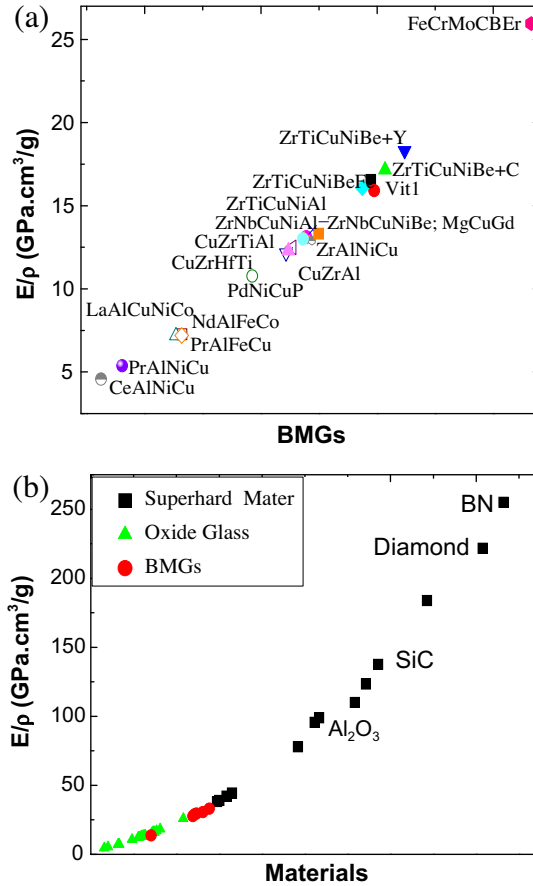


Fig. 5. (a) A comparison of  $K$  and  $E$  for various BMGs. (b) Young's modulus at room temperature and glass transition temperature  $T_g$  of various glasses [172].

typical non-metallic glasses (listed in Table 1). The feature of variation of  $G$  with  $E$  shown in Fig. 7 indicates that a similar relation like other isotropic materials also exists in metallic glasses. All the BMGs have different compositions and properties prepared by different methods, while all data points fall on a solid line of  $E/G = 0.261$  for these metallic glasses and other non-metallic glasses. The results indicate that for the metallic glasses the  $G$  (or  $E$ ) can be easily evaluated from  $E$  (or  $G$ ). It is known that the  $K$  is volume-nonpreserving and closely related to the volume [50].

For an isotropic solid, its elastic behavior is fully described by the longitudinal modulus ( $L = c_{11}$ ) and shear modulus ( $G = c_{44}$ ), and there is an isotropic relation between the components of the related elastic stiffness tensor [26]:  $c_{11} = c_{12} + 2c_{44}$ . The Cauchy identity  $c_{12} = c_{44}$  holds when in addition the atoms interact through a central potential. Then one obtains a reduction to only one independent elastic constant  $c_{11} = 3c_{44}$  (or  $L = 3G$ ). For an isotropic solid composed of molecular interacting with two-body central force, the Cauchy's identity is stated as:  $K = \frac{5}{3}G$ , which implies that  $L$  and  $K$  are equal to 0 when  $G = 0$ . For the Lennard-Jones interaction potential such as in metallic materials, this identity changes to [41]:  $K = a + (b - 1.333)G$ , where  $a$  and  $b$  are constants. This is known as the generalized Cauchy relation. The parameters  $a$  and  $b$  remain constant with changing temperature and pressure, but are sensitive to small changes in the potential. This relation was found to be valid for liquids and glasses [42]. To check the valid of the Cauchy identity in metallic glasses, we compared the values of  $K$  and  $G$  for various bulk metallic glasses listed in Table 1. Fig. 8a shows that relationship between  $K$  and  $G$  for



**Fig. 6.** (a) The ratio of Young's modulus and density of BMGs; and (b) the comparison of  $E/\rho$  between BMGs and oxide glasses and some super hard materials.

various metallic glasses. One can see that all the BMG deviate the Cauchy relation of  $K = 5/3G$ . The degree of deviation from the Cauchy relation is related to the anharmonicity of the material [42]. For some systems, such as rare earth and Mg-, Sr-, Ca-based BMGs, they is indeed in the form of  $K = a + bG$ , which fits the generalized Cauchy relation. While for different systems, the parameters  $a$  and  $b$  change and are sensitive to the minor difference in banding nature or small in changes of potential of the BMGs. This indicates that the elastic properties of various BMGs cannot described by only one elastic constant and the BMGs have differences in bonding nature and interaction potential. Actually, the systematically studies show that these BMGs indeed have markedly different properties and features. For example, the Fe-based BMGs with some metalloid elements of P, C, and B have covalent-like banding nature, and the Pd- and Pt-based BMGs have different structural features compared with that of the BMGs based on transition metals such as Zr and Cu, and then these BMG systems have much different parameters of  $a$  and  $b$ . The results indicate that the extent of deviation from the Cauchy relation related to the anharmonicity of the material reflects the bonding nature or atomic interaction potentials of BMGs.

The value of  $b$  is fitted for different metallic glass systems to show the degree of deviation from the Cauchy relation. The Pd- and Pt-based metallic glasses have largest  $b$  value of  $\sim 4.7$ , and Mg-, Ca-, and Sr-based BMGs have the smallest  $b$  value of  $\sim 2.10$ . Fig. 8b shows the relation of the degree of deviation from the Cauchy relation using the parameters of  $b$  and the Poisson's ratio of these metallic glasses.

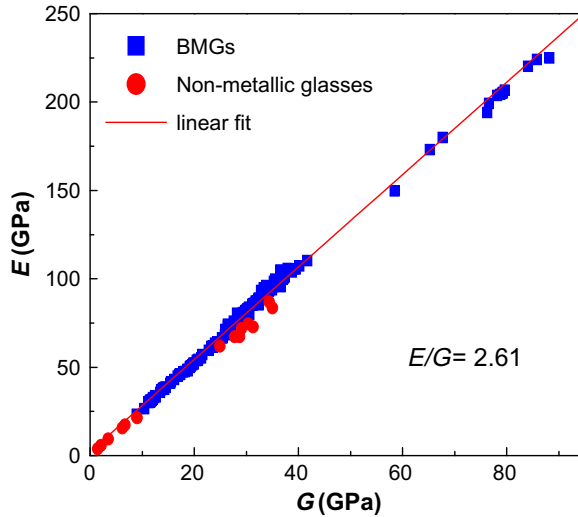
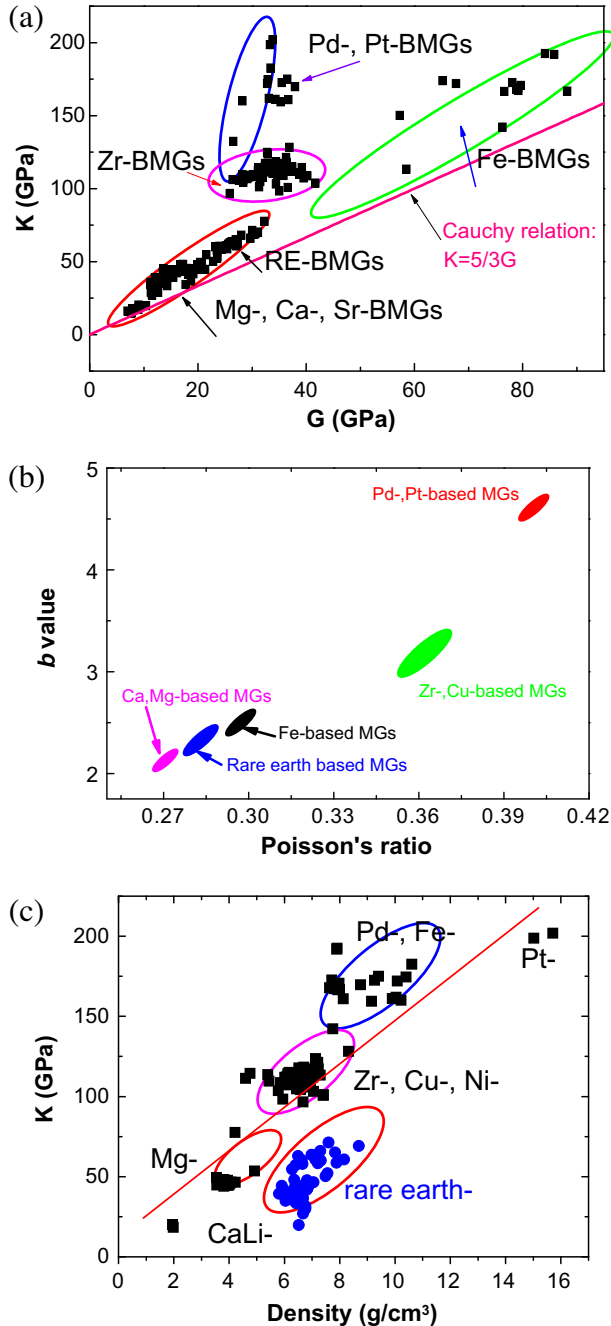


Fig. 7. Variation of the shear modulus  $G$  vs. Young's modulus  $E$  for various BMGs and other non-metallic glasses list in Table 1.

The degree of deviation from the Cauchy relation exhibits clearly correlation with the Poisson's ratio of these BMGs, and the BMG with larger Poisson's ratio  $\nu$  has larger  $b$  value or higher degree of deviation from the Cauchy relation. For example, the  $\nu$  value of Au-, Pt-, and Pd-based BMGs is larger than 0.40, and these BMGs show obviously larger deviation from the Cauchy relation of  $K = 5/3G$ ; the values of  $\nu$  of the Zr- and Cu-based BMGs are about 0.34–0.38, and the BMGs have intermediate degree of deviation; and the Fe- and rare earth based BMGs have low value of  $\nu$  and slight deviation from Cauchy relation. The degree of deviation from the Cauchy relation is related to the anharmonicity of a metallic glass, and the anharmonic effect can be determined by the Grüneisen parameter  $\gamma = -d \ln \omega / d \ln V$  (where  $\omega$  is frequency, and  $V$  is volume) [25], which relates microscopically to the vibrational frequencies of atoms and macroscopically relates to thermodynamic properties such as heat capacity and thermal expansion in a material.

Fig. 8c shows the relationship between density and  $K$  for various BMGs listed in Table 1. One can see a clear tendency that the metallic glass with higher density has high bulk modulus  $K$ .

Poisson's ratio  $\nu$ , which covers a wide interval of values for various non-metallic glasses and BMGs, reflects the information and insight on the microstructure, nature and physical and mechanical properties of glassy materials. Therefore, it deserves a special focus on this parameter of glasses. When a cylinder of a material such as rubber or polymer is compressed along its axis, common experience says that it should expand radically from this axis. This everyday phenomenon is embodied by the material's Poisson's ratio, which is defined as the relative transverse expansion divided by the relative compression in the direction of an applied force [177]. Fig. 9 illustrates the definition of the Poisson's ratio [178]. Poisson's ratio is the negative of the ratio of transverse contraction strain to longitudinal extension strain in the direction of elastic loading. Hence,  $\nu$  reflects the resistance of a material opposes to volume change with respect to shape change, and provides insight into chemical bonding of atoms regarding the variations of bond angle and bond length. Note that Poisson's ratio is strictly defined only for small strain linear elastic behavior. It is small for shear-resistant compressible materials such as cellular solid, and cork has a Poisson's ratio of close to 0, for which no lateral expansion occurs. For incompressible bodies such as rubber, it tends toward 0.5 for which the expansion acts to keep the total volume of the solid constant. Most materials have a positive Poisson's ratio of between 0 and 0.5. Metallic beryllium is of an ultralow value of  $\sim 1/20$ . Most familiar metallic materials such as steels have Poisson's ratio close to 0.3. Most materials with low Poisson's ratio, such as amorphous silica, exhibit highly strain dependent elastic properties. For the solids with  $\nu > 1/8$  (when  $G = K$ , then  $\nu = 1/8$ ), the resistance to bond-length change exceeds that to bond-angle change, and vice versa [179].



**Fig. 8.** (a) The relationship between  $K$  and  $G$  for various BMGs. (b) The relation between the Poisson's ratio and  $b$  value (the generalized Cauchy relation in the form of  $K = a + bG$ , and  $b$  represents the degree of the deviation from the Cauchy relation) of the MGs. (c) The relationship between density and  $K$  in various BMGs. The solid line is for guiding the eyes.

Phenomenologically, it is generally accepted that the materials with low Poisson's ratio are brittle [30,180]. For example, ductile face centered cubic metals have high Poisson's ratio, whereas brittle

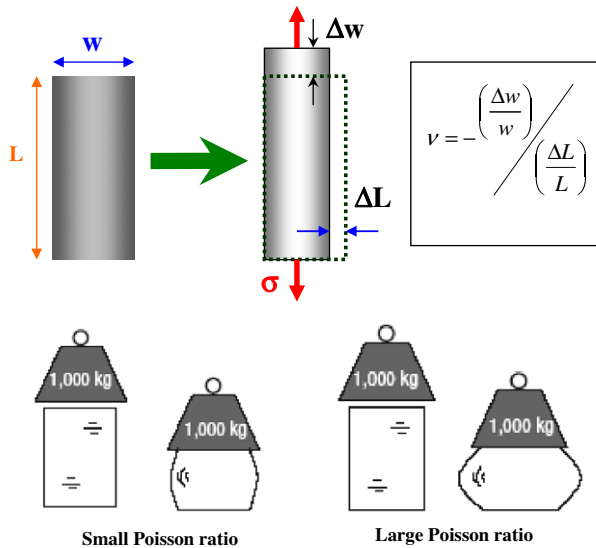


**Fig. 9.** The definition of Poisson's ratio and the illustration and contrast of the solid possesses a small or a large Poisson's ratio [178].

bcc metals have low values [30]. However, the above standpoint does not imply that the materials with high Poisson's ratio should be ductile, as evidenced by a large group of brittle ordered intermetallic compounds with high Poisson's ratio [179–181]. The first law of thermodynamics predicts the bound of  $\nu$  as  $-1 < \nu < 0.5$ . The theory of isotropic elasticity allows  $\nu$  values have negative values which indeed have been observed at low strain in some polymeric foams structures and anisotropic materials only [182–184].

Glassy materials exhibit a wide range of values of Poisson's ratio from 0.1 to 0.45. The value of  $\nu$  of the various BMGs is close to that of their base metals or determined by the base component [56]. The  $\nu$  and elastic constants of base elements for BMGs at room temperature are collected in Table 2. For example, the values of  $\nu$  of the Zr-based BMGs are about 0.34–0.37, which are similar to that of Zr (0.34) and Cu (0.37) (another main component in the BMG). For Au-, Pt-, and Pd-based BMGs, their  $\nu$  values are around 0.41, which are close to that of Pt, Au and Pd. The Fe (0.29) and rare earth elements have low values of  $\nu$  (see Table 2), and then the Fe- and rare earth based BMGs have low values of  $\nu$ . For a solid with covalent bonds such as silicate glass, its value of  $\nu$  is lower than 0.25, which is much smaller than that of BMGs. The markedly difference in the value of Poisson's ratio indicates the different microstructural characteristics between the metallic glasses and non-metallic glasses. In various glassy materials, Poisson's ratio, the atomic packing density and the glass network dimensionality appear to be strongly correlated [172]. The Poisson's ratio also correlates with other properties or natures of glassy materials [56,81,178]. For example, achieving high Poisson's ratio has even been considered as a means to improve toughness of BMGs [109].

The variation of Poisson's ratio with acoustic velocity is given by relation of 
$$\nu = \left(1 - 2\left(\frac{v_s}{v_l}\right)^2\right) / 2 \left(1 - \left(\frac{v_s}{v_l}\right)^2\right)$$
. Fig. 10 graphically shows the variation of  $\nu$  vs. acoustic velocity ratio for about 200 metallic glasses listed in Table 1. Some representative non-metallic glasses are also shown for comparison. It can clearly see from the figure that the  $\nu$  of the glass increases with the decrease of the velocity ratio, and the Poisson's ratio of the metallic glasses ranges from 0.42 to 0.27. Most BMGs have  $\nu$  values between 0.3 and 0.4. The Pt-, Au- and Pd-based BMGs have the largest  $\nu$  value of 0.42 [111,113], and the Fe-based and some rare earth based (such as Yb-based) BMGs have the lowest  $\nu$  value of 0.27. The  $\nu < 0.25$  is associated to nonmetallic glasses with a highly cross-linked network

**Table 2**

The density  $\rho$ , melting temperature,  $T_m$ , Poisson's ratio  $\nu$  and elastic constants (Young's modulus,  $E$ , shear modulus  $G$ , and bulk modulus  $K$ ) of base elements for BMGs at room temperature. Data from American Institute of Physics Handbook (Mc Graw-Hill, 1972 and Website: <http://www.webelements.com>).

Element	$E$ (GPa)	$G$ (GPa)	$K$ (GPa)	$\nu$	$H_v$ (GPa)	$\rho$ (g/cm <sup>3</sup> )	$T_m$ (K)
Zr	68	33	–	0.34	9.03	6.508	1125
Ti	116	44	110	0.32	9.70	4.54	1941
Cu	130	48	140	0.34	3.69	8.954	1356
Ni	200	76	180	0.31	6.38	8.902	1726
Nb	105	38	170	0.40	13.2	8.58	2741
Mg	45	17	45	0.29	–	1.738	922
Fe	211	82	170	0.29	6.08	7.874	1808
Al	70	26	76	0.35	1.67	2.70	933
Zn	108	43	70	0.25	4.2	7.14	692
Co	209	75	180	0.31	10.43	8.89	1768
Cr	279	115	160	0.21	10.06	7.19	2163
Be	287	132	130	0.03	16.7	1.847	1551
Hf	78	30	110	0.37	17.6	13.31	2500
Pd	121	44	180	0.39	4.61	12.02	1827
Au	78	27	220	0.44	2.5	19.32	1337
Pt	74	29	57	0.28	5.49	21.45	2045
Ca	20	7.4	17	0.31	1.75	1.54	1112
Sr		6.1		0.28		2.64	1050
W	411	161	310	0.28	34.3	19.25	3683
B			320		9.3	2.35	2373
C			33			3.514	3820
Si	47		100		6.5	2.33	1685
Sc	74	29	57	0.28	–	2.989	1814
Y	64	26	41	0.24	–	4.47	1783
La	37	14	28	0.28	4.91	6.15	1193
Ce	34	14	22	0.24	2.70	7.14	795
Pr	37	15	29	0.28	4.00	6.64	1208
Nd	41	16	32	0.28	3.43	6.80	1297
Sm	50	20	38	0.27	4.12	7.353	1345
Gd	55	22	38	0.26	5.70	7.90	1583
Tb	56	22	39	0.26	8.63	8.22	1629
Dy	61	25	41	0.25	5.40	8.55	1680
Ho	65	26	40	0.23	4.81	8.80	1734
Er	70	28	44	0.24	5.89	9.07	1770
Tm	74	31	45	0.21	5.2	9.321	1818
Yb	24	9.9	31	0.21	2.6	6.570	1097
Lu	69	27	48	0.26	11.6	9.842	1936

structure. For SiO<sub>2</sub> glass, its  $\nu$  is equal to 0.15. One way of classifying solids is to plot their bulk modulus against shear modulus. From the elastic relation of  $K/G = 2(\nu + 1)/3(1 - 2\nu)$ , one can see that if  $G = K$  then  $\nu = 1/8$ . In other words, when  $K < G$ , then  $\nu < 1/8$ ;  $K > \frac{8}{3}G$ , then  $\nu > 1/3$ . Fig. 11 summarizes the relation among bulk and shear moduli and Poisson's ratio of most BMGs, typical non-metallic glasses, some metals and alloys. It clearly shows that for most BMGs,  $K > \frac{8}{3}G$ ; only in some rare earth based BMGs,  $K$  is slightly smaller than  $\frac{8}{3}G$ . In non-metallic glasses,  $K$  is even smaller than  $G$ .

An important task for studying metallic glassy materials is in search of the application. The systematical data of elastic moduli for BMGs is useful for identifying the attributes of the new glassy materials and to show which are better than those of existing materials, and which attributes that are worse. A series of obtained BMGs with markedly different elastic moduli provides more material selections for applications. The search for glasses possessing high elastic moduli is a relatively old topic, and it is of paramount interest today with the need for new light and durable materials stiffer than those presently available. For instance, in order to increase both the rotating speed and the durability of computer hard disks, Al–Mg alloys are being more and more replaced by high Young's modulus glassy materials. An enhancement of the elastic moduli allows also for a decrease of the weight of windows (for a given glass density) and thus for a significant decrease of the energy consumption in the

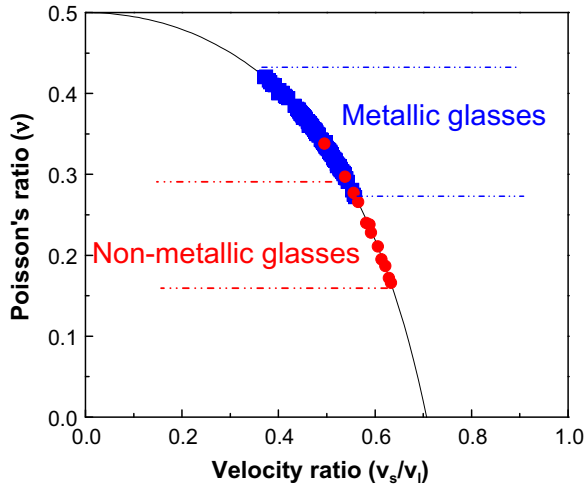


Fig. 10. Summary of Poisson's ratio of BMGs and other non-metallic glasses.

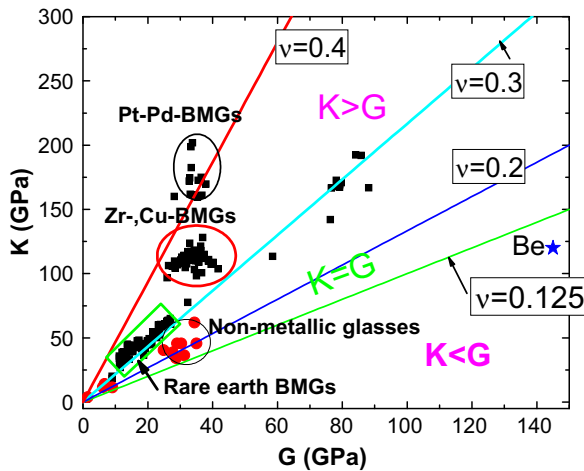
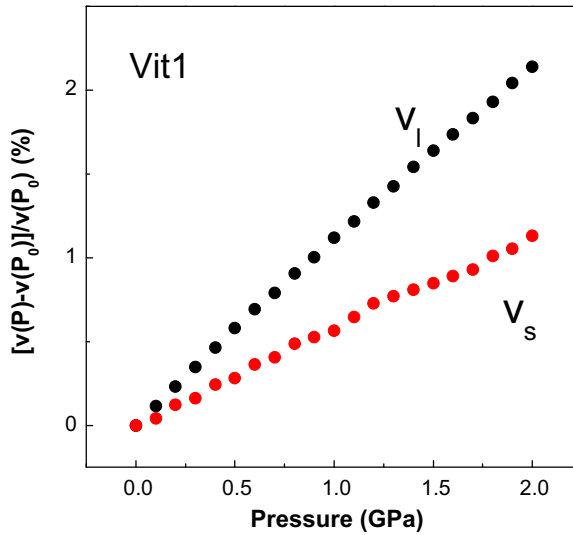


Fig. 11. Summary of relationship among shear and bulk moduli and Poisson's ratio of various metallic glasses and other non-metallic glasses.

transportation industry [172]. The elastic moduli and related correlations with physical and mechanical properties are useful for glassy materials design and searching new glassy materials with unique properties [56]. As shown later the metallic glasses exploration and design based on the elastic moduli are indeed effective.

### 5. Pressure dependence of elastic properties of metallic glasses

The pressure,  $P$ , dependence of the structural and physical properties of the bulk metallic glasses can be accurately investigated by the ultrasonic method benefiting from the bulky size of BMGs which are suitable for measurements of elastic wave propagation even under high pressure [166–171]. The pressure dependence of acoustic velocities can provide critical information on the microstructural,



**Fig. 12.** Variation of longitudinal and transverse velocities ( $v = v_l, v_s$ ) of the  $Zr_{41}Ti_{14}Cu_{12.5}Ni_{10}Be_{22.5}$  BMG upon pressure at room temperature [166]. The frequency of the ultrasonic wave is 20 MHz, and  $v$  is normalized by  $v_0(P)$  at ambient pressure  $P_0$ .

elastic and thermal characteristics, equation of state, anharmonicity and their evolution upon pressure of glassy materials. The pressure dependence of acoustic and elastic properties of BMGs has been systematically study recently [166–171].

To determine the pressure dependence of the elastic moduli exactly, it is necessary to know the dimensional or density changes of the samples with compression. Cook's method [71], by which the elastic constants and sample dimensions can be calculated simultaneously and self-consistently, was used for the density correction under high pressure. When using the Cook's method, a mesh of 0.1 GPa pressure intervals and a value for the quantity  $1 + \Delta$  of 0.001, which is the ratio of the adiabatic to the isothermal bulk moduli, were used.

As an example, Fig. 12 presents the pressure dependence of  $v_l$  and  $v_s$  of the typical  $Zr_{41}Ti_{14}Cu_{12.5}Ni_{10}Be_{22.5}$  BMG (Vit1). The data of  $v_l$  and  $v_s$  show no measurable hysteresis effects in the pressure loading and release cycle, and there are no observable permanent changes in acoustic velocities and density increase up to 2.0 GPa [166]. The pressure-dependent tend of acoustic velocities of the BMG is similar and independent of the carries ultrasonic frequency. These results indicate the perfectly elastic behavior in the BMG under homogeneous hydrostatic pressure up to 2.0 GPa. The  $P$ -dependence of acoustic velocities of a series of different BMGs with markedly different physical and mechanical properties has been systematically studied. The  $P$  dependence of  $v_l$  and  $v_s$  up to 2 GPa for these BMGs except Ce-based BMG (will be shown later) show similar change tendency, and increase smoothly with increasing  $P$  and show an approximately linear  $P$ -dependence [56,165–170]. For most BMGs, the change of  $v_l$  upon  $P$  is much larger than that of the  $v_s$ , and  $|dv_l/dP| \approx a|dv_s/dP|$ , and  $a = 2-5$ . The  $v_l$  is more sensitive to homogeneous hydrostatic pressure comparing to  $v_s$ , because the longitudinal wave is compressional wave and is sensitive to the change of volume, while  $v_s$  is a signature of transverse interaction and sensitive to the bonding between atoms [50]. The response of the acoustic and elastic properties of metallic glasses and non-metallic glasses has been compared. Fig. 13 shows pressure variations of  $v_l$  and  $v_s$  of the typical silicate Ti-glass ( $SiO_2 + 8.4 \text{ wt\% TiO}_2$ ) [144]. Similar to that of BMGs, the data of  $v_l$  and  $v_s$  show no measurable hysteresis effects in the pressure loading and release cycle. However, in contrast to BMGs, the  $v_l$  and  $v_s$  of the silicate glass decrease almost linearly with increasing  $P$ . This indicates that oxide glass with covalent atomic structure has different response to pressure compared to that of BMGs (with dense random packed metallic structure) [185], and the  $P$ -dependent acoustic properties reflect the structural difference of the different glasses.

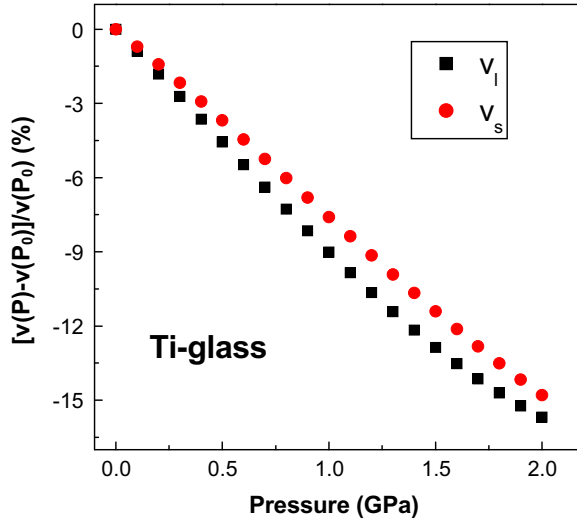


**Fig. 13.** Variation of longitudinal and transverse velocities ( $v = v_l, v_s$ ) of the Ti-glass upon pressure at room temperature. The  $v$  is normalized by  $v_0(P)$  at ambient pressure  $P_0$  [144].

The corresponding  $P$ -dependence of elastic constants  $Y$  ( $Y = E, G, K$ , and  $\nu$ ) calculated from the acoustic velocities for Vit1 and Ti-glass are shown in Figs. 14 and 15. For Vit1 or other BMGs,  $E, G, K$ , and  $\nu$  increase monotonically and linearly with increasing pressure. The  $dE/dP, dG/dP$  and  $dK/dP$  of BMGs are positive, i.e. the elastic constants exhibit a positive deviation with pressure from linearity, showing that the BMGs stiffen under hydrostatic pressure [165–170]. The application of pressure leads to a smaller change of  $\nu_s$  (1.2%) and  $G$  (4.1%) and does not induce acoustic mode softening for the BMGs, and no phase transition occurs under pressure up to 2 GPa. In the absence of phase changes, such

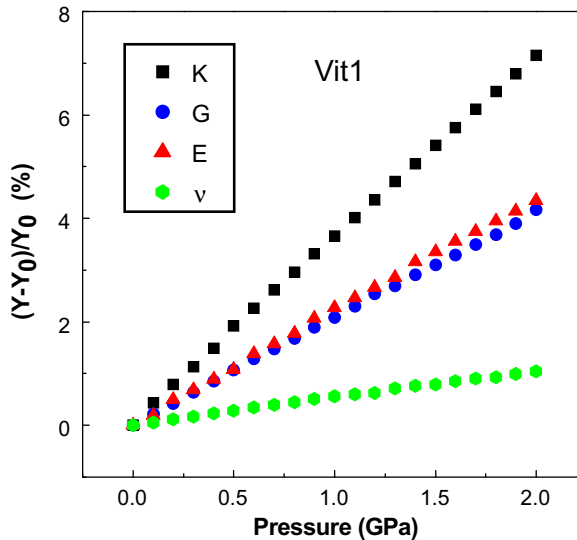


**Fig. 14.** The variation of elastic constants  $Y$  ( $Y = E, G, K$ , and  $\nu$ ) of the Vit1 with pressure,  $Y$  is normalized by  $\Delta Y/Y_0 = (Y - Y_0)/Y_0$ , where  $Y_0$  is a normal modulus at  $P_0$  [166].

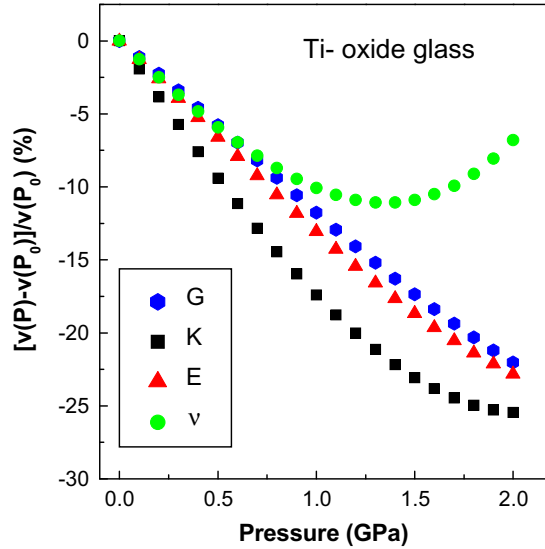


**Fig. 15.** The variation of elastic constants  $Y$  of the Ti-oxide glass ( $Y = E, G, K,$  and  $\nu$ ) with pressure,  $Y$  is normalized by  $\Delta Y/Y_0 = (Y - Y_0)/Y_0$ , where  $Y_0$  is a normal modulus at  $P_0$  [144].

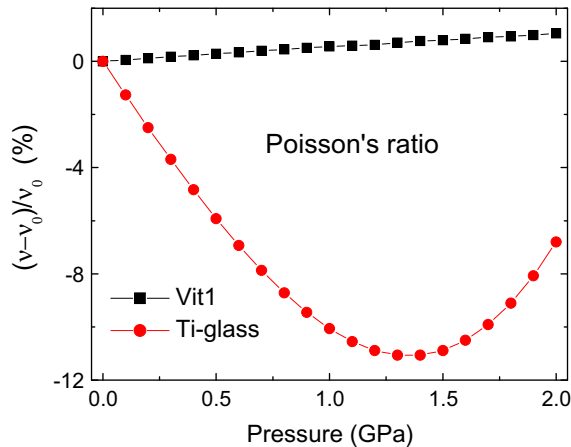


**Fig. 16.** A comparison of the Poisson's ratio changing upon pressure for metallic glass of Vit1 and Ti-oxide glass. The  $\nu_0$  is the Poisson's ratio at ambient pressure.

monotonic increase of elastic moduli with increasing pressure is attributed to the denser packing of the BMGs [165–170,186]. The pressure leads to relatively larger changes of  $\nu_l$  (2.2%) and  $K$  (7.1%) for Vit1, meaning that pressure has larger effect on the longitudinal acoustic phonons than the transverse phonons in the BMG. This is different from the case induced by crystallization in the BMGs, which normally causes obvious stiffening of transverse acoustic phonons [151]. While for Ti-oxide glass, on the contrary, the  $E, G, K,$  and  $\nu$  decrease monotonically and nonlinearly with increasing pressure and  $dE/dP < 0, dG/dP < 0$  and  $dK/dP < 0$ , indicating pressure induce acoustic mode softening (as shown in Fig. 15). This is markedly different from that of BMGs. At higher pressure, especially  $K$  and  $\nu$  show obviously nonlinear behavior upon  $P$ , and  $\nu$  increase upon pressure when  $P$  is larger than

**Table 3**

Relative pressure-induced variations of  $\rho$ ,  $v_l$ ,  $v_s$ ,  $G$ ,  $E$ ,  $K$  and  $\nu$  for various BMGs, oxide glasses and amorphous carbon. All the variations for these glasses are measured at 0.5 GPa except for fused quartz at 0.43GPa, water white glass and window glass at 0.42 GPa [56,165–170].

Glasses	$\Delta\rho/\rho_0$ (%)	$\Delta V_l/V_{l0}$ (%)	$\Delta V_s/V_{s0}$ (%)	$\Delta K/K_0$ (%)	$\Delta G/G_0$ (%)	$\Delta E/E_0$ (%)	$\Delta\nu/\nu_0$ (%)
Fused quartz (0.43 GPa)	1.24	-2.90	-2.49	-5.47	-3.75	-4.14	-2.87
Amorphous carbon	4.09	2.18	-3.09	20.30	-2.24	1.77	26.36
Water white glass (0.42 GPa)	0.92	-0.08	-0.64	1.71	-0.37	-0.01	1.87
Window glass (0.42 GPa)	1.08	-0.06	-1.19	3.14	-1.31	-0.48	4.81
SiO <sub>2</sub> + TiO <sub>2</sub> glass	1.58	4.57	-3.69	-9.41	-5.77	-6.59	-5.92
Zr <sub>41</sub> Ti <sub>14</sub> Cu <sub>12.5</sub> Ni <sub>10.2</sub> Be <sub>22.5</sub>	0.46	0.57	0.30	1.84	1.07	1.14	0.28
Zr <sub>48</sub> Nb <sub>8</sub> Cu <sub>12</sub> Fe <sub>8</sub> Be <sub>24</sub>	0.44	0.55	0.23	1.59	0.91	0.99	0.31
Zr <sub>50.6</sub> Ti <sub>15.2</sub> Cu <sub>18.8</sub> Ni <sub>14.1</sub> Al <sub>14.3</sub>	0.44	0.64	0.36	1.97	1.16	1.23	0.27
Pd <sub>39</sub> Ni <sub>10</sub> Cu <sub>30</sub> P <sub>21</sub>	0.32	0.75	0.51	1.98	1.34	1.38	0.15
Cu <sub>60</sub> Zr <sub>20</sub> Hf <sub>10</sub> Ti <sub>10</sub>	0.39	0.68	0.39	1.97	1.17	1.24	0.27
Ce <sub>70</sub> Al <sub>10</sub> Ni <sub>10</sub> Cu <sub>10</sub>	1.89	-2.66	-0.29	-6.08	1.30	0.34	-3.91
Nd <sub>60</sub> Al <sub>10</sub> Fe <sub>20</sub> Co <sub>10</sub>	1.07	0.97	0.39	3.72	1.86	2.10	1.00
Yb <sub>62.5</sub> Zn <sub>15</sub> Mg <sub>17.5</sub> Cu <sub>5</sub>	2.73	2.07	1.14	8.06	5.67	5.01	2.82

1.3 GPa. Poisson's ratio is small for shear-resistance compressible glasses. Fig. 16 shows a comparison of Poisson's ratio changes upon pressure for the typical BMG of Vit1 and non-metallic glasses (Ti-glass). The BMG with much larger  $\nu$  shows an increase of  $\nu$  with its densification under pressure, while the  $\nu$  of Ti-oxide glass further decreases upon compression. This is due to the strong resistance toward contraction in transverse direction. The high-pressure experiments indicate that volume conservative shear flow predominates in BMGs whereas the densification plays a dominant role in silicate glasses. The data for pressure induced change in acoustic velocities and elastic constants for typical BMGs and non-metallic glasses are listed in Table 3. Fig. 17 shows a comparison of the changes of volume, acoustic velocities,  $K$ ,  $E$ ,  $G$  under 0.5 GPa for various BMGs. One can see that the BMGs show markedly different changes in density, acoustic velocities,  $K$ ,  $E$ ,  $G$  under high pressure. The Yb-based BMG show much bigger change which denotes that the bonding between the atoms increase much more enormously.

Further physical insight into the acoustic vibrational behaviors of a metallic glass can be gained by investigating the anharmonicity of the long-wavelength acoustic modes. The Grüneisen parameters of a metallic glass can be determined using the following equations [50,112]:

$$\gamma_l = -\frac{K}{6C_{11}} \left[ 3 - \frac{3C_{12}}{K} - \frac{3dK}{dp} - 4 \frac{dG}{dp} \right] \quad (5.1)$$

$$\gamma_s = -\frac{1}{6G} \left[ 2G - 3K \frac{dG}{dp} - \frac{3}{2}K + \frac{3}{2}C_{12} \right] \quad (5.2)$$

and

$$\gamma_{av} = \frac{1}{3}(\gamma_l + 2\gamma_s) \quad (5.3)$$

where  $\gamma_l$ ,  $\gamma_s$  and  $\gamma_{av}$  are the longitudinal, shear and average Grüneisen parameters, respectively, and  $C_{11} = \rho v_l^2$ ,  $C_{12} = C_{11} - 2C_{44}$ ,  $G = C_{44} = \rho v_s^2$ . From the linear fit of the elastic constants vs. pressure, the  $\gamma_l$ ,  $\gamma_s$  and  $\gamma_{av}$  can be obtained using Eqs. (5.1)–(5.3). The Grüneisen constant  $\gamma$ , which is related to the derivative of  $K$ , can also be estimated by using the Slater's equation [187]:

$$\gamma = -\frac{1}{6} + \frac{1}{2} \left( \frac{\partial K}{\partial P} \right)_T \quad (5.4)$$

For example, the  $\gamma$  of Vit1 is 1.85 as estimated from Fig. 14. For Ti-glass,  $\gamma$  is -4.02 as estimated from Fig. 15. The available Grüneisen parameters of various BMGs, oxide glasses and amorphous carbon are collected in Table 4. The values of  $\gamma$  of BMGs are close to the reported values of fused silica (-2.9)

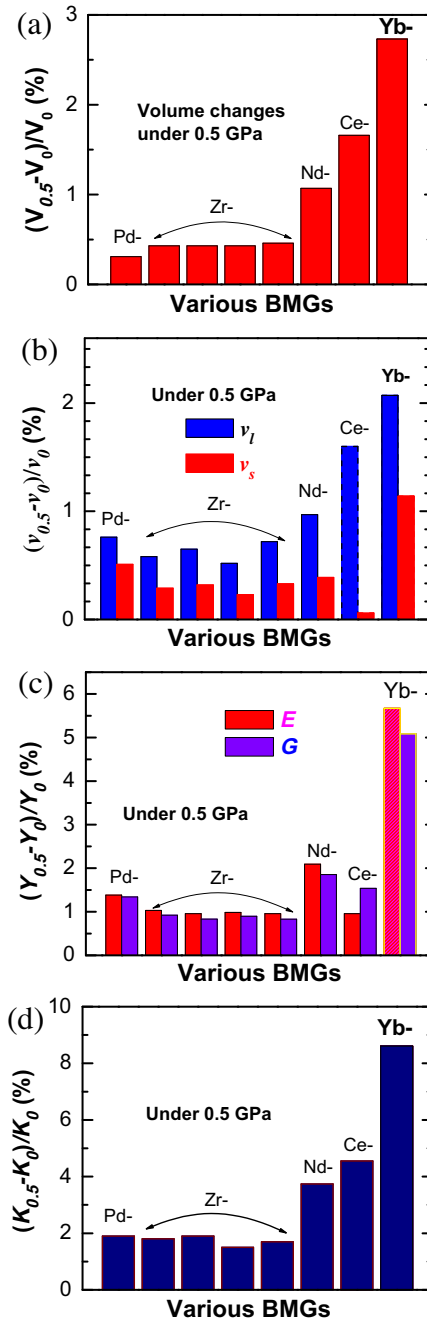


**Fig. 17.** (a) The comparison of relative volume changes under 0.5 GPa for various BMGs. (b) The comparison of the velocities changes under 0.5 GPa for various BMGs. (c) and (d) show the comparison of the changes of  $E$  and  $G$ , and  $K$  for various BMGs, respectively.

[188], etched soda glass (2.5) [188], iron (3.4) [189] and silicon (0.8 to  $-1.5$ ) [190]. This classifies the BMGs among the solids with larger anharmonicity [191].

**Table 4**

Pressure derivatives of longitudinal velocity  $v_l$  and transverse velocity  $v_t$  and Grüneisen parameters  $\gamma_l$ ,  $\gamma_s$  and  $\gamma_{av}$  and Slater's Grüneisen parameter  $\gamma_{sla}$  for different glasses including BMGs, silicate glasses and carbon glass [56,165–170].

Glasses	$dv_l/dP$ (km/s GPa)	$dv_t/dP$ (km/s GPa)	$dK/dP$	$\gamma_l$	$\gamma_s$	$\gamma_{av}$	$\gamma_{sla}$
Zr <sub>41</sub> Ti <sub>14</sub> Cu <sub>12.5</sub> Ni <sub>10</sub> Be <sub>22.5</sub> (vit1)	0.055	0.014	4.058	1.65	0.86	1.12	1.85
Zr <sub>48</sub> Nb <sub>8</sub> Cu <sub>12</sub> Fe <sub>8</sub> Be <sub>24</sub>	0.055	0.011	4.099	1.54	0.88	1.10	1.84
Zr <sub>50.6</sub> Ti <sub>5.2</sub> Cu <sub>18.8</sub> Ni <sub>14.1</sub> Al <sub>14.3</sub>	0.062	0.017	4.344	1.76	0.67	1.03	1.95
Pd <sub>39.1</sub> Ni <sub>10.1</sub> Cu <sub>29.9</sub> P <sub>20.9</sub>	0.072	0.021	6.277	2.75	2.02	2.26	2.97
Pd <sub>40</sub> Ni <sub>40</sub> P <sub>20</sub>	0.064	0.019		3.30	2.23	2.59	
Cu <sub>60</sub> Zr <sub>20</sub> Hf <sub>10</sub> Ti <sub>10</sub>	0.063	0.016	5.12	2.10	1.34	1.59	2.40
Crystallized Cu <sub>60</sub> Zr <sub>20</sub> Hf <sub>10</sub> Ti <sub>10</sub>	0.062	0.019	5.21	2.05	1.40	1.61	2.46
Nd <sub>60</sub> Al <sub>10</sub> Fe <sub>20</sub> Co <sub>10</sub>	0.97	0.389	3.42	1.37	0.64	0.89	
Yb <sub>62.5</sub> Zn <sub>15</sub> Mg <sub>17.5</sub> Cu <sub>5</sub>	0.095	0.029	3.16	1.17	0.70	0.86	
Ce <sub>70</sub> Al <sub>10</sub> Ni <sub>10</sub> Cu <sub>10</sub>	-0.133	-0.007	-3.33	-1.11	0.20	-0.23	-1.831
Amorphous Carbon	0.150	-0.153	4.404	0.76	-0.45	-0.04	2.03
Window glass	-0.009	-0.097	2.880	0.27	-0.78	-0.43	1.27
Water white glass	-0.015	-0.053	1.777	0.22	-0.38	-0.18	0.71
Float glass	0.008	-0.046	2.096	0.27	-0.42	-0.19	0.88
SiO <sub>2</sub> + TiO <sub>2</sub> glass	-0.462	-0.273	-7.713	-2.25	-2.10	-2.15	-2.42
Microcrystal glass	-0.390	-0.180		-3.17	-2.60	-2.79	-3.59
Fused quartz	-0.403	-0.218	-4.666	-2.10	-1.75	-1.86	-2.50

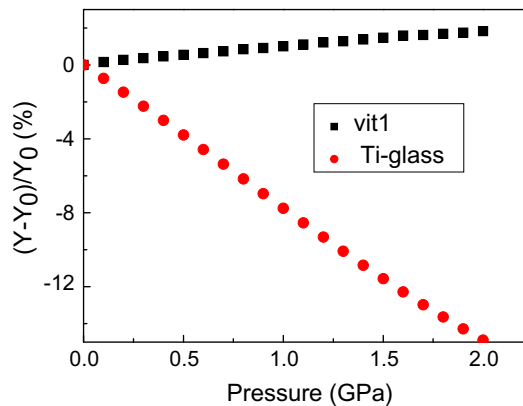


**Fig. 18.** The relative variation of the Debye temperature  $\theta_D$  of Vit1 and Ti-glass with pressure,  $Y$  is normalized by  $\Delta Y/Y_0 = (Y - Y_0)/Y_0$ , where  $Y_0$  is a normal Debye temperature at  $P_0$  [166].

The pressure variation of  $\theta_D$  reflects the rigidity of a solid change with pressure. Fig. 18 shows the comparison of pressure variation of  $\theta_D$  for Vit1 and Ti-glass in the range of 0–2 GPa. For the BMG,  $\theta_D$  increases monotonically and slightly with increasing pressure, implying an increase in rigidity of the BMG with pressure [51]. While for Ti-glass,  $\theta_D$  decreases monotonically and significantly with increasing pressure, meaning that the rigidity of the oxide glass is very sensitive to pressure and decreases rapidly with increasing pressure. In contrast to that of Vit1, large changes in  $v_s$  (–15.7%),  $v_l$  (–14.8%),  $K$  (–25.4%),  $G$  (–22.0%) and  $\theta_D$  (–15.1%) under 2 GPa occur in Ti-glass, indicating pressure induces obvious softening of acoustic phonons relative to Ti-glass at ambient condition. The softening is comparable to the softening in BMGs induced by crystallization [192,193].

The different responses to pressure of silicate and metallic glasses are due to completely different structural characteristic of BMGs (random close packing (*rcp*) atomic configuration) and oxide glasses [continuous-random networks (*crn*)]. Oxide glass is a covalent bonded glass with a significant spread in Si–O–Si bond angles. Under high pressure, the change of the bond angles between atoms in oxide glass leads to relatively larger volume change, which can sensitively induce changes in the electron

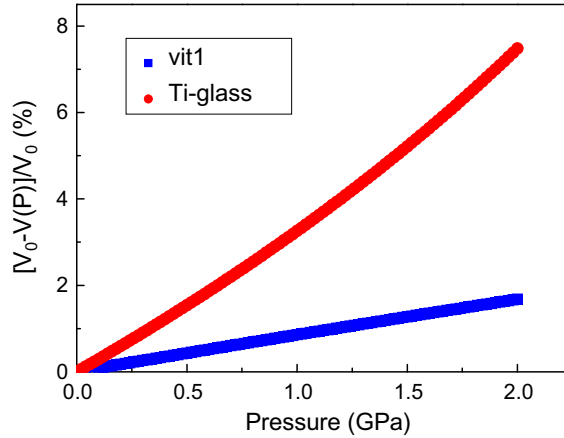


**Fig. 19.** A comparison of pressure and volume relation or equation of state (EOS) of the metallic glass (Vit1) and oxide glass (Ti-glass) [166].

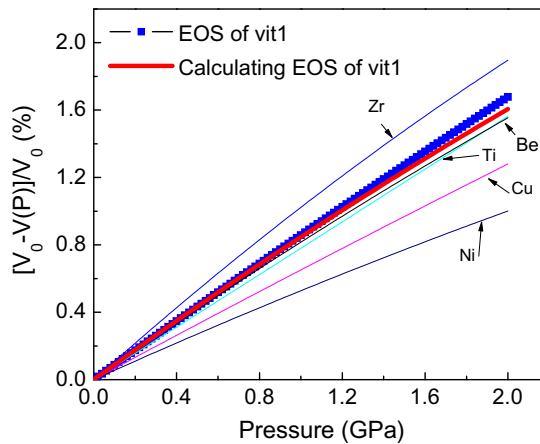


**Fig. 20.** The pressure and volume relation (EOS) of the Vit1 got from acoustic measurement. A comparison of the EOS of Vit1 and its crystalline components of Zr, Ti, Cu, Ni, and Be [166].

configuration, atomic interaction force and the relative flow between atoms. So, the oxide glasses have a large  $\theta_D$  and shear modulus change upon pressure.

The equation of state (EOS) of a solid plays an important role in condensed matter physics, geophysics and application. However, little information about EOS is obtained for metallic glasses, because the measurements of EOS have been impeded mainly by the inability to prepare bulk metallic glassy specimens. The large size and high thermal stability of the BMGs make the detailed and accurate studies of elastic properties in large pressure range become possible by ultrasonic method, and provide opportunity for studying the EOS of the metallic glasses. From the data of  $K_0$  and  $K'_0$  ( $K_0$  and  $K'_0$  are the bulk modulus and its pressure derivation at  $P_0$  respectively), the volume compression  $V_0/V(P)$  and their hydrostatic-pressure dependence or the EOS of BMGs in the non-phase transitional case, can be obtained using the Murnaghan form [195]:

$$P = \left(\frac{K_0}{K'_0}\right) \left[ \left(\frac{V_0}{V(P)}\right)^{K'_0} - 1 \right] \text{ GPa} \tag{5.5}$$

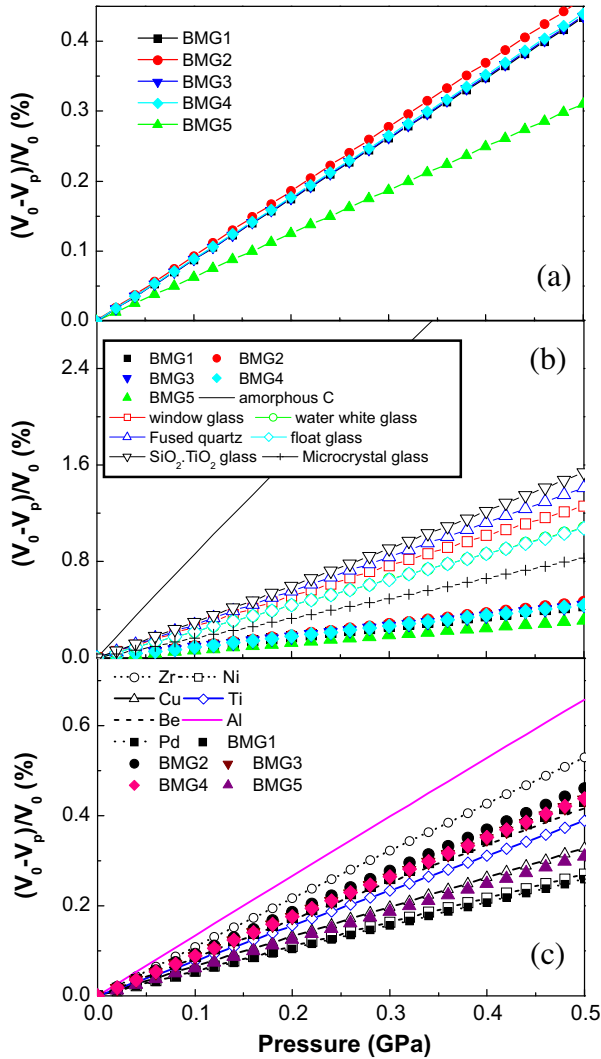


**Fig. 21.** The EOS of various BMGs. (a) EOS of  $Zr_{41}Ti_{14}Cu_{12.5}Ni_{10}Be_{22.5}$  (BMG1),  $Zr_{41}Ti_{14}Cu_{12.5}Ni_9Be_{22.5}C_1$  (BMG2),  $Zr_{48}Nb_8Cu_{12}Fe_8Be_{24}$  (BMG3),  $Zr_{50.6}Ti_{5.2}Cu_{18.8}Ni_{14.1}Al_{14.3}$  (BMG4) and  $Pd_{39}Ni_{10}Cu_{30}P_{21}$  (BMG5). (b) A comparison of the EOS of silicate glasses and BMGs (c). A comparison of EOS of crystalline components and BMGs [56,166].

As an example, the  $P - V$  relation of the Vit1 and Ti-glass are plotted in Fig. 19. The  $K_0$  and  $K'_0$  for the two glasses are obtained from Figs. 14 and 15. The equation of state of the Vit1 is obtained as:

$$p = 28.3 \left[ \left( \frac{V_0}{V(p)} \right)^{4.06} - 1 \right] \tag{5.6}$$

The obtained EOS of Vit1 is close to that obtained by direct  $P - V$  measurements at room temperature [99]. Comparing with oxide glass, the Zr-based BMG exhibits much smaller volume change upon pressure as shown in Fig. 19.

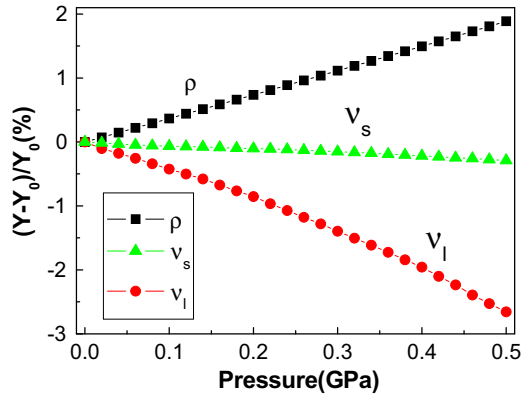


Fig. 22. Relative variations  $\Delta Y(P)/Y(P_0) = [Y(P) - Y(P_0)]/Y(P_0)$  of  $\rho$ ,  $v_l$ , and  $v_s$  with pressure up to 0.5 GPa for Ce-based BMG at room temperature.  $P_0$  is ambient pressure [169].

The volume compressibility or EOS of metallic elements can be expressed as [196]:

$$\Delta V/V_0 = -aP + bP^2 \quad (5.7)$$

where  $a$  and  $b$  are constants, volume compression,  $\Delta V = V(P) - V_0$ . The compression curves of the components of Zr, Ti, Cu, Ni and Be obtained by directly volume and pressure measurements [196] are plotted in Fig. 20 [166]. Remarkably, the compression curves of Vit1 is interposed among their metallic components, e.g. the compression curve of the  $Zr_{41}Ti_{14}Cu_{12.5}Ni_{10}Be_{22.5}$  BMG is interposed among that of Zr, Ti, Cu, Ni, and Be as shown in Fig. 20. The volume compression of the BMG can be calculated as a mean value of all volume compression curves of the Zr, Ti, Cu, Ni, and Be based on the atomic percents of these constituent elements. The calculating result is also shown in Fig. 20. It can be seen that the calculating EOS for Vit1 in terms of Eq. (5.7) agrees well with its EOS derived from experimental data using the Murnaghan form. The phenomenon has been found in a series of various BMGs as shown in Fig. 21 [166]. This indicates that the compression curve or EOS of BMGs correlates with that of their metallic components and exhibits a roughly weighted average EOS of these elements. Since the compressibility of a solid is determined by the nature of the interatomic potential and the atomic configurations, the total compression of BMGs can be ascribed to the contribution of individual metallic elements. Furthermore, the pressure dependence of volume change of the BMGs is similar with their crystallized state, and they all roughly exhibit an average result of their metallic components (see Table 4) [167]. The above results therefore imply that the short-range order structure of the BMG has close correlation with the atomic configurations in their metallic components. Since those metallic components are of cubic close-packed structures, it is very likely that the similar atomic close-packed configurations dominate the short-range structure of the BMGs. These highly packed structures have also been confirmed by density measurements. The relative density change of the BMGs between amorphous and fully crystallized states is less than 1.0% [56]. The found correlation is fit to almost all known BMGs and could be used to estimate the EOS of a novel BMG.

The only known exception so far is Ce-based BMGs. The Ce-based BMGs do show unusual features and properties such as extremely low glass transition temperature ( $\sim 85^\circ\text{C}$ ), low elastic moduli (close to those of non-metallic glasses such as some polymers), large supercooled liquid temperature region, high stability and a very large electron effective mass [123–128]. In near-boiling water, these materials can be repeatedly shaped, and can thus be regarded as metallic plastics. Their resistance to crystallization permits extended forming times above  $T_g$  and ensures adequate lifetime at room temperature. Such materials, combining polymer-like thermoplastic behavior with the distinctive properties of metallic glasses, have potential in structural and functional applications and can facilitate studies of the supercooled liquid state [125,127]. The Ce-based BMGs also show an unusual response of acoustic and elastic properties to hydrostatic pressure. Fig. 22 shows the pressure variations of  $\rho$ ,  $v_l$ , or  $v_s$  for a  $Ce_{70}Al_{10}Ni_{10}Cu_{10}$  BMG at room temperature up to 0.5 GPa. The  $\rho$  follows

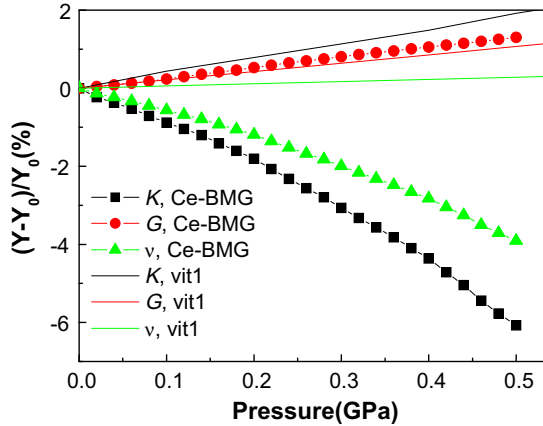


Fig. 23. A comparison of the relative variations of  $G$ ,  $K$ , and  $\nu$  with pressure up to 0.5 GPa for the Ce-based BMG and Vit 1 at room temperature [169].

a linear relation to pressure with an unusually high increase with increasing pressure (up to 1.9% at 0.5 GPa) [169]. The value is much higher than that of other BMGs and similar to or even larger than that of the non-metallic glasses such as oxides glasses as shown in Table 3. The relative change of acoustic velocities as a function of pressure is negative i.e.  $dv_l/dP < 0$ ,  $dv_s/dP < 0$ . This is markedly different from other BMGs but rather similar to nonmetallic glasses. As shown in Table 3, except for the Ce-based BMG having negative  $dv_l/dp$  and  $dv_s/dp$ , all other BMGs have a positive pressure dependence of acoustic velocities. Meanwhile, the pressure-induced decrease of  $\nu_l$  of Ce-based BMG is about 20 times larger than that of  $\nu_s$ :  $|dv_l/dp| \approx 20|dv_s/dp|$ , while for other BMGs,  $|dv_l/dp| \approx 2 \sim 5|dv_s/dp|$ . Such a large difference between  $|dv_l/dp|$  and  $|dv_s/dp|$  even has not been observed in oxide glasses. This indicates that the longitudinal phonon mode is much softer than the shear mode in the Ce-based BMG under pressure, which is similar to that of some non-metallic glasses [54]. This is unusual for BMG with metallic bonding structure. Fig. 23 presents the pressure dependence of the  $G$ ,  $K$  and  $\nu$  for the Ce-based BMG. The  $G$  has a comparably small increase with pressure while  $K$  and  $\nu$  exhibit the largest decreases up to  $-6.1\%$  and  $-3.9\%$  at 0.5 GPa, respectively. According to the relation  $G = \rho v_s^2$ , the increased  $G$  comes in large part from the large increase of  $\rho$  under pressure because  $dv_s/dp < 0$ . The Poisson ratio  $\nu$ , as a density independent parameter, directly reflects the relative change of  $\nu_l/\nu_s$ , so, it is very sensitive to microstructure. The large variation of  $\nu$  under pressure suggests a pressure-induced structural change in a material. This phenomenon has not been observed in Zr-, Cu-, and Pd-based BMGs [54,110,144,166–171], whose Poisson's ratio remains constant or shows small variations under pressure as listed in Table 3. Apparently, the Ce-based BMG exhibits much larger and different variations of  $\rho$ ,  $\nu_l$ ,  $K$  and  $\nu$  compared to those of Vit1, strongly indicating that the Ce-based BMG has a unique structure that is quite different from those of other BMGs [169]. Actually, an apparent amorphous to amorphous phase transition indeed has been reported in Ce-based metallic glasses [197–200].

The Grueneisen constants  $\gamma_l$ ,  $\gamma_s$  and  $\gamma_{av}$  for the Ce-based BMG are  $-1.10$ ,  $0.20$  and  $-0.23$ , respectively. The BMG has large negative  $\gamma_l$  value but comparably small positive  $\gamma_s$  and thus has negative  $\gamma_{av}$ . The large negative  $\gamma_l$  of the Ce-BMG is comparable to that of silicate glasses [201]. In other words, the softening vibrational behaviors in the long-wavelength limit of the Ce-based BMG under high pressure are mainly controlled by the longitudinal acoustic mode. The opposite signs of  $\gamma_l$  and  $\gamma_s$  in the Ce-BMG are similar to that of carbon glass [202], which has a special mixed structure: the C–C linkage is a mixture of covalent and metallic bonds, while the linkage between layers is van der Waals bonding. Previous structural analyses have demonstrated the covalently bonded short-range ordering structures in Al–Ni–Ce melt-spin glasses [203], and the covalent like short-range ordering is the “rigid” structural units such as tetrahedra in oxide glasses and icosahedral cluster in some BMGs. The

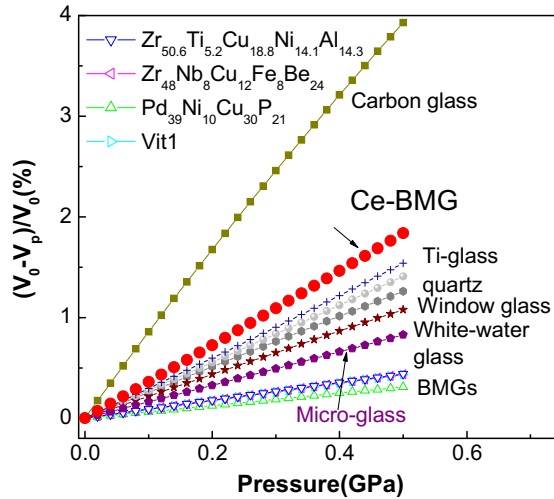


Fig. 24. The comparison of EOS of  $Ce_{70}Al_{10}Ni_{10}Cu_{10}$  BMGs, other BMGs, silicate glasses and amorphous carbon [169].

glass with a structure composed of the weakly linked “rigid” structural units, and the soft modes are low energy deformation of these “rigid” structural units [54,204]. Thus, the normal local structure similar to that of other BMGs and covalent bonding structures similar to those of oxide glasses may coexist in the Ce-based BMGs, and the intrinsic glassy structure containing short-range covalent like bonds causes the anomalous acoustic behaviors under pressure [169]. The EOS of the Ce-based BMG is presented in Fig. 24. The compressibility of the Ce-based BMG is also similar to that of silicate glasses but much higher than that of the other BMGs. The elastic properties study confirms that the Ce-based BMG contains short-range covalent like bonds similar to those of silicate glasses [169].

The elasticity investigations under high pressure in non-metallic glasses also reveal interesting structural changes regarding either the coordination number or the atomic packing density [172]. Kurkjian et al. [205] predicted that the tetrahedral glasses such as  $SiO_2$ ,  $BeF_2$ , and  $GeO_2$  all exhibit a negative pressure dependence of their shear moduli and found a direct correlation with Poisson’s ratio: the smaller the  $\nu$ , the more negative the pressure dependence becomes. It is found experimentally that for silica, the elastic moduli first decrease with pressure up to 2.5 GPa. At higher pressure the elastic moduli increase as is the case for most materials [206]. In silica and silicate glasses, and in low Poisson’s ratio glasses in general, high pressure induces permanent densification. Above 20 GPa, the density of  $\alpha$ - $SiO_2$  approaches the one of quartz. This results in a gradual increase of  $\nu$  with pressure, from 0.15 to 0.3 above 20 GPa. In the case of glassy water,  $K$  increases but  $G$  decreases with increasing pressure. Rouxel et al. [207] performed pressure experiments up to 25 GPa at 293 K on silica, soda-lime-silica, chalcogenide, and bulk metallic glasses. Their results show that markedly different sensitivity in elastic moduli of these glasses from very different chemical systems to high pressure, and this is linked to the different atomic structure of these glasses. The elastic properties investigation under high-pressure indeed can provide insight on the information of microstructural characteristics and bonding nature of the glasses.

## 6. Temperature dependence of elastic properties of metallic glasses

Elastic constants and their temperature behaviors provide information about atomic configurations, excitations in solids including the anharmonicity of the lattice vibrations [208,209], the density of electron states at the Fermi level and the shape of the Fermi surface [210], and the activation barriers for thermally activated relaxations [211]. Ultrasonic may be the only method which enables

the measurements of high-frequency elastic and loss moduli resulting from atomic motions underlying relaxation processes, and the elastic moduli data cannot be obtained by extrapolation of low-frequency mechanical data because of the invalidity of the implicit assumptions [212]. The ultrasonic method provides sensitive tool for locating phase transitions induced by temperature, determining phase diagrams, and studying the phase-transition order. The metallic glasses are thermodynamic and kinetic metastable, and their mechanical and physical properties are very sensitive the temperature. The temperature dependence of elastic properties of metallic glasses can provide important information on various transitions such as the temperature induced relaxation, structural change, crystalline phase nucleation and growth, crystallization, glass transition, and mechanical and physical properties changes in metallic glasses. We have systematically studied the acoustic and elastic properties changes of metallic glasses upon temperatures both in *in situ* and *ex situ* modes in wide temperature range from liquid nitrogen temperature to several hundreds Centigrade.

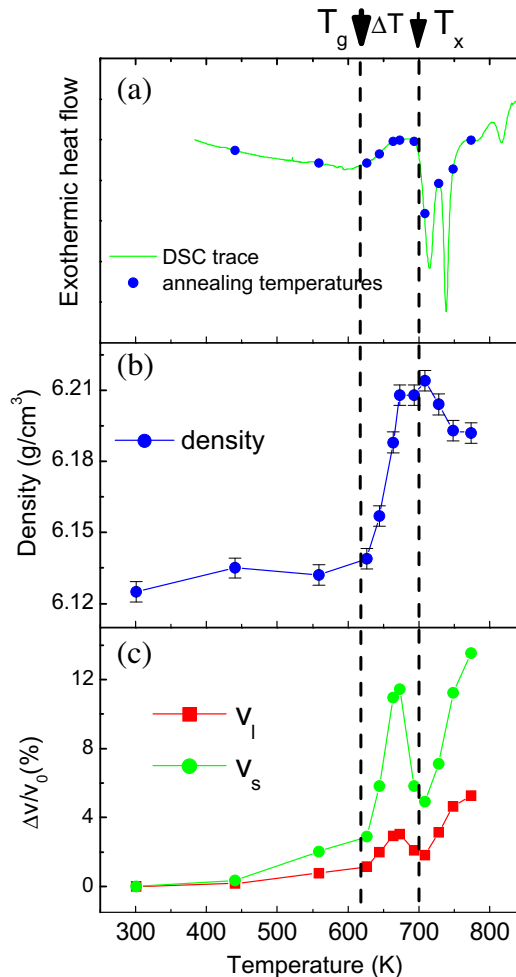


**Fig. 25.** (a) DSC trace of Vit1. The points are chosen annealing temperatures for density, and acoustic velocities measurements. (b) The variation of density with  $T$ . (c) The relative longitudinal and transverse velocities change with  $T$ , ( $v = v_l, v_s$ ),  $\Delta v/v_0 = (v - v_0)/v_0$ , where  $v_0$  is velocity for as-prepared BMG [192].

### 6.1. The elastic property of BMGs upon annealing temperatures

The BMGs exhibits obvious glass transition and wide supercooled liquid region and provide a system to study the glass transition, relaxation, and crystallization, and to accurately measure the structural and physical properties concomitant with these transitions [54]. The Vit1 (its  $T_g$ , the onset temperature of the first crystallization  $T_x$ , are 623 K and 698 K, respectively) is an ideal model system for study of glass transition and crystallization. The Vit1 was annealed at each temperature for 0.5 h, and then was cooled to room temperature (RT) for ultrasonic measurements [192]. Below 673 K, no obvious crystallization happens. When annealed near calorimetric  $T_x$ , nanocrystalline phases precipitate in the glassy matrix. Above 693 K, the BMG is completely crystallized [192]. Fig. 25a–c shows the temperature dependence (from RT to 773 K) of  $\rho$ ,  $v_l$ , and  $v_s$ , which can sensitively reflect the microstructural change during glass transition and crystallization of Vit1 [192]. The  $\rho$  increases slightly below calorimetric  $T_g$ , and significantly increases near  $T_g$  and reaches a maximum in the supercooled liquid region, followed by a slightly decrease below  $T_x$ . After fully crystallization, the  $\rho$  keeps almost unchanged. The relative change of  $\rho$  in the supercooled state and fully crystallized state are 1.3% and 1.1%, respectively. The marked density change indicates an amount of vacancy-like defects or free volume is quenched in the BMG even Vit1 was formed at a low cooling rate of 1 K/s, and large volume change accompanies the glass transition. The volume change in Vit1 has also been observed by positron annihilation studies [213] and volume–pressure relation measurements [99]. The acoustic velocities have a sudden increase near calorimetric  $T_g$ , and forms a peak in the supercooled liquid region [see Fig. 25b]. They reach a minimum near  $T_x$  and increase again with increasing temperature. The  $v_s$  has much larger relative change during the glass transition and in the supercooled liquid region. The drastic microstructural change during the glass transition process results in the variation of the acoustic parameters. The relative variations of the elastic constant  $E$ ,  $G$ ,  $K$ ,  $\nu$  and  $\theta_D$  upon temperature for Vit1 are shown in Fig. 26. The  $E$ ,  $G$  and  $\theta_D$  show a sudden increase near  $T_g$  indicating the stiffening at the onset of glass transition and reach maximum in the supercooled liquid region, the  $\nu$  also show a drastic change near  $T_g$  but reach a minimum in the supercooled liquid region, while the  $K$  does not show the similar change trends. The microhardness  $H_v$  also shows a drastically increase near  $T_g$  confirms the stiffening and a subsequent monotonic increase [192]. Similar phenomenon has also been found in Pd-based BMG, ZrTiCuNiAl and ZrNbCuNiAl BMGs. Fig. 27 exhibits the relative longitudinal and transverse velocities,  $E$ ,  $G$ ,  $K$ , and  $\nu$  change with temperature for as-prepared Zr<sub>53</sub>Ti<sub>5</sub>Cu<sub>20</sub>Ni<sub>12</sub>Al<sub>10</sub>

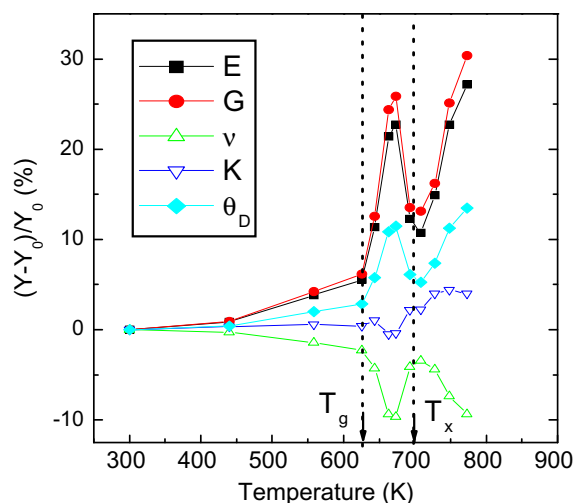


**Fig. 26.** The relative changes  $\Delta Y/Y_0 = (Y - Y_0)/Y_0$  of variation of  $E$ ,  $G$ ,  $K$ ,  $\nu$  and  $\theta_D$  ( $Y$  stands for  $E$ ,  $G$ ,  $K$ ,  $\nu$  and  $\theta_D$ ) of Vit1 with temperatures [192].

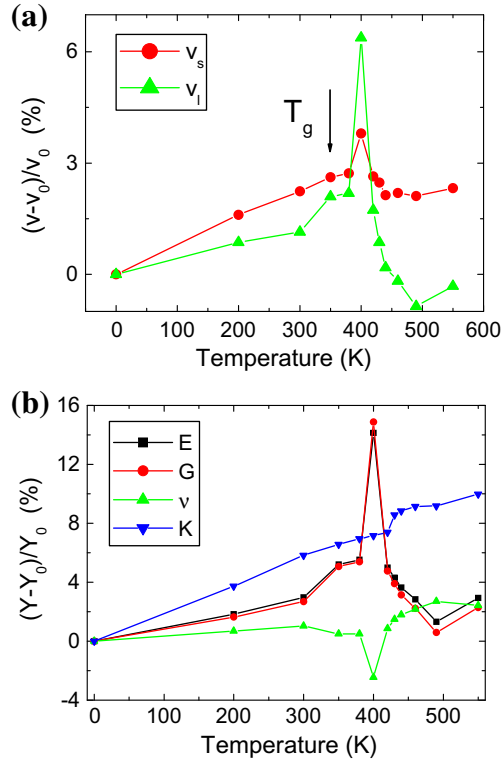


**Fig. 27.** (a) The relative longitudinal and transverse velocities change with  $T$ , ( $v = v_t, v_s$ ),  $v$  is normalized by  $\Delta v/v_0 = (v - v_0)/v_0$ , where  $v_0$  is velocity for as-prepared  $Zr_{53}Ti_5Cu_{20}Ni_{12}Al_{10}$ BMG. (b) The relative changes  $\Delta Y/Y_0 = (Y - Y_0)/Y_0$  of variation of  $Y$  ( $Y$  stands for  $E, G, K$ , and  $v$ ) of the BMG with temperature.

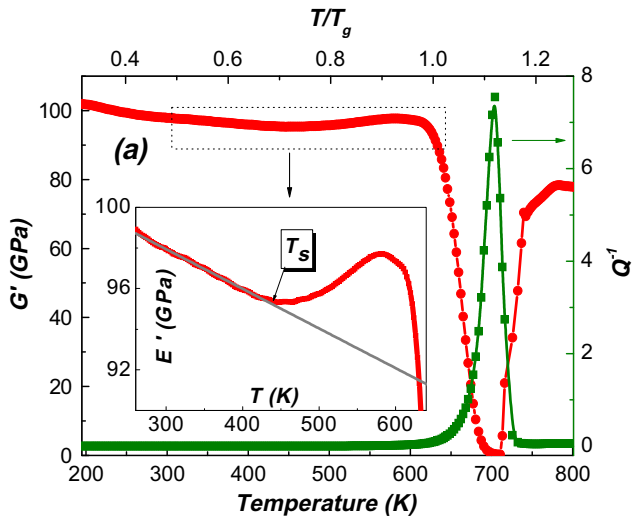


**Fig. 28.** Storage modulus  $G'$ , internal friction  $Q^{-1}$  of Vit4. Inset: Partially amplified indicating the modulus stiffening before glass transition [216],  $T_s$  is the stiffening temperature.

BMG. Similar to Vit1, the BMG also show an obvious stiffening onset of glass transition which confirms the markedly microstructural change during glass transition [214,215].

In contrast to common metals and alloys, whose modulus generally decreases with increasing temperature, the metallic glasses, which resemble rubber and protein like materials, become even much stiffer demonstrated with an enhanced elastic modulus before glass transition. Fig. 28 shows the modulus stiffening behavior of a typical  $Zr_{46.75}Ti_{8.25}Cu_{7.5}Ni_{10}Be_{27.5}$  BMG (Vit4) [216]. Before the sharp loss at glass transition, the elastic modulus manifests a distinct increase onset at 445 K as highlighted in the inset of the figure. For instance, the liner predicted modulus is 92.4 GPa at 585 K ( $0.94T_g$ ), while the actual modulus is 97.3 GPa, which is about 6% enhanced. This indicates a modulus stiffening behavior before glass transition in the BMG. It is found that the modulus stiffening behavior before glass transition in BMGs is ubiquitous depending on cooling and heating rates, testing frequencies, physical aging. The possible physical reasons are attributed to the evolution of the ordered structure during relaxation [216]. The results indicate that similar to rubber and proteins the BMGs also show obvious stiffening onset of glass transition. The above results confirm that the sensitive structural change and unique phenomenon can be sensitively reflected by elastic properties measurements.

The investigations of the acoustic velocities and elastic constants of BMGs upon annealing temperature indicate that the characteristics of glass transition: (1) the discontinue changes of acoustic velocity, density and mechanical properties demonstrate that an obvious stiff phenomenon happens just before the glass transition; (2) a large volume change accompanies the glass transition of the BMG; (3) the glass transition has a marked kinetic nature. The dramatic change of the acoustic velocities, density, mechanical properties and the striking stiffness of transverse acoustic phonons near  $T_g$  also demonstrate that the glass transition is related to relatively abrupt microstructural change [217–219].

A striking softening of long-wavelength transverse acoustic phonons relative to its crystallized state of BMGs is widely observed by comparison the elastic moduli between BMGs and their crystallized phases [54,57,151]. Large changes in  $v_s$ ,  $\theta_D$ , and  $G$  and small changes in  $\rho$ ,  $v_l$  and  $K$  between the glassy and crystallized states are observed in various BMGs. For example, for Vit1, the changes of  $v_s$ ,  $\theta_D$ , and  $G$  between the amorphous and crystallized states are 13.5%, 13.4%, and 30.3%, respectively. While the changes in  $v_l$  and  $K$  are only 5.2% and 3.9%, respectively. Table 5 shows the changes of  $v_s$ ,  $\theta_D$ , and  $G$  between the amorphous and crystallized states of various BMGs. The changes of  $v_s$ ,  $\theta_D$ , and  $G$  between the glassy and crystallized states are larger than 10%. And the changes in  $v_l$  and  $K$  are only  $\sim 5\%$ . The decrease in  $\theta_D$ , i.e., the decrease in the maximum frequency allowed, leads to an increase in the effective atomic distance in BMGs and degradation of bonding strength compared with their crystalline state. The softening phenomenon has also been observed in amorphization process of thin film induced by irradiation, and is similar to that associated with melting [147]. For the BMGs, with denser packed microstructure, its density change is about 1.0% and much smaller than that of the oxide glasses [148], while the oxide glasses exhibit a large density change between crystal and glass state, e.g. for vitreous  $SiO_2$ ,  $\Delta\rho/\rho \approx 20\%$  [149]. Thus, the softening is mainly attributed to the unique microstructural characteristics of the BMGs [54,57,151]. The softening phenomenon also indicates that markedly differences in the electronic state, and atomic interaction between the glassy and crystalline states exists, even though the coordination number and nearest-neighbor distance of the BMG are not obviously changed after crystallization. In contrast, the application of pressure does not induce acoustic shear mode softening for BMGs. The pressure-induced changes of  $v_l$ ,  $v_s$ ,  $G$ , and  $K$  for BMGs are different from the changes of these parameters induced by crystallization as shown in Table 6. The pressure leads to a smaller change of  $v_s$  (1.2%) and  $G$  (4.1%), and relatively larger changes of  $v_l$  (2.2%) and  $K$  (7.1%) for Vit1. This result means that pressure has larger effect on the longitudinal acoustic phonons than the transverse phonons in the BMG. Meanwhile, crystallization causes a striking stiffening of transverse acoustic phonons relative to the BMG.

There are few studies of the acoustic waves in glass-forming liquids even though in certain viscous liquids (close to melting) the propagating shear elastic modes are found to be existence [164]. This is due to extremely difficult to perform acoustic measurements at high temperatures. Johnson et al. developed a smart way to indirectly study the temperature dependence of the liquid shear and bulk moduli  $G_\infty$  and  $K_\infty$  which depends on the liquid configuration by using ultrasonic measurements performed at a high frequency [220–224]. It is provided that the  $\alpha$ -relaxation time of the glass-forming liquid  $\tau = \eta(T)/G_\infty$  is much greater than the inverse of the measuring frequency. To probe the

**Table 5**

A comparison of the properties of the glassy state ( $Y_a$ ,  $Y$  stands for  $v_h$ ,  $v_s$ ,  $\rho$ ,  $K$ ,  $G$ ,  $E$ ,  $v$ , and  $\theta_D$ ) and crystallized state ( $Y_c$ ) for various alloys.  $\Delta Y/Y_0 = (Y_{\text{Crystalline}} - Y_{\text{Amorphous}})/Y_{\text{Amorphous}}$  (%).

BMGs	Zr <sub>41</sub> Ti <sub>14</sub> Cu <sub>12.5</sub> - Ni <sub>5</sub> Be <sub>22.5</sub>	Zr <sub>46.75</sub> Ti <sub>8.25</sub> Cu <sub>5.5</sub> - Ni <sub>10</sub> Be <sub>27.5</sub>	Zr <sub>48</sub> Nb <sub>8</sub> Cu <sub>14</sub> - Ni <sub>12</sub> Be <sub>18</sub>	Zr <sub>48</sub> Nb <sub>8</sub> Cu <sub>12</sub> - Fe <sub>8</sub> Be <sub>24</sub>	Zr <sub>53</sub> Ti <sub>5</sub> Cu <sub>20</sub> - Ni <sub>12</sub> Al <sub>10</sub>	Pd <sub>39.1</sub> Ni <sub>10.1</sub> - Cu <sub>29.9</sub> P <sub>20.9</sub>	Nd <sub>60</sub> Al <sub>10</sub> - Fe <sub>20</sub> Co <sub>10</sub>	Cu <sub>60</sub> Zr <sub>20</sub> - Hf <sub>10</sub> Ti <sub>10</sub>	Ce <sub>70</sub> Al <sub>10</sub> - Ni <sub>10</sub> Cu <sub>10</sub>	Mg <sub>65</sub> Cu <sub>25</sub> Tb <sub>10</sub>	Pr <sub>60</sub> Al <sub>10</sub> Ni <sub>10</sub> Cu <sub>20</sub>
$T_g$ (°C)	350	350	383	388	395	291	302	461	86	141	127
$T_x$ (°C)	425	458	448	460	450	364	510	509	104	214	179
Annealing $T$ (°C) and time (h)	500, 2	550, 1	448, 2	600, 1	680, 1	423, 1.5	510, 1	598, 1.5	257, 1	240, 1	390, 1
$\Delta v_i/v_{i0}$	5.3	4.4	5.5	4.52	2.32	3.2	2.2	3.8	13	7.5	8.6
$\Delta v_s/v_{s0}$	13.5	10.8	8.7	10.9	-0.32	12.4	3.9	11	21	10.3	17.1
$\Delta \rho/\rho_0$	1.1	1.05	0.98	1.21	2.94	0.7	0.41	0.58	0.6	0.4	0.35
$\Delta K/K_0$	4.0	2.6	9.9	4.09	10.0	2.2	2.9	2.4	22.9	12.3	10.8
$\Delta E/E_0$	27.2	27.7	18.4	22.2	54	25.0	7.74	21.9	43.5	20.8	34.7
$\Delta G/G_0$	30.3	31.0	19.2	24.5	48	27.2	8.4	24.2	47.0	22.2	37.6
$\Delta v/v_0$	-9.4	-9.5	-2.7			-6.0	-2.8	-7.0	-9.9	-4.8	-5.2
$\Delta \theta_D/\theta_{D0}$	13.44	10.8		11.0	22	12.3	3.95	11.0	20.6	10.3	16.8

**Table 6**

A comparison of acoustic and elastic properties of the  $Zr_{41}Ti_{14}Cu_{12.5}Ni_{10}Be_{22.5}$  BMG under high pressure and after crystallization.  $Y_0$  stand for as-state ( $Y_0 = v_l, v_s, G, K$  and  $\theta_D$ ),  $Y_p$  high pressure (2.0 GPa) state and  $Y_c$  crystallized state.

	$v_l$ (km/s)	$v_s$ (km/s)	$G$ (GPa)	$K$ (GPa)	$\theta_D$ (K)
$(Y_c - Y_0)/Y_0$ (%)	5.2	13.5	30.3	3.9	13.4
$(Y_p - Y_0)/Y_0$ (%)	2.2	1.2	4.3	7.7	1.8

dependence of  $G_\infty$  on the configurational state of the liquid, the acoustic velocities of the glassy specimens were measured after thermal relaxation to the equilibrium liquid state in the supercooled liquid temperature region. The ultrasonic measurements were performed *ex situ* on the relaxed BMG sample at RT after being quenched rapidly from the processing temperature in the supercooled liquid temperature region. The total annealing time at each temperature  $T_A$  was chosen to be less than the time to the onset of detectable crystallization as determined by the time–temperature transformation for the BMG samples and comparable to the previously determined time for viscosity relaxation to occur [220]. This ensures that the samples are in a fully relaxed glassy state. Provided the rapid quenching time is short compared to the  $\alpha$ -relaxation time at  $T_A$ , the relaxed liquid can be configurationally captured, and the acoustical properties at room temperature are characteristic of the equilibrium liquid at  $T_A$ . The isoconfigurational shear modulus at  $T_A$  were then estimated by extrapolating the room temperature measurements using a linear Debye–Grüneisen constant to account for the thermal expansion effect on the shear modulus of the frozen glass. By using this method, the  $T$  dependences of  $G_\infty$  and  $K_\infty$  in the liquid state for various BMGs are obtained and directly related to the viscosity and fragility of the glass-forming liquids [220–224]. However, this method can only be applied to the BMG systems with high GFA and very stable supercooled liquid state. For most known BMG systems, their supercooled liquid state temperature range is not large enough for the method.

## 6.2. *In situ* measurement of temperature dependence of elastic moduli of BMGs

The precise measurements on temperature dependence of elastic constants of BMGs are essential to understand the physical and mechanical properties as well as the glass transition displayed in BMGs. However, the  $T$  dependence of elastic moduli data of metallic glasses is sparse due to experimental difficulties in measurements and lower resistance to crystallization of most metallic glasses. It remains relatively difficult to obtain good estimations of the elastic moduli at elevated temperature in glasses until the 1950s, with the progress in high-temperature ultrasonic method and direct mechanical vibration including mechanical spectroscopy. Efforts have been made recently to study the behavior of the elastic modulus around  $T_g$  for typical glass and BMGs [225–237].

### 6.2.1. *In situ* measurement of temperature dependence of elastic moduli during glass transition

The resonant ultrasound spectroscopy (RUS) method was recently developed to determine the full elastic tensor of the solid from a single frequency scan. The method could be applied to *in situ* measure the acoustic velocities of glasses at high temperature [64–68]. The advantages of this technique lies in the ability to work with small, mm sized samples and the sample can be heat treated during the ultrasound spectroscopy measurements, which is very useful for study the elastic moduli changes during phase transition and glass transition [225,226]. The RUS method can even be applied to study the elastic properties of melt. For instance, the speed of longitudinal sound waves has been measured in liquid, supercooled, and amorphous selenium ( $T_g = 35^\circ\text{C}$ , one of the simplest glass-forming substances), including the region around the  $T_g$  by RUS [165]. Four temperature regions with strongly different relaxation times can be distinguished between  $RT$ ,  $T_g$ ,  $T_x$  and the melting point by the measurements. Each region is marked by a change in the slope of the temperature dependence of the sound velocity. Near  $T_g$  the velocities of longitudinal and transverse sound exhibit hysteresis with a step-like drop on heating and a more continuous rise on cooling. The  $T$  dependence of the velocity in supercooled selenium can be interpreted as a phase diagram. The phase diagram contains a melting temperature, at which no feature occurs in the sound velocity on heating from, or cooling to, the

supercooled state. In contrast, a step-like anomaly occurs in both the longitudinal and transverse velocities of sound near the  $T_g$ . It is speculated that this anomaly in the sound velocity may be a general feature of the glass transition [165].

The RUS method has also been applied to study the elastic properties changes and features of BMGs during glass transition and crystallization processes. Similarly to conventional crystalline metals, the elastic moduli of the BMGs monotonically decrease upon heating. However, the ratio of changes in the shear and bulk moduli ( $\Delta G/\Delta K$ ) (for example, for the PdNiCuP BMG) from 20 °C to 290 °C is 7.5, which is much larger than that of conventional crystalline metals of about 2 [226]. For Ca-based BMGs, below  $T_g$ , both Young's modulus and shear modulus decrease with increasing temperature, and the Poisson's ratio increases with increasing temperature. A decrease in the softening rate above  $T_g$  suggests that structural changes are important, and these trends reverse due to crystallization [225]. The temperature dependences of the density, viscosity, ultrasound velocities and attenuation of the PdSi alloy in liquid state have also been measured. A difference during heating and subsequent cooling with a ranching temperature at 1380–1430 K was observed for all measured quantities. An abnormally high attenuation of ultrasound was furthermore observed during several hours after that the sample was melted. The results are interpreted in terms of metastable inhomogeneities existing in the melt [235].

Some BMGs with exceptional low  $T_g$  and exceptionally stable supercooled liquid state were recently developed [63,125,173,238,239]. These BMGs enable their  $T$ -dependent elastic constants to be *in situ* determined well into the supercooled liquid state in a  $N_2$  flushed atmosphere using a pulse echo overlap method. Since the used carrying frequency of 10 MHz was  $10^{10}$  times the relaxation rate of  $\sim 1$  mHz for the BMG in the measuring temperature range, the measured elastic constants were taken as the instantaneous elastic moduli. The insignificant temperature effects on the quartz transducers and the bonding resin in the measuring temperature range were determined by using standard samples and ruled out to minimize their influence on the ultrasonic velocities measurements. Fig. 29 shows *in situ* temperature dependent acoustic velocities around  $T_g$  (=343 K) of a  $Ce_{68}Al_{10}Cu_{20}$ - $Co_2$  BMG and a breakaway polymeric glass with very low  $T_g$  (=323 K) for comparison [232]. At calorimetric  $T_x$ , a discontinuously sudden increase of  $v_l$  corresponding to the crystallization of the BMG is seen in Fig. 29b, which suggests that the transition temperatures ( $T_g$  and  $T_x$ ) determined by DSC and the acoustic method are well consistent. Below  $T_g$ , both  $v_l$  and  $v_s$  of the BMG show weak  $T$  dependence and similar  $T$  derivatives to that of the crystallized BMG. Importantly, at calorimetric  $T_g$ , a sharp drop (1.68%) of  $v_s$  happens while no obvious change of  $v_l$  is detected, and the softening temperature  $T_{g-v_l}$  of  $v_l$  [as indicated in Fig. 29c] is about 6 K higher than that of  $v_s$ . For breakaway glass [Fig. 29d], the dramatic softening of  $v_s$  also occurs at calorimetric  $T_g$ (323 K) while the softening temperature of  $v_l$ ,  $T_{g-v_l}$  is about 14 K higher than that of  $v_s$ . The two cases show that only  $v_s$  becomes softening at  $T_g$  while the softening of  $v_l$  happens in a separate temperature above  $T_g$ . The  $T$ -dependences of  $v_s$  and  $v_l$  of the BMG are distinctively different not only in the decrease magnitude but also in their corresponding softening temperature around glass transition. The softening temperature of  $v_s$  corresponds well with calorimetric  $T_g$  in the two glasses, while the softening of  $v_l$  occurs about 10 K above calorimetric  $T_g$ . The  $v_s$  is a signature of transverse interaction and sensitive to the bonding between atoms, while  $v_l$  is sensitive to the change of volume because the longitudinal wave is compressional wave [50]. The results indicate that a sudden change of volume does not occur at calorimetric  $T_g$ . Fig. 30a and b shows that a pronounced softening is observed in the  $T$ -dependent volume-preserving  $G$  curves of both glasses, while the volume-nonpreserving  $K$  consistently shows very weak  $T$  dependence around calorimetric  $T_g$ . Especially for the breakaway glass, nearly no obvious variation was observed in the  $K$ - $T$  curve around  $T_g$ , and the values of  $dK/dT$  in glass and supercooled liquid state are similar. In supercooled liquid state,  $dG/dT$  is more than three times larger than  $dK/dT$  in glassy state for the two glasses. These experimental results clearly imply that the  $G$  is an effective parameter for governing the glass transition in the glasses, and the  $T$ -dependent  $G$  can accurately describe the change of the viscosity and fragility in the two glass-forming liquids [232].

Using the temperature dependent data of  $G$  and  $K$ , the  $m$  values of the glasses can be determined from the correlation existing between the softening rate and relaxation kinetics [240]. The  $m$  values calculated from the elastic and potential energy landscape models for the two glasses are close to the experimental result. For both glasses, the  $m$  value obtained from the "shoving" model is close to that of PEL estimation [232]. The results therefore experimentally demonstrate that the "shoving"

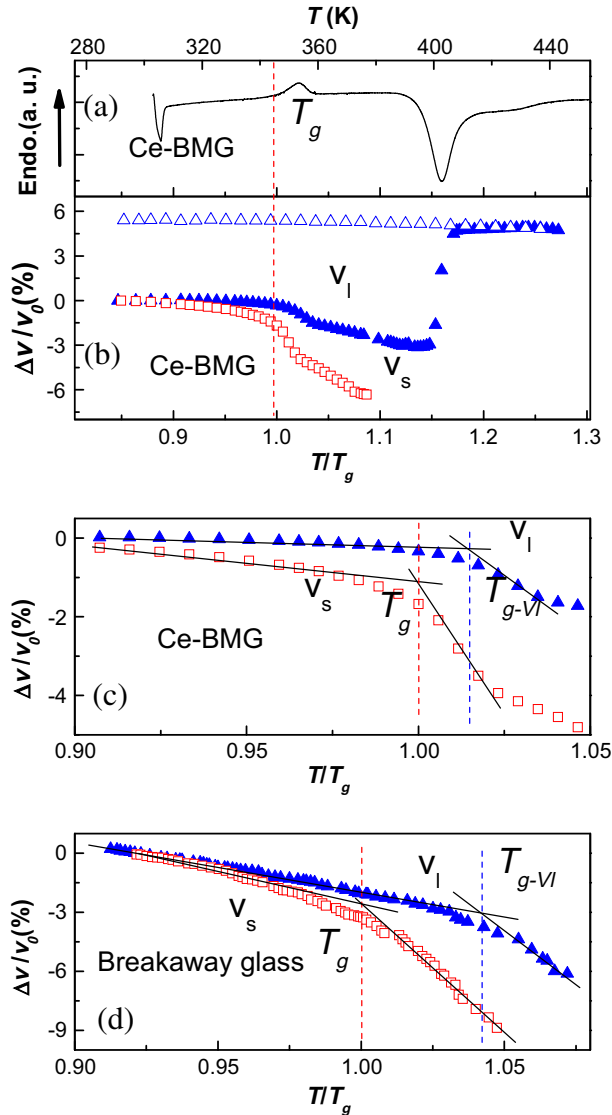


**Fig. 29.** (a): DSC trace at a heating rate of 2 K/min for  $\text{Ce}_{68}\text{Al}_{10}\text{Cu}_{20}\text{Co}_2$  BMG. (b): Relative changes  $\Delta v/v_0[(v - v_0)/v_0]$  vs.  $T/T_g$  of  $v_l$  and  $v_s$  for the BMG at 2 K/min, and  $\Delta v/v_0$  of  $v_l$  for its crystallized sample. (c): Detailed results around  $T_g$  showing  $\Delta v/v_0$  vs.  $T/T_g$  of  $v_l$  and  $v_s$ . (d):  $\Delta v/v_0$  of  $v_l$  and  $v_s$  as a function of  $T/T_g$  for breakaway glass. The  $v_0$  is room temperature value of  $v_l$  or  $v_s$  [232].

model is equivalent to potential energy landscape on the description of the relaxation activation energy. The result also supports that the  $G$  can be used to explain the liquid behavior near  $T_g$  at least in the two glasses. Assuming that  $\tau_0 = 10^{-13}$  s and  $\tau(T_g) = 10^3$  s at  $T_g$  [240,241], the calculated  $\ln\tau$  vs.  $T_g/T$  according to the “shoving” model for the two glasses are plotted in Fig. 31. It clearly shows that the  $T$ -dependent  $G$  near  $T_g$  is directly responsible for the liquid fragility and a larger decrease of  $G$  with temperature approaching  $T_g$ . For comparison, the viscosity of the Ce-based BMG and the breakaway glass were measured using dynamic mechanical analysis method as shown in Fig. 31. One can see that the calculated and experimental  $T$ -dependent relaxation time data roughly fit for the Ce-based BMG and breakaway glass. The experimental  $\tau$  data of breakaway glass also fit well to that of the

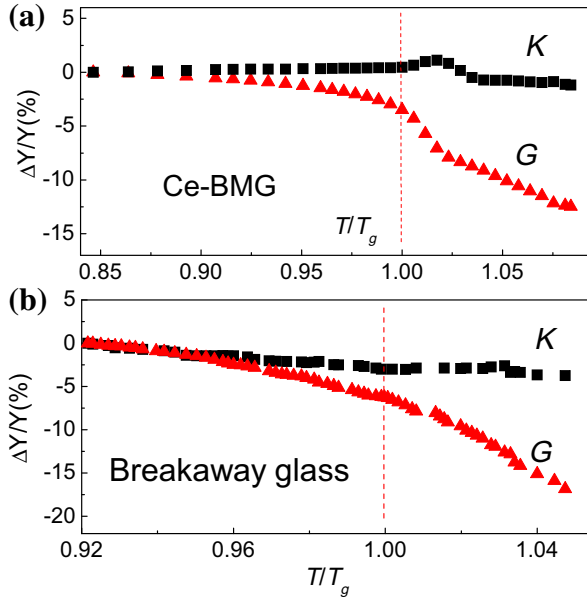


**Fig. 30.** Relative changes  $\Delta Y/Y_0 = (Y - Y_0)/Y_0$  of K and G vs.  $T/T_g$  for Ce-based BMG (a) and breakaway glass (b).  $Y_0$  represents K or G at room temperature [232].

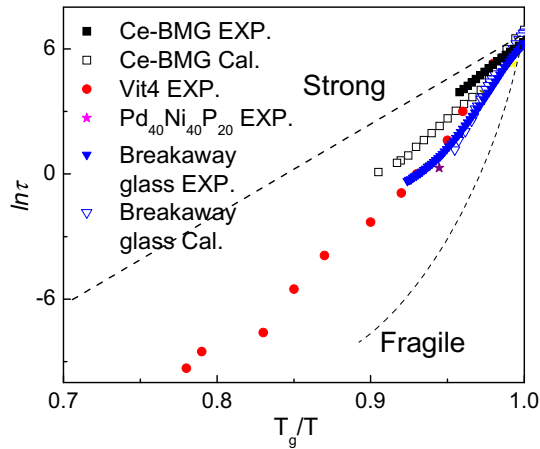


**Fig. 31.** Fragility plots between  $\ln \tau$  and  $T_g/T$  for the BMG and breakaway glass from the “shoving” mode. For comparison, the experimental relaxation times for Ce-BMG, breakaway glass, Vit4 ( $m = 43$ ), and Pd<sub>40</sub>Ni<sub>40</sub>P<sub>20</sub> ( $m = 51$ ) obtained from viscosity measurements are plotted. It clearly shows that the calculated and independent experimental relaxation time data for the Ce-based glass and breakaway glass roughly fit [232].

Pd<sub>40</sub>Ni<sub>40</sub>P<sub>20</sub> glass with similar  $m$  value. The *in situ* instantaneous elastic moduli measurements well into supercooled liquid show manifestations of critical important of shear during glass transition. The results provide direct experimental evidences for confirming that the activation energy for viscosity slow down and configurational changes in the liquid potential energy landscape scales with shear modulus. The temperature dependence of elastic moduli such as  $E$  and Poisson’s ratio for a series of non-metallic glasses indeed exhibit a transition range between slow softening rate and a faster one,

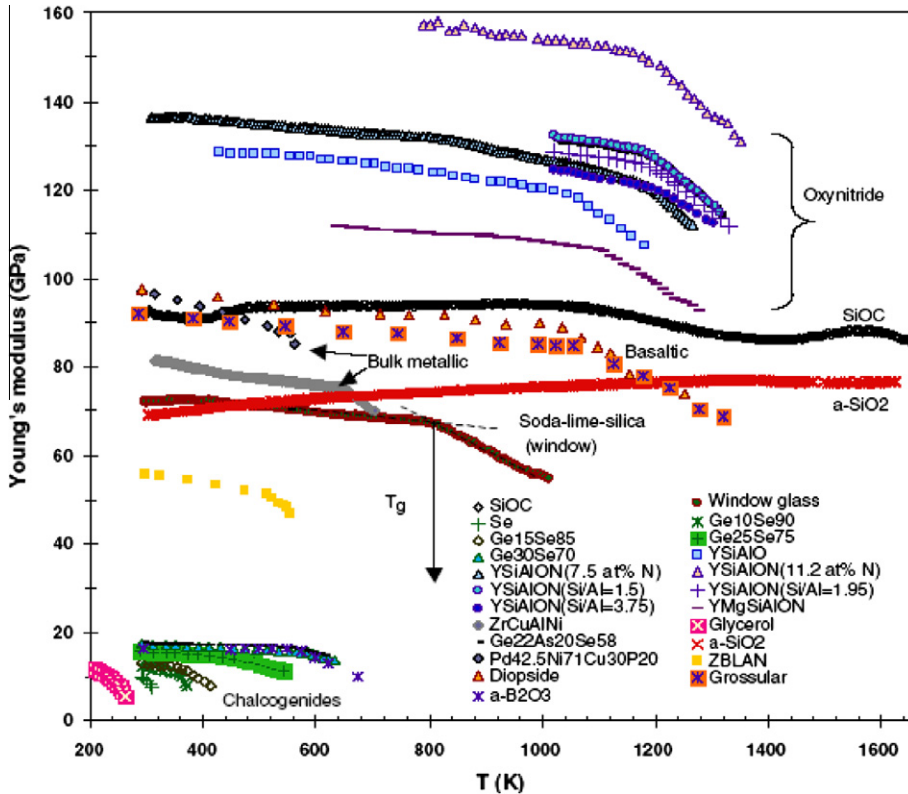


Fig. 32. Temperature dependence of Young's modulus of various non-metallic glasses [172].

corresponding to glass transition as shown in Fig. 32 [172]. The temperature dependence of the elastic moduli above  $T_g$  can be discussed in terms of the fragile vs. strong character of liquid, and the rate of softening is indicative of the glass-forming liquid fragility.

Thermal mechanical analyzer (DMA) can monitor temperature and frequency dependence of both storage and loss moduli of BMGs [83,97,242–248]. DMA measurements were performed on a series of strong and fragile metallic glasses in isochronous and isothermal routes to study the dynamic mechanical relaxation in BMGs and their supercooled liquid state close to their  $T_g$ . The metastable glasses will relax into more stable states, and the inevitable relaxation accordingly makes it a powerful means for deep understanding the nature of glass and glass transition. There are two relaxation modes which attract most interest of researchers [34–38]: one is the primary relaxation or  $\alpha$ -relaxation, which is closely related to the glass transition process; another is the secondary Johari–Goldstein relaxation or slow  $\beta$ -relaxation [34–38,249,250]. The slow  $\beta$ -relaxation is considered to be a near universal feature of glass-forming liquids at low temperatures. At the crossover temperature  $T_c$  above  $T_g$ , the  $\alpha$ - and slow  $\beta$ -relaxations merge into one effective process [249,250]. However, many supercooled liquids, especially for rather strong ones, do not exhibit the well-resolved  $\beta$ -process, but an excess wing contribution to the high-frequency wing of the  $\alpha$ -peak [249–251]. The slow  $\beta$ -relaxation, as a faster and more local relaxation mode, can be regarded as a precursor of  $\alpha$ -relaxation and it may probably relate to the superior mechanical performance of metallic glasses. (For example, the slow  $\beta$ -relaxation is regarded to correspond the activation of shear transformation zone during plastic deformation of BMGs [82].) However, there has so far been no consensus on this issue even on a qualitative level, and the physical origins of the excess wing and slow  $\beta$ -relaxation are commonly considered as one of the great mysteries of glass physics [249–251]. The  $\beta$ -relaxation was originally seen to indicate local

diffusion, both rotational and translational, in loosely packed isolated regions, and represents the motion of 'island' [249,250]. Another view based on the dipolar correlation function is that the slow  $\beta$ -relaxation may be attributed to faster, small angle reorientational motion of all molecules. It is still unclear if this process has an intermolecular or intramolecular origin, or whether it reflects small or relatively large-angle jumps. The dynamical mechanical relaxation arising from the elastic dipole reorients after the removal an external stress has been found to be available to the dynamics of the supercooled liquids with an assembly of equal-size or different-size [252,253]. The method could provide more direct evidences for the underlying physics of the excess wing and slow  $\beta$ -relaxation, since in the system reorientation of elastic dipole cannot occur by the reorientation of the spheres about their axis [253]. Metallic liquid is the very systems with atoms which interact through metallic bonding, and its structure is close to a dense random packing of spheres. The BMG-forming supercooled liquids offer a wide experimental temperature and time windows for investigating the dynamical characteristics in supercooled liquids and for verifying that if exist the excess wing and how universal it is in the supercooled liquids.

High-precision dynamical mechanical relaxation measurements were performed on a TA DMA2970. A sinusoidal strain was applied during all dynamic mechanical measurements with frequency range from  $10^{-2}$  to 200 Hz. The temperature and frequency dependent modulus measuring accuracies for the DMA were better than 2%. A complex modulus  $G^*(\omega, T) = G'(\omega, T) + iG''(\omega, T)$  can be obtained from the DMA results [254]. The elastic modulus such as shear modulus  $G(T)$  can be determined as [254]:  $G(T) = G'(\omega, T)(1 + \tan^2\delta) = G''(\omega, T)(\tan\delta + 1/\tan\delta)$ , where  $\tan\delta = G''/G'$  is the internal friction. Specimen in the shape of rectangular sheet was tested in a single-cantilever bending configuration and protected in an argon atmosphere. Before DMA measurements, all samples had been

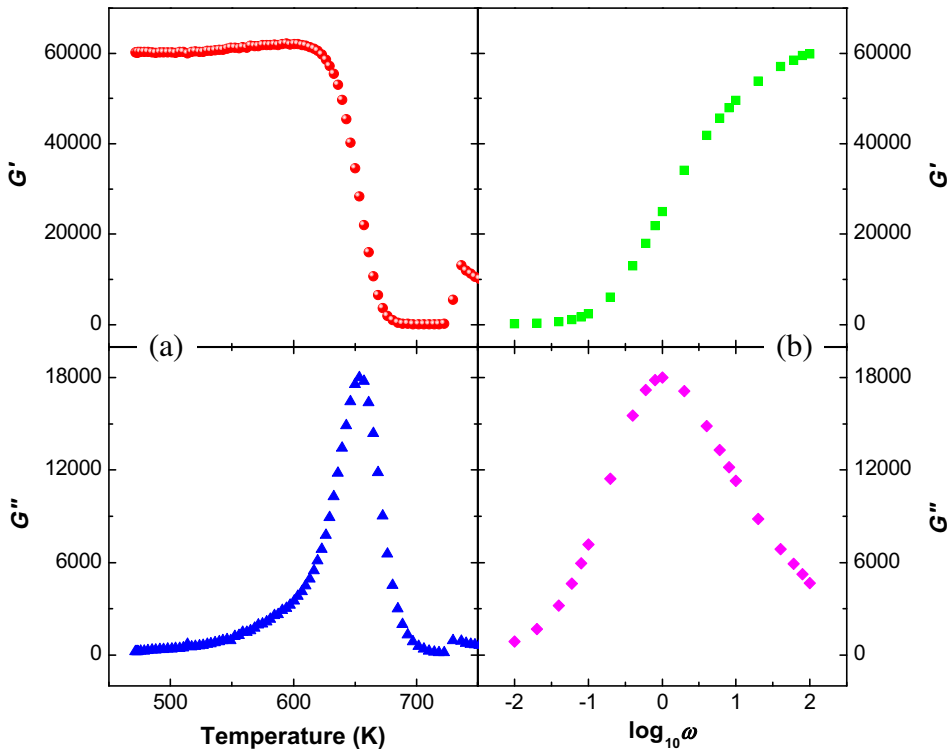


**Fig. 33.** The storage  $G'$  and loss moduli  $G''$  of  $Zr_{46.75}Ti_{8.25}Cu_{7.5}Ni_{10}Be_{27.5}$  (Vit4) determined in a heating process (a); and isothermal process (changing the frequency  $\omega$ ) (b). The measurement accuracy is better than 2% [243].

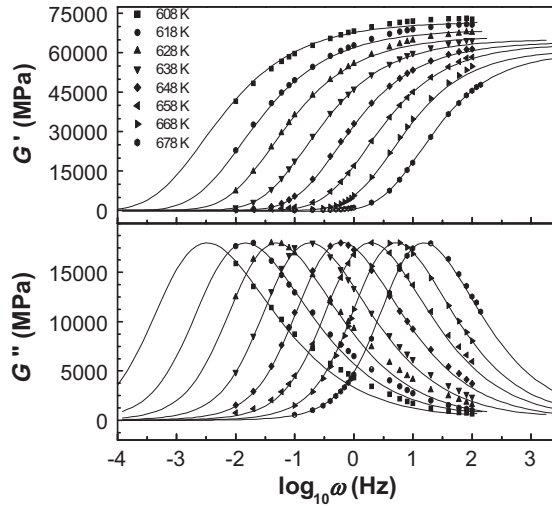


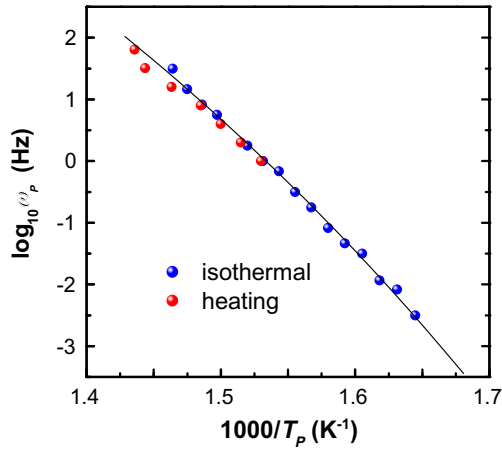
**Fig. 34.** The  $\omega$ -dependence of  $G'$  and  $G''$  of Vit4 supercooled liquid determined isothermally by DMA at different temperatures. The solid lines are the fits using the KWW equation [242].

heated into respective supercooled liquid region and cooled at constant rate ( $\leq 40$  K/min) to RT in order to erase the interfering of the formation of the as-cast samples.

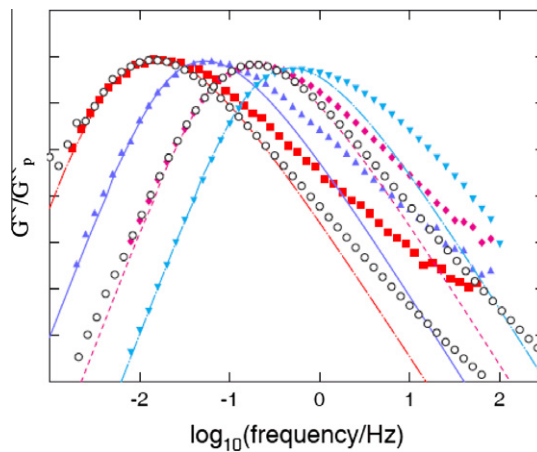
Fig. 33a exhibits the typical storage ( $G'$ ) and loss ( $G''$ ) moduli of  $Zr_{46.75}Ti_{18.25}Cu_{7.5}Ni_{10}Be_{27.5}$  (Vit4) determined from 473 K to 750 K at a heating rate of 3 K/min and a frequency  $\omega$  of 1 Hz [243]. In glassy state  $G'$  and  $G''$  are slightly dependent of temperature increasing from 300 to 500 K. From 500 K to the onset temperature of glass transition (603 K), both  $G'$  and  $G''$  increases slowly and gradually due to the physical aging occurring during heating. In the supercooled liquid region, an obvious asymmetrical peak characterized by a smaller slope at low- $T$  side can be found in the  $G''$ -curve, while the  $G'$  decreases to zero at higher  $T$ , exhibiting a typical liquid characteristic. The occurrence of the crystallization is exhibited with an abrupt increasing of  $G'$  at 725 K. Fig. 33b shows that  $G'$  and  $G''$  as function of  $\omega$  at 653 K. An asymmetrical peak is also exhibited well in the  $G''$ -curves, and  $G'$  increases from zero to a constant value with increasing  $\omega$ . The change of the  $G'$  and  $G''$  in Fig. 33a and b has an inverse tendency.

Fig. 34 presents the  $\omega$ -dependence of  $G'$  and  $G''$  of supercooled liquid state of Vit4 determined isothermally by DMA from 608 to 678 K. The dynamical characteristic of the supercooled liquid is exhibited well by the  $G''$ -curves. The values of  $\log_{10}\omega_p$  ( $\omega_p$  is the peak frequency) directly indicate the frequencies of the molecular fluctuation which are relevant for the susceptibilities. The  $T$ -dependence of  $\log_{10}\omega_p$ , usually called as molecular mobility, is relevant for the dynamical relaxation [252,253]. Fig. 35 shows  $\log_{10}\omega_p$  vs. reciprocal peak temperature  $1/T_p$  of  $G''$ -curves determined from the isothermal and continuous heating processes. The consistence in the molecular mobility between isothermal and continuous heating processes affirms the correlation between them, and the isothermal process is the limitation of the continuous heating process. The  $T$ -dependent  $\omega_p$  of the  $G''$ -curves is fitted by the Vogel–Fulcher–Tamman (VFT) expression:  $\omega_p = \omega_0 \exp\left(\frac{-B}{T-T_0}\right)$  [239–241]. From the fit, the parameters of  $\omega_0$ ,  $B$  and  $T_0$  for Vit4 are determined to be  $4.6559 \times 10^{14}$  Hz, 10134.6 K and 352 K, respectively. The fragility  $m$  of Vit4 is then calculated to be 38. The values of  $B$ ,  $T_0$  and  $m$  are almost same as those determined from the  $T$ -dependent viscosity [255].

From Fig. 34 one can see that all spectra of  $G''$  for Vit4 dominated by a single and asymmetrical peak shifting through the  $\omega$ -axis with temperature exhibit a typical relaxation behavior, which has been considered to represent mainly the  $\alpha$ -relaxation process [252,253]. The data were fitted with the Kohlrausch–Williams–Watts (KWW) form (or the Havriliak–Negami function) [252,253]: The Fourier transforms of  $d\left\{\Delta G \exp\left[-\left(\frac{t}{\tau}\right)^{\beta_{KWW}}\right]\right\}/dt$ , where  $\Delta G = G(\omega = \infty) - G(\omega = 0)$ ,  $\beta_{KWW}$  a stretched coefficient,



**Fig. 35.** The plots of  $\log_{10}\omega_p$  vs.  $1000/T_p$  of the  $G''$ -curves in Vit4 supercooled liquid determined in isothermal processes and continuous heating processes [242].



**Fig. 36.** Comparison with the dielectric relaxation loss data of a small molecule glass former of MTHF (has the same  $\beta_{KWW}$  as the Vit4 metallic glass) at two same temperatures (638 K and 648 K, black open circles) [247,248].

and  $\tau$  the averaged relaxation time. The originally and purely phenomenological KWW form is used because the KWW function has been theoretically derived from a system with a distribution of relaxation times, and can describe the  $\alpha$ -relaxation well which represents the process with a distribution of relaxation time. It can be clearly found in Fig. 34 that a departure or excess wing at high- $\omega$  flank of the  $\alpha$ -peak exists and becomes more pronounced with decreasing temperature. The departure from the KWW form has also been observed in dielectric measurements on the molecular supercooled liquids without obvious slow  $\beta$ -peak [252,253]. Fig. 36 shows the comparison of the data with the dielectric relaxation loss data of a small molecule glass-former called MTHF at two temperatures [248]. The MTHF has obvious excess wing in the dielectric relaxation loss curve and the same  $\beta_{KWW}$  as that of Vit4. One can see that the excess wing in Vit4 over the KWW fit is larger than that of MTHF, which further confirms the existence of excess wing in BMGs.

The superposition of the  $\alpha$ - and  $\beta$ -processes is exhibited in  $G''$ -curves determined in the continuous heating process. Fig. 37 exhibits the best fits for the  $G''$ -curves of Vit4 determined in continuous

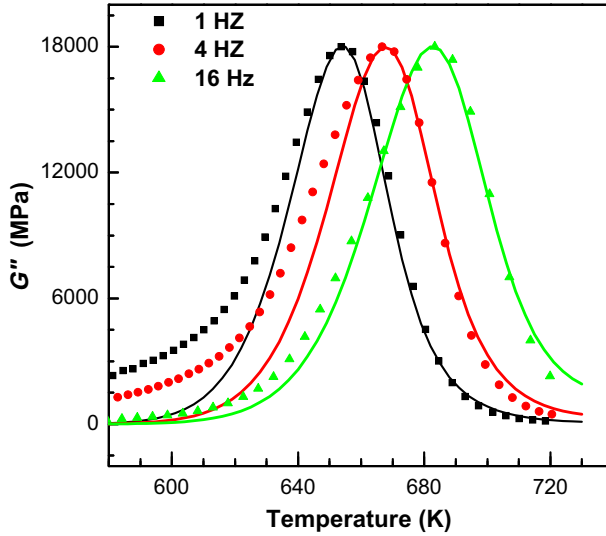


**Fig. 37.** Temperature-dependent  $G''$  of Vit4 for three frequencies. The solid lines are fits using the KWW equation with the relaxation time  $\tau = 1.6 \times 10^{-15} \exp\left(\frac{9668.42}{T-352}\right)$  and  $\beta_{KWW}$  equal to 0.65 [246].

heating processes (heating rate of 5 K/min) at 1, 4, and 16 Hz. The fitting  $\tau$  has a form:  $\tau = 1.6 \times 10^{-15} \exp\left(\frac{9668.42}{T-352}\right)$ . The fits yield a better representation of the peak part above  $T_p$ , but the low- $T$  data display higher value than the fits. Similar to the observation in loss modulus curves determined isothermally, an excess wing on the  $\alpha$ -curve in  $G''$ -curves is exhibited. The slow  $\beta$ -process existing in the metallic supercooled is faster than the  $\alpha$ -process and appears firstly during continuous

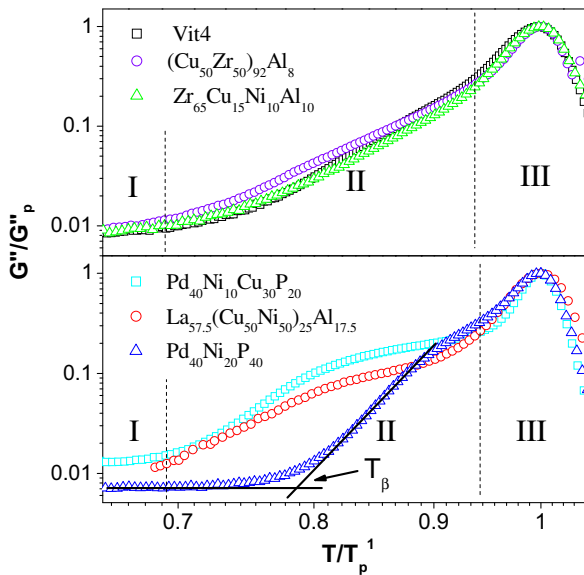


**Fig. 38.** The temperature dependence of the reduced loss modulus  $G''/G''_p$  measured at 1 Hz on different metallic glass-forming liquids in ramp mode (3 K/min). The  $T$  is normalized to  $T_p^1$  (the peak temperature determined at 1 Hz) for comparison [246].

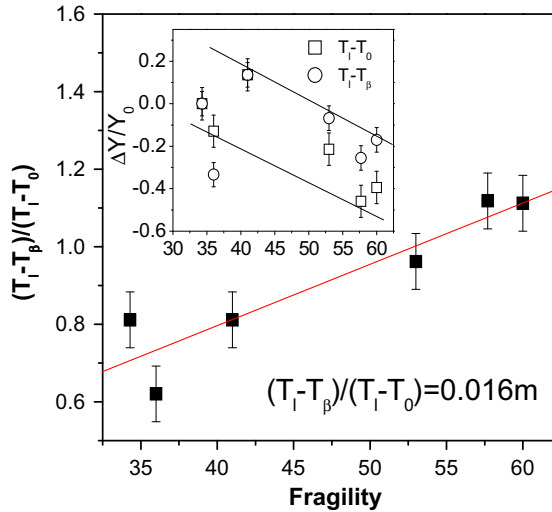


**Fig. 39.** Relationship between the onset temperature of slow  $\beta$ -relaxation- $T_\beta$  and fragility- $m$  in various BMGs, the solid line is drawn by linear fit with  $(T_1 - T_\beta)/(T_1 - T_0) = 0.016m$ . The relative change  $[\Delta Y/Y_0 = (Y_1 - Y_0)/Y_0, Y_0$ —the value for Vit4] of  $T_1 - T_\beta$  and  $T_1 - T_0$  to that of Vit4 is shown in the inset [246].

heating, and then the  $\alpha$ -process follows. Because of the intrinsic dynamical characteristic of the metallic supercooled liquids the slow  $\beta$ -process is not fully decoupled from the  $\alpha$ -process.

DMA measurements were performed on a series of strong and fragile metallic glass-forming liquids in isochronous and isothermal routes. Fig. 38 shows the reduced loss modulus  $G''/G_p'$  of the six BMGs [Vit4,  $Zr_{65}Cu_{15}Ni_{10}Al_{10}$ ,  $(Cu_{50}Zr_{50})_{92}Al_8$ ,  $Pd_{40}Ni_{10}Cu_{30}P_{20}$ ,  $Pd_{40}Ni_{40}P_{20}$  and  $La_{57.5}(Cu_{50}Ni_{50})_{25}Al_{17.5}$ ] in temperature domain measured at 1 Hz with the heating rate of 3 K/min.  $G_p'$  is the loss modulus at the peak and the temperature is also scaled by the peak temperature  $T_p^1$ . Common characteristics of all these curves can be divided into three regions: Region I is the low  $T$  range where  $G''$  is nearly independent of temperature; Region II has a characteristic shoulder which is affirmed to be related to the slow- $\beta$  relaxation. The results indicate that the slow  $\beta$ -relaxation is universal for these BMGs. Region III is the one where the  $G''$ -peak can be found. The peak is a typical characteristic of supercooled liquid, and related to the  $\alpha$ -relaxation. The three regions have more or less individual characteristics, and the individuality depends on the dynamical characteristic of different BMGs.

For the six BMGs,  $Pd_{40}Ni_{10}Cu_{30}P_{20}$ ,  $Pd_{40}Ni_{40}P_{20}$  and  $La_{57.5}(Cu_{50}Ni_{50})_{25}Al_{17.5}$  liquids have larger fragility index  $m$ , and the other three liquids are rather strong with small  $m$ . It is noted that the individuality of region II in the reduced  $G''-T$  curves corresponds to the fragility  $m$ ; i.e. the larger  $m$  the BMG has, the more obvious its region II is. This can be qualitatively explained as: for strong liquids, if the size of cooperative rearrangement region does not change significantly during  $T$  changes, the relaxation times of the primary and secondary relaxations do not differ a lot, and only an inconspicuous bump below  $T_g$  can be discerned in the strong glass-forming liquids. On the contrary, the slow  $\beta$ -relaxation could evolve into an obvious shoulder in fragile glass-forming liquids. A relationship between a scaled parameter related to  $\beta$ -relaxation in the form  $(T_1 - T_\beta)/(T_1 - T_0)$  and fragility of BMGs is established in Fig. 39.  $T_\beta$  is the onset temperature of the secondary relaxation.  $T_1 - T_\beta$  is scaled to  $T_1 - T_0$  to diminish the large difference among various BMGs. For the metallic liquids,  $(T_1 - T_\beta)/(T_1 - T_0)$  shows an increasing trend with increasing fragility although relative change of  $T_1 - T_\beta$  and  $T_1 - T_0$  to that of Vit4 tends to decrease with fragility (inset in Fig. 39). The quantitative relationship is:  $(T_1 - T_\beta)/(T_1 - T_0) = 0.016m$ . The distance between  $T_1$  and  $T_\beta$  also decrease with increasing fragility (up to  $-17\%$ ) which means that the absolute distance between  $T_1$  and  $T_\beta$  is larger for strong system. But the  $(T_1 - T_\beta)/(T_1 - T_0)$  increases with fragility, which indicates a obvious correlation between the

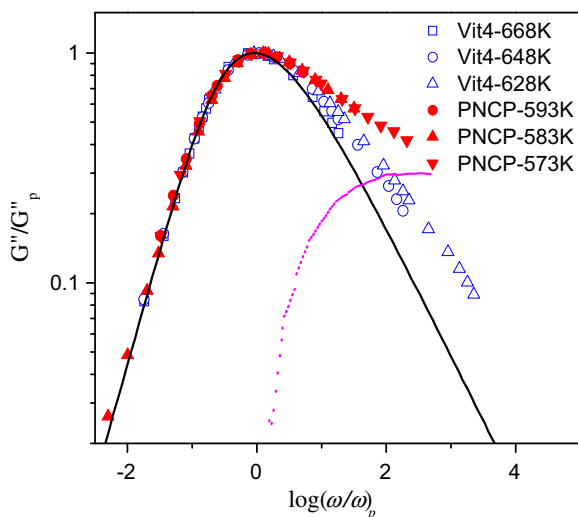


**Fig. 40.** DMA master curves for Vit4 and Pd<sub>40</sub>Ni<sub>10</sub>Cu<sub>30</sub>P<sub>20</sub> BMG. The solid line is the KWW fit to the master curve of Pd<sub>40</sub>Ni<sub>10</sub>Cu<sub>30</sub>P<sub>20</sub> with  $\beta = 0.57$ . The dash line indicates the possible contribution from slow- $\beta$  mode by subtracting the KWW fit from the master curve. Logarithmic scales are chosen for the reduced loss modulus  $G''/G''_p$  [243].

degree of coupling between  $\alpha$  and slow  $\beta$ -relaxation modes and the intrinsic dynamic characteristic of the BMGs indicated by their fragilities.

Frequency sweeps was conducted on Pd<sub>40</sub>Ni<sub>10</sub>Cu<sub>30</sub>P<sub>20</sub> (573–593 K) and Vit4 (628–668 K) samples and their respective master curves are shown in Fig. 40. Both BMGs show a prominent  $\alpha$ -relaxation peak in frequency domain. On the low frequency side of the loss peak, the two BMGs behave in the same way within experimental error but they differ significantly at high frequencies. After bifurcated at about 1 decade frequency, the spectra of Pd<sub>40</sub>Ni<sub>10</sub>Cu<sub>30</sub>P<sub>20</sub> possess larger value of normalized  $G''$  and the difference tends to increase with frequency. The KWW fit to the experimental spectra of Pd<sub>40</sub>Ni<sub>10</sub>Cu<sub>30</sub>P<sub>20</sub> with  $\beta = 0.57$  (solid line) is plotted in Fig. 39, and the dash line is the result of subtracting the fit curve from the experimental data. The difference provides another evidence of the existence of slow  $\beta$ -relaxation in Pd<sub>40</sub>Ni<sub>10</sub>Cu<sub>30</sub>P<sub>20</sub>.

The dynamic elastic modulus analysis results indicate that slow  $\beta$ -relaxation mode is ubiquitous in metallic glass-forming systems though it may manifest as an excess wing in strong glasses due to strong coupling with the  $\alpha$ -relaxation. The degree of coupling between  $\alpha$  and slow  $\beta$ -relaxations correlates with the fragility of the glass-forming liquids and causes an obvious violation of the time–temperature superposition principle in rather strong metallic glass-forming liquids. The finding of existence of  $\beta$ -relaxation in the metallic supercooled liquids affirms that the separation of the  $\alpha$ - and  $\beta$ -relaxations is universal and the  $\beta$ -relaxation process arises from the small-scale translational motions of atoms which are hindered in its metastable atomic solid-like islands [83,97,282,248]. These results indicate that the dynamic elastic modulus analysis upon temperature and frequency is effective method for relaxation study in metallic glasses and glass-forming liquids.

### 6.2.2. *In situ* measurement of temperature dependence of elastic moduli at low temperatures

The velocities of ultrasonic waves  $v_l$  and  $v_s$  of representative Vit1, other Zr-based BMGs, (Cu<sub>50</sub>Zr<sub>50</sub>)<sub>95</sub>Al<sub>5</sub>, Cu-, La-, Ca-, and Ce-based BMGs as a function of temperature were *in situ* measured down to liquid nitrogen temperature [256–261]. The temperature variations of  $v_l$  and  $v_s$  for these BMGs are shown in Fig. 41a–c. Both  $v_l$  and  $v_s$  increase roughly in linear with decreasing  $T$  in cooling process for these BMGs. This suggests that bonding strength in the glassy alloys decreases with increasing temperature and has similar temperature dependence of sound velocities to that of crystalline alloys [262]. The  $T$  dependence of acoustic velocities shows no measurable hysteresis effects down to the

liquid nitrogen temperature. The  $v_s$  has larger change compared with that of  $v_l$  upon the decreasing temperature meaning that temperature has larger effect on the transverse acoustic phonons than that of the longitudinal phonons in the BMGs [256].

The variations of the  $E$ ,  $G$ , and  $K$  of these BMGs obtained from the acoustic measurements are shown in Fig. 42. All the elastic moduli monotonously increase with decreasing temperature, indicating the continuous stiffness of these BMGs with decreasing temperature. The  $G$  and  $E$  exhibit markedly increment with the drop of temperature while the  $K$  only shows a slightly reduction. The changes of the shear and bulk moduli ratio ( $dG/dK$ ) from the liquid nitrogen temperature to ambient temperature [Vit1: 2.61,  $(\text{Cu}_{50}\text{Zr}_{50})_{95}\text{Al}_5$ : 2.63,  $\text{La}_{68}\text{Al}_{10}\text{Cu}_{20}\text{Co}_2$ : 3.14 and  $\text{Mg}_{65}\text{Cu}_{25}\text{Gd}_{10}$ : 2.69] is larger than that of conventional crystalline alloys ( $dG/dK = 2$ ) [226]. The variations of Poisson's ratio as a function of  $T$  (normalized to  $T_g$ ) for the four BMGs are shown in Fig. 43. The  $\nu$  shows the decreases with the decreasing temperature indicating that the temperature variation of  $\nu$  does not markedly depend on the type of the BMGs [256]. The change trend of the  $\nu$  upon temperature is also consistent with the behavior of conventional alloys [262]. Because the large  $\nu$  is correlated to a better ductility [56], the decrease of  $\nu$  in low temperature could suggest more disappointed deformation ability.

The temperature dependence of elastic constants of metallic glass can be universally modeled by the Varshni expression [225,263]

$$C(T) = C(0) - \frac{s}{\exp(\theta_E/T) - 1} \quad (6.1)$$

where  $C(0)$  is the value of the elastic constant at 0 K,  $\theta_E$  the effective Einstein temperature, and  $s$  an adjustable parameter related to the strength of the anharmonic interactions. This expression is based on the assumption that the thermal phonons, which are responsible for the anharmonic effects, can be represented approximately by  $\theta_E$ . The elastic moduli of these BMGs are well fitted with the Varshni expression as shown in Fig. 42. Through the Varshni fitting, the elastic moduli at 0 K are obtained and listed in Table 7. The parameter  $s$ , which is determined from temperature dependence of  $K$ , can

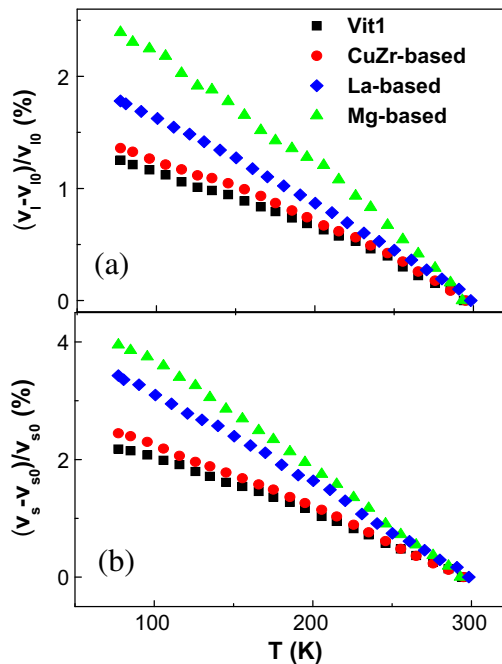


**Fig. 41.** The temperature dependences of  $\nu_l$  (a) and  $\nu_s$  (b) of Vit1,  $(\text{Cu}_{50}\text{Zr}_{50})_{95}\text{Al}_5$ ,  $\text{La}_{68}\text{Al}_{10}\text{Cu}_{20}\text{Co}_2$ ,  $\text{Mg}_{65}\text{Cu}_{25}\text{Gd}_{10}$  BMGs;  $\nu_l$  and  $\nu_s$  are the acoustic velocities at ambient temperature [256].

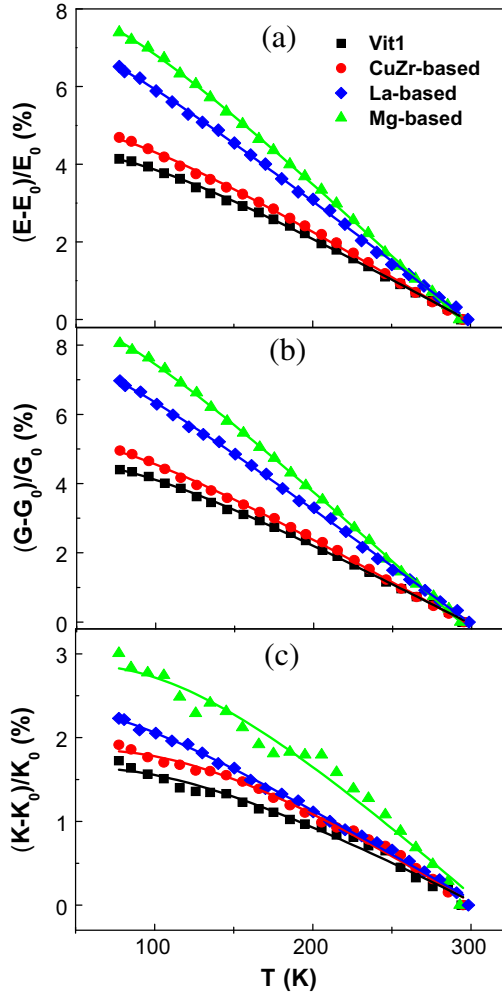


**Fig. 42.** The variations of the  $E$  (a),  $G$  (b), and  $K$  (c) of Vit1,  $(\text{Cu}_{50}\text{Zr}_{50})_{95}\text{Al}_5$ ,  $\text{La}_{68}\text{Al}_{10}\text{Cu}_{20}\text{Co}_2$ ,  $\text{Mg}_{65}\text{Cu}_{25}\text{Gd}_{10}$  BMGs with temperature. The  $E_0$ ,  $G_0$  and  $K_0$  are the elastic moduli at ambient temperature. The Varshni fits are shown in solid line [256].

be expressed as [264]:  $s = \frac{3k_B\theta_E}{\Omega_0} \gamma(\gamma + 1)$ , where  $\Omega_0$  represents the mean atomic volume, and  $\gamma$  is the Grüneisen parameter. Using the fitting parameters  $\theta_E$  and  $s$  from the Varshni expression for bulk modulus, the  $\gamma$  of the BMGs can be obtained and listed in Table 7. The values of  $\gamma$  for the BMGs are in the range of 1.3–1.8, which are consistent with that obtained by other method and much larger than that of the non-metallic glasses (less than 1.0) (see Table 4). The positive Grüneisen parameters indicate stiffness mode under low temperature.

The long wavelength phonon contribution to the heat capacity can be calculated from the elastic moduli by [50,51]:

$$C_p = \frac{2\pi^2 k_B^4}{5h^3 v_0^3} T^3 \quad (6.2)$$

where  $k_B$  and  $h$  is Boltzmann's constant and Planck's constant, and  $v_0$  is an average sound velocity given by:  $\frac{1}{v_0^3} = \frac{1}{3} \left( \frac{1}{v_l^3} + \frac{2}{v_s^3} \right)$ . The  $v_l$  and  $v_s$  at the low temperature limit (0 K) can be calculated through the moduli  $G(0)$  and  $K(0)$  yielding from the Varshni fitting:  $v_l(0) = \sqrt{(4G(0)/3 + K(0))/\rho}$  and

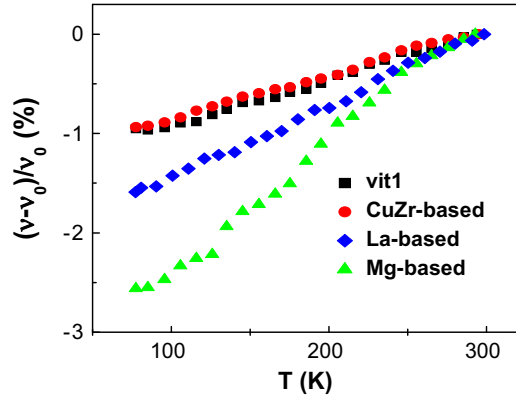


Fig. 43. The variations of Poisson's ratio  $\nu$  on temperature for Vit1,  $(\text{Cu}_{50}\text{Zr}_{50})_{95}\text{Al}_5$ ,  $\text{La}_{68}\text{Al}_{10}\text{Cu}_{20}\text{Co}_2$ ,  $\text{Mg}_{65}\text{Cu}_{25}\text{Gd}_{10}$  BMGs [256].

$\nu_s(0) = \sqrt{G(0)/\rho}$  [225]. Using these values, the acoustic contribution to the low temperature molar specific heat for the BMGs is obtained (listed in Table 7). The  $\theta_D$  for the MBGs (listed in Table 7) extended to 0 K can also be obtained by [50]:  $\theta_D = \frac{\nu v_0}{k_B} \left( \frac{3}{4\pi\Omega_0} \right)^{1/3}$ .

From above results, the entire temperature dependence of the shear and bulk moduli can be written as:

$$G(T) = G(RT) + \frac{S}{e^{\theta_E/RT} - 1} - \frac{S}{e^{\theta_E/T} - 1} \tag{6.3}$$

$$K(T) = K(RT) + \frac{S}{e^{\theta_E/RT} - 1} - \frac{S}{e^{\theta_E/T} - 1} \tag{6.4}$$

where  $RT$  is room temperature. The predictive ability of Eqs. (6.3) and (6.4) has been tested using experimental data obtained on a number of BMGs [256–261].

For comparison, the acoustic data of the non-metallic water-white glass with covalent bond (main constituent is  $\text{SiO}_2$ ) were measured at low temperatures. The water-white glass has a rather small

Table 7

The density  $\rho$ ,  $v_l$ ,  $v_s$ ,  $E$ ,  $G$ ,  $K$ , and Poisson's ratio  $\nu$  at ambient temperature.  $E(0)$ ,  $G(0)$ ,  $K(0)$ , and  $v_l(0)$ ,  $v_s(0)$ , which are the elastic moduli and ultrasonic velocities at low temperature limit, respectively, are calculated from the Varshni expression. The  $v_0(0)$  and  $C_p/T^3$  are the average sound velocity and molar specific heat at 0 K.  $\gamma$  is Grueneisen constant [256,259].

Sample	Vit1	$(\text{Cu}_{50}\text{Zr}_{50})_{95}\text{Al}_5$	$\text{Mg}_{65}\text{Cu}_{25}\text{Gd}_{10}$	$\text{La}_{68}\text{Al}_{10}\text{Cu}_{20}\text{Co}_2$	$\text{Ce}_{68}\text{Al}_{10}\text{Cu}_{20}\text{Co}_2$
$T_g$ (K)	625	695	406	374	341
$v_l$ (km/s)	5.116	4.699	4.272	2.911	2.612
$v_s$ (km/s)	2.415	2.120	2.232	1.379	1.322
$E$ (GPa)	96.3	88.7	49.8	31.7	31.4
$G$ (GPa)	35.5	32.3	19.0	11.7	11.8
$K$ (GPa)	112.0	115.8	44.2	36.6	30.3
$\nu$	0.357	0.372	0.312	0.355	0.328
$E(0)$ (GPa)	100.5	93.1	53.8	34.2	–
$G(0)$ (GPa)	37.1	34.0	20.7	12.6	–
$K(0)$ (GPa)	113.8	117.9	45.5	39.6	–
$v_l(0)$ (km/s)	5.180	4.763	4.382	3.028	–
$v_s(0)$ (km/s)	2.469	2.174	2.332	1.431	–
$v_0(0)$ (km/s)	2.777	2.450	2.606	1.610	–
$\gamma$	1.6	1.8	1.5	1.3	–
$C_p/T^3$ (J/mol K <sup>4</sup> )	$5.619 \times 10^{-5}$	$8.643 \times 10^{-5}$	$8.595 \times 10^{-5}$	$4.552 \times 10^{-4}$	–
$\theta_D(0)$ (K)	325.9	282.1	282.8	162.3	–

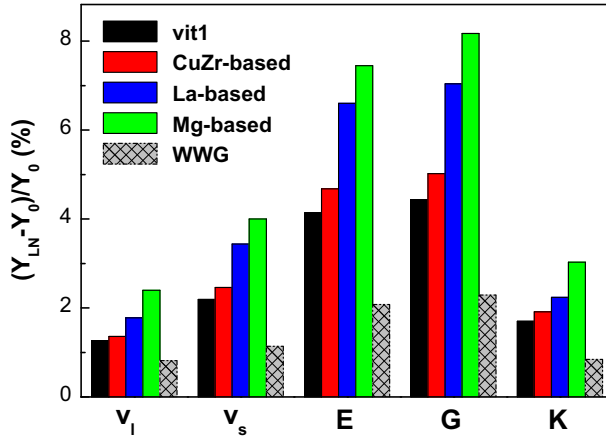


**Fig. 44.** The comparison for the relative changes  $\Delta Y = (Y_{LN} - Y_0)/Y_0$  ( $Y = v_l, v_s, E, G,$  and  $K$ ) between the state ( $Y_{LN}$ ) of liquid nitrogen temperature and the ambient state ( $Y_0$ ) for Vit1,  $(\text{Cu}_{50}\text{Zr}_{50})_{95}\text{Al}_5$ ,  $\text{La}_{68}\text{Al}_{10}\text{Cu}_{20}\text{Co}_2$ ,  $\text{Mg}_{65}\text{Cu}_{25}\text{Gd}_{10}$ , and oxide water-white glass (WWG) [256].

temperature effect on its elastic behavior in contrast to metallic glasses as contrasted in Fig. 44. The change of temperature has slight effect on oxide glass because of the strong directionality and large energy of the covalent bonding, while in BMGs, the metallic bond without directionality can be easily and continuously affected by temperature [265].

Cerium-based BMGs have attracted great attention due to their unique properties [123–128,169,187–199,266,267]. The pressure dependence of elastic moduli of Ce-based BMGs, unlike that of other BMGs with normal mode stiffening, exhibits anomalous elastic and acoustic behaviors under pressure [169]. This anomalous behavior is attributed to the intrinsic features of Ce element and the unique structure of the Ce-based BMGs. The cryogenic and acoustic experiments are performed on a representative  $\text{Ce}_{68}\text{Al}_{10}\text{Cu}_{20}\text{Co}_2$  BMG. The  $T$ -dependences of  $v_l$  and  $v_s$  of the Ce-based BMG are shown in Fig. 45. For the  $\text{Ce}_{68}\text{Al}_{10}\text{Cu}_{20}\text{Co}_2$ ,  $v_l$  and  $v_s$  show very different behavior with the decreasing temperature from that of other BMGs and conventional alloys [259]. Their dependences on temperature seriously deviate from the linear relationship. Furthermore, the  $v_s$  exhibits positive temperature coefficient which indicates the mode softening under cooling, and this is contrary to the regularity of other BMGs. The response to temperature of acoustic behaviors similar to that under high pressure

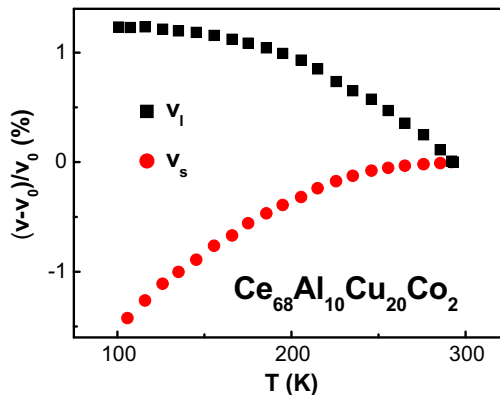


**Fig. 45.** The temperature dependences of  $v_l$  and  $v_s$  of  $\text{Ce}_{68}\text{Al}_{10}\text{Cu}_{20}\text{Co}_2$  BMG;  $v_0$  is the velocity at ambient temperature [259].

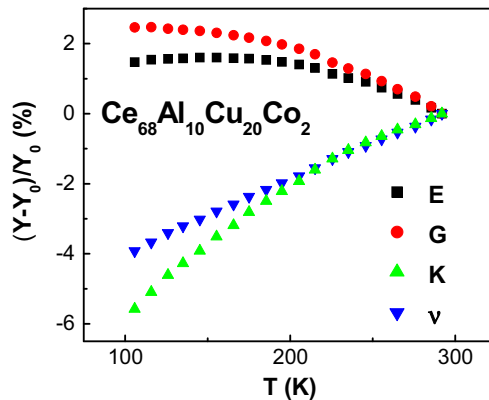


**Fig. 46.** The dependences of  $E$ ,  $G$ ,  $K$ , and  $\nu$  of  $\text{Ce}_{68}\text{Al}_{10}\text{Cu}_{20}\text{Co}_2$  BMG on temperature. The  $Y_0$  is the modulus at ambient temperature [259].

is unusual compared to other BMGs and crystalline alloys. The variations of the  $E$ ,  $G$ ,  $K$  and  $\nu$  as a function of temperature of the Ce-based BMG are shown in Fig. 46. Although  $E$  and  $G$  display stiffening mode with decreasing temperature,  $K$  abnormally decreases with decreasing temperature. The decrease of  $K$  directly indicates the softening of Ce-based BMG under cooling process. Moreover,  $E$ ,  $G$ , and  $K$  all completely deviate from the quasi-linear tendency in the measured temperature range [259]. In contrast to other BMGs, the  $K$  and Poisson's ratio of Ce-based BMG have the larger variations upon decreasing temperature [257,259]. These results show that the elastic moduli of Ce-based BMG are much more sensitive to cooling temperature. The monotonously increases of  $G$  and  $E$  under cooling indicate that there is a stiffening of transverse acoustic phonons in the Ce-based BMG.

As a major component of Ce-based BMGs, Ce plays a key role in the physical behavior and properties of the BMGs. For Ce element, because the energy level of the inner  $4f$  electrons is very closed to that of the outer or valence  $5d$  and  $6s$  levels, and thus only small amounts of energy can change the relative occupancy of these electronic levels giving rise to a variable electronic structure [268]. The valence of Ce can be changed by low temperature and high pressure. Under 100 K, the valence of Ce becomes a non-integral valence 3.67 from the valence 3 at room temperature, which corresponds to the lattice collapse arising from the change in electronic structure [269,270]. The mutable electronic structure leads to a complex phase diagram and the solid–solid isostructural  $\gamma \leftrightarrow \alpha$  phase transition of Ce element [268–270]. For the Ce-based BMGs, the abnormal elastic moduli response to pressure and temperature are closely related to the evolution of electronic configuration of Ce at low temperatures or under high pressure. The softening of longitudinal acoustic phonons and the sharp drop of  $K$  are corresponding to the relaxed structure and the shrinkage of atomic radius owing to the continuous increased valence of Ce under cooling. Without  $4f$  electrons and changeful electronic structure, La-based BMG displays a normal acoustic and elastic behavior under cooling, which confirms the abnormal elastic moduli of Ce-based BMG root in the alterative electronic configuration of Ce. The volume shrinkage of Ce-based sample upon cooling down to liquid nitrogen temperature was measured and compare to other representative BMGs [259]. The Ce-based BMG indeed exhibits larger contraction under cooling more than other BMGs, which indicates the intensive reduction of interatomic distance. Except for the normal cooling shrinkage, the shrinkage of atomic radius of Ce from the increasing valence occurs obviously. This implies a possible electronic phase transition in Ce-based BMGs at lower temperatures, most likely amorphous-to-amorphous phase transition, which also found under high pressure [197–199].

The elastic moduli are directly dominated by the second derivative of potential energy in the metastable structural state between atoms. Although the process of relaxation in metastable metallic glasses is very slow under low temperatures, it can be reflected by  $T$  dependent elastic moduli. It is found that the mechanical behavior of BMGs has been markedly changed at low temperatures

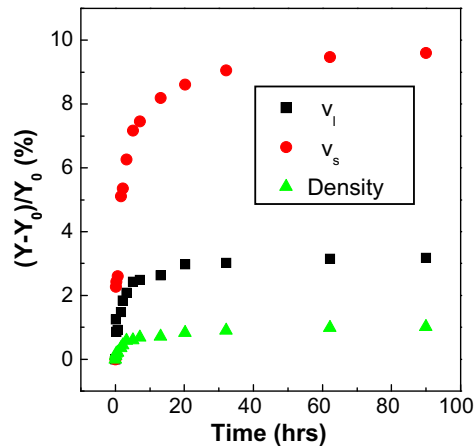


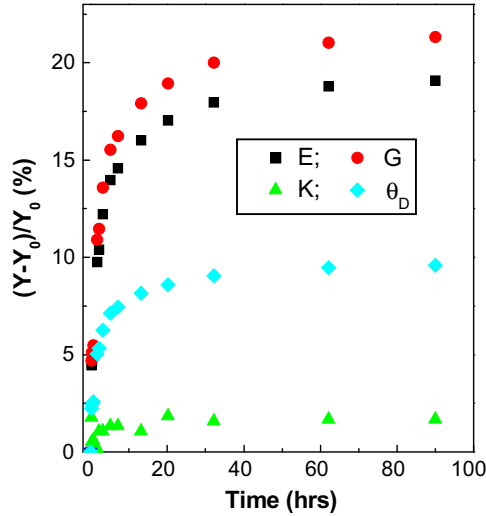
**Fig. 47.** The relative longitudinal and transverse velocities (a), and density (b), changes upon annealing time at 633 K for Vit1 ( $Y = \rho$ ,  $v_l$  and  $v_s$ ,  $Y_0$  is corresponding value for the as-prepared Vit1 [277–279]).

[271], and the change can be reflected by the Poisson's ratio [56,272,273]. So, the dependences of elastic moduli on temperature can provide useful information for understanding the relaxation, mechanical and physical properties of BMGs. Since the longitudinal wave interacts with electrons and the transverse one lacks such interactions, simultaneous longitudinal and shear waves measurements upon temperature can provide useful information about structural changes, phase-transition, and elastic and electronic contributions for glassy alloys [274,275].

## 7. Time dependence (structural relaxation) of elastic constants of metallic glasses

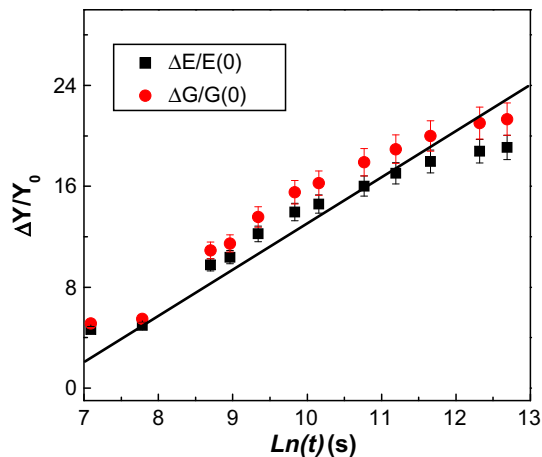
The properties of glasses change with time due to the structural relaxation. When kept isothermally, their density, optical, electrical, mechanical and elastic properties change spontaneously and continuously with time and progressively approach the properties of a disordered structure of lower energy [34–38]. Ultrasonic is the effective method which enables the measurements of high-frequency elastic moduli resulting from atomic motions underlying relaxation processes [275]. Since glassy alloys show a nonideal elastic behavior due to anelasticity similar to organic and inorganic glasses [276], it is expected that the elastic moduli measurements can reflect information on the structural relaxation induced changes of the physical properties of the BMGs [54]. The ultrasonic is also the effective method for detecting the microstructural changes resulting from ageing-induced primary nanocrystallization, phase separation and short-range order to medium range order change in BMGs, which are difficult to detect by other methods such as XRD and DSC methods.

Fig. 47 presents the variations of  $v_l$ ,  $v_s$ , and density of Vit1 isothermal annealed at 633 K ( $\sim 1.02T_g$ ) [the annealing temperature is in its supercooled liquid region (623–698 K)] for different times [277–279]. The acoustic measurements were performed on the annealed Vit1 at RT. The XRD patterns of the annealed Vit1 for various annealing times exhibiting no obvious crystalline peaks are observed up to 90 h annealing. While micro-structural change happens when Vit1 was annealed for prolonged time in the supercooled liquid region, and the annealed BMG have smaller first nearest-neighbor distance compared with the as-prepared state [278,279]. DSC traces confirm that the glass transition and the crystallization are significantly affected by annealing [279]. Both  $v_l$  and  $v_s$  increase with increasing annealing time as indicated in Fig. 47a. The change of  $v_s$  upon annealing time is much larger than that of  $v_l$ . The large density difference, 1% (the relative density change between as-prepared and fully crystallized BMG is about 1.2% [279]) can be seen in Fig. 47b, which demonstrates the densification of the BMG with increasing annealing time. The corresponding elastic constants  $E$ ,  $G$ , and  $K$  shown in Fig. 48 show similar change trend with increasing time. The large changes in the  $v_s$  (9.6%),  $\theta_D$  (9.6%),  $G$  (21.4%),



**Fig. 48.** The relative changes  $\Delta Y/Y_0 = (Y - Y_0)/Y_0$  of elastic constants and Debye temperature ( $Y = E, G, K$  and  $\theta_D$ ) of Vit1 with increasing annealing time. A large relative change of  $G, E$  and  $\theta_D$  and a smaller change of  $K$  in 90 h annealed sample relative to the as-prepared glassy state can be clearly seen [278].

$\rho$  (1.0%), and  $\nu$  (3.2%) between the BMG in as-prepared and 90 h annealed states confirms the microstructural change induced by isothermal annealing near  $T_g$ . The properties changes of  $G$  and  $E$ , which are structure-sensitive, are chosen to plot vs.  $\ln(t)$  in Fig. 49. It can be seen that the change of the  $G$  and  $E$  varies roughly linearly with  $\ln(t)$ , and an approximate relation  $\Delta Y/Y_0 \propto \ln(t)$ . This corresponds to a continuous spectrum of activation energies for the relaxation in the BMGs [280–284]. The change in the shear modulus of non-metallic glasses has been measured with time, and it has been suggested that the change follows a non-exponential, nonlinear change in the relaxation rate with time [285,286]. Olsen et al. [287] found that the MHz frequency shear modulus of Siloxane glass, kept at a temperature close to its  $T_g$ , decreases with time in a nonexponential nonlinear manner. Granato



**Fig. 49.** The relative changes  $\Delta Y/Y_0$  ( $Y = E, G$  for Vit1 with the logarithm of the isothermal annealing time  $\ln(t)$ ). The solid line is for guiding the eyes.

[288] concluded that the elastic moduli, enthalpy, and volume of a glass change in the same manner upon structural relaxation.

The change in elastic and vibrational properties with annealing time for one of the most stable  $Zr_{46.75}Ti_{8.25}Cu_{7.5}Ni_{10}Be_{27.5}$  BMG (Vit4) was studied to examine the structural-dependent properties of glasses [29]. The Vit4 was kept in a pure argon atmosphere at 100 Pa pressure for a prechosen period at  $523 \pm 0.1$  K ( $\sim 0.86T_g$ ), which is 127 K below its  $T_g$  for annealing. The annealing temperature is close to  $T_0$  of the Vogel–Fulcher–Tammann equation for viscosity [289]. After certain time, the sample was removed from this container and allowed to cool to room temperature to measure the acoustic velocities. Fig. 50 plots the  $v_l$ ,  $v_s$  and Poisson ratio  $\nu$  against the logarithmic annealing time  $t$  [29]. All the three quantities increase with  $\log(t)$  qualitatively in a stretched sigmoid shape manner approaching a limiting plateau value. The measured increase in  $v_l$  and  $v_s$  is  $\sim 2\%$ , while  $\nu$  decreases by  $\sim 1\%$  in a stretched sigmoid manner thereby indicating that the Vit4 becomes laterally stiffer on isothermal annealing. It is conceivable that some of Poisson's ratio decrease is due to the collapse of the weakly bonded regions or island of mobility in the glass structure. Because the high ultrasonic wave frequency of 10 MHz, the  $\nu$ ,  $G$ ,  $K$  and  $E$  values determined here are equal to the instantaneous or limiting high-frequency values. The  $G$ ,  $K$  and  $E$  are plotted against  $\log(t)$  in Fig. 51. The plots of  $K_\infty$  and  $G_\infty$  against  $\log(t)$  show that the two moduli increase according to,

$$K_\infty(t) = K_\infty(0) + [K_\infty(\infty) - K_\infty(0)](1 - \exp - [kt]^n) \quad (7.1)$$

with  $K_\infty(0) = 108.6$  GPa,  $K_\infty(\infty) = 111.7$  GPa, the rate constant,  $k = 7.37 \times 10^{-6} \text{ s}^{-1}$ , and the parameter  $n = 0.5$ , and

$$G_\infty(t) = G_\infty(0) + [G_\infty(\infty) - G_\infty(0)](1 - \exp - [kt]^n) \quad (7.2)$$

with  $G_\infty(0) = 34.91$  GPa,  $G_\infty(\infty) = 36.96$  GPa and the same values of  $k$  and  $n$  as for  $K$ . The value of  $n$  is comparable to  $n = 0.3\text{--}0.7$  observed for different glasses [286,287]. The bulk and shear moduli remain linearly related to each other as:  $K_\infty(t) = 54.83 \pm 0.76 + (1.54 \pm 0.02)G_\infty(t)$ . This is expected from the generalization of the Cauchy identity [41,290,291]. Annealing treatments reduce the free volume

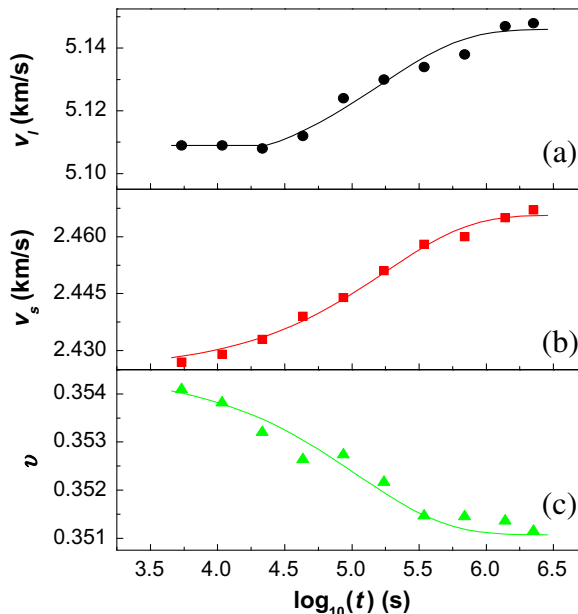


**Fig. 50.** (a) The plots of the density and the longitudinal sound velocity against logarithmic time for Vit4 at 523 K. (b) The corresponding plot of the transverse velocity. (c) The corresponding plot of the Poisson's ratio [29].

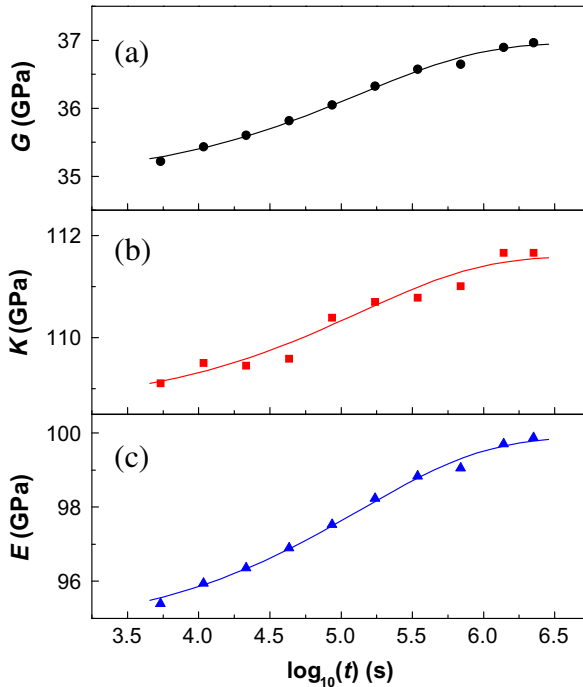


**Fig. 51.** (a) The bulk modulus  $K$  of Vit4 at 523 K is plotted against  $\log(t)$ . (b) The corresponding plot of the shear modulus. (c) The corresponding plot of the Young's modulus [29].

content and increase the atomic packing density, and then slight increase of the elastic moduli of various glasses. For instance, a 15% increase of  $E$  in a borosilicate glass ( $B_{22}\% B_2O_3$ ) after annealing of a quenched sample has been reported [292]. A large  $E$  increase from 106 (as-quenched) to 115 GPa in a  $Cu_{60}Zr_{22}Ti_{18}$  BMG was reported after annealing at  $T_g$ . A further improvement, up to 142 GPa, was observed after a 120-min long plateau at  $T_g$  [293].

The relaxation process can also be described as a decrease in the fictive temperature ( $T_f$ ) of a glass, i.e., the temperature at which the glass properties would correspond to that of a liquid if it is heated extremely rapidly, without allowing further relaxation to occur. Although a glass has no configurations available to its structure, it is said to have configurational entropy which is seen to be equal to the configurational entropy at  $T_f$  [284]. The configurational and vibrational properties, and elastic moduli of a glass change during its structural relaxation [284], but this does not explain why the rate of structural relaxation and configurational entropy at a fixed temperature decrease concomitantly [29]. In energy landscape paradigm [294–296], with annealing time, state point of the glass shifts to a deeper minimum of higher curvature and both the vibrational and configurational contributions to its properties decrease.

## 8. Correlations between elastic moduli and microstructure, glass formation, glass transition, fragility and melting

Understanding of the nature of glass, the temperature dependent slowing down of relaxation in glass-forming liquids, the flow in the glass and glass-forming liquids, the structural characteristics and the relation between microstructure and properties of glasses, and the dynamics in glasses are the central issues in glassy physics. However, when one tries to formulate an atomistic theory of glasses, one right away faces a major difficulty that it is a challenge even to describe the atomic

structure of glasses accurately. The glasses and liquids have a structure characterized by disorder and randomness, and yet they are condensed matter with strong interatomic correlation. This ‘many-body’ nature of glass makes it difficult to proceed theoretically [297] because we cannot benefit of the translational symmetry and resultant Bloch theorem. A glassy state is thought to be an unsuitable basis for understanding structure and properties, and the understanding the nature of glass and glass transition is regarded as the deepest and most interesting unsolved problem in modern condensed matter theory [298]. It is still rather vague how the structure affects the mechanical and physical properties for metallic glasses. In the absence of reliable theories the most frequently used concept by experimentalists is the old idea of free-volume advanced by Cohen and Turnbull [299–301]. While this theory has been successful as a phenomenology and its physical reality as applied to metallic glasses is questionable [302–304]. Over the last three decades, several other phenomenological theories have also been proposed to understand the nature of glass, glass transition, flow in glasses and glass formation. However, it has not been possible to quantitatively predict the experimental phenomena by these models [36,88]. The lack of a reliable theory of glass physics has led to the pursuit of correlations between various glasses or viscous liquids parameters, and the situation is similar in metallic glass field [56,82,87,145,272,305–363]. It is remarkable that metallic glasses with isotropic structure show behaviors that are in some way much more regular than that of crystals which can be readily measured by ultrasonic method.

Instantaneous elastic moduli of a glass are related to the curvature of the potential energy minimum and the anharmonic force contributions [35,364,365]. The deeper energy minima of lower energy have a higher curvature and would correspond to higher instantaneous elastic moduli [79]. Knuyt and Stals [366] have derived simple expressions for the shear and bulk moduli for amorphous metals. The derivation was accomplished by using a Gaussian distribution for the nearest-neighbor distance and a two-particle interatomic potential. The theory explains the lower values of Poisson’s ratio for a crystal in comparison with a glass of the same composition due to structural ordering. The theory can also describe qualitatively the dependence of Poisson’s ratio on changes of atomic structure in structural relaxation and hydrostatic compression of metallic glasses [49]. In structure point of view, the elastic characteristics (say Young’s modulus and shear modulus) at the continuum scale allow getting insight into the short- and medium-range orders existing in glasses [80,341]. In particular, the atomic packing density,  $C_g$ , and the glass network dimensionality appear to be strongly correlated with elastic moduli. Moreover, the temperature dependence of the elastic moduli brings light on the structural changes occurring above the glass transition temperature and on the depolymerization rate in the supercooled liquids. The softening rate depends on the level of cooperativity of atomic movements during the deformation process [80,341]. Furthermore, the elastic properties have the essential role for materials selection in mechanical design [80,367] because they closely correlate with mechanical properties of materials. In a word, the elastic moduli are key parameters which link the liquid and its glassy state, and correlate the microstructural features and macroscopic properties in glasses. The possible correlations among the properties or features and elastic constants could assist in understanding the long-standing issues of glass formation and structure, the nature of glass and searching for new glasses.

The ultrasonic studies of the elastic properties of more and more bulk metallic glasses have yielded a wealth of experimental elastic data previously inaccessible in metallic glasses owing to their small size. Significant amounts of data have been collected on thermal, mechanical and physical properties as well as the information on the microstructural characteristics for various BMGs with markedly different properties (e.g. fracture strength  $\sigma_F$ , fracture toughness  $K_{IC}$ , Vicker’s hardness  $H_v$ , thermodynamic parameters like  $T_g$ ,  $T_x$ ,  $T_m$  and fragility) [54,56,58,90,368–372]. For example, the La-, Sr-, Zn- and Ce-based BMGs with the ultralow elastic moduli values (e.g. Young’s modulus  $E < 30$  GPa) are comparable to those of oxides fused quartz and close to those of polymers [123–128,173], and the CaLi-based BMGs with lowest density and elastic moduli ( $\sim 23$  GPa) comparable to that of human bones [238]; and Co-based glassy alloy exhibits ultrahigh fracture strength of 5185 MPa, high Young’s modulus of 268 GPa [175]. Mg-, and Fe-based BMGs are very brittle, their fracture toughness  $K_{IC}$  value of  $1 \sim 2$  MPa  $m^{1/2}$  approaching the ideal brittle behaviors associated with brittle oxide silica glasses [373–376], and some BMGs with excellent plasticity have also been obtained [85,113,377–394]; the  $T_g$  of the BMGs ranges from as low as 299 K of Sr-based BMGs [173] to as high as 1151 K of tungsten

based metallic glass. The excellent glass-forming ability of the BMG systems has also permitted better characterization of the thermodynamics and kinetics of metallic glass formation, and plentiful data of fragility, viscosity, thermal stability, melting temperature, reduced glass transition temperature,  $T_{rg} = T_g/T_l$  (the key parameter to evaluate the GFA of an alloy) are obtained for various BMGs [54,56,58,90,368–371,395]. Therefore, the availability of various BMG samples, with marked differences in physical properties, thermodynamic and kinetic features and GFA, make it possible to establish some correlations among the properties or features and elastic constants. Based on these data, indeed, some clear correlations have been found. These correlations, as we listed in the following, could lead to smart searches for new BMGs with desirable properties rather than the trial-and-error method, and assist in the understanding of the glass nature, properties and formation.

### 8.1. The correlations between elastic properties and microstructure of metallic glasses

Elastic properties of a glass can reflect the information of its microstructure. In various glasses including non-metallic and metallic glasses, the elastic characteristics at the continuum scale allow to get insight into the short- and medium-range orders existing in glasses [42,49]. Poisson's ratio  $\nu$  is determined by the relation of the energy necessary for pure shear realization to the energy necessary for the separation of a body into particles remote from each other for infinitely large distances. Simultaneously,  $\nu$  is also determined by the indices of interatomic potential which characterize the stiffness of interatomic forces. That is, the values of  $\nu$  is determined both by the structure of the substance and the parameters of the interatomic potential. (The structural interpretation of Poisson's ratio is possible today only within semi-empirical correlations resulted from the relation of Grueneisen's theory [397] and Nemilov's theory [290,398].)

The structure of glass can be described by the atomic packing density,  $C_g$ . The  $C_g$ , which reflects the structural characteristics of glasses, is defined as the ratio between the minimum theoretical volume occupied by the ions and the corresponding effective volume of glass [172,341]:

$$C_g = \rho \sum f_i V_i / \left( \sum f_i m_i \right) \quad (8.1)$$

with for the  $i$ th constituent with  $A_x B_y$  chemical formula:  $V_i = 4/3\pi N(xr_A^3 + yr_B^3)$ , where  $N$  is the Avogadro number,  $r_A$  and  $r_B$  are the ionic or atomic radii,  $f_i$  is the molar fraction, and  $m_i$  is the molar mass. The  $C_g$  is estimated to be about 0.52 for a standard window glass and 0.45 for a-SiO<sub>2</sub>. An estimation of the packing density in metallic glasses was obtained by giving the atomic radius of each element its value in the corresponding pure metal. The relatively high values (>0.75) are obtained for multicomponent BMGs [172,341]. The various glasses have a wide range of value of  $\nu$  depending on glassy structure according to the survey [56,290,341]. It is found that the  $\nu$ ,  $C_g$ , and the glass network dimensionality appear to be strongly correlated in various glasses [341]. Fig. 52 presents the relation between  $\nu$  and  $C_g$  of various glasses [172]. The wide spectrum of glasses with different types of atomic bonds shows a clear trend. Maximum values for  $C_g$  ( $C_g > 0.7$ ) are observed for metallic glasses (based on cluster-like structural units) with larger Poisson's ratio. Atomic networks consisting primarily of chains and layers units (chalcogenides, low Si-content silicate, and phosphate glasses) correspond to  $C_g < 0.56$  and lower Poisson's ratio. The  $C_g$  increases monotonically with  $\nu$  from about 0.41 of a SiOC glass ( $\nu = 0.11$ ) to about 0.87 for a PdCuNi metallic glass ( $\nu = 0.4$ ). The glasses experience densification under high pressure. Various glasses of silica, soda-lime-silica, chalcogenide, and bulk metallic glasses under 25 GPa at RT show that there is a direct correlation between  $\nu$  and the maximum post-decompression density change:  $\Delta\rho/\rho \propto \exp(-b\nu)$  ( $b$  is constant) [207]. This indicates that  $\nu$  can be regarded as a useful index to predict the extent of densification of a glass with an arbitrary composition, and the Poisson's ratio closely correlates with the microstructure of various glassy materials.

The Poisson's ratio also correlates to the glass network connectivity [333]. Experimental data show that  $\nu$  decreases monotonically with the mean coordination number  $\langle n \rangle$  as shown in Fig. 53. The  $\langle n \rangle$ , which is a useful parameter to correlate the physical properties to the structural changes of glasses, is defined as  $\langle n \rangle = \sum f_i n_i$ , where  $f_i$  and  $n_i$  are the atomic fraction and the coordination number of the  $i$ th constituent, respectively. A highly cross-linked network, as exemplified by amorphous silica (a-SiO<sub>2</sub>), leads to a small  $\nu$  ( $\nu = 0.15$ ), whereas weakly correlated networks, such as for chain-based chalcogen-

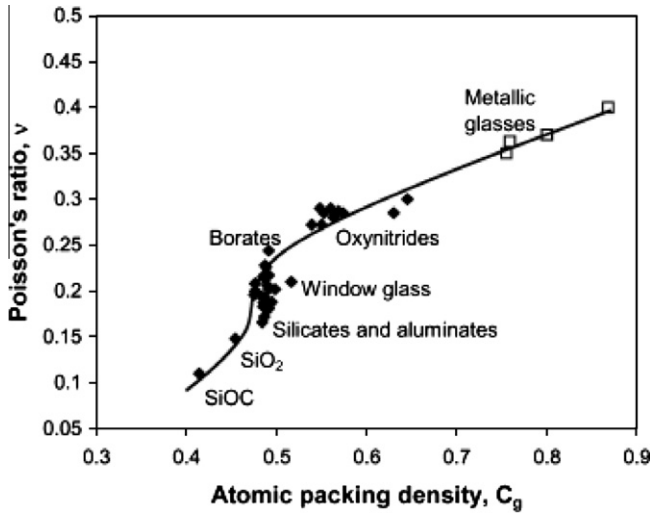


Fig. 52. Poisson's ratio vs. atomic network packing density for various glasses including metallic glasses [172].

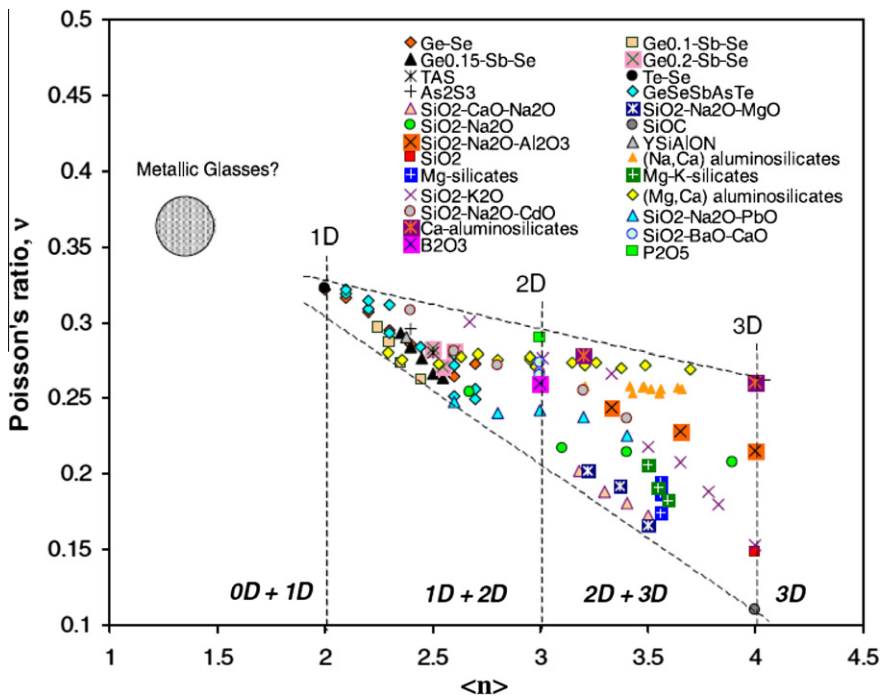


Fig. 53. Poisson's ratio vs. the average coordination number  $\langle n \rangle$  for different kind of glasses [341].

ide glasses or clusters packed metallic glasses, exhibit values of  $\nu$  higher than 0.3 (up to 0.4). Poisson's ratio also depends on the dimensionality ( $D$ ) of the structural units of glasses [341]. This tendency is shown in Fig. 54, and the tendency is particularly pronounced when elements with very different valences substitute one for the other [341]. It is noted that  $\nu$  from 0.30 to 0.40, which is the range for

BMGs consisting of quasi-equivalent cluster-type units eventually packed with an icosahedral-like medium-range order [89,90,399], is predicted by extrapolating the bounds of the Poisson's ratio domain to smaller cross-link degree or to 0D structural units.

The microstructure of various glasses also links to the bulk modulus. There is a correlation between  $K$  and the volume or density of various glasses [172]. The density or molar volume of an alloy reflects the information of the microstructure and has close relation with glass-forming ability, plasticity, and other properties for some BMGs [358,360,400,401]. The statistical survey of elastic moduli vs. density is applied to various rare earth (RE) based BMGs [402]. Fig. 55a shows  $K$  vs.  $\rho$  for different kinds of RE-based BMGs. One can see that the data are rather dispersed, and  $K$  and  $\rho$  do not exhibit a clear correlation. However, when the abscissa is changed into average molar volume,  $V_m$  ( $V_m = \text{molar mass/density}$ ), as shown in Fig. 55b, the  $K$  and  $V_m$  shows clear exponential correlation. To further verify the correlation, the survey is applied to much more different kinds of BMGs for those their  $K$  and  $V_m$  data are available. These BMGs include 54 kinds of Ca-, Mg-, RE-, Zr-, Cu-, Ni-, Fe-, Pt-, Pd-, Au-based BMGs with markedly different physical properties, and the data are listed in Table 8. Fig. 56 shows the relationships of  $K$  vs.  $\rho$  [Fig. 56a] and  $K$  vs.  $V_m$  [Fig. 56b]. Similarly, the  $K$  vs.  $\rho$  is quite scattered, while their  $K$  and  $V_m$  show clear correlation for these markedly different BMG systems.

The bulk modulus for a solid can be expressed as [32]:  $K = \Omega_0 \left( \frac{\partial^2 U}{\partial \Omega^2} \right)_{\Omega_0}$ , where  $U$  is the potential energy,  $U = \frac{1}{2} \sum z u_{ij}$ ;  $u_{ij}$  is the potential energy between two atoms of  $i$  and  $j$ ,  $u_{ij} = -Ar^{-n} + Br^{-m} = -A\Omega^{-n/l} + B\Omega^{-m/l}$ ,  $\Omega = r^3$  is the atomic volume;  $\Omega_0$  is the equilibrium atomic volume,  $V_m \sim N_A \Omega_0$ ,  $N_A$  is

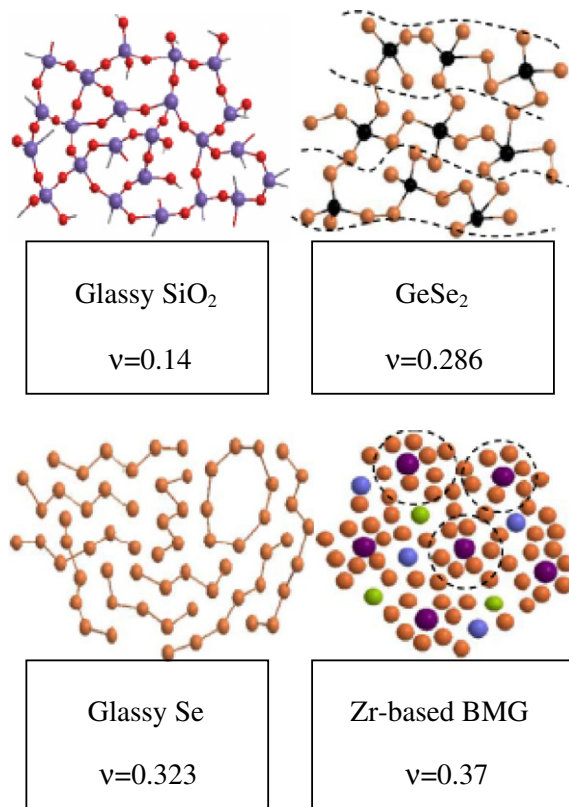


**Fig. 54.** Schematic drawings of glass atomic network structural units with increasing Poisson's ratio: a-SiO<sub>2</sub>, with each Si atoms bonded to four oxygen atoms; GeSe<sub>4</sub>, where layers of germanium (black spheres) are sandwiched between layers of selenium; a-Se that mainly consists of chain units but some rings (here Se<sub>8</sub>) may form too; and a Zr-based metallic glass possibly based on icosahedral-like clusters [341].

Avogadro constant;  $A$ ,  $B$ ,  $m$  and  $n$  are constants;  $z$  is the number of near-neighbor atoms. The first term of  $-A\Omega^{-n/3}$  represents the longer-range attractive energy and the second term of  $B\Omega^{-m/3}$  represents the corresponding short-range repulsive energy. The long-/short-range nature of the two forces is satisfied if  $m > n$ , which is also needed for solid stability. Minimum total potential energy is achieved when  $\partial u_{ij}/\partial r|_{r=r_0} = 0$ . This induces  $\frac{An}{Bm} = r_0^{-m+n}$ . By substituting  $B$  with:  $B = \frac{An}{mr_0^{-m+n}}$ ,  $K$  can be expressed as:  $K = \sum_{ij} \frac{An(m-n)}{9} z\Omega_0^{-\frac{n+3}{3}}$ , or  $K \propto V_m^{-\alpha}$ . From the data fit in Fig. 56b, the value of  $\alpha$  is determined to be about 2.6 for these BMGs. Then, the exponent  $n$  ( $\alpha = \frac{n+3}{3}$ ) of the attractive part of the Lennard-Jones potential is estimated to be 4.8. This physical analysis confirms the correlation between  $K$  and  $V_m$ . Actually, in crystals, the compounds that with similar atomic structure and electronic physical properties will share the same form in  $K \sim \Omega_0^{-\alpha}$  correlation [32]. It is thought that the BMGs have short-range order similar to crystals, and then, the similar  $K \sim V_m^{-\alpha}$  correlation existing in metallic glasses indicates that correlation derives from the short-range nature of atomic bonding.

Fig. 57a shows the relation between shear modulus  $G$  and  $V_m$  for various BMGs. The  $G$  also shows roughly correlation upon  $V_m$  for all the investigated BMGs systems, while  $K$  shows much stronger increase tendency with decreasing of  $V_m$ . For the systems with smaller  $V_m$ , such as Pd-, Pt-, Zr-, Ni-, Cu-, Au-based BMGs, the  $G$  is relatively smaller than that of the rare-earth- and Ca-based BMG. The different changing tendency of  $K$  and  $G$  stimulates us to survey the relationship between Poisson's ratio  $\nu$  (which is equivalent to the ratio  $K/G$ ) and  $V_m$  among various BMGs. Fig. 57b shows the data of  $\nu$  vs.

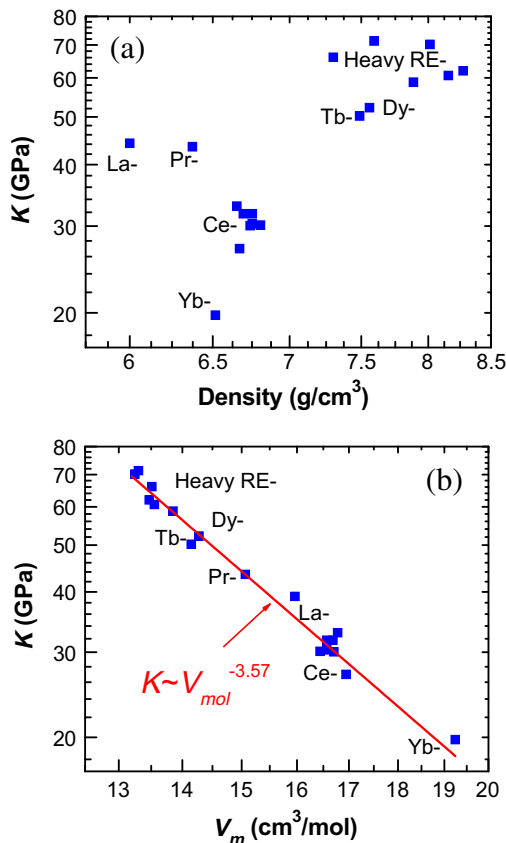


Fig. 55. (a) Bulk modulus  $K$  of 18 kinds of RE-based BMGs vs. density. (b) Much better correlation when change the abscissa axis to molar volume,  $V_m$ , shown in logarithmic coordinates. The red line is the linear fitting data [402].

**Table 8**

The bulk modulus  $K$ , shear modulus  $G$ , Poisson's ratio  $\nu$ , density  $\rho$  and average molar volume  $V_m$  for more than 50 kinds of different BMGs [54,56,58, and references therein].

Compositions	$\rho$ (g/cm <sup>3</sup> )	$V_m$ (cm <sup>3</sup> /mol)	$K$ (GPa)	$G$ (GPa)	$\nu$
Ca <sub>65</sub> Mg <sub>8.54</sub> Li <sub>9.96</sub> Zn <sub>16.5</sub>	1.956	20.249	20.15	8.95	0.307
Ca <sub>65</sub> Mg <sub>8.31</sub> Li <sub>9.69</sub> Zn <sub>17</sub>	1.983	20.1	18.45	8.98	0.291
Yb <sub>62.5</sub> Zn <sub>15</sub> Mg <sub>17.5</sub> Cu <sub>5</sub>	6.516	19.244	19.78	10.4	0.276
Ce <sub>70</sub> Al <sub>10</sub> Ni <sub>10</sub> Cu <sub>10</sub>	6.67	16.943	27	11.5	0.313
(Ce <sub>20</sub> La <sub>80</sub> ) <sub>68</sub> Al <sub>10</sub> Cu <sub>20</sub> Co <sub>2</sub>	6.653	16.777	32.93	11.86	0.334
Ce <sub>68</sub> Al <sub>10</sub> Cu <sub>20</sub> Nb <sub>2</sub>	6.738	16.703	30.06	11.65	0.328
(Ce <sub>80</sub> La <sub>20</sub> ) <sub>68</sub> Al <sub>10</sub> Cu <sub>20</sub> Co <sub>2</sub>	6.694	16.687	31.79	11.64	0.337
Ce <sub>68</sub> Al <sub>10</sub> Cu <sub>20</sub> Co <sub>2</sub>	6.752	16.568	30.33	11.8	0.333
Ce <sub>68</sub> Al <sub>10</sub> Cu <sub>20</sub> Ni <sub>2</sub>	6.753	16.565	31.77	11.98	0.332
Ce <sub>68</sub> Al <sub>10</sub> Cu <sub>20</sub> Co <sub>2</sub>	6.806	16.436	30.13	11.36	0.333
La <sub>55</sub> Al <sub>25</sub> Cu <sub>10</sub> Ni <sub>5</sub> Co <sub>5</sub>	6.0	15.896	44.2	15.6	0.335
Nd <sub>60</sub> Al <sub>10</sub> Ni <sub>10</sub> Cu <sub>20</sub>	6.689	16.12	42.8	13.5	0.358
Pr <sub>55</sub> Al <sub>25</sub> Co <sub>20</sub>	6.373	15.0683	43.48	15.42	0.324
Dy <sub>55</sub> Al <sub>25</sub> Co <sub>20</sub>	7.56	14.274	52.22	23.52	0.304
Tb <sub>55</sub> Al <sub>25</sub> Co <sub>20</sub>	7.488	14.148	50.19	22.85	0.302
Ho <sub>55</sub> Al <sub>25</sub> Co <sub>20</sub>	7.888	13.849	58.81	25.42	0.311
Er <sub>55</sub> Al <sub>25</sub> Co <sub>20</sub>	8.157	13.5509	60.7	27.08	0.306
Tm <sub>39</sub> Y <sub>16</sub> Al <sub>25</sub> Co <sub>20</sub>	7.301	13.511	66.1	29.7	0.304
Tm <sub>55</sub> Al <sub>25</sub> Co <sub>20</sub>	8.274	13.469	62	25.6	0.302
Lu <sub>39</sub> Y <sub>16</sub> Al <sub>25</sub> Co <sub>20</sub>	7.593	13.301	71.3	30	0.316
Lu <sub>45</sub> Y <sub>10</sub> Al <sub>25</sub> Co <sub>20</sub>	8.014	13.246	70.2	31.1	0.31
Lu <sub>55</sub> Al <sub>25</sub> Co <sub>20</sub>	8.694	13.200	69.2	30.6	0.316
Mg <sub>65</sub> Cu <sub>25</sub> Gd <sub>10</sub>	3.79	12.509	45.1	19.3	0.313
Mg <sub>65</sub> Cu <sub>25</sub> Y <sub>9</sub> Gd <sub>1</sub>	3.336	12.368	39.045	20.427	0.27
Mg <sub>65</sub> Cu <sub>25</sub> Y <sub>10</sub>	3.284	12.357	41.36	18.87	0.329
Mg <sub>65</sub> Cu <sub>25</sub> Y <sub>8</sub> Gd <sub>2</sub>	3.4285	12.233	39.854	20.12	0.29
Mg <sub>65</sub> Cu <sub>25</sub> Y <sub>5</sub> Gd <sub>5</sub>	3.65	12.053	39.1	19.7162	0.29
Mg <sub>65</sub> Cu <sub>25</sub> Tb <sub>10</sub>	3.98	11.9548	44.7	19.6	0.32
Zr <sub>64.13</sub> Cu <sub>15.75</sub> Ni <sub>10.12</sub> Al <sub>10</sub> (S2)	6.604	11.682	106.63	28.46	0.377
Zr <sub>65</sub> Cu <sub>15</sub> Ni <sub>10</sub> Al <sub>10</sub>	6.642	11.652	106.65	30.27	0.355
Zr <sub>61.88</sub> Cu <sub>18</sub> Ni <sub>10.12</sub> Al <sub>10</sub> (S1)	6.649	11.508	108.33	29.1	0.377
Zr <sub>55</sub> Al <sub>19</sub> Co <sub>19</sub> Cu <sub>7</sub>	6.2	11.442	114.9	30.8	0.352
Zr <sub>57</sub> Nb <sub>5</sub> Cu <sub>15.4</sub> Ni <sub>12.6</sub> Al <sub>10</sub>	6.69	11.438	107.7	32	0.379
Zr <sub>57</sub> Ti <sub>5</sub> Cu <sub>20</sub> Ni <sub>8</sub> Al <sub>10</sub>	6.52	11.425	99.2	30.1	0.375
At <sub>149</sub> Ag <sub>5.5</sub> Pd <sub>2.3</sub> Cu <sub>26.9</sub> Si <sub>116.3</sub>	11.6	10.911	132.3	26.5	0.406
(Zr <sub>0.59</sub> Ti <sub>0.06</sub> Cu <sub>0.22</sub> Ni <sub>0.13</sub> ) <sub>85.7</sub> Al <sub>14.3</sub>	6.608	10.739	112.6	34	0.370
Cu <sub>45</sub> Zr <sub>45</sub> Al <sub>7</sub> Gd <sub>3</sub>	7.122	10.707	105.86	33.163	0.358
Au <sub>55</sub> Cu <sub>25</sub> Si <sub>20</sub>	12.2	10.642	139.8	24.6	0.417
Cu <sub>46</sub> Zr <sub>54</sub>	7.62	10.301	128.5	30	0.391
Zr <sub>46.75</sub> Ti <sub>8.25</sub> Cu <sub>10.15</sub> Ni <sub>10</sub> Be <sub>27.25</sub>	6.014	10.205	111.9	37.2	0.356
Zr <sub>48</sub> Nb <sub>8</sub> Cu <sub>12</sub> Fe <sub>8</sub> Be <sub>24</sub>	6.436	10.173	113.6	35.2	0.367
Zr <sub>41</sub> Ti <sub>4</sub> Cu <sub>12.5</sub> Ni <sub>10</sub> Be <sub>22.5</sub>	6.125	9.786	114.1	37.4	0.354
Ni <sub>45</sub> Ti <sub>20</sub> Zr <sub>25</sub> Al <sub>10</sub>	6.4	9.608	129.6	40.2	0.359
Cu <sub>60</sub> Zr <sub>20</sub> Hf <sub>10</sub> Ti <sub>10</sub>	8.315	9.502	128.2	36.9	0.36
Fused quartz	2.201	9.096	36.9	31	0.17
Pd <sub>77.5</sub> Cu <sub>6</sub> Si <sub>16.5</sub>	10.4	8.742	166	31.8	0.409
Ni <sub>60</sub> Sn <sub>6</sub> (Nb <sub>0.8</sub> Ta <sub>0.2</sub> ) <sub>34</sub>	9.24	8.667	189	59.41	0.357
Pt <sub>57.5</sub> Cu <sub>14.7</sub> Ni <sub>5</sub> P <sub>22.8</sub>	15.2	8.652	243.2	33.4	0.434
Ni <sub>60</sub> Nb <sub>35</sub> Sn <sub>5</sub>	8.64	8.526	267	66.32	0.385
Pt <sub>60</sub> Ni <sub>15</sub> P <sub>25</sub>	15.7	8.509	202	33.8	0.42
Pd <sub>60</sub> Cu <sub>20</sub> P <sub>20</sub>	9.78	8.462	167	32.3	0.409
Pd <sub>64</sub> Ni <sub>16</sub> P <sub>20</sub>	10.1	8.286	166	32.7	0.405
window glass (SiO <sub>2</sub> )	2.421	8.2721	38.8	27.7	0.211
Pd <sub>40</sub> Cu <sub>40</sub> P <sub>20</sub>	9.3	7.97647	158	33.2	0.402
Pd <sub>39</sub> Ni <sub>10</sub> Cu <sub>30</sub> P <sub>21</sub>	9.152	7.96996	159.1	35.1	0.399
Fe <sub>53</sub> Cr <sub>15</sub> Mo <sub>14</sub> Er <sub>1</sub> C <sub>15</sub> B <sub>6</sub>	6.92	7.94116	180	75	0.32
(Fe <sub>74.5</sub> Mo <sub>5.5</sub> )P <sub>12.5</sub> (C <sub>5</sub> B <sub>2.5</sub> )		6.850	145.0	59.9	
Fe <sub>70</sub> Mo <sub>5</sub> Ni <sub>5</sub>   P <sub>12.5</sub>   C <sub>5</sub> B <sub>2.5</sub>		6.89	150.1	59.3	
Fe <sub>61</sub> Mn <sub>10</sub> Cr <sub>4</sub> Mo <sub>6</sub> Er <sub>1</sub> C <sub>15</sub> B <sub>6</sub>	6.89	7.47745	146	75	0.28

**Table 8** (continued)

Compositions	$\rho$ (g/cm <sup>3</sup> )	$V_m$ (cm <sup>3</sup> /mol)	$K$ (GPa)	$G$ (GPa)	$\nu$
Toughened glass (SiO <sub>2</sub> )	2.556	7.83516	61.9	34.4	0.266
Amorphous carbon	1.559	7.69872	11.4	9.01	0.18

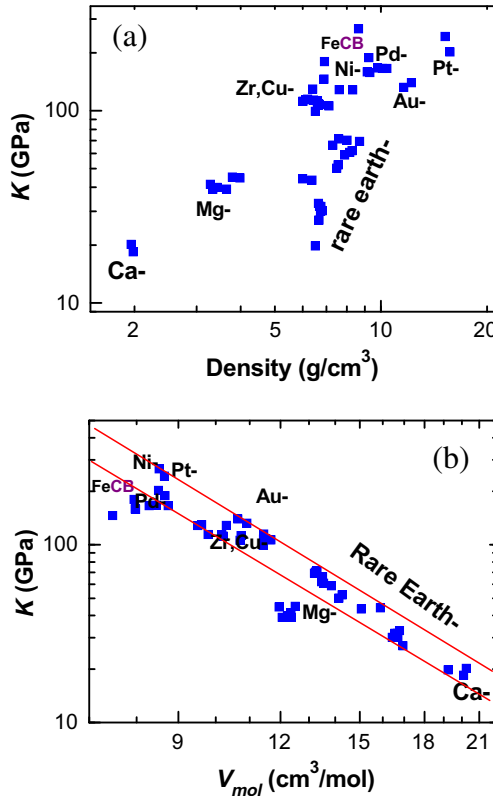


**Fig. 56.** (a)  $K$  vs. density for 54 kinds of various BMGs (including Ca-, Mg-, RE-, Zr-, Cu-, Ni-, Fe-, Pt-, Pd-, Au-based BMGs). (b) The data of  $K$  vs.  $V_m$  of the corresponding BMGs in logarithmic coordinates. The red line is the linear fitting data [402].

$V_m$  for various BMGs and some metalloid glassy materials. Remarkably, there is a clear trend that the BMGs with smaller  $V_m$  possess larger  $\nu$ . In the plasticity and Poisson's ratio correlation (we will show later), there exists a critical value of Poisson's ratio of 0.34 dividing plasticity from brittleness of various BMGs [56]. Below 0.34 brittle behavior is obtained or, values for  $K/G$  less than approximately 2.5 similarly result in a low toughness glass, and higher values of  $\nu$  give higher toughness and better plasticity. A similar critical value of  $V_m$  for metallic glasses (11.8 cm<sup>3</sup>/mol) exists to determine the tough and brittle in various BMGs, which is in rather good consistency with that of the plasticity and Poisson's ratio correlation. One can see from Fig. 57b that the cyan zone (including Mg-, RE-, Ca-based BMGs) shows the brittle behavior characterized with smaller  $\nu$  (<0.34) and bigger  $V_m$  (>11.8 cm<sup>3</sup>/mol). The magenta-colored zone (mainly including Pd-, Pt-, Zr-, Ni-, Cu-, Au-based BMGs) contains the ductile systems that is characterized with bigger  $\nu$  (>0.34) and smaller  $V_m$  (<11.8 cm<sup>3</sup>/mol). The cyan-colored zone (including typical brittle glasses such as amorphous-SiO<sub>2</sub>, amorphous-carbon, and two carbon and boron alloyed Fe-based BMGs of Fe<sub>61</sub>Mn<sub>10</sub>Cr<sub>4</sub>Mo<sub>6</sub>Er<sub>1</sub>C<sub>15</sub>B<sub>6</sub> and Fe<sub>53</sub>Cr<sub>15</sub>-Mo<sub>14</sub>Er<sub>1</sub>C<sub>15</sub>B<sub>6</sub>) containing the covalent bonding amorphous materials is characterized with small

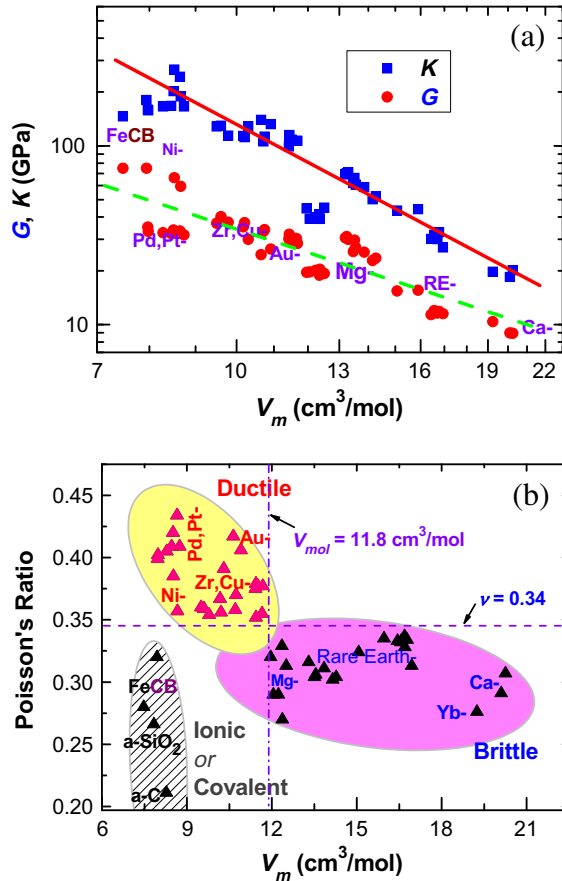


**Fig. 57.** (a) The shear modulus  $G$  of 54 kinds of BMGs shows a weak  $V_m$ -determined behavior, comparing to the  $K \sim V_m$  correlation. (b) The Poisson's ratio of various BMGs vs.  $V_m$ . The map can be divided by two lines as shown,  $\nu = 0.34$  and  $V_m = 11.8 \text{ cm}^3/\text{mol}$ , which determine the tough and brittle in various BMGs [402].

$V_m$  ( $V_m < 11.8 \text{ cm}^3/\text{mol}$ ) and small  $\nu < 0.34$ ). The result indicates that the plasticity of BMGs could be related to  $V_m$ . The plausible correlations between  $V_m$  and elastic moduli further confirm that the elastic moduli can effectively reflect the structural features of metallic glasses, and the close links between  $V_m$  and elastic moduli of BMGs can be used to sensitively reflect their structural change in BMGs induced by aging, crystallization, compositional change or microalloying, pressure and temperature, and mechanical treatments, which can assist in understanding of the microstructure features and nature of glasses.

Fig. 58 exhibits an example to study the aging induced structural change of a  $\text{Ce}_{68}\text{Al}_{10}\text{Cu}_{20}\text{Fe}_2$  BMG by monitoring their elastic moduli changes [403]. One can see that the minor relative change of the density, demonstrating the microstructural relaxation of the BMG, monotonically increase with the Poisson's ratio decreasing. This indicates that the microstructural change induced by aging can be reflected well by elastic moduli. Fig. 59 presents the variations density and Poisson's ratio of the Vit1 annealed at 633 K (10 K above  $T_g$ ) for various times. The large density difference of 1% (the relative density change between as-prepared Vit1 and its fully crystallized state is about 1.2%) indicating markedly structural change induced by isothermal annealing process (structural relaxation). The  $\nu$  shows reverse density change trend with increasing annealing time. The marked  $\nu$  change matches the density change confirming that elastic properties can sensitively reflect the structural information during relaxation process [29,192,278].

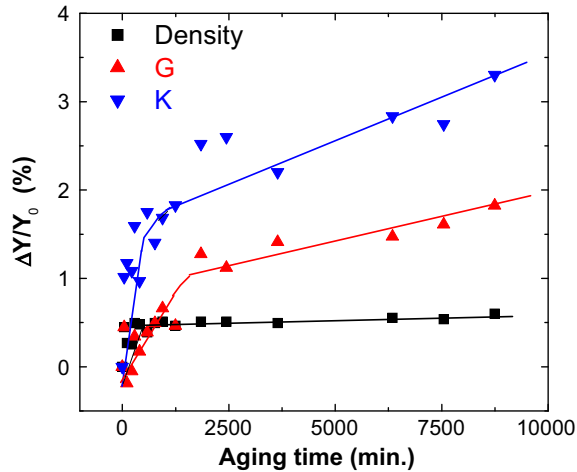


**Fig. 58.** The relative density and elastic moduli ( $K$  and  $G$ ) changes of the  $\text{Ce}_{68}\text{Al}_{10}\text{Cu}_{20}\text{Fe}_2$  BMG upon annealing time below its  $T_g$  (at  $60\text{ }^\circ\text{C}$ ). ( $Y = \rho, G, \text{ and } K$ ),  $Y$  is normalized by  $\Delta Y/Y_0 = (Y - Y_0)/Y_0$ , where  $Y_0$  is a corresponding value for the as-prepared BMG. The solid lines are for guiding the eyes.

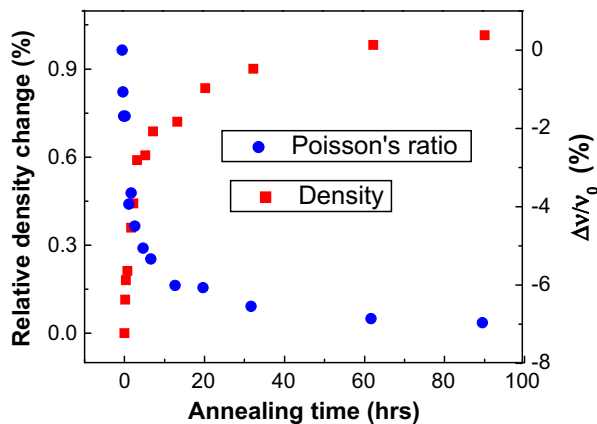


**Fig. 59.** The comparison of the relative density and Poisson's ratio changes of the Vit1 upon annealing time around its  $T_g$ .

The evolution of microstructure of BMGs tuned by composition changing can also be sensitively reflected by monitoring their elastic moduli change. Fig. 60 exhibits the evolution of microstructure of  $(\text{Zr}_{0.59}\text{Ti}_{0.06}\text{Cu}_{0.22}\text{Ni}_{0.13})_{100-x}\text{Al}_x$  ( $10 \leq x \leq 16$ ) BMGs as function of Al content [102]. The number of the atoms in unit volume,  $n$  (calculated by  $n = \rho/A$ , where  $A$  is the average atomic weight),  $G$ ,  $\theta_D$  and  $T_g$  are found to monotonically increase with increasing Al content. The relative increase of  $n$  is 1.4% when Al content increases from 10 to 16 at.%, and the corresponding increases of  $G$  and  $\theta_D$  are 12.4% and 6.4%, respectively. It can be clearly seen that a small change of  $n$ , meaning the subtle change of the microstructure of the alloy, leads to larger changes in  $G$ . Fig. 61 shows pressure induced increase in atomic packing density and the corresponding changes of  $G$  and  $\theta_D$ . Even the increase in atomic packing density resulting from pressure is only about 0.4% under 0.5 GPa, the  $G$  and  $\theta_D$  of the BMG show marked corresponding change and fit very well to the changing tendency of density or the microstructure, indicating that elastic properties can sensitively reflect subtle change of microstructure in the short-range scale induced by pressure [102]. Similarly, the temperature induced subtle structural changes can also be sensitively reflected by the changes of the elastic moduli.

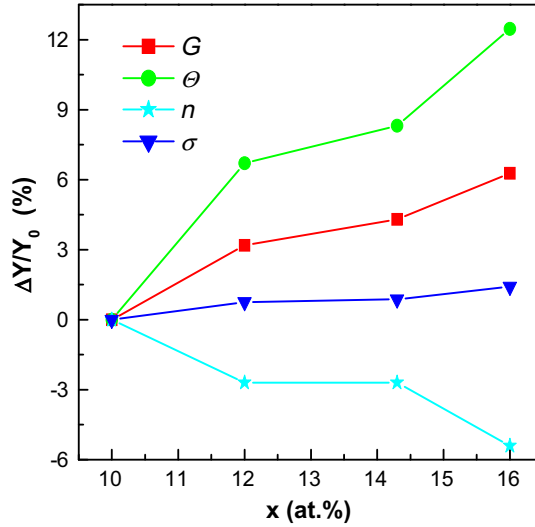


**Fig. 60.** The relative change of  $\Delta Y/Y_0 = (Y - Y_0)/Y_0$  ( $Y = n, G, \theta_D, T_g, Y_0$  is a normal value for the BMG with 10 at.% of Al) upon Al content for the  $(Zr_{0.59}Ti_{0.06}Cu_{0.22}Ni_{0.13})_{100-x}Al_x$  BMG. The number of the atoms in unit volume  $n$  is calculated by  $n = \rho/A$ , where  $A$  is the average atomic weight [102].

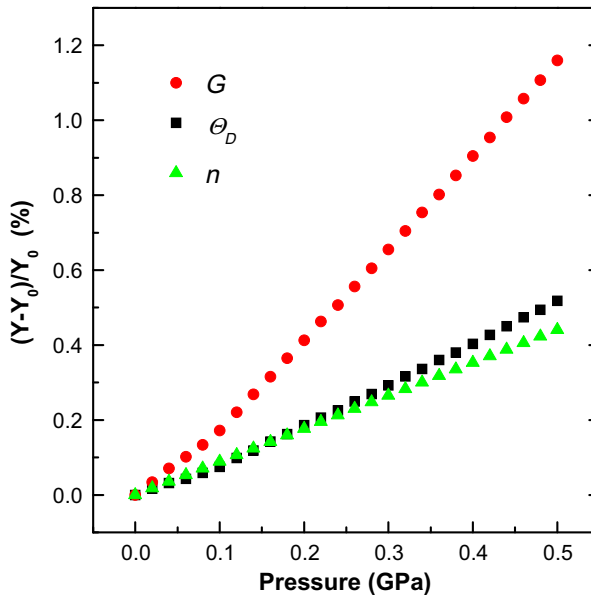


**Fig. 61.** The relative change of  $\Delta Y/Y_0 = (Y - Y_0)/Y_0$  ( $Y = n, G, \theta_D, Y_0$  is a normal value for the BMG at ambient pressure) upon pressure for the  $(Zr_{0.59}Ti_{0.06}Cu_{0.22}Ni_{0.13})_{86.7}Al_{14.3}$  BMG. The number of the atoms in unit volume  $n$  is calculated by  $n = \rho/A$ , where  $A$  is the average atomic weight [102].

Microalloying even in a minute trace can also induce significantly change of microstructure of the BMGs [126]. Fig. 62 exhibits that as low as 0.2 at.% of Co addition can dramatically change the density in a simple cerium-based  $Ce_{70-x}Al_{10}Cu_{20}Co_x$  ( $0 \leq x \leq 5$  at.%) BMG accompanying with a fragile to

strong transition and markedly  $G$  and  $K$  changes [126]. Further experimental results show that the sharp increase of density and  $G$  and  $K$  of  $Ce_{70-x}Al_{10}Cu_{20}Co_x$  alloys induced by Co addition is correlated with a dramatic increase of Al site symmetry, as reflected by decreasing quadrupole frequency measured by  $^{27}Al$  nuclear magnetic resonance (NMR) [267]. The comparison of the change of quadrupole frequency induced by minor tuning of Co concentration shows the change and evolution of cluster symmetry of the Al-centered icosahedral clusters, which is the predominant structural building block according to the structure model [89,90,267]. Similar phenomenon has also been observed in CuZrAl BMG-forming alloys with minor Gd addition [115,404]. The results indicate that the geometric property of site symmetry (the subtle local atomic-scale structural change) in metallic glasses, which is another important but less known characteristic of local structures, can also be effectively characterized by elastic moduli.

The metallic glasses exhibit a high elastic deformability about 2% and totally different deformation mechanism compared to their crystalline counterparts. It is proposed that irreversible deformation occurs at a high stress within the elastic region based on molecular-dynamics simulations of noncrystalline system during the prolonging compression process, while the irreversible deformation is very small and overwhelmed by the ordering process of structural relaxation. Pre-compression within the elastic region have been conducted on a typical  $Zr_{46.75}Ti_{8.25}Cu_{7.5}Ni_{10}Be_{27.5}$  BMG and ultrasonic method was used to monitor the structural change. Measurements show that the elastic moduli and the density of the specimen decrease with loading time indicating that an irreversible change of configuration occurs in the elastic region. Fig. 63 presents the variation of densities, acoustic velocities, and elastic moduli with different pre-compression times in elastic regime. The acoustic velocities and elastic moduli decrease obviously with increasing preloading time. And the sample pre-compression with greater stress shows a larger decrease in the moduli and the velocities, which indicates the pre-compression induced irreversible structural changes and softening of the glass in elastic region. Despite the large scatter in Fig. 63a, it can be seen that there is a slight decreasing tendency in densities, implying excess free volume created during the process of pre-compression. Due to that the longitudinal acoustic phonons are softer than the transverse phonons in the BMG, it can be seen from Fig. 63b that the change of longitudinal acoustic velocity is much larger than the transverse acoustic velocity. The relative variation of elastic moduli are presented in Fig. 63c, the  $E$  and  $G$  changes little and in an insignificant difference, whereas the  $K$  changes as much as twice of  $E$  and  $G$ . The bulk modulus represents the response to hydrostatic which involves bond stretching, it decreases with increasing equilibrium separation between atoms and it demonstrates that excess free volume can be created during the precompression. The irreversible structure changing should be related with the structural characteristic of metallic glasses and the local rearrangement of atoms. The fundamental unit of atomic motion that undergoes a shear deformation from one relatively low energy configuration to a

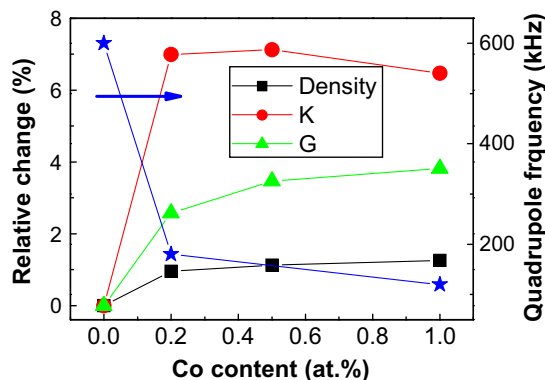
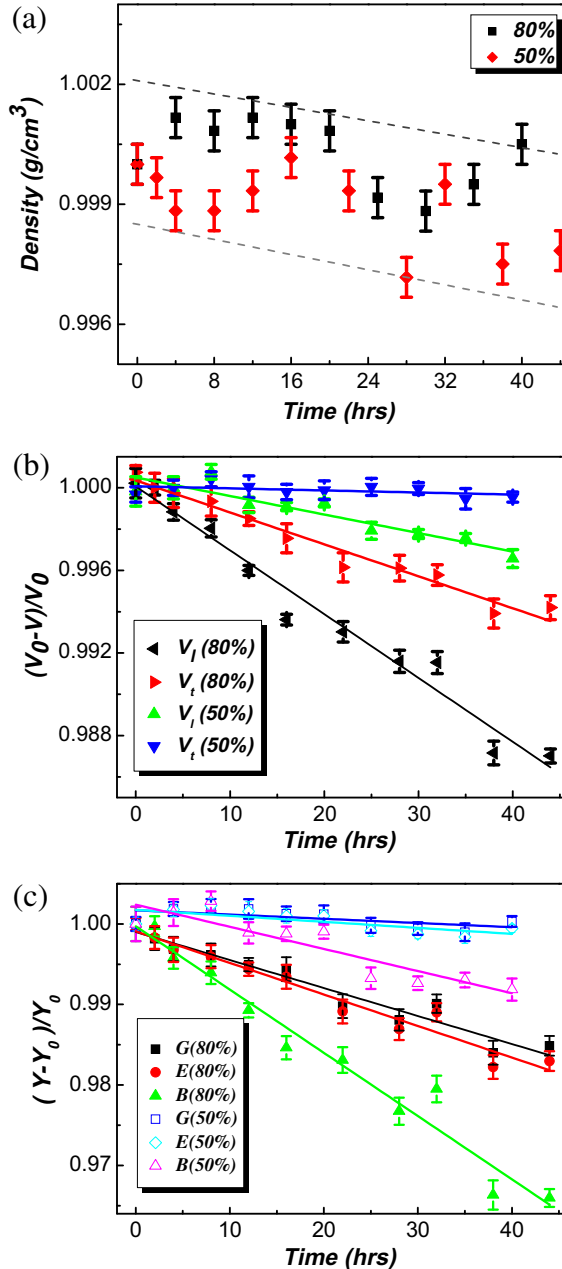


Fig. 62. The comparison of the change of quadrupole frequency (reflects the change and evolution of cluster symmetry upon minor tuning of Co concentration, or reflects the change of the local structure [267]), density and elastic constants of  $K$  and  $G$  [126].

second such configuration should exist in BMG. Before the yielding, some structural changing must have occurred in the BMG, which should be related with the plastic units. When the pre-compression was applied to the BMG, the plastic units can be activated by the durative stress. The irreversible rearrangements of constitute atoms in the plastic units corresponds to the structural change occurred



**Fig. 63.** Variation of (a) density, (b) acoustic velocity and (c) moduli with prolonging pre-compression time pre-compressed at 50% and 80% of the yield strength. The dash line in (a) is drawn to guide the eyes.

during our experiment. We note that the anisotropy of the metallic glasses induced by directional solidification and external treatments such as pre-loading, applied pressure, shot peening can be detected by the elastic stiffness coefficients.

Above correlations between microstructure and elastic moduli of metallic glasses indicate that the elastic moduli can sensitively reflect the subtle microstructural change of BMGs induced by changing of composition, internal or external stress, and so on. This is important because even though it is still a major challenge to describe the atomic structure of glasses accurately due to the ‘many-body’ random nature one can establish the links between the microstructural change (can be characterized by elastic moduli) and properties of glasses, and then provides insight on the characteristic of the microstructure and the relationship between structure and properties or features of glasses.

## 8.2. Correlation between elastic constants of metallic glasses and elastic constants of their constituents

In metallic composite materials, the elastic modulus of a composite is an average of the moduli of the constituent phases according to the so-called “rule of mixture” [405–407]. Because the metallic glasses inherit the structure of metals and alloys, the “rule of mixture” can be applied to metallic glasses for estimation of their elastic moduli from their compositions and the constitute elements with known elastic constants in crystalline form.

Applying the “rule of mixture” to a metallic glass for the mixing of constituent elements  $A_{f_1}B_{f_2}C_{f_3}\dots\dots(\sum f_i = 1)$ , the elastic moduli,  $M$  of the metallic glass can be calculate according to:

$$M = \sum \left( \frac{V_i \cdot f_i}{\sum V_i \cdot f_i} \cdot M_i \right) \quad (8.2)$$

and

$$\frac{1}{M} = \sum \left( \frac{V_i \cdot f_i}{\sum V_i \cdot f_i} \cdot \frac{1}{M_i} \right) \quad (8.3)$$

Assuming all elements have the same atomic volume, the equation can be simplified to [54,87,170]:

$$M^{-1} = \sum \left( f_i \cdot \frac{1}{M_i} \right) \quad (8.4)$$

and

$$M = \sum (f_i \cdot M_i) \quad (8.5)$$

where  $M_i$  is the modulus of constituent element,  $f_i$ , atomic percent of element  $i$ .  $V_{mi}$ , atomic volume, the values are calculated from:

$$V_{mi} = \frac{m_i}{\rho_i N_A} \quad (8.6)$$

where  $m_i$  and  $\rho_i$  are the molar atomic weight and density of the  $i$ -th component element.

Therefore, the elastic modulus of metallic glasses can be estimated by Eqs. (8.2) and (8.3) as function of composition and atomic volume. As is known from composite mechanics, this calculation gives an upper bound on the predicted elastic modulus. The lower bound is given by an assumption of uniform stress rather than strain (corresponding to an average of compliances) [408]. Following the above equations, as an example, the Young’s modulus, the best-known and most commonly used elastic constant in engineering design, were calculated for more than 50 typical metallic glass systems with different components and compositions. It should be noted that the experimental Young’s modulus data from different groups were derived either by mechanical test or by ultrasonic method. The calculated values and the experimental derived ones are summarized in Table 9. A comparison plot between the calculated results and the experimental data is given in Fig. 64. Fig. 64a exhibits the results calculated by Eq. (8.2), and Fig. 64b is that by Eq. (8.3). Due to the experimental  $E$  data are from different groups measured by different methods which bring errors, some composition-dependent discrepancies maybe exist. However, it is clear that the results calculated by Eq. (8.2) are accord with the line

**Table 9**Data of experimentally and theoretically ( $E_c$ ) derived Young's moduli of typical BMGs [54,56,58,78,84, and references therein].

BMG	$E$ (GPa)	$E_c$ (GPa) Calculated by Eq. (8.2)	$E_c$ (GPa) Calculated by Eq. (8.3)	$E_c$ (GPa) Calculated by Eq. (8.4)
Vit1	101	113.8	88.7	105.5
Zr <sub>46.75</sub> Ti <sub>18.25</sub> Cu <sub>7.5</sub> Ni <sub>10</sub> Be <sub>27.5</sub>	100.5	113.6	85.8	103.9
Zr <sub>45.4</sub> Ti <sub>9.6</sub> Cu <sub>10.15</sub> Ni <sub>8.6</sub> Be <sub>26.25</sub>	100.9	113.0	86.3	103.8
Zr <sub>48</sub> Nb <sub>8</sub> Cu <sub>12</sub> Fe <sub>8</sub> Be <sub>24</sub>	95.7	109.3	84.5	100.4
Zr <sub>65</sub> Al <sub>10</sub> Ni <sub>10</sub> Cu <sub>15</sub>	83	81.1	74.0	79.1
Zr <sub>57</sub> Ti <sub>5</sub> Cu <sub>20</sub> Ni <sub>8</sub> Al <sub>10</sub>	82	84.2	76.5	82.1
Zr <sub>57</sub> Nb <sub>5</sub> Cu <sub>15.4</sub> Ni <sub>12.6</sub> Al <sub>10</sub>	87.3	85.4	76.6	82.6
Zr <sub>52.25</sub> Cu <sub>28.5</sub> Ni <sub>4.75</sub> Al <sub>9.5</sub> Ta <sub>5</sub>	90	88.9	78.9	85.2
Ti <sub>50</sub> Cu <sub>23</sub> Ni <sub>20</sub> Sn <sub>7</sub>	85.3	122.2	107.2	117.9
Ti <sub>50</sub> Ni <sub>24</sub> Cu <sub>20</sub> B <sub>1</sub> Si <sub>2</sub> Sn <sub>2</sub>	110	130.4	116.8	125.4
Ti <sub>40</sub> Zr <sub>25</sub> Ni <sub>3</sub> Cu <sub>12</sub> Be <sub>20</sub>	92.6	118.7	98.6	112.4
Sc <sub>36</sub> Co <sub>20</sub> Y <sub>20</sub> Al <sub>24</sub>	85.2	84.0	74.6	80.8
Dy <sub>46</sub> Y <sub>10</sub> Al <sub>24</sub> Co <sub>18</sub> Fe <sub>2</sub>	64.2	76.6	67.3	74.1
Gd <sub>36</sub> Y <sub>20</sub> Al <sub>24</sub> Co <sub>20</sub>	62.2	73.6	63.8	68.0
Nd <sub>60</sub> Fe <sub>20</sub> Al <sub>10</sub> Ni <sub>10</sub>	54.1	65.3	47.4	57.1
Pr <sub>60</sub> Al <sub>10</sub> Ni <sub>10</sub> Cu <sub>20</sub>	37.2	54.5	42.5	50.8
La <sub>66</sub> Al <sub>14</sub> Ni <sub>10</sub> Cu <sub>10</sub>	35.7	49.5	41.0	47.4
Ce <sub>70</sub> Al <sub>10</sub> Ni <sub>10</sub> Cu <sub>10</sub>	30.3	46.7	37.5	42.9
Cu <sub>50</sub> Zr <sub>50</sub>	84	88.9	81.0	89.3
(Cu <sub>50</sub> Zr <sub>50</sub> ) <sub>96</sub> Al <sub>4</sub>	88.7	88.2	80.5	88.3
(Cu <sub>50</sub> Zr <sub>50</sub> ) <sub>92</sub> Al <sub>8</sub>	93.7	87.4	80.0	87.4
Cu <sub>55</sub> Zr <sub>30</sub> Ti <sub>10</sub> Co <sub>5</sub>	130	103.8	92.6	102.6
Cu <sub>60</sub> Hf <sub>30</sub> Ti <sub>10</sub>	124	106.0	99.9	107.3
Cu <sub>60</sub> Hf <sub>10</sub> Zr <sub>20</sub> Ti <sub>10</sub>	101	102.7	94.3	103.1
Ni <sub>45</sub> Ti <sub>20</sub> Zr <sub>25</sub> Al <sub>10</sub>	114	119.6	96.9	110.1
Ni <sub>40</sub> Cu <sub>6</sub> Ti <sub>16</sub> Zr <sub>28</sub> Al <sub>10</sub>	111	115.3	93.9	106.5
Ni <sub>40</sub> Cu <sub>5</sub> Ti <sub>16.5</sub> Zr <sub>28.5</sub> Al <sub>10</sub>	122	114.8	93.6	106.1
Ni <sub>40</sub> Cu <sub>5</sub> Ti <sub>17</sub> Zr <sub>28</sub> Al <sub>10</sub>	133.9	115.2	93.9	106.4
Ni <sub>39.8</sub> Cu <sub>5.97</sub> Ti <sub>15.92</sub> Zr <sub>27.86</sub> Al <sub>9.95</sub> Si <sub>0.5</sub>	117	114.8	93.4	105.8
Ni <sub>60</sub> Nb <sub>35</sub> Sn <sub>5</sub>	183.7	143.6	118.6	136.4
Ni <sub>60</sub> Sn <sub>6</sub> (Nb <sub>0.8</sub> Ta <sub>0.2</sub> ) <sub>34</sub>	161.3	149.3	120.8	139.7
Ni <sub>60</sub> Sn <sub>6</sub> (Nb <sub>0.6</sub> Ta <sub>0.4</sub> ) <sub>34</sub>	163.7	156.2	126.2	145.5
Pd <sub>77.5</sub> Si <sub>16.5</sub> Cu <sub>6</sub>	96	105.1	90.1	96.4
Pd <sub>80</sub> Si <sub>20</sub>	70	101.7	85.8	92.0
Pd <sub>40</sub> Ni <sub>40</sub> P <sub>20</sub>	108	101.3	13.1	22.1
Pt <sub>60</sub> Ni <sub>15</sub> P <sub>25</sub>	96	106.1	12.0	18.4
Pd <sub>40</sub> Ni <sub>10</sub> Cu <sub>30</sub> P <sub>20</sub>	98	87.4	13.2	21.7
Mg <sub>65</sub> Cu <sub>25</sub> Gd <sub>10</sub>	56	57.5	50.3	54.4
Mg <sub>65</sub> Y <sub>10</sub> Cu <sub>15</sub> Ag <sub>5</sub> Pd <sub>5</sub>	59	58.8	52.1	55.0
Mg <sub>75</sub> Ni <sub>15</sub> Y <sub>10</sub>	61	59.2	50.0	52.7
Mg <sub>65</sub> Cu <sub>20</sub> Y <sub>15</sub>	69	58.1	52.0	54.6
Fe <sub>61</sub> Zr <sub>8</sub> Y <sub>2</sub> Co <sub>6</sub> Mo <sub>7</sub> Al <sub>1</sub> B <sub>15</sub>	222	210.4	153.1	186.5
(Fe <sub>0.75</sub> B <sub>0.2</sub> Si <sub>0.05</sub> ) <sub>96</sub> Nb <sub>4</sub>	180	218.6	163.6	190.5
[(Fe <sub>0.8</sub> Co <sub>0.2</sub> ) <sub>0.75</sub> B <sub>0.2</sub> Si <sub>0.05</sub> ] <sub>96</sub> Nb <sub>4</sub>	205	218.4	163.1	190.2
[(Fe <sub>0.8</sub> Co <sub>0.1</sub> Ni <sub>0.1</sub> ) <sub>0.75</sub> B <sub>0.2</sub> Si <sub>0.05</sub> ] <sub>96</sub> Nb <sub>4</sub>	208	227.4	122.8	167.3
Fe <sub>65.5</sub> Cr <sub>4</sub> Mo <sub>4</sub> Ga <sub>4</sub> P <sub>12</sub> C <sub>5</sub> B <sub>5.5</sub>	161	157.0	16.2	26.1
(Fe <sub>0.75</sub> B <sub>0.15</sub> Si <sub>0.1</sub> ) <sub>96</sub> Nb <sub>4</sub>	175	198.7	134.7	162.3
Fe <sub>77</sub> Ga <sub>3</sub> P <sub>9.5</sub> C <sub>4</sub> B <sub>4</sub> Si <sub>2.5</sub>	182	155.3	19.5	31.5
Fe <sub>48</sub> Cr <sub>15</sub> Mo <sub>14</sub> Er <sub>2</sub> C <sub>15</sub> B <sub>6</sub>	200	224.6	55.6	39.9
(Fe <sub>44.3</sub> Cr <sub>5</sub> Co <sub>5</sub> Mo <sub>12.8</sub> Mn <sub>11.2</sub> C <sub>15.8</sub> B <sub>5.9</sub> ) <sub>98.5</sub> Y <sub>1.5</sub>	257	214.1	53.2	38.4
Co <sub>43</sub> Fe <sub>20</sub> Ta <sub>5.5</sub> B <sub>31.5</sub>	268	258.5	233.9	249.0
W <sub>46</sub> Ru <sub>37</sub> B <sub>17</sub>	309	415.5	414.9	417.9
Ca <sub>65</sub> Ag <sub>35</sub>	20	31.0	23.0	27.2
Ca <sub>57</sub> Mg <sub>19</sub> Cu <sub>24</sub>	38	33.2	23.6	28.9
Au <sub>49</sub> Ag <sub>5.5</sub> Pd <sub>2.3</sub> Cu <sub>26.9</sub> Si <sub>16.3</sub>	74.4	83.2	74.7	78.9

$E = E_c$  well, indicating the suitability of Eq. (8.2) for calculation of the elastic moduli of the metallic glasses. Compared with the data in Fig. 64a, that in Fig. 64b exhibits remarkable spread, especially

the calculated results of Fe-based BMGs consisting of metalloids (B, C, P, for which the bond type changes on alloying, and metallic and covalent bonds coexist in the Fe-based BMGs). The calculation results of Zr–Be based and rare-earth based systems by Eq. (8.2) are slightly higher than experimental results. Contrarily, Eq. (8.3) gives a bit lower values. Actually, in composite materials Eq. (8.2) gives an upper bound of the predicted modulus, while Eq. (8.3) gives a lower bound of that. In Zr–Be based BMGs, the element Be is of extremely high modulus compared with other components, and that, the atomic percentage of Be is relatively high. These factors will over-weight the influence of Be, consequently, overestimate the calculation values by Eq. (8.2) but underestimate that by Eq. (8.3).

The simplified Eq. (8.4) can produce rather good results in most BMG systems though the effect of atomic volume is ignored. The effects of high modulus or huge atomic volume of component may be balanced by the ignorance of atomic volume. Eq. (8.4) is applied to different families of BMGs (about 20 various BMGs) and the calculated elastic constants ( $E$ ,  $G$ ,  $K$  and  $K/G$ ) are listed in Table 10. Fig. 65 shows the ratio between the experimental and calculated  $E$ ,  $G$ ,  $K$  and  $K/G$  (or alternatively  $\nu$ ) for these BMGs. The ratios range from 0.93 to 1.2 indicating that the elastic constants of the BMGs calculated using Eq. (8.4) is roughly in agreement with those obtained by the ultrasonic method. The results indicate that elastic constants of BMGs show a correlation with a weighted average of the elastic constants of the constituent elements, and the elastic moduli of the BMGs depend strongly on their metallic components, and can be calculated as a mean value of all elements based on the atomic percents of constituent elements [56]. This result also indicates that the BMGs can be considered as highly dense packing structure.

The theoretically derived data for various BMGs show good consistency with their corresponding experimental ones [56,124,139,169,408]. Thus, one can approximately adopt the calculated results even if the experimental data of a metallic glass are not known, or one can predict the elastic moduli for a non-existing metallic glass. This is of significance because as will be shown in the following the elastic constants correlate with some mechanical and physical properties,  $T_g$ , GFA, and even liquid fragility in the BMGs. These correlations then provide useful guidelines for the development of new BMGs with desirable properties by controlling the elastic moduli of the alloy through selection of constituents with suitable elastic moduli.

### 8.3. Correlation between elastic properties and glass formation

The mechanism of glass formation and the design of metallic glassy composition with excellent glass-forming ability and controllable physical, chemical and mechanical properties are one of the

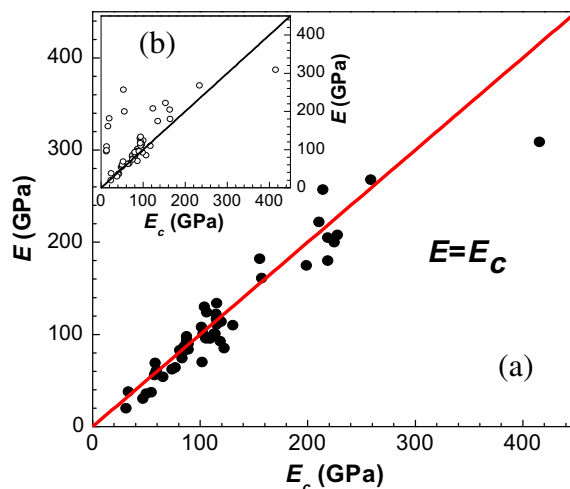


**Fig. 64.** Comparison plot between the calculated Young's modulus  $E_c$  and the experimentally derived  $E$  for different BMGs. (a) Calculated values with Eq. (8.2), (b) calculated values with Eq. (8.3).

**Table 10**

Calculated [according to Eq. (8.4) of  $M^{-1} = \sum (f_i \cdot \frac{1}{M_i})$ ] and experimental elastic constants for various typical BMGs, all the experimental elastic constants from Ref. [54,56,58,78,82, and references therein].

BMGs	K (GPa)		G (GPa)		E (GPa)		K/G	
	Exp.	Cal.	Exp.	Cal.	Exp.	Cal.	Exp.	Cal.
Zr <sub>41</sub> Ti <sub>14</sub> Cu <sub>12.5</sub> Ni <sub>10</sub> Be <sub>22.5</sub>	114.8	115.0	37.4	47.1	101.3	105.5	3.1	2.44
Zr <sub>46.75</sub> Ti <sub>18.25</sub> Cu <sub>7.5</sub> Ni <sub>10</sub> Be <sub>27.5</sub>	113.4	113.7	35.2	47.6	95.7	103.9	3.22	2.39
Zr <sub>53</sub> Ti <sub>5</sub> Cu <sub>20</sub> Ni <sub>12</sub> Al <sub>10</sub>	106.8	106.9	32.1	37.3	87.6	84.8	3.32	2.86
Zr <sub>48</sub> Nb <sub>8</sub> Cu <sub>12</sub> Be <sub>24</sub> Fe <sub>8</sub>	113.4	116.1	35.2	45.6	95.7	100.4	3.22	2.55
Zr <sub>57</sub> Nb <sub>5</sub> Cu <sub>15.4</sub> Ni <sub>12.6</sub> Al <sub>10</sub>	107.7	107.4	32.0	36.6	87.3	82.6	3.37	2.93
Zr <sub>65</sub> Al <sub>10</sub> Ni <sub>10</sub> Cu <sub>15</sub>	106.7	103.4	30.3	35.7	83.0	79.1	3.52	2.89
Nd <sub>60</sub> Al <sub>10</sub> Fe <sub>20</sub> Co <sub>10</sub>	46.5	45.9	19.4	22.2	51.2	57.2	2.39	2.07
Pd <sub>77.5</sub> Cu <sub>6</sub> Si <sub>16.5</sub>	174.7	156.6	32.9	35.0	92.9	96.4	5.31	4.48
La <sub>55</sub> Al <sub>25</sub> Cu <sub>10</sub> Ni <sub>5</sub> Co <sub>5</sub>	44.1	41.3	15.6	19.1	41.9	50.8	2.83	2.16
La <sub>66</sub> Al <sub>14</sub> Cu <sub>10</sub> Ni <sub>10</sub>	34.9	37.5	13.4	17.9	35.7	47.4	2.60	2.10
Cu <sub>60</sub> Zr <sub>20</sub> Hf <sub>10</sub> Ti <sub>10</sub>	128.2	122.3	36.9	41.4	101.1	103.1	3.47	2.96
Pr <sub>55</sub> Al <sub>12</sub> Fe <sub>30</sub> Cu <sub>3</sub>	41.4	44.4	18.2	22.0	47.6	54.9	2.27	2.02
Mg <sub>65</sub> Cu <sub>25</sub> Tb <sub>10</sub>	44.7	53.2	19.6	20.8	51.3	55.1	2.28	2.55
Cu <sub>50</sub> Zr <sub>50</sub>	101.2	114.3	32.0	39.1	87.0	89.3	3.16	2.92
(Cu <sub>50</sub> Zr <sub>50</sub> ) <sub>96</sub> Al <sub>4</sub>	113.7	112.1	32.4	38.3	88.7	88.3	3.51	2.92
(Cu <sub>50</sub> Zr <sub>50</sub> ) <sub>90</sub> Al <sub>7</sub> Gd <sub>3</sub>	117.1	104.4	32.4	36.9	89.0	86.0	3.61	2.82
Gd <sub>40</sub> Y <sub>16</sub> Al <sub>24</sub> Co <sub>20</sub>	58.0	53.5	23.5	27.6	62.2	70.6	2.47	1.94
Dy <sub>46</sub> Y <sub>10</sub> Al <sub>24</sub> Co <sub>18</sub> Fe <sub>2</sub>	58.5	55.8	24.4	29.3	64.2	74.1	2.40	1.90
Ni <sub>50</sub> Nb <sub>50</sub>	168.3	174.9	48.2	50.7	132.0	137.7	3.49	3.45
Ce <sub>68</sub> Al <sub>10</sub> Cu <sub>20</sub> Fe <sub>2</sub>	31.0	30.0	11.8	17.0	30.8	42.0	2.60	1.76
Er <sub>50</sub> Al <sub>24</sub> Co <sub>20</sub> Y <sub>6</sub>	65.1	58.5	27.0	31.2	71.1	80.2	2.41	1.88

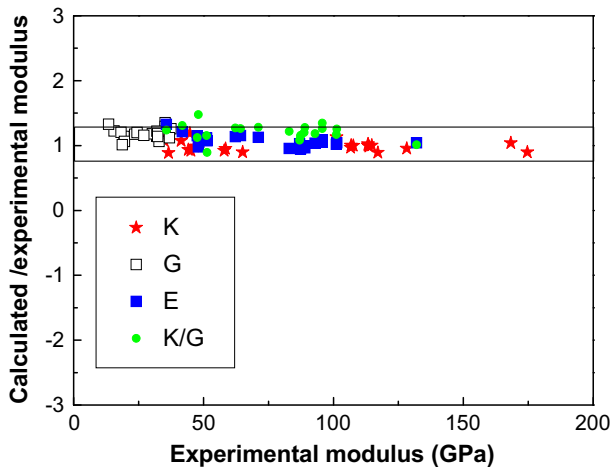


**Fig. 65.** The ratio of calculated elastic constants (according to Eq. (8.4)) to experimental results for various BMGs listed in Table 9 [56].

central issues in material science [1–14]. The GFA is extremely important in the glass-formation process in industries and, at the same time, it is also related to the fundamental issues of glass transition and glass nature. Substantial progress has been made in understanding these issues over the past decades, yet many key questions remain [54–58,368–371]. About hundreds bulky glass-forming alloy compositions, with wide critical glass-forming cooling range from 0.01 K/s to  $10^4$  K/s, are obtained. Although some rather general empirical rules, based on the thermodynamic, kinetic, nucleation and microstructural features, give useful directions in general [48–52,305–308,409–420], the

development of new BMGs in practical has always been “hit or miss” whether the resulting glass has excellent GFA or would turn out to be excellent in some properties. Therefore, a specific criterion for BMG formation, based on the insightful understanding of the nature of the glass, is of highly significance.

The quantitative measure of the GFA is given by the critical cooling rate  $R_c$ , which is the minimum cooling rate required for the formation of fully glass. The  $R_c$  can be estimated by [416]:  $dT/dt$  (K/s) =  $10/D^2$  (cm), where  $D$  is the typical dimension of the formed glassy alloy. In the past, a variety of schemes have been proposed to attain an understanding of why systems can be vitrified and of what determines the composition ranges over which glasses can be made [14,54–56,313,314,409–420]. These approaches are difficult to be quantified in the realistic practices.

The correlation between elastic moduli and GFA could provide another choice for the development of new BMGs with controllable properties. Poisson's ratio appears to be composition dependent and can reflect the GFA of a glass-forming alloy. The available data of  $R_c$  and Poisson ratio for various BMGs

**Table 11**

The  $T_{rg} = T_g/T_i$ ,  $\Delta T = T_x - T_g$ ,  $\gamma = T_x/(T_g + T_i)$  critical cooling rate for glass formation  $R_c$  and Poisson's ratio (or  $K/G$ ) for typical oxide glasses and various representative BMGs. (The data of  $T_{rg}$ ,  $\Delta T$ ,  $\gamma$  and  $R_c$  were taken from Refs. [54,409–419] and the references herein. The data of Poisson's ratio or  $K/G$  were taken from Refs. [54,56] and the references herein.)

Glasses	$T_{rg}$	$\gamma$	$\Delta T$ (K)	$R_c$ (K/s)	$\nu$	$K/G$
Zr <sub>41</sub> Ti <sub>14</sub> Cu <sub>12.5</sub> Ni <sub>10</sub> Be <sub>22.5</sub>	0.626	0.415	49.0	1.4	0.352	3.047
Zr <sub>46.75</sub> Ti <sub>8.25</sub> Cu <sub>7.5</sub> Ni <sub>10</sub> Be <sub>27.5</sub>	0.525	0.402	105.0	28.0	0.350	3.008
Zr <sub>48</sub> Nb <sub>8</sub> Cu <sub>12</sub> Fe <sub>8</sub> Be <sub>24</sub>	0.600	0.404	93.0	15.0	0.359	3.22
Zr <sub>65</sub> Al <sub>10</sub> Ni <sub>10</sub> Cu <sub>15</sub>	0.561	0.403	79.5	4.1	0.377	3.521
Zr <sub>45.4</sub> Ti <sub>9.6</sub> Cu <sub>10.15</sub> Ni <sub>8.6</sub> Be <sub>26.25</sub>	0.503	0.397	117	17.5	0.350	3.00
Zr <sub>65</sub> Cu <sub>12.5</sub> Be <sub>22.5</sub>	0.533	0.406	99	67.0	0.39	4.07
Zr <sub>35</sub> Ti <sub>30</sub> Cu <sub>8.25</sub> Be <sub>26.75</sub>	0.554	0.454	159	4.5	0.35	3.04
Zr <sub>33</sub> Ti <sub>30</sub> Cu <sub>7.5</sub> Be <sub>27.5</sub> Al <sub>2</sub>	0.550	0.439	144	3.0	0.332	2.65
Ti <sub>45</sub> Zr <sub>20</sub> Be <sub>35</sub>	0.531	0.380	57	25	0.36	3.12
Ti <sub>45</sub> Zr <sub>20</sub> Be <sub>30</sub> Cr <sub>5</sub>	0.530	0.390	77	20	0.35	2.92
Cu <sub>50</sub> Zr <sub>50</sub>	0.550	0.379	47	250	0.360	3.238
(Cu <sub>50</sub> Zr <sub>50</sub> ) <sub>92</sub> Al <sub>8</sub>	0.607	0.422	82	40	0.366	3.394
(Cu <sub>50</sub> Zr <sub>50</sub> ) <sub>92</sub> Al <sub>7</sub> Gd <sub>1</sub>	0.613	0.420	73	10	0.377	3.760
Cu <sub>60</sub> Zr <sub>20</sub> Hf <sub>10</sub> Ti <sub>10</sub>	0.630	0.407	43	110	0.368	3.75
Pd <sub>40</sub> Ni <sub>10</sub> Cu <sub>30</sub> P <sub>20</sub>	0.690	0.464	78.9	0.1	0.397	4.52
Pd <sub>77.5</sub> Si <sub>16.5</sub> Cu <sub>4</sub>	0.585	0.392	40.0	500	0.410	5.307
Pd <sub>40</sub> Ni <sub>40</sub> P <sub>20</sub>	0.585	0.409	63.0	0.17	0.403	4.795
Pt <sub>57.5</sub> Cu <sub>14.7</sub> Ni <sub>5.3</sub> P <sub>22.5</sub>	0.640	0.465	98	5.7	0.420	5.952
Mg <sub>65</sub> Cu <sub>25</sub> Tb <sub>10</sub>	0.573	0.425	73	40	0.309	2.283
Mg <sub>65</sub> Cu <sub>25</sub> Y <sub>10</sub>	0.551	0.401	54.9	50	0.305	2.299
Mg <sub>59.5</sub> Cu <sub>22.9</sub> Ag <sub>6.6</sub> Gd <sub>11</sub>	0.579	–	47	1.5	~0.30	2.3
Ca <sub>65</sub> Li <sub>9.96</sub> Mg <sub>8.54</sub> Zn <sub>16.5</sub>	0.550	0.347	22	40	0.307	2.2
Fe <sub>60</sub> Cr <sub>10</sub> Mo <sub>9</sub> C <sub>13</sub> B <sub>6</sub> Er <sub>2</sub>	0.557	0.379	46	16.0	0.297	2.128
Fe <sub>64</sub> Cr <sub>10</sub> Mo <sub>9</sub> C <sub>15</sub> Er <sub>2</sub>	0.562	0.381	47	40.0	0.275	1.887
La <sub>55</sub> Al <sub>25</sub> Cu <sub>10</sub> Ni <sub>5</sub> Co <sub>5</sub>	0.540	0.399	76.6	37.5	0.340	2.832
Pr <sub>60</sub> Cu <sub>20</sub> Ni <sub>10</sub> Al <sub>10</sub>	0.580	0.372	43	40	0.360	3.311
Sc <sub>36</sub> Al <sub>24</sub> Co <sub>20</sub> Y <sub>20</sub>	0.630	0.444	98	110	0.317	2.398
Ce <sub>68</sub> Al <sub>10</sub> Cu <sub>20</sub> Fe <sub>2</sub>	0.497	0.399	71	100	0.313	2.625
Nd <sub>60</sub> Fe <sub>20</sub> Co <sub>10</sub> Al <sub>10</sub>	0.51	0.372	–	150	0.317	2.611
Er <sub>50</sub> Al <sub>24</sub> Co <sub>20</sub> Y <sub>6</sub>	0.603	0.406	51	1.0	0.318	2.410
Dy <sub>46</sub> Al <sub>24</sub> Co <sub>18</sub> Fe <sub>2</sub> Y <sub>10</sub>	0.633	0.410	50	40.0	0.317	2.439
Tb <sub>36</sub> Y <sub>20</sub> Al <sub>24</sub> Co <sub>20</sub>	0.62	0.418	67	30.0	0.325	2.500
Tm <sub>39</sub> Al <sub>25</sub> Co <sub>20</sub> Y <sub>16</sub>	0.582	0.407	71	10	0.274	2.55
Yb <sub>62.5</sub> Zn <sub>15</sub> Mg <sub>17.5</sub> Cu <sub>5</sub>	0.575		20	55	0.276	1.98
Float glass				<0.01	0.23	1.50
Ti-glass				<0.01	0.17	1.20
Window glass				<0.01	0.211	1.40
Water-white glass				<0.01	0.238	1.57
Fused quartz				<0.01	0.17	1.26
Microcrystal glass				<0.01	0.266	1.80
Borosilicate glass				<0.01	0.24	1.60
Carbon glass				<0.01	0.187	1.26

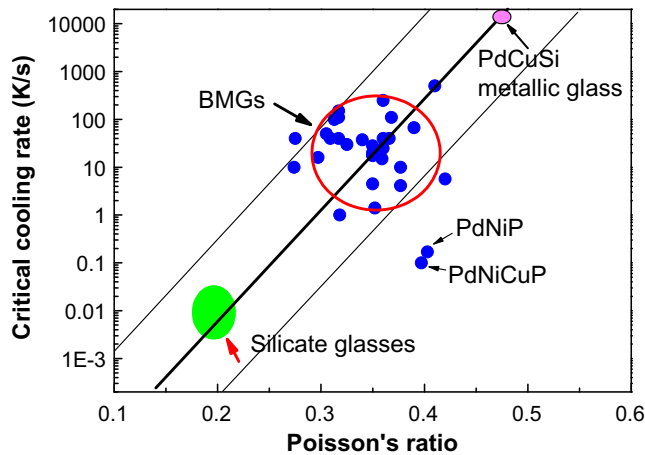


**Fig. 66.** The relation of critical glass formation cooling rate and the Poisson ratio  $\nu$  for oxide glasses, conventional metallic glasses available and BMGs.

are collected and listed in Table 11. Except  $\text{Pd}_{40}\text{Ni}_{40}\text{P}_{20}$  and  $\text{Pd}_{40}\text{Ni}_{10}\text{Cu}_{30}\text{P}_{20}$  metallic glasses (the two metallic glasses have been demonstrated to have special microstructural feature compared to other BMGs [369]), the BMGs and typical non-metallic oxide glasses listed in Table 11 have a roughly correlation between  $R_c$  and  $\nu$  as shown in Fig. 66. The glass with small value of  $\nu$  has higher GFA. The non-metallic glasses (e.g. oxide glass), whose  $\nu$  is less than 0.25, are of the lowest value of critical cooling rate of  $R_c$ . In contrast, the conventional metallic glasses such as  $\text{PdSiCu}$  with poor GFA, have high value of  $\nu$ . For BMGs with GFA between oxide glasses and conventional melt-spun metallic glasses, their value of  $\nu$  is between that of the conventional metallic glasses and oxide glasses.

It is found that the GFA and Poisson's ratio show remarkable correlation upon the changing of composition in some BMG-forming systems. Fig. 67 shows the clear correlation between GFA and Poisson's ratio in Ce-based and CuZr-based BMGs. The GFA of the Ce-based and CuZr-based BMGs are very sensitive to the minor addition of some minor elements. For example, in  $\text{Ce}_{70-x}\text{Al}_{10}\text{Cu}_{20}\text{Co}_x$  BMGs, even a trace of Co addition (0.2 at.%) can substantially improved the GFA of the alloy as shown in Fig. 67a. Significantly, one can see that the minor addition can also induce markedly Poisson's ratio change, and the critical diameter ( $D$ ) (representing the GFA of an alloy) as function of Co concentration in Ce-based BMGs, showing clear correlation between GFA and Poisson's ratio with the changing of the composition. The similar correlation can be seen in another typical CuZr-based BMG as shown in Fig. 67b.

The relation between fragility and GFA has been reported in various BMG-forming systems [315,420], and the fragility  $m$  (links to Poisson's ratio [56]) is regarded as an indicator of an alloy's GFA. The  $G$ , which depends on the interatomic distance and especially the repulsive branch of the interatomic potential, is closely related to the  $T_g$  and melting temperature,  $T_i$ . A good rule of thumb, associated with the ratio of  $T_g$  and  $T_i$ , has for many years been proposed for evolution of GFA by Turnbull [299,300]. That is, good metallic glass formers require  $T_g/T_i$  to be higher than 0.67 (the "2/3 rule"). It is successful empirical rule for finding new metallic glass system. The  $T_g$  and  $T_i$  themselves are correlated with  $E$  and  $G$  (see following section), respectively. The relationship between volumetric change (related to bulk modulus  $K$ ) and GFA has also been found in various BMGs [345]. Those results indicate that the GFA of an alloy is in connection with the elastic moduli. The plausible correlation between elastic moduli and GFA would provide a new route for metallic glasses design.

A possible phenomenological explanation for the correlations between the Poisson's ratio (or  $K/G$ ) and GFA of BMGs is based on the framework of the potential energy landscapes, PEL [421]. The GFA of a metallic glass-forming liquid is closely related to its flow, and the GFA characterizes how easily the occurrence of the flow and how easily of the flow of the melt can be frozen without crystallization, and

thus a glassy state can be obtained from its liquid state upon cooling. In liquid state, the alloy is supposed to locate at local minima (inherent state) in PEL, and the flow is the process that the system escapes from one local minimum to another or the disappearance of barrier between the neighbor local minima. The average barrier,  $\Delta E^*$ , between local minima in the PEL as schematically shown in Fig. 68 is mainly related to shear modulus  $G$  [82]. For the BMGs with low  $G$  or larger Poisson's ratio, the  $\Delta E^*$  is as small as such that the barrier is easy to be surmounted via small strain energy. On the other hand, surmounting the large energy barrier (small value of Poisson's ratio) will take some finite time and large energy, in order for the system to track the changes in the PEL through structural rearrangements [422]. The small  $\nu$  means atoms or molecules can hardly rearrange themselves to cooling, and the large  $\nu$  indicates the ease of atomic rearrangement. Therefore, the small  $\nu$  indicates the ease of freezing atomic rearrangement or form glass from liquid or high GFA in a glass forming system.

#### 8.4. Correlation between elastic moduli and glass transition

The glass-forming liquids are frozen into glasses at certain temperature through glass transition, and the dependence of glass transition temperature  $T_g$  on the cooling rate is weak. In general, the  $T_g$  changes by 3–5 K when the cooling rate changes by an order of magnitude

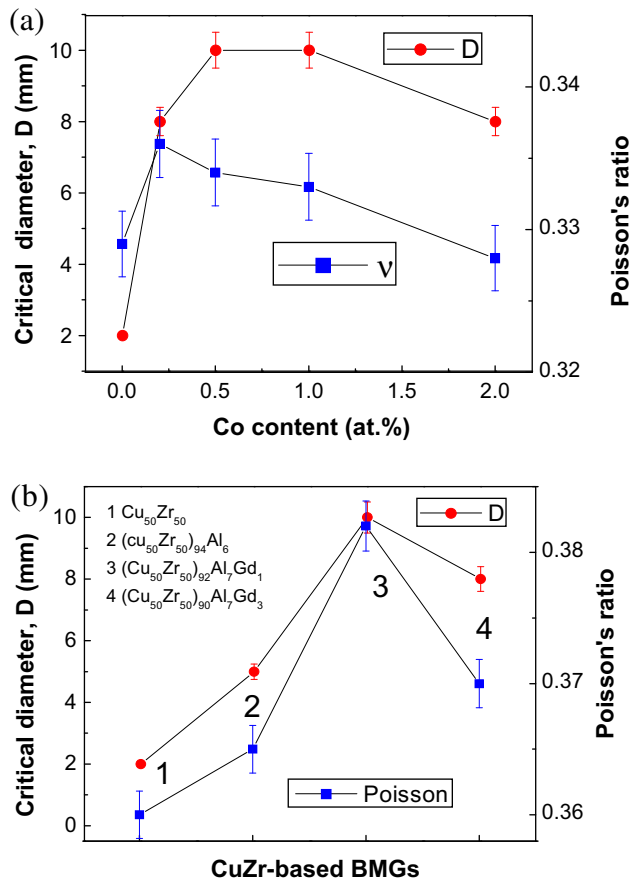


**Fig. 67.** (a) Critical diameter ( $D$ ) as function of Co concentration in  $\text{Ce}_{70-x}\text{Al}_{10}\text{Cu}_{20}\text{Co}_x$  ( $x = 0.2-2$  at.%) BMGs, showing clear correlation between GFA and Poisson's ratio. (b) Critical diameter as function of concentration changing induced by minor addition in CuZr-based BMGs, showing clear correlation between GFA and Poisson's ratio.

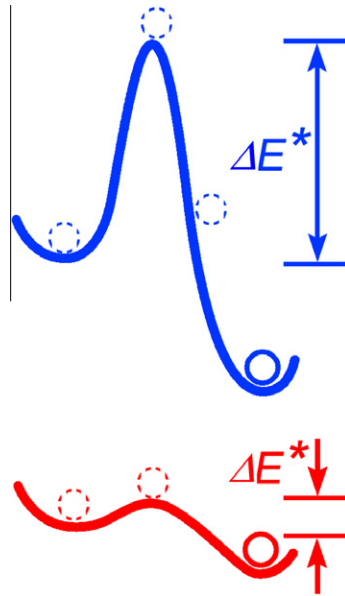


**Fig. 68.** Schematic diagram illustrating the correlation between flow behavior and the energy barrier  $\Delta E^*$  in Potential energy landscape.

[54,55,79,368,369,371], and the transition scope is narrow. Therefore, the  $T_g$  determined by atomic cohesive energy is an important materials characteristic [35,295]. The bulk glass-forming alloys, which exhibit distinct glass transition in their DSC trace and exceptional large supercooled liquid temperature range, permit better characterization of their glass transition and elastic properties [35,295], and the availability of various BMGs provides significant data of glass transition and elastic constants. Both the  $T_g$  and elastic moduli are determined by atomic cohesive energy, thus, the glass transition is expected to be closely related to the elastic moduli of BMGs. Table 12 collects all available relevant data on typical metallic glasses in the literatures. The BMGs include almost all kinds of developed BMGs based on different elements with representative compositions and markedly different values of  $T_g$  and elastic moduli. For example, the Sr-, Ce-, CaLi-, and La-based BMGs have ultraslow  $E$  value ( $\sim 30$  GPa, is comparable to those of polymers) and ultralow  $T_g$  ( $\sim 300$  K, approaching room temperature) [113–128,173,234,423] and W-based glassy alloy exhibits ultrahigh  $T_g$  (1151 K) and high  $E$  (309 GPa) [424]. These data can be used to check the possible correlation between  $T_g$  and elastic moduli in metallic glasses.

Even though the original data are obtained from different groups with various testing conditions, the data on these metallic glasses, plotted in Fig. 69, show clear correlations between glass transition temperature  $T_g$  and elastic modulus  $E$ . The similar correlation has also been reported in silica and other glasses [341,398]. The correlation between  $T_g$  and  $E$  in metallic glasses can also be expressed in terms of  $T_g$ . That is:

$$T_g = 2.5E \quad (8.7)$$

Higher value of  $T_g$  of a metallic glass gives higher value of  $E$ . Fig. 70 presents the relation of  $T_g$  and shear modulus  $G$  for various BMGs. It can be seen that  $T_g$  and  $G$  in these BMGs also have a roughly correlation of:

$$T_g \propto M \cdot G \quad (8.8)$$

where  $M$  is the molar mass of a metallic glass. A linear relationship between  $T_g$  and  $G$  in four types of glasses (silica-based optical glasses, germanate glasses, BeF<sub>2</sub>-based glasses, and chalcogenide glasses)

**Table 12**Data of  $E$ ,  $G$ ,  $\sigma_f$ ,  $\theta_D$ ,  $H_V$ , and  $T_g$  collected on representative metallic glasses (all compositions in at.%) and other non-metallic glasses.

Glasses	$\sigma_f$ (GPa)	$H_V$ (GPa)	$E$ (GPa)	$G$ (K)	$T_g$ (K)	$\theta_D$ (K)	Refs.
Zr <sub>41</sub> Ti <sub>14</sub> Cu <sub>12.5</sub> Ni <sub>10</sub> Be <sub>22.5</sub>	1.8	5.23	101	37.4	620	327	[54,369]
Zr <sub>46.75</sub> Ti <sub>8.25</sub> Cu <sub>7.5</sub> Ni <sub>10</sub> Be <sub>27.5</sub>	1.83	6.1	100	37.2	623	327	[54,369]
Zr <sub>65</sub> Al <sub>10</sub> Ni <sub>10</sub> Cu <sub>15</sub>	1.45	5.6	83	30.3	652	267	[54,371]
Zr <sub>52.25</sub> Cu <sub>28.5</sub> Ni <sub>4.75</sub> Al <sub>9.5</sub> Ta <sub>5</sub>	1.909	–	90	–	705	–	[54]
Zr <sub>61</sub> Cu <sub>17.3</sub> Ni <sub>12.8</sub> Al <sub>7.9</sub> Sn <sub>1</sub>	1.77	–	77.4	28.2	665	256.7	This work
Zr <sub>57</sub> Ti <sub>5</sub> Cu <sub>20</sub> Ni <sub>8</sub> Al <sub>10</sub>	1.77	5.4	82	30.1	657	270.1	[54,371]
Zr <sub>57</sub> Nb <sub>5</sub> Cu <sub>15.4</sub> Ni <sub>12.6</sub> Al <sub>10</sub>	1.8	5.9	87.3	31.9	687	274	[54]
Zr <sub>35</sub> Ti <sub>30</sub> Cu <sub>8.25</sub> Be <sub>26.75</sub>	–	–	86.9	31.8	578	–	[160]
Zr <sub>50</sub> Cu <sub>25</sub> Be <sub>25</sub>	–	–	96.8	35.8	633	–	[160]
Ti <sub>50</sub> Cu <sub>23</sub> Ni <sub>20</sub> Sn <sub>7</sub>	1.3	–	85.3	–	681	–	[416]
Ti <sub>50</sub> Ni <sub>24</sub> Cu <sub>20</sub> B <sub>1</sub> Si <sub>2</sub> Sn <sub>2</sub>	2.1	6.1	110	–	726	–	[56]
Ti <sub>45</sub> Zr <sub>20</sub> Be <sub>35</sub>	1.86	–	96.8	35.7	597	–	[159]
Ti <sub>45</sub> Zr <sub>20</sub> Be <sub>30</sub> Cr <sub>5</sub>	1.72	–	105.6	39.2	602	–	[159]
Cu <sub>50</sub> Zr <sub>50</sub>	1.92	5.8	85	32	733	231	[56]
Cu <sub>50</sub> Zr <sub>45</sub> Al <sub>5</sub>	1.89	5.4	102	33.3	701	278	[56,427]
Cu <sub>55</sub> Zr <sub>30</sub> Ti <sub>10</sub> Co <sub>5</sub>	2.31	–	130	–	714	–	[56]
Cu <sub>60</sub> Hf <sub>30</sub> Ti <sub>10</sub>	2.16	–	124	–	725	–	[56]
Cu <sub>60</sub> Hf <sub>10</sub> Zr <sub>20</sub> Ti <sub>10</sub>	1.95	7	101	36.9	754	282	[56]
Pd <sub>40</sub> Ni <sub>10</sub> Cu <sub>30</sub> P <sub>20</sub>	1.52	5.0	98	35.1	560	280	[56]
Pd <sub>77.5</sub> Si <sub>16.5</sub> Cu <sub>6</sub>	1.55	4.5	96	34.8	630	250	[428–430]
Pd <sub>40</sub> Ni <sub>40</sub> P <sub>20</sub>	1.7	5.3	108	38.6	583	292	[428–430]
Pd <sub>64</sub> Fe <sub>16</sub> P <sub>20</sub>	–	–	–	33.1	630	256	[428–430]
Pd <sub>80</sub> Si <sub>20</sub>	1.34	–	70	–	607	–	[428–430]
Pd <sub>80</sub> P <sub>20</sub>	–	–	–	27.1	607	224	[428–430]
Pt <sub>74.7</sub> Cu <sub>1.5</sub> Ag <sub>0.3</sub> P <sub>18</sub> B <sub>4</sub> Si <sub>1.5</sub>	1.20	3.95	–	32.4	479	–	113
(Fe <sub>0.75</sub> B <sub>0.2</sub> Si <sub>0.05</sub> ) <sub>96</sub> Nb <sub>4</sub>	3.16	10.5	180	–	835	–	[427]
[(Fe <sub>0.8</sub> Co <sub>0.2</sub> ) <sub>0.75</sub> B <sub>0.2</sub> Si <sub>0.05</sub> ] <sub>96</sub> Nb <sub>4</sub>	4.17	12.0	205	–	830	–	[427]
Fe <sub>61</sub> Zr <sub>8</sub> Y <sub>2</sub> Co <sub>6</sub> Mo <sub>7</sub> Al <sub>1</sub> B <sub>15</sub>	–	11.4	222	–	899	–	[56]
Fe <sub>68</sub> Cr <sub>3</sub> Mo <sub>10</sub> P <sub>6</sub> C <sub>10</sub> B <sub>3</sub>	3.1	9.0	180	67.7	714	–	[163]
Ni <sub>50</sub> Nb <sub>50</sub>	2.26	8.93	132	48.1	875	–	[56,425]
Ni <sub>45</sub> Ti <sub>20</sub> Zr <sub>25</sub> Al <sub>10</sub>	2.37	7.75	114	–	733	–	[56,425]
Ni <sub>40</sub> Cu <sub>5</sub> Ti <sub>17</sub> Zr <sub>28</sub> Al <sub>10</sub>	2.3	8.45	133.9	–	762	–	[56,425]
Co <sub>43</sub> Fe <sub>20</sub> Ta <sub>5.5</sub> B <sub>31.5</sub>	5.185	–	268	–	910	–	[175]
Co <sub>56</sub> Ta <sub>9</sub> B <sub>35</sub>	5.80	15.4	240.6	91.5	945	–	[672]
Mo <sub>52</sub> Cr <sub>14</sub> Fe <sub>14</sub> P <sub>12</sub> B <sub>8</sub>	–	12.6	–	–	1135	–	[424]
Mo <sub>40</sub> Co <sub>20</sub> Fe <sub>20</sub> B <sub>20</sub>	–	17.5	–	–	1108	–	[424]
Ta <sub>42</sub> Ni <sub>36</sub> Co <sub>22</sub>	2.7	9.7	170	–	983	–	[664]
W <sub>46</sub> Ru <sub>37</sub> B <sub>17</sub>	–	16.8	309	–	1151	–	[424]
W <sub>46</sub> Ru <sub>37</sub> B <sub>12</sub> Si <sub>5</sub>	–	13.2	229	–	1110	–	[424]
W <sub>45</sub> Ru <sub>36</sub> B <sub>17</sub> Hf <sub>2</sub>	–	16.5	262	–	1129	–	[424]
Mg <sub>65</sub> Cu <sub>25</sub> Tb <sub>10</sub>	0.80	2.83	51.3	19.6	417	272.9	[56]
Mg <sub>65</sub> Y <sub>10</sub> Cu <sub>15</sub> Ag <sub>5</sub> Pd <sub>5</sub>	0.77	–	59	–	437	–	[423]
Mg <sub>65</sub> Cu <sub>20</sub> Y <sub>15</sub>	0.82	2.6	69	–	420	–	[56]
Sr <sub>60</sub> Li <sub>5</sub> Mg <sub>15</sub> Zn <sub>20</sub>	0.30	0.95	19.7	7.71	331	156	[173]
Zn <sub>20</sub> Ca <sub>20</sub> Sr <sub>20</sub> Yb <sub>20</sub> Li <sub>11</sub> Mg <sub>9</sub>	0.40	0.82	16.0	6.30	323	–	This work
Zn <sub>40</sub> Mg <sub>11</sub> Ca <sub>31</sub> Yb <sub>18</sub>	0.66	1.80	28.8	–	396	–	This work
Al <sub>88</sub> Ni <sub>9</sub> Ce <sub>2</sub> Fe <sub>1</sub>	1.35	–	~70	–	–	–	[56]
Ca <sub>65</sub> Ag <sub>35</sub>	–	1.5	20	–	400	–	[56,426]
Ca <sub>57</sub> Mg <sub>19</sub> Cu <sub>24</sub>	0.545	–	38	–	387	–	[56,426]
Ca <sub>65</sub> Li <sub>9.96</sub> Mg <sub>8.54</sub> Zn <sub>16.5</sub>	0.53	1.35	23.4	8.95	320	220.7	[238]
Ce <sub>70</sub> Al <sub>10</sub> Ni <sub>10</sub> Cu <sub>10</sub>	0.40	1.5	30	11.5	359	144.1	[56]
Nd <sub>60</sub> Al <sub>10</sub> Fe <sub>20</sub> Co <sub>10</sub>	0.45	2.2	51	35.1	493	189	[56]
Gd <sub>36</sub> Y <sub>20</sub> Al <sub>24</sub> Co <sub>20</sub>	–	–	62.2	23.6	603	221.4	[56]
Hf <sub>39</sub> Al <sub>25</sub> Co <sub>20</sub> Y <sub>16</sub>	–	–	69.1	26.2	649	226.5	[56]
Tm <sub>39</sub> Al <sub>25</sub> Co <sub>20</sub> Y <sub>16</sub>	1.98	6.07	75.0	29.4	664	236	[118]
Lu <sub>45</sub> Y <sub>10</sub> Al <sub>25</sub> Co <sub>20</sub>	1.89	6.12	79.1	31.1	689	231	[119]
Yb <sub>62.5</sub> Zn <sub>15</sub> Mg <sub>17.5</sub> Cu <sub>5</sub>	–	1.52	26.5	10.4	381	132	[63]
La <sub>55</sub> Al <sub>25</sub> Cu <sub>10</sub> Ni <sub>5</sub> Co <sub>5</sub>	~0.5	3.0	41.9	15.6	466	183	[56]
La <sub>55</sub> Al <sub>25</sub> Co <sub>20</sub>	0.99	3.48	40.9	15.42	477	181	[138]

(continued on next page)

Table 12 (continued)

Glasses	$\sigma_f$ (GPa)	$H_v$ (GPa)	$E$ (GPa)	$G$ (K)	$T_g$ (K)	$\theta_D$ (K)	Refs.
Pr <sub>55</sub> Al <sub>25</sub> Co <sub>20</sub>	1.01	2.58	45.90	17.35	509	190	[138]
Tb <sub>55</sub> Al <sub>25</sub> Co <sub>20</sub>	0.83	4.42	59.53	22.85	612	203	[138]
Dy <sub>55</sub> Al <sub>25</sub> Co <sub>20</sub>	0.72	4.70	61.36	23.52	635	205	[138]
Ho <sub>55</sub> Al <sub>25</sub> Co <sub>20</sub>	0.87	4.14	66.64	25.42	649	210	[138]
Er <sub>55</sub> Al <sub>25</sub> Co <sub>20</sub>	1.12	5.45	70.72	27.08	667	215	[138]
Au <sub>76.9</sub> Si <sub>9.45</sub> Ge <sub>13.66</sub>				–	297	240	[56]
Au <sub>49</sub> Ag <sub>5.5</sub> Pd <sub>2.3</sub> Cu <sub>26.9</sub> Si <sub>16.3</sub>			74.4	26.5	401		[114]
Au <sub>70</sub> Cu <sub>5.5</sub> Ag <sub>7.5</sub> Si <sub>17</sub>		2.64			339		[431]
Pt <sub>60</sub> Ni <sub>15</sub> P <sub>25</sub>		4.1	96	33.8	485	205	[56]
Pt <sub>60</sub> Cu <sub>16</sub> Co <sub>2</sub> P <sub>22</sub>	1.1	4.02	~96		506	206	[56]
Pt <sub>57.5</sub> Cu <sub>14.7</sub> Ni <sub>5.3</sub> P <sub>22.5</sub>	1.4		94.8	33.3	508	206	[56,113]

are also found [398]. Some other physical parameters of metallic glass such as strength and linear thermal expansion coefficient which are directly associated with the atomic bond are also found to be correlated to  $T_g$ . For example, the fracture strength  $\sigma_f$  of various metallic glasses correlates with  $T_g$  as [323]:  $\sigma_f = 55 \frac{\rho}{M} (T_g - T_0)$ ,  $T_0$  is strength measuremental temperature. The linear thermal expansion coefficient and  $T_g$  are found to have a unique correlation for a number of BMGs with markedly different properties and  $T_g$  [326]. Egami had theoretically predicts that there is the correlation between of bulk modulus  $K$  and  $T_g$  which can be expressed as [302,303]:  $T_g = 6.14 \times 10^{-3} \langle \Omega \rangle \langle K \rangle / k_B$ , where  $\langle \Omega \rangle$  is the average local volume,  $k_B$  is the Boltzmann constant. Recently, Egami suggests that  $T_g$  depends not only on  $K$  but both  $K$  and  $G$  [322]. Actually, it is generally known that the  $T_g$  is dominated by the bonding force among the constituents. Consequently, the high value of elastic moduli of the metallic glasses, which is due to the stronger bonding force among the constituent elements, corresponds to high value of  $T_g$ .

The relationship for between  $E$  and  $T_g$  for various glasses including soft and brittle chalcogenide glasses, rare-earth glasses, silicon oxynitride glasses, oxycarbide glasses, alkali–alkaline–earth–silicate and aluminosilicate glasses, borate, phosphate, germanate, and basaltic glasses, and metallic glasses is summarized [341]. These glasses with  $E$  extending from 5 to 180 GPa and  $T_g$  ranging from 136 K (amorphous ice) to 1600 K (SiC<sub>0.33</sub>O<sub>1.33</sub> glasses). The Young's modulus is plotted as a function of  $T_g$  in Fig. 71. Although the general tendency is an increase of  $E$  with  $T_g$ , it is noteworthy that the highest values for  $E$  are not reported for the most refractory glasses (SiOC glasses) which are characterized by a low atomic packing density. On the contrary, the high packing density of metallic glasses

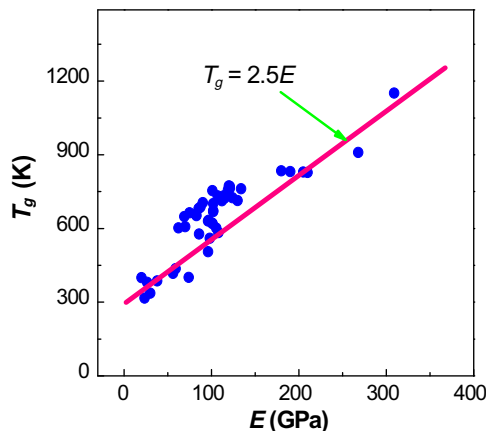


Fig. 69. The correlation of the elastic modulus  $E$  with glass transition temperature  $T_g$  for all the metallic glasses for which relevant data are available (listed in Table 12) [87]. The line is the guidance for eyes.

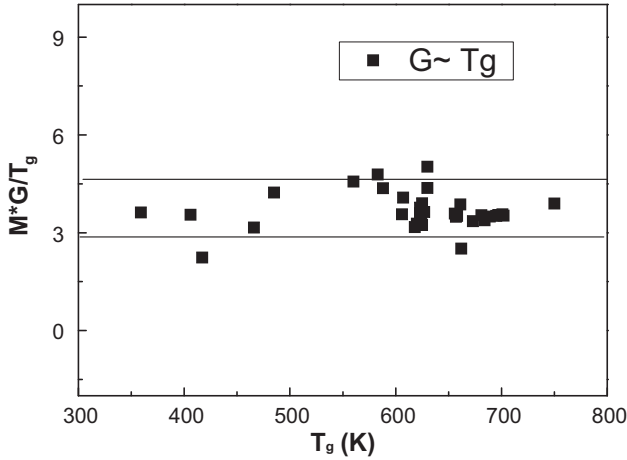


Fig. 70. The relation of glass transition temperature  $T_g$  and shear modulus  $G$  for various BMGs listed in Table 12 ( $M$  is the molar mass of a BMG) [87].

counterbalances their low bonding energy [432]. Elastic moduli depend much on temperature, and their values at temperature stem both intrinsically from the fine details of the atomic packing and the atomic bonding types and extrinsically from how far the glass transition of the glass is from the actual temperature. There are indeed two ways to meet a specific value for an elastic modulus at a given temperature. The first is the atomic packing density and the second one on the bond strength

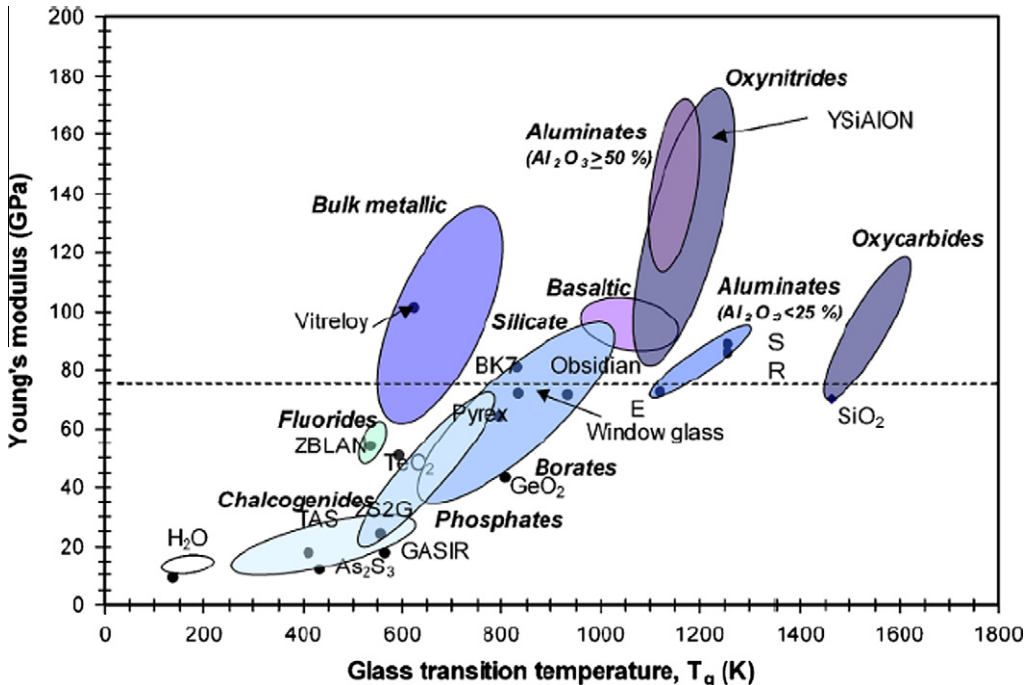


Fig. 71. Young's modulus and  $T_g$  for different inorganic chemical glass systems [341].

[432]. The  $T_g$  is related to a mean atomic bonding energy regardless of the packing density. So that  $T_g$  increases monotonically as the fraction of weakest bonds decreases to the benefit of stronger ones, consistently with the classical order: van der Waals < metallic < ionic < covalent. Therefore, for different types of glasses with different atomic bonding, contrary to the common wisdom that  $E$  scales with  $T_g$ , it turns out that one can easily find glasses with very different  $T_g$  exhibiting the same value for  $E$ .

Nevertheless, for the metallic glasses with similar the packing density and atomic bonding energy, the  $T_g$  and  $E$  indeed have clear correlation. It is important to find the relation between  $T_g$  and Young's modulus, which is by far the most frequently reported elastic characteristic, in these glassy alloys, because the design of glasses with high elastic moduli is an important issue in glass science and glassy materials application. The correlation between elastic moduli and  $T_g$  can be basic guidelines for developing glasses with high or low elastic moduli. The correlation is also the basis for establishing the elastic models [79]. The  $T_g$  and  $E$  correlation demonstrates that the glass transition is kind of moduli softening process similar to melting and is helpful for understanding the nature of BMGs.

### 8.5. Correlation between elastic moduli and melting

Melting of a crystalline solid like amorphization is a kind of transformation that results in a topologically disordered atomic structure. Born proposed that melting occurs when one of the shear elastic moduli vanishes ( $G = 0$ ) [26], which links the melting phenomenon to the elastic parameter. For a cubic crystal, the three generally accepted stability criteria are [26]:

$$C_{11} + 2C_{12} > 0, \quad C_{11} - C_{12} > 0, \quad C_{44} > 0 \quad (8.9)$$

where  $C_{11}$ ,  $C_{12}$ , and  $C_{44}$  are the independent elastic constants in the Voigt notation. Subsequent experimental investigations have shown that shear modulus does not fully vanish at  $T_m$  [433]. Based on the Lindemann melting criterion, Varshni [225] suggested that melting occurs when  $G$  is reduced to a value given by  $G(T) = f_m G(0)$ , where  $f_m$  is a factor that would depend on the crystal structure and the nature of binding. For pure crystalline metals,  $f_m$  is proposed to be 0.55.

A glass can be considered as a frozen liquid that has a static structure similar to supercooled liquids [1–10]. It is generally known that the  $T_g$  like  $T_m$  is dominated by the bonding force among the constituents, and striking parallels in the way of melting and amorphization have been recognized. The onset amorphization is preceded by a shear softening very similar to that which precedes the onset of melting during heat of most metals and alloys [147,430,434].

The Debye temperature,  $\theta_D$ , which is an important characteristic of a material, represents the temperature at which nearly all modes of vibrations in a solid are excited [51]. The Debye model was developed for crystal lattices, it seems inapplicable to the amorphous structure, yet the phenomena to be described in crystalline and amorphous alloys are very similar. For instance, the specific heat of the BMGs and other glasses at low temperature follows the same path in temperature as that of their crystalline states [435]. Under the circumstance, the metallic glasses can be treated as a monoatomic lattice with an average cellular volume, by using acoustic data obtained by ultrasonic method or the specific heat data, the  $\theta_D$  of the metallic glasses can be readily obtained [54,436]. The attempt to relate the glass transition to vibrational characteristics of the solids is long-standing issue and is of significant, because the possible correlation could assist the understanding of the glass transition and relaxation in glasses [437–439].

According to the Lindemann melting criterion, the melting temperature  $T_m$  of a solid is related to  $\theta_D$  as [440]  $T_l = \frac{Mk_B\theta_D^2\langle\mu_{crit}^2\rangle}{9h^2}$ , where  $k_B$  is the Boltzmann constant,  $M$  is the atomic mass,  $h$  is Planck's constant,  $\langle\mu_{crit}^2\rangle$  is critical mean-square thermal displacement. The original work of Lindemann is related to the Einstein temperature, not the Debye temperature. However, Einstein approximation [51] is much deviates the real situation in solids comparing with Debye approximation. So it is more reasonable to deduce the Debye temperature from acoustic data [51]. On the other hand, the relationship between  $E$  and melting temperature,  $T_l$  for various crystalline metallic alloys can be described as [441–443]:  $E = 97.9 \times q(RT_l/V_m)$ , where  $q$  is the number of atoms in the chemical formula,  $V_m$  is the molar volume and  $R$  is the gas constant. Granato [444] derived the Lindemann rule from a thermodynamic viewpoint

with no connection to a critical value and gives the melting temperature proportional to the shear modulus, which depends on the interatomic distance especially the repulsive branch of the interatomic potential.

It is found that some phenomena are common features underlie melting and vitrification processes. For example, the volume change, the decrease of the Debye temperature upon glass formation, and the elastic softening have also been observed in the formation of metallic glasses [54–57,151,445]. It is also found that the  $T_g$  and  $G$  of metallic glasses have a roughly correlation in various BMGs [57], and the ratios of the shear modulus at 0 K to the shear modulus at the glass transition temperature,  $G(T_g)/G(0)$ , for various BMGs are almost the same and have a value around 0.85, which indicates that the glass transition occurs when the shear modulus decreases to 85% of the shear modulus at 0 K, i.e.  $G(T_g) = 0.85G(0)$  [362]. (For melting,  $G(T_m) = 0.55G(0)$  [233].) On other hand, the average melting temperature  $\langle T_m \rangle$  ( $\langle T_m \rangle = \sum f_i(T_m)_i$ , where  $f_i$  and  $(T_m)_i$  are the atomic fraction and melting temperature of component  $i$ , respectively.) and glass transition temperature  $T_g$  have a linear correlation of  $T_g = 0.385\langle T_m \rangle$  [446]. These correlations and the similarity between melting and glass transition process imply the similarity between the melting and glass transition. Actually, a generalized Lindemann melting hypothesis later was proposed to connect the melting and the some vitrification processes [147].

The similarity between melting and glass transition process implies the possible intrinsic connection (Lindemann like criterion) between Debye temperature  $\theta_D$  and glass transition temperature  $T_g$  [57]. The bulky glass-forming alloys are model systems for study the common features underlies the glass transition and the melting process, and the sufficient data on  $\theta_D$  of metallic glasses make it possible to revisit the topic on the correlation between  $T_g$  and  $\theta_D$  in metallic glasses [57]. Table 12 lists  $\theta_D$  and  $T_g$  of various typical BMGs. For BMGs,  $T_g$  is much larger than  $\theta_D$ , and the ratio of  $T_g/\theta_D$  is between 1.85–2.55 and quite scattering. This means that  $T_g$  and  $\theta_D$  cannot be considered to have good linear correlation. Fig. 72 presents the data of  $T_g$  and  $\theta_D$  for BMGs listed in Table 12 according to Lindemann formula [57]. These BMGs are assumed to have the same static and dynamic mean-square displacements  $\langle \mu_{cri}^2 \rangle$ , which measuring the topological and thermal disorder of an alloy. (The values of mean square displacement of atoms at  $T_g$  and at the melting temperature can be assumed and interpreted to be the same [439–441,445].) An apparent correlation between  $\theta_D^2$  and  $T_g$  is clearly shown for BMGs available. That is:

$$T_g = aM\theta_D^2 \quad (8.10)$$

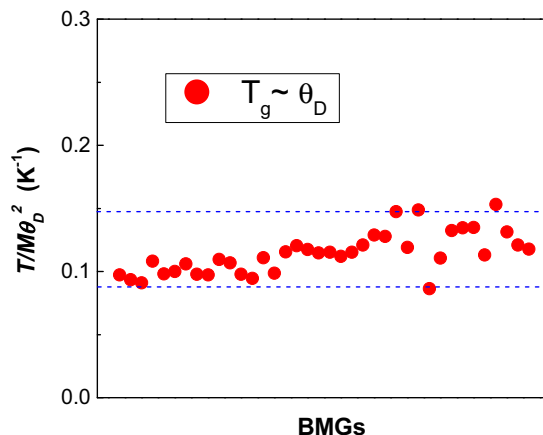


**Fig. 72.** The relation of  $T_g$  and Debye temperature,  $\theta_D$  for various metallic glasses listed in Table 12.  $M$  is the average atomic mass. The solid lines are for guiding the eyes.  $T_g$  of the BMGs was determined by DSC a constant heating rate of 0.167 K/s with the error about  $\pm 2$  K [57].

where  $a$  is the constant, and its value for BMGs ranges from  $1.0 \times 10^{-4}$  to  $1.4 \times 10^{-4}$  (K mol) $^{-1}$ , and its average value is  $1.1 \times 10^{-4}$  (K mol) $^{-1}$ . The correlation between  $T_g$  and  $\theta_D^2$  in BMGs confirms that the glass transition of the BMG-forming alloys has the characteristic of melting and a Lindermann type criterion exists for glass transition [57]. By analogy of Lindermann criterion for melting, the glass transition is considered to occur when the amplitude of motion of atoms reaches a critical value which is somewhat small for a solid to melt [57]. The Lindermann like criterion for glass transition more or less indicates that the glass transition is in connection with anharmonicity coupling of the vibration and configurational energy manifolds [438]. According to the phonon theory [50], the vibrational quantum states in glass can be regarded as short-lived wave disturbances propagating randomly through the material. The phonon interactions in solids including metallic glasses become dominant near  $\theta_D$  and give microscopic region of high potential energy. The apparent correlation between Debye temperature and glass transition temperature or the existence of the Lindermann type criterion in various BMGs indicates that the glass transition, approaching from the solid, is associated with a vibration, which provides clues for understanding of glass transition.

The formation of metallic glass through cooling a liquid is commonly believed to be closely related to the melting temperature of an alloy. This is based on the known Turnbull's  $T_{rg}$  criterion ( $T_{rg} = T_g/T_l$ , where  $T_l$  is the liquidus temperature) [409]. This criterion has led to the general practice of locating glass formers specifically in the deep-eutectics. Therefore, the relationships between  $\theta_D$  and  $T_g$ , between  $T_g$  and  $T_m$ , and elastic moduli to  $T_g$  ( $T_m$ ) can be used to predict and design BMGs with a desired glass transition temperature  $T_g$ .

### 8.6. Correlation between elastic moduli and fragility

The phenomenon of so-called fragility is one of the very important and interesting unsolved issues left of the 20<sup>th</sup> century [290,447–452]. The viscosity,  $\eta$ , with the temperature approaching  $T_g$  of glass-forming liquids can be classified according to the concept of “fragility” [447]. The kinetic fragility  $m$ , which is directly related to the slowing down of the dynamics, is defined in terms of the shear viscosity as:

$$m = \left. \frac{\partial \log \eta(T)}{\partial (T_g/T)} \right|_{T=T_g} \quad (8.11)$$

Therefore,  $m$  is an index of how fast the viscosity increases while approaching the structural arrest at  $T_g$ , the temperature at which the structural relaxation time  $\tau \sim 100$  s or alternatively  $\eta = 10^{12}$  Pa s [446,447]. Plotting the viscosity curves for glasses of different nature as a function of reduced co-ordinate  $T_g/T$  one obtains all substances forming a sheaf of curves converging in the point  $T_g/T = 1$ . At extremely high temperatures ( $T_g/T \rightarrow 0$ ) all curves strive to a common limit which corresponds to  $\log \eta = -(4.5 \pm 1)$ . For all glasses, the fragility values typically range between  $m = 16$  (least value) for “strong” systems and  $m = 200$  for “fragile” systems [446,447]. The meaning of term ‘fragility’ implies that the substances having the least curvature in such coordinate system have the most conservative structure against the temperature rising [290,446,447]. The substances with small curvature were named by Angell as ‘strong’ glass formers. The rising of the curvature was explained by the facility of structure destruction, and such glass forming melts are ‘fragile’.

One of the puzzles that remains unsolved is the correlation of the fragility and other macroscopic properties of the liquids or the resulting glasses [56,81,178,305,307–310,312,313,315–317,453]. Recently, attempts have been made to correlate the fragility of a glass-forming liquid and the relative strength of  $K/G$  (or alternatively Poisson's ratio  $\nu$ ) of its corresponding glass [81]. Novikov et al. [81] found, based on the analysis of a large number of non-metallic glasses (including covalent and hydrogen-bonded, van-der-Waals and ionic glasses) the  $m$  and  $K/G$  of the respective glasses can be well described by:  $m = 29(K/G - 0.41)$ . To put this relationship in more quantitative terms, Novikov et al. [81] assumed that the viscosity at high  $T$  is considered to follow the Arrhenius law  $\eta = \eta_0 \exp(\Delta E/T)$ , where  $\Delta E$  is a single activation, based on the observation that the temperature dependence of the viscosity in the region of the liquid state is linear on an Angell plot. As the derivative of the relaxation time with respect to scaled inverse temperature  $T_g/T$  is equal to  $\Delta E/T_g$  in the liquid state. They then proceed to fit

the experimental values of  $m$  vs.  $\Delta E/T_g$  to obtain:  $\frac{\Delta E}{T_g} = \frac{19.2^2 \ln 10}{m}$ . On the other hand, based on empirical grounds—that the transition temperature  $T_g$  correlates with both the  $K$  and the  $G$  of the glass in the way:  $T_g = K + xG$  (where  $x$  is a fitted constant); and from elastic model [36],  $\Delta E \propto G$ . Then, one gets  $m \propto K/G$ .

Priya and Das tried to put this correlation on sound theoretical ground by a first-principles treatment in terms of the mode-coupling theory studied for a system of hard spheres [449]. Using a scaled packing fraction as the analogy to temperature, the relaxation time, equivalently the fragility, in the model is correlated with the change in elastic moduli. When a specific value is picked for the upper wave vector cutoff of the density fluctuations considered in the theory, the behavior of the ratio  $K/G$  as a function of  $m$  exhibits remarkable agreement with the found correlation of Novikov et al. [81]. Rouxel [341] suggests that the temperature dependent of  $E$  and Poisson's ratio reflects the degree of fragility of the glass based on *in situ* measurements of temperature dependence of elastic moduli for various glass systems (as shown in Fig. 73). The rate of softening immediately above  $T_g$  can be used to evaluate the fragility of liquid from the correlation existing between the softening rate and the relaxation kinetics.

However, Johari et al. [306,311,314] debated that the linear form of this  $m \sim \nu$  correlation is unjustified, and they demonstrated that a quadratic dependence of  $m$  on the Poisson's ratio fits the data as well as a linear one. The interpretation of the reasons of the correlations between fragility and Poisson's ratio has not yet successfully arrived at a fair and acknowledged theory, and concerns have been raised on the correlations [300,306,311,314]. Nevertheless, even though the correlation is still controversial, the work suggests that a systematic study of the correlation between fragility and Poisson's ratio of glasses is expected to yield important information about the nature and properties of glasses.

The values of fragility of BMGs can be directly taken by using Vogel–Fulcher (VF) equation fits to viscosity data [240,446,447,454]. On the other hand, the liquid fragility can be determined from purely

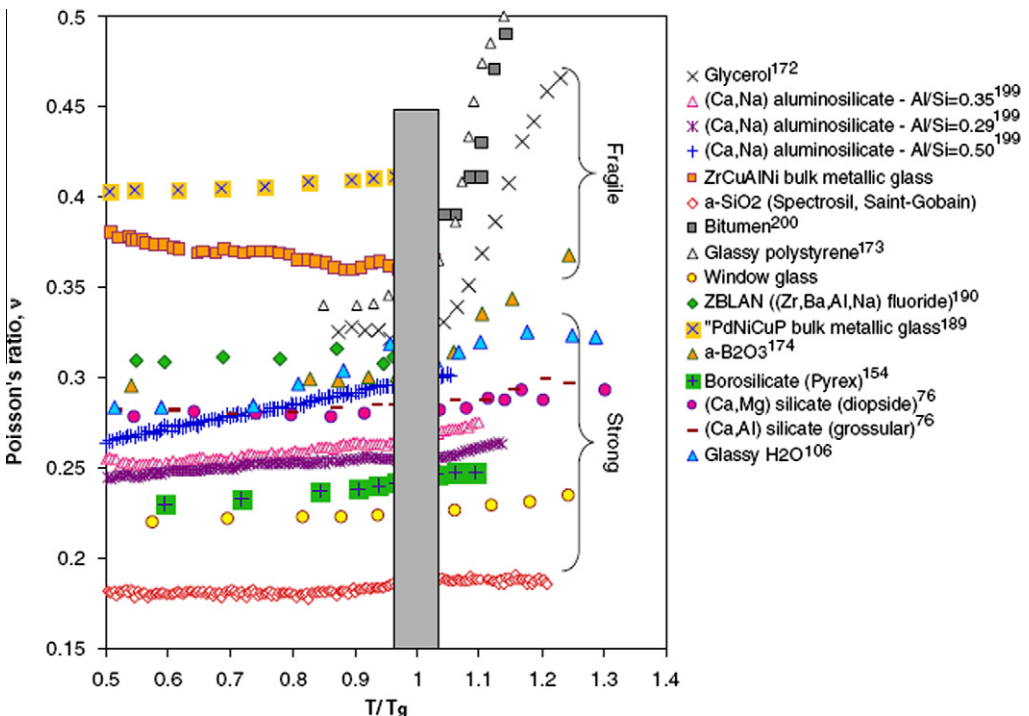


Fig. 73. Temperature dependence of Poisson's ratio for different glass systems [341].

thermodynamic way near  $T_g$ , and the value of  $m$  estimated this way is consistent with those obtained by the kinetic method [455]. Since viscosity relaxation and the glass transition measured by calorimetric methods occur on the same time scale, the heating rate  $\phi$  dependent glass transition can be used as an alternative way to determine the fragility of the metallic glasses [56,114,130]. Previous studies confirm that the  $\phi$ -dependent  $T_g$  describes the fragility equally well as complementary viscosity measurements [456], and the dependent  $T_g$  on  $\phi$  can also be described by a VFT type relation:

$$\phi(T_g) = A \exp\left(D^* T_g^0 / (T_g^0 - T_g)\right) \quad (8.12)$$

where  $A$  is a constant,  $T_g^0$  is the VF temperature and  $D^*$  is the strength parameter. From the fit of the relationship of  $T_g$  vs.  $\ln \phi$  of the metallic glasses using the VFT equation, the VFT parameter  $A$ ,  $T_g^0$  and  $D^*$  are obtained, and the  $m$  can be obtained as:

$$m = (D^* / \ln 10) * (T_g^0 / T_g) * (1 - T_g^0 / T_g)^{-2} \quad (8.13)$$

**Table 13**

The thermodynamic fragility values of  $m_t$  for various typical BMGs. The available values of kinetic fragility  $m_k$  are also listed for comparisons.

Metallic glasses	G (GPa)	K (GPa)	E (GPa)	K/G	$\nu$	$m_k$	$m_t$	Refs.
Zr <sub>41</sub> Ti <sub>14</sub> Cu <sub>12.5</sub> Ni <sub>10</sub> Be <sub>22.5</sub>	37.4	114.1	101.2	3.047	0.352	50	39	[369,455]
Zr <sub>46.75</sub> Ti <sub>18.25</sub> Cu <sub>7.5</sub> Ni <sub>10</sub> Be <sub>27.5</sub>	37.2	111.9	100.5	3.008	0.350	44	34	[455]
Zr <sub>65</sub> Al <sub>10</sub> Ni <sub>10</sub> Cu <sub>15</sub>	30.3	106.6	83.0	3.521	0.370		35	[56,369,455]
Zr <sub>35</sub> Ti <sub>30</sub> Cu <sub>8.25</sub> Be <sub>26.75</sub>	31.8		86.9	3.51	0.37	66	66	[160]
Cu <sub>50</sub> Zr <sub>50</sub>	31.3	101.2	85.0	3.238	0.360		62	[456]
(Cu <sub>50</sub> Zr <sub>50</sub> ) <sub>92</sub> Al <sub>8</sub>	34.3	116.4	93.7	3.394	0.366		43	[456]
(Cu <sub>50</sub> Zr <sub>50</sub> ) <sub>92</sub> Al <sub>7</sub> Gd <sub>1</sub>	32.9	123.7	90.6	3.760	0.377		29	[456]
(Cu <sub>50</sub> Zr <sub>50</sub> ) <sub>86</sub> Al <sub>7</sub> Be <sub>7</sub>	38.1	122.6		3.22	0.359		42	[453]
(Cu <sub>50</sub> Zr <sub>50</sub> ) <sub>86</sub> Al <sub>7</sub> Ag <sub>7</sub>	32.7	156.1		4.77	0.402		45	[453]
Cu <sub>46</sub> Zr <sub>42</sub> Al <sub>7</sub> Y <sub>5</sub>	31	104.1		3.36	0.364		49	[453,425]
Ca <sub>65</sub> Mg <sub>15</sub> Zn <sub>20</sub>	10.1	22.6	22.4	2.23	0.300		21	[152,501]
Pd <sub>39.1</sub> Ni <sub>10.1</sub> Cu <sub>29.9</sub> P <sub>20.9</sub>	35.2	158.7	98.2	4.52	0.397	59	52	[369,455,457]
Pd <sub>77.5</sub> Si <sub>16.5</sub> Cu <sub>6</sub>	32.9	174.6	92.9	5.31	0.411	73	52	[457,458]
Pd <sub>40</sub> Ni <sub>40</sub> P <sub>20</sub>	38.6	184.9	108.2	4.79	0.403	54	41	[457,458]
Pt <sub>60</sub> Ni <sub>15</sub> P <sub>25</sub>	33.8	201.9	96.1	5.97	0.421	68	86	[113,453,458]
Pt <sub>57.5</sub> Cu <sub>14.7</sub> Ni <sub>5.3</sub> P <sub>22.5</sub>	33.3	198.7		5.98	0.42		68	[113,453,458]
Au <sub>77.8</sub> Ge <sub>13.8</sub> Si <sub>8.4</sub>	–	–	–	8.28	0.442		92	[436,437]
Au <sub>49</sub> Ag <sub>5.5</sub> Pd <sub>2.3</sub> Cu <sub>26.9</sub> Si <sub>16.3</sub>	132.3	26.5		4.99	0.406		70	[114]
Ce <sub>70</sub> Al <sub>10</sub> Ni <sub>10</sub> Cu <sub>10</sub>	11.5	27.0	30.3	2.34	0.313		21	[56]
Pr <sub>60</sub> Al <sub>10</sub> Ni <sub>10</sub> Cu <sub>20</sub>	13.6	45.2	37.2	3.31	0.363		31	[56]
Gd <sub>40</sub> Y <sub>16</sub> Al <sub>24</sub> Co <sub>20</sub>	23.5	58.0	62.2	2.46	0.321		32	[56]
La <sub>55</sub> Al <sub>25</sub> Cu <sub>10</sub> Ni <sub>5</sub> Co <sub>5</sub>	15.6	44.2	41.8	2.83	0.342		28	[457,458]
Nd <sub>60</sub> Al <sub>10</sub> Fe <sub>20</sub> Co <sub>10</sub>	20.7	46.5	54.1	2.24	0.306	33	32	[56]
Ho <sub>39</sub> Al <sub>25</sub> Co <sub>20</sub> Y <sub>16</sub>	26.2	63.6	69.1	2.43	0.319		49	[140]
Tm <sub>39</sub> Y <sub>16</sub> Al <sub>25</sub> Co <sub>20</sub>	55.3	29.4	75.0	1.88	0.274		39	[118]
Tm <sub>40</sub> Zr <sub>15</sub> Al <sub>25</sub> Co <sub>20</sub>	68.1	28.0	73.8	2.43	0.319		35	[118]
Yb <sub>62.5</sub> Zn <sub>15</sub> Mg <sub>17.5</sub> Cu <sub>5</sub>	10.4	19.8	26.5	1.90	0.276		26	[63]
La <sub>55</sub> Al <sub>25</sub> Co <sub>20</sub>	15.42	39.34	40.90	2.65	0.327		27	[138]
Pr <sub>55</sub> Al <sub>25</sub> Co <sub>20</sub>	17.35	43.48	45.90	2.64	0.324		38	[138]
Tb <sub>55</sub> Al <sub>25</sub> Co <sub>20</sub>	22.85	50.19	59.53	2.61	0.302		32	[138]
Dy <sub>55</sub> Al <sub>25</sub> Co <sub>20</sub>	23.52	52.22	61.36	2.61	0.304		30	[138]
Ho <sub>55</sub> Al <sub>25</sub> Co <sub>20</sub>	25.42	58.81	66.64	2.62	0.311		25	[138]
Er <sub>55</sub> Al <sub>25</sub> Co <sub>20</sub>	27.08	60.70	70.72	2.61	0.306		28	[138]
Mg <sub>65</sub> Cu <sub>25</sub> Gd <sub>10</sub>	19.3	45.1	50.6	2.338	0.313		41	[56,458,460]
Mg <sub>65</sub> Cu <sub>25</sub> Y <sub>10</sub>	19.4	44.7		2.30	0.305		45	[453]
Ca <sub>65</sub> Li <sub>9.96</sub> Mg <sub>8.54</sub> Zn <sub>16.5</sub>	8.95	20.2	23.4	2.26	0.307		20	[237]
Fe <sub>70</sub> B <sub>5</sub> C <sub>5</sub> Si <sub>3</sub> Al <sub>5</sub> Ga <sub>2</sub> P <sub>10</sub>	58.5	113.4	149.7	1.938	0.280		34	[459]
Fe <sub>41.5</sub> Ni <sub>41.5</sub> P <sub>17</sub>				10.1	0.452		99	[458]
Ni <sub>60</sub> Nb <sub>35</sub> Sn <sub>5</sub>	66.3	267		4.03	0.385		60	[453]

The changes in  $T_g^0$  result in changes in  $D^*$  that keep the value of  $m$  reasonably constant [455–464]. Table 13 lists the values of  $m$  for various BMGs available. The available values of kinetic fragility are also listed to show that both thermodynamic and kinetic fragility give the same tendency. The values of  $m$  normally range from 20 to 70 for the BMGs. According to the Angell's classification [446,447], the BMGs are intermediate strong glasses.

As the structural state of a glass is inherited from the equilibrium liquid, the elastic properties of the BMGs are expected to be inherited from the infinite frequency elastic response ( $G^\infty$  and  $K^\infty$ ) of the equilibrium liquid at fictive temperature  $T_f$  [465–467]. Therefore, it would be intriguing to see if there exists a similar correlation between fragility and Poisson's ratio in BMGs. Egami proposes an approach based on the exchange and fluctuation of atomic bonds described in terms of the atomic level stresses to theoretically explain the relation of fragility and Poisson's ratio in metallic glasses [302]. By using the model, the relation between fragility and Poisson's ratio is given by:  $m = 39(1 - \nu)/2(1 - 2\nu)$ . The survey of fragility and elastic moduli for various typical metallic glasses has been made to attempt to establish the correlation between elastic moduli and fragility [56]. Fig. 74 presents the relation of  $m$  and  $K/G$  (alternatively Poisson's ratio  $\nu$ ) of a variety of BMG systems available. The Novikov–Sokolov correlation  $m = 29(K/G - 0.41)$  [81] for non-metallic glasses is also shown for comparison. The collects all available relevant data on BMGs show that there a very roughly tendency between the fragility and elastic properties in BMGs. The thermodynamic fragility upon the relative strength of  $K/G$  rough described by the relationship:

$$m = 11.0(K/G - 0.27) \quad (8.14)$$

The correlation coefficient (11.0) is much different from that of the Novikov–Sokolov correlation (29.0). The difference is assigned to the contribution of the free electron gas to the bulk modulus in metallic glasses with complex chemical composition [308]. Novikov et al. claim that the ratio of  $T_g$  or  $T_m$  to the activation energy of viscous flow in normal metallic liquid correlates with fragility just as in other nonmetallic liquids [308]. Dai et al. [312] claim that there is an intrinsic correlation between fragility of a liquid and bulk modulus of its glass [ $mRT_g/(M/\rho) - 0.729 = 0.198K$ ], and the linear correlation between the fragility and the  $K/G$  exists strictly at either absolute zero temperature or very high frequency. Moreover, an inverse linear correlation between fragility and bulk dilatation induced by shear-dominant activation energy was discovered. Park et al. find that  $m$  can be formulated with  $\nu$  as [315]:  $\nu = -0.179 + 0.312 \log m$ , which means that  $m$  and  $\nu$  have a nonlinear correlation. They further suggest high  $m$  as well as large  $\nu$  values might be regarded as indicators of the BMGs plasticity [315]. Nemilov claims that the  $m \sim \nu$  correlation exist only within special groups of glasses which have

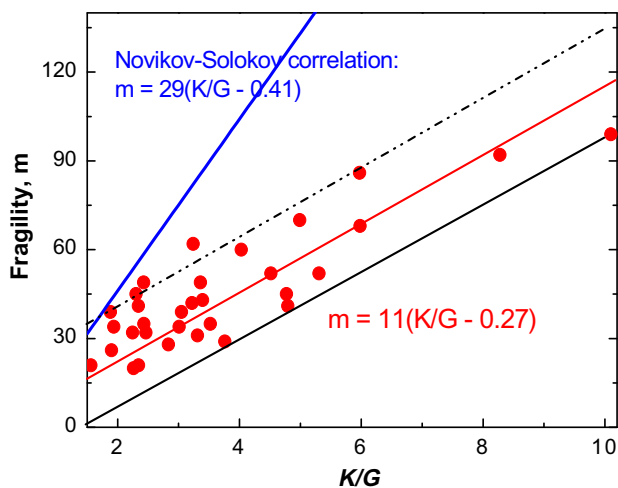


Fig. 74. The correlation between  $m$  and  $K/G$  for the available metallic glasses.

related structure, and the relation between the variation of the vibrational properties during the glass transition and the fragility of the liquid would explain the highly debated Poisson's ratio vs. fragility correlation [290].

We note that the relation between  $m$  and  $B/G$  (or  $m$  and  $\nu$ ) inevitably contains large ambiguity because of the narrow range of  $m$  values for the available BMGs. Unfortunately, at this moment, there are not so many BMG formers, whose kinetic fragility and elastic constants are all known. The kinetic fragility is calculated at a well defined  $T_g$ , the calorimetric fragility is usually calculated at a higher and not well defined  $T_f$ . This introduces an additional source of uncertainty; both the elastic constants and the calorimetric fragility depend on a not very well-known value of  $T_f$  which, in addition, can be different for different kind of experiments. Thus, the  $m \sim \nu$  correlation should be carefully checked and improved for more BMG systems in future. On the other hand, to clarify the validity of the correlation between the  $K/G$  ratio and the fragility of the liquid, measurements of the high-frequency elastic constants of the equilibrium liquid at the same  $T_g$  where the glass fragility is calculated should be performed. The estimation of the elastic constants of the equilibrium liquid at  $T_g$  from the elastic constants of the glass at room temperature introduces a certain amount of error. Unfortunately, there is few such available data in literature for metallic glasses. The validity of the correlation shown in Fig. 74 has to be taken with precautions. More experimental measurements, theoretical calculations of the infinite frequency response of liquids near glass transition and analysis of data for more different BMGs and other glass-forming materials different from metallic glasses are crucial to check this hypothesis. There is no clear model for a mechanism of such correlations either, and more works are needed to clarify the issue.

### 8.7. Correlation between elastic properties and boson peak

One of the most intriguing universal features of glasses, observable in Raman or inelastic neutron scattering or specific heat at low temperatures, is so called boson peak (BP), which is defined as excess with respect to the Debye contribution in the low-frequency vibrational density of state (VDOS) [468–472]. At low temperatures, accordingly, the specific heat  $C_p$  of glasses often presents a distinct excess in  $C_p/T^3$  compared to the Debye theory above 1 K, which is related to the BP contribution. However, the physical origin of BP is still a debated issue and is commonly considered as one of the great mysteries of glass physics [468–472]. Interest in this issue is further stimulated by the finding that the amplitude of BP is even correlated with the liquid fragility  $m$  in non-metallic glasses [331].

The low-temperature  $C_p$  anomalies associated with boson peak in various BMGs have been recently studied [321,473–480]. The CuZr-based BMGs with significant differences in GFA, elastic properties, and configurational features induced by minor additions were chosen as model systems. These BMGs cover a substantial part of the Angell diagram in terms of fragility. The availability of such glasses makes it possible to study the low temperature  $C_p$  anomaly associated with the generation of low-frequency modes, and to identify how the low-frequency mode changes with the fragility, Poisson ratio  $\nu$ , GFA, and microstructural feature in metallic glasses [321]. Table 14 lists the parameters of GFA, fragility, elastic properties and microstructural features of these BMGs. The  $\text{Cu}_{50}\text{Zr}_{50}$  is fragile BMGs,  $(\text{Cu}_{50}\text{Zr}_{50})_{90}\text{Al}_7\text{Gd}_3$  is strong BMGs, and  $(\text{Cu}_{50}\text{Zr}_{50})_{96}\text{Al}_4$  BMG possess an intermediate degree of fragility [58]. Fig. 75 shows the  $(C_p - \gamma T)/T^3$  ( $\gamma$  is the electronic coefficient of  $C_p$ ) of the BMGs without the mask of the electronic and/or magnetic contributions. The results clearly exceed the Debye model and show an anomaly. The fragile CuZr glass shows hardly pronounced bump, while the bump becomes more pronounced, and the  $T_{\text{max}}$  corresponding to the maximum excess  $C_p$  shift to lower  $T$  for the stronger BMGs. As in many nonmetallic glasses, it is reasonable to believe that the humps arise from low-frequency vibrations and corresponds to the boson peak [470]. The value  $((C_p - \gamma T)/T^3)_{\text{max}}$  at the maximum for the BMGs increases with the decreasing fragility, and the excess  $C_p$  becomes much stronger in the strong BMGs. The  $C_{BP}$  is obtained from subtracting the Debye contribution  $C_D$ ,  $\gamma T$  and/or the magnetic contribution from the measured  $C_p$ . The boson peak has been found in a series of various BMGs [474]. After scaled by  $C_D$ , the different Debye contributions, which are usually the maximal one to  $C_p$ , is eliminated, and the  $C_{BP}/C_D$  values of these BMGs, oxide glasses and organic glasses obey a clear correlation between the BP and  $m$  only with an exception of  $\text{SiO}_2$  (see Fig. 76) [474,481]. The results provide new evidences for the correlation between the thermodynamic and kinetic properties in various glasses.

**Table 14**

The fragility  $m$ , and critical sample thickness  $d_c$ , volume per mole  $V_m$ , and Poisson's ratio  $\nu$  for CuZr-based BMGs. The markedly increase of  $d_c$  indicates that the significantly increase of the GFA of the alloys by minor additions. The BP amplitude  $((C_p - \gamma T)/T^3)_{\max}$  and position  $T_{\max}$ , the Debye temperature  $\theta_D$ , and the Einstein temperature  $\theta_E$  are also listed [321].

Parameter	Cu <sub>50</sub> Zr <sub>50</sub>	(Cu <sub>50</sub> Zr <sub>50</sub> ) <sub>96</sub> Al <sub>4</sub>	(Cu <sub>50</sub> Zr <sub>50</sub> ) <sub>90</sub> Al <sub>7</sub> Gd <sub>3</sub>
$d_c$ (mm)	2	5	10
$m$	62	40	30
$V_m$ (cm <sup>3</sup> )	10.4	10.5	10.7
$\nu$	0.359	0.369	0.373
$T_{\max}$ (K)	17.5	10.1	7.8
$((C_p - \gamma T)/T^3)_{\max}$	0.125	0.181	0.202
$\theta_D$ (K)	283	281	268
$\theta_E$ (K)	88	73	67

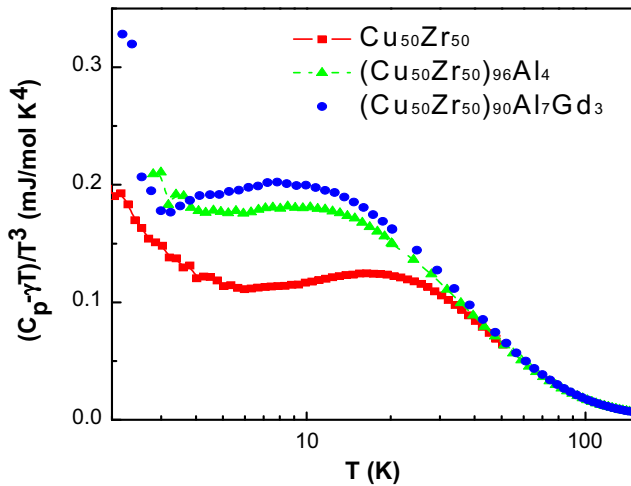


**Fig. 75.** The  $(C_p - \gamma T)/T^3$  vs.  $T$  plots of Cu<sub>50</sub>Zr<sub>50</sub>, (Cu<sub>50</sub>Zr<sub>50</sub>)<sub>96</sub>Al<sub>4</sub> and (Cu<sub>50</sub>Zr<sub>50</sub>)<sub>90</sub>Al<sub>7</sub>Gd<sub>3</sub> BMGs after subtracting the electronic contribution or/and the magnetic contribution [321].

The inset of Fig. 76 and Table 14 also show that the  $((C_p - \gamma T)/T^3)_{\max}$  increases linearly with the increasing Poisson's ratio  $\nu$ . The glass with higher  $\nu$  has stronger BP. The correlation can be extended to more BMG systems [474].

The  $C_p$  anomalies associated with the boson peak in BMGs can be fitted well using an additional Einstein mode [475–479]. The presence of an Einstein oscillator suggests the existence of the vibrations of loose atoms or clusters in an independent localized harmonic mode in the glasses [475–479]. In crystalline materials, the vibrations of the loose “rattler” atoms in oversized cage structure or large voids are regarded to result in the localized modes [482,483]. It is assumed that the localized vibrational mode has a Gaussian distribution with a dominant frequency corresponding to the Einstein frequency. Therefore, the mode's contribution to VDOS has a Gaussian distribution which deviates from the Debye mode. At higher temperature ( $>10$  meV), the hybridization with other modes is stronger, and the peak is considerably broader, which cannot be separated from the measurement. In the alloys, the minor addition of atoms (Al and Gd) with markedly different atomic size induces an increase of the amount of the solute atoms and vacancies and then changes the localized vibrations in the alloys. This causes the change of the peak position, the intensity and broadness of the BP. Ultrasonic and density measurements confirm that the additions and annealing below  $T_g$  do induce markedly change in elastic moduli and molar volume indicating obviously structural change. This proposed model is also useful for the understanding the observed correlations. In BMG-forming liquids, the local

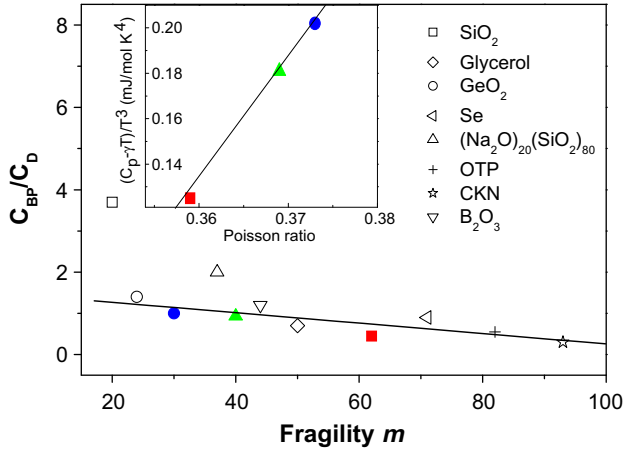


**Fig. 76.** The ratio of the BP contribution to the Debye contribution around the maximum (at 7–18K) vs. the fragility  $m$  of  $\text{Cu}_{50}\text{Zr}_{50}$  (■),  $(\text{Cu}_{50}\text{Zr}_{50})_{96}\text{Al}_4$  (▲), and  $(\text{Cu}_{50}\text{Zr}_{50})_{90}\text{Al}_7\text{Gd}_3$  (●) BMGs and other non-metallic glasses. The inset is the  $((C_p - \gamma T)/T^3)_{\max}$  vs. Poisson ratio  $\nu$  of  $\text{Cu}_{50}\text{Zr}_{50}$  (■),  $(\text{Cu}_{50}\text{Zr}_{50})_{96}\text{Al}_4$  (▲), and  $(\text{Cu}_{50}\text{Zr}_{50})_{90}\text{Al}_7\text{Gd}_3$  (●) BMGs [321].

structure controls  $m$ ,  $\nu$  and GFA. Both the elastic moduli and the low- $T$   $C_p$  anomaly (or boson peak) are “finger-mark” properties of glass when the liquid freezes into glass, it is therefore reasonable to exist correlation between the excess vibrational contribution in the BMGs and the representative properties of liquid such as  $m$  and Poisson’s ratio.

### 8.8. Other correlations

For various BMGs, there exist correlation between average Grüneisen parameter  $\gamma_{av}$  and bulk modulus  $K$ . Table 4 lists pressure derivative of velocities,  $dv_l/dP$  and  $dv_s/dP$ , and Grüneisen parameters,  $\gamma_l$ ,  $\gamma_s$  and  $\gamma_{av}$  of various glassy materials, and the  $K$ ,  $\nu$  of these glasses are listed in Table 1. The  $\gamma_l$ ,  $\gamma_s$  and  $\gamma_{av}$  are the longitudinal, shear and average Grüneisen parameters, respectively. Fig. 77a shows smooth correlation between  $\gamma_{av}$  and  $K$  for various BMGs. There seems to be abrupt increase of  $\gamma_{av}$  at  $K \sim 110$  GPa, and the systems with  $K < 110$  GPa tends to have similar  $\gamma_{av}$  value around 0.9, while the systems with  $K > 110$  GPa increase sharply. Fig. 77b shows a clear correlation exists between  $\gamma_{av}$  and Poisson’s ratio, indicating that the BMGs with bigger Poisson’s ratio tend to have stronger anharmonic effects. System with bigger Poisson’s ratio tends to have bigger  $\gamma_{av}$ . The anharmonic effect in BMGs under pressures correlates with  $K$ , and Poisson’s ratio, and the BMGs with smaller  $K$  and smaller Poisson’s ratio perform weaker anharmonic effects [484]. We will show later that the plasticity of BMGs correlates with Poisson’s ratio  $\nu$  [56]. A large  $\nu$  is regarded as the indicator of the plastic characteristic of a BMG and could therefore be used as a means of identifying plastic BMGs. The correlation between anharmonic behavior and Poisson’s ratio indicates the proposition that the plasticity of metallic glasses is related to the anharmonic effect or Grüneisen parameter. That is, the BMG system with stronger anharmonic effect (larger Grüneisen constant  $\gamma_{av}$ ) has better plasticity (alternatively, the bigger  $\nu$ ).

Poisson’s ratio  $\nu$  can be calculated as [56]:  $\nu = \frac{v_l^2 - 2v_t^2}{2(v_l^2 - v_t^2)}$ . Unlike other elastic constants, to get  $\nu$  value one does not need to measure the density which is hard to be measured *in situ* during experimental process. This characteristic makes Poisson’s ratio a suitable probe for investigating temperature and pressure behaviors of a material [56]. Recently, Rouxel et al. [207] reported that there is a direct correlation between  $\nu$  and the maximum post-decompression density change in various glasses. However, most of the researches focus on establishing relations between Poisson’s ratio and other physics parameters, and little work involving in temperature or pressure dependent behaviors of  $\nu$  which are closely related to atomic configurations and potentials has been reported. The Poisson’s

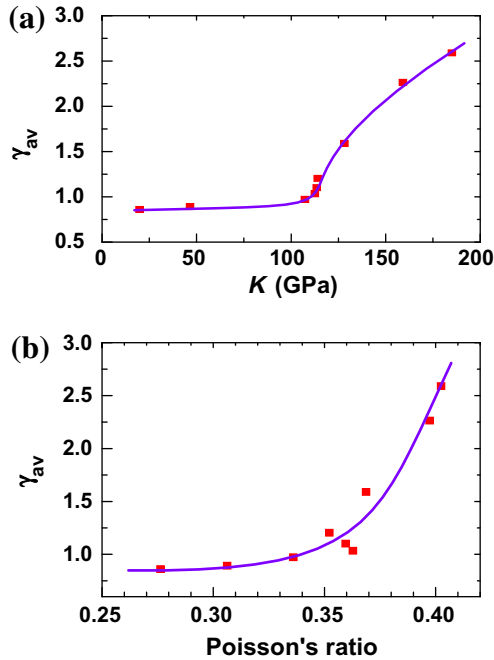


**Fig. 77.** The average Grüneisen parameter shows clear correlation with (a)  $K$ , and (b) Poisson's ratio. The scattered symbols are experiment data, and the lines are drawn to guide eyes [484].

ratio variations under high pressure and low temperature (270–100 K) of a variety of bulk metallic glasses and non-metallic glasses were recently investigated [485]. It is found that the microstructure of metallic glasses with high  $\nu$  is difficult to be changed under pressure or low temperature compared with that low  $\nu$  ones, and there are direct correlations between Poisson's ratio and its differential upon pressure or temperature. The pressure variations of  $\nu$  for various glasses at room temperature are shown in Fig. 78a. To avoid any possibility of plastic behavior, the pressure was raised to 0.5 GPa, which is much lower than the yielding strength of measuring BMGs and glasses. The  $\nu$  of all the glasses changes roughly linearly with increasing  $P$  but shows markedly different slopes. For silica glasses, their  $\nu$  decreases with increasing  $P$  and  $dv/dP$  of the silica glasses has a negative value [485]. While for various BMGs with different values of  $\nu$ , their  $\nu$  increases with increasing  $P$  and their  $dv/dP$  has a positive value. The different pressure responses of BMGs and oxide glasses reflect their different structures and chemical bonding. For a  $Ce_{70}Al_{10}Ni_{10}Cu_{10}$  metallic plastic, it has markedly different structural characteristics and features compared to other BMGs, and its bonding between Al and Ce atoms have a strong covalence-like characteristic [169]. It then shows similar response of  $\nu$  under pressure like silica glasses and negative  $dv/dP$ . Fig. 78b shows the data of  $dv/dP$  vs.  $\nu_0$  (Poisson's ratio at ambient temperature and pressure) for BMGs and some silica glasses. From Fig. 78b one can see that  $dv/dP$  vs.  $\nu_0$  can be distinctly divided into three zones. The red-circled zone contains the BMGs which are characterized with bigger  $\nu_0$  ( $>0.27$ ) and positive  $dv/dP$ . The green-circled zone of the silica glasses is characterized with smaller  $\nu_0$  ( $<0.27$ ) and negative  $dv/dP$ . And the Ce-based metallic plastic in the blue circle are characterized with bigger  $\nu_0$  ( $>0.3$ ) and negative  $dv/dP$ . The variation of  $\nu$  with  $T$  for different BMGs and non-metallic glasses is also investigated and shown in Fig. 78c. In contrast to the  $\nu$  variation under  $P$ , both silica glasses and BMGs have a negative  $dv/dT$ . Similarly, the data of  $dv/dT$  and  $\nu_0$  can also be divided into three zones as shown in Fig. 78c. The result indicates that the  $dv/dP$  or  $dv/dT$  can be used to reflect or distinguish the chemical bonding or structure in different glasses.

Though the  $\nu$  of the BMGs increase linearly with the increasing  $P$  [Fig. 79a], different BMGs display different changing rates upon  $P$ . The  $dv/dP$  of Yb-based BMG with smaller  $\nu$  is more than 20 times

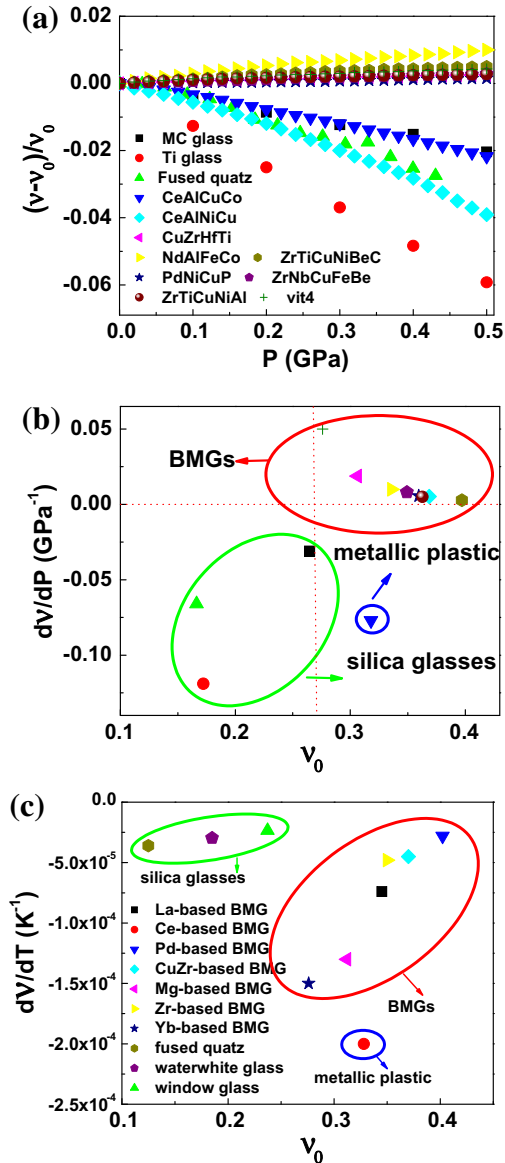


**Fig. 78.** (a) Variation of Poisson's ratio of silica glasses and BMGs with pressure,  $P$ . MC stands for microcrystal glass, Ti-glass is  $\text{TiO}_2$ - $\text{SiO}_2$  glass, Vit4:  $\text{Zr}_{47}\text{Ti}_8\text{Cu}_{7.5}\text{Ni}_{10}\text{Be}_{27.5}$ , ZrTiCuNiBeC:  $\text{Zr}_{41}\text{Ti}_{14}\text{Cu}_{12.5}\text{Ni}_9\text{Be}_{22.5}\text{C}_1$ , ZrNbCuFeBe:  $\text{Zr}_{48}\text{Nb}_8\text{Cu}_{12}\text{Fe}_8\text{Be}_{24}$ , ZrTiCuNiAl:  $\text{Zr}_{50.6}\text{Ti}_{5.2}\text{Cu}_{18.8}\text{Ni}_{14.1}\text{Al}_{14.3}$ , PdNiCuP:  $\text{Pd}_{39}\text{Ni}_{10}\text{Cu}_{30}\text{P}_{21}$ , CeAlCuCo:  $\text{Ce}_{69}\text{Al}_{10}\text{Cu}_{20}\text{Co}_1$ , CeAlNiCu:  $\text{Ce}_{70}\text{Al}_{10}\text{Ni}_{10}\text{Cu}_{10}$ , CuZrHfTi:  $\text{Cu}_{60}\text{Zr}_{20}\text{Hf}_{10}\text{Ti}_{10}$  and NdAlFeCo:  $\text{Nd}_{60}\text{Al}_{10}\text{Fe}_{20}\text{Co}_{10}$ . (b) The  $dv/dP$  vs.  $v_0$  of various glasses including BMGs, metallic plastic of Ce-based metallic glasses and silica glasses. La-based BMG:  $\text{La}_{68}\text{Al}_{10}\text{Cu}_{20}\text{Co}_2$ , Zr-based BMG:  $\text{Zr}_{41}\text{Ti}_{14}\text{Cu}_{12.5}\text{Ni}_{10}\text{Be}_{22.5}$ , CuZr-based BMG:  $\text{Cu}_{47.5}\text{Zr}_{47.5}\text{Al}_5$ , Mg-based BMG:  $\text{Mg}_{65}\text{Cu}_{25}\text{Gd}_{10}$ , Ce-based BMG:  $\text{Ce}_{68}\text{Al}_{10}\text{Cu}_{20}\text{Co}_2$ , Pd-based BMG:  $\text{Pd}_{42.5}\text{Ni}_{7.5}\text{Cu}_{30}\text{P}_{20}$ , and Yb-based BMG:  $\text{Yb}_{62.5}\text{Zn}_{15}\text{Mg}_{17.5}\text{Cu}_5$ . [485].

larger than that of Pd-based BMG with larger  $v$ . This means that the increase of  $v$  of Yb-based BMG upon  $P$  is more than 20 times larger than that of Pd-based BMG. Remarkably, the  $v_0$  of various BMGs

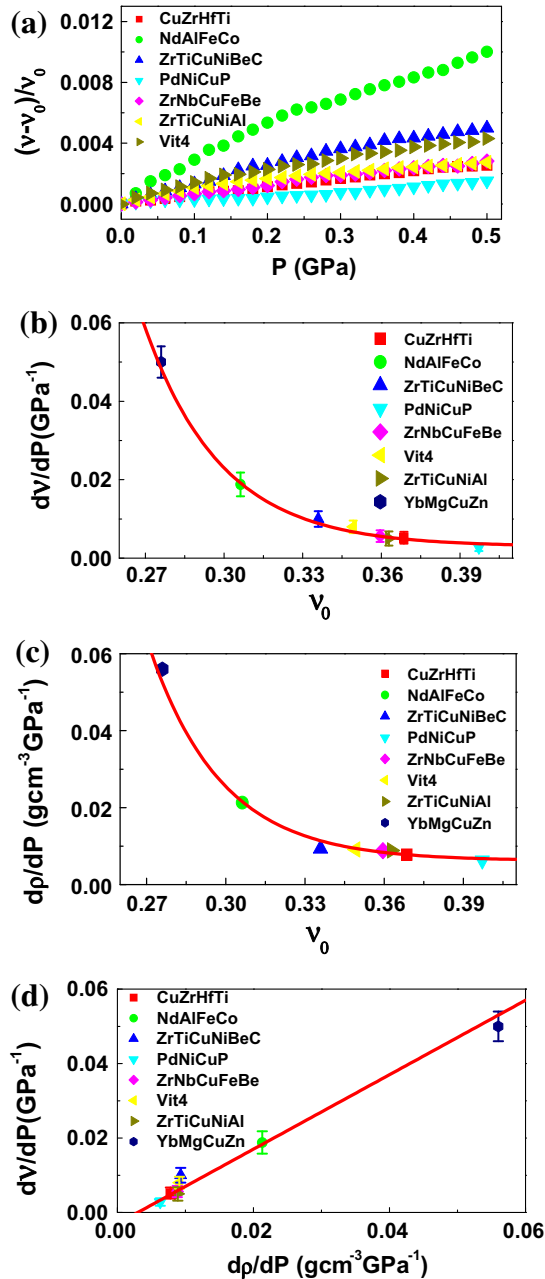


**Fig. 79.** (a) Variation of Poisson's ratio of BMGs with  $P$ . (b) The correlation between  $dv/dP$  and  $v$  of BMGs. YbMgCuZn BMG: Yb<sub>62.5</sub>Zn<sub>15</sub>Mg<sub>17.5</sub>Cu<sub>5</sub>. (c) The correlation between  $v$  and  $dp/dP$  (calculated by using the Cook's methods). (d) The correlation between  $dv/dP$  and  $dp/dP$  [485].

correlates with their slope of  $dv/dP$ , and the BMG with smaller  $v_0$  has larger  $dv/dP$ . As shown in Fig. 79b, the  $dv/dP$  vs.  $v_0$ , for BMGs can be expressed by an equation:

$$\frac{d\nu}{dP} = 0.00295 + 540 \exp(-34 \cdot \nu_0) \quad (8.15)$$

The results indicate that  $\nu$  can be viewed as a useful index to predict the extent of the change rate of  $\nu$  under  $P$  of a metallic glass, and there should exist distinct structural difference among these BMGs with similar structural characteristic consisting of efficiently packed clusters.

The  $P$ -induced density changes ( $d\rho/dP$ ) of these BMGs are calculated using the Cook's methods [71]. Under 0.5 GPa, the density of the Yb-based BMG with smallest  $\nu$  among these BMGs, has largest increase of  $\sim 5\%$  [484], and for Nd-based BMG (smaller  $\nu$ )  $\rho$  increases more than 2%, and the density of Pd-based BMG with bigger  $\nu$  increases only about 0.6%. It can be found that both  $d\rho/dP$  and  $d\nu/dP$  show very similar changing tendency with the increasing  $\nu_0$  as shown in Fig. 79c and d. The BMGs with high  $\nu$  are more difficult to be changed under pressure both in density and in Poisson's ratio itself.

The variation of  $\nu$  of various BMGs vs. temperature is shown in Fig. 80a. The  $\nu$  of all the BMGs monotonously decrease with decreasing  $T$  and the  $T$  dependence of the  $\nu$  of various BMGs can be modeled by the Varshni expression [225]. It is noted that the  $\nu$  of BMGs exhibits opposite changing tendency when lowering  $T$  and increasing  $P$ . This is due to the different response of volume-nonpreserving bulk modulus  $K$  and volume conservative shear modulus  $G$  upon lowering  $T$  and increasing  $P$ . The  $\nu$  can be expressed by the two elastic constants as:  $\frac{K}{G} = \frac{2}{3} \frac{1+\nu}{1-2\nu}$ , and it is obvious that the increase of  $K/G$  corresponds to the increase of  $\nu$ . Experimentally, the increase of  $K$  is larger than that of  $G$  when raising pressure. On the contrary, the increase of  $G$  plays a dominant role when lowering temperature,

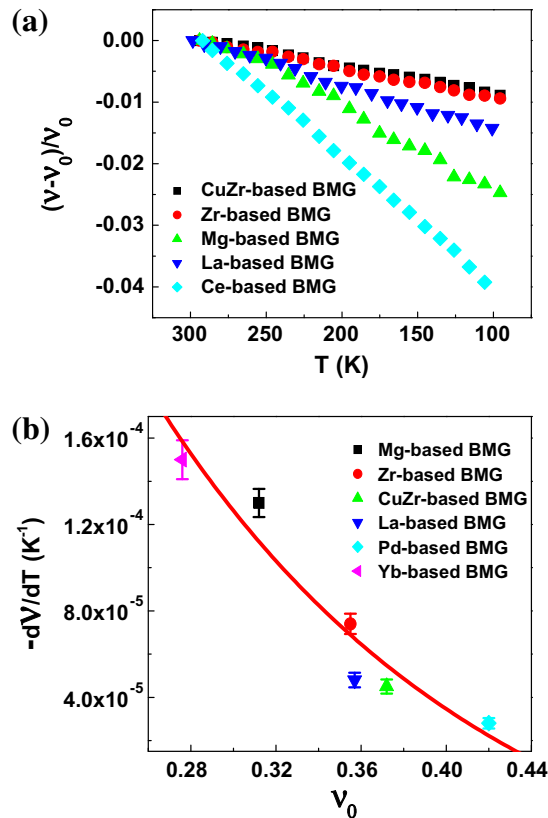


Fig. 80. (a) Variation of Poisson's ratio of BMGs with temperature. (b) The correlation between  $-d\nu/dT$  and  $\nu$  of BMGs [485].

and the  $G$  shows steep decrease while  $K$  undergoes weak  $T$  dependence. Therefore, different responses of  $K$  and  $G$  upon lowering  $T$  and increasing  $P$  lead to the opposite changing tendency of  $\nu$ . The opposite change of  $\nu$  is related to the structural features of a metallic glass and is corroborated by a recent theoretical study of Poisson's ratio changes in glasses [49].

When  $T < 100$  K, the decrease of  $\nu$  of Mg-based BMG (>2%) is two times larger than that of CuZr-based BMG (<1%). The difference further confirms structural difference in these BMGs. The correlation between  $-d\nu/dT$  and  $\nu$  of various BMGs at room temperature is shown in Fig. 80b. The absolute value of  $d\nu/dT$ , which represents the change of the atomic structure and density of the BMGs, decreases with the increasing  $\nu$ . It is found that even though the  $\nu$  of BMGs exhibits opposite changing tendency upon lowering  $T$  and increasing  $P$ , the  $T$  and  $P$  derivatives of the Poisson's ratio vs.  $\nu_0$  have similar tendency. That is, derivatives of  $\nu$  decrease with the increasing  $\nu_0$ , and the tendency can be fitted by similar equation:

$$-\frac{d\nu}{dT} = -0.00007 + 0.0013 \exp(-6.3 \cdot \nu_0) \quad (8.16)$$

The correlation shows that the BMGs with higher  $\nu$  are more stable upon lowering temperature, and can be used to predict the change rate of  $\nu$  of a BMG under low temperature.

The correlations further demonstrate that the Poisson's ratio is an important parameter for effectively reflecting free volume fraction which is key structural characteristic of glasses. The derivatives of  $\nu$  upon  $P$  or  $T$  can distinguish the chemical bonding nature of different kind of glasses. In addition, the results indicate that the  $\nu$  can reflect the free volume fraction in metallic glasses. The finding of free volume of BMGs with higher  $\nu$  is hard to be annihilated under pressure or upon lowering  $T$  compared to that of the BMGs with low  $\nu$  confirms that the volume conservative shear flow predominates in metallic glasses. Free volume is related to the formation, relaxation and deformation of metallic glasses. The free volume in a metallic glass increases as the plastic deformation proceeds because of the shear induced dilatation [3,23,486]. The links between  $\nu$  and free volume in glassy materials can assist in understanding of many fundamental issues in the metallic glasses such as plastic flow, relaxation and formation. The shear transformation zones, STZs or plastic units occur preferentially in the regions with plentiful of free volume in BMGs and evolve into shear bands upon loading. So, if the fraction of the free volume in BMGs hard to be annihilated (more free volume are left in the sample), their plasticity will be improved. The finding, that the free volume annihilation in BMGs with high  $\nu$  is more difficult under pressure or upon decreasing temperature compared with low  $\nu$  ones, means that the more STZs could be activated concurrently in the BMGs with higher  $\nu$ . Consequently, numerous shear band nuclei are formed concurrently in the BMGs which leads to good plasticity in the high  $\nu$  BMGs. The density change of brittle BMG (e.g. Yb-based BMG) is much larger than that of tough BMGs (e.g. Zr-based BMG), and the free volume fraction in high  $\nu$  BMGs is smaller than the fraction in the low  $\nu$  ones. Generally speaking, this indicates that more atoms between two nearest free volume sites in the tough BMGs with higher  $\nu$ , and the STZ of the high  $\nu$  BMGs generally contains more atoms comparing to that of the low  $\nu$  ones. And STZs of a large size reinforce the shear capability of the BMGs and promote the formation of multiple shear bands, which is consistent with the fact that a higher  $\nu$  represents a higher ductility [56]. The Poisson's ratio, which has loosed links with free volume fraction and bonding feature of glasses, is an important parameter for reflecting the microstructural features, deformation of glasses, and for providing predictability and formation design for the apparently disordered metallic glasses.

## 9. Correlations between elastic moduli and mechanical properties

The intrinsic relationships between mechanical properties and their crystal and electronic structures of crystalline materials have been well established with the development of dislocation theory and electronic theory, which can explain the atomic and electronic origins of the strength, deformation and plasticity of crystalline materials [487,488]. While for glassy materials, such as metallic glasses, the definite correlations between mechanical behavior and their atomic and electronic structures have not been properly established due to the complicated disorder structure. The underlying

physics of the strength and plasticity of metallic glasses at temperature well below glass transition temperature is poorly understood. Currently, efforts are being made in order to understand the elastic behavior of metallic glasses, mainly because the elastic properties of a metallic glass, which can be easily determined, are closely related to many of its mechanical qualities such as strength, hardness, toughness and plasticity. Elastic modulus  $E$ , hardness  $H_v$ , fracture strength  $\sigma_f$ , toughness  $K_c$  and plasticity are essential parameters of structural materials including metallic glasses, and the relationships among them are of keen interest to material scientists. The availability of various BMGs with a minimum dimension of  $\geq 1$  mm has permitted better characterization of their mechanical properties, and significant data have been collected on the mechanical properties (e.g. fracture strength and toughness, Vicker's hardness, and plasticity) and elastic constants for various metallic glasses [54–58]. Even if no comprehensive understanding of the mechanism for the strength, plasticity and deformation mechanism in BMGs, it would be intriguing to see if there exist relations between mechanical behaviors and elastic properties in these glassy alloys. The empirical correlations are useful for the design and exploration of BMGs with desired mechanical properties and for understanding the behaviors of metallic glasses.

### 9.1. Correlation between elastic moduli and strength

Structural materials are the workhorse of our infrastructure. Stronger and tougher metallic materials are always needed to reduce weight and improve safety [489]. The fracture strength of materials depends on various characteristics of the materials and represents a fundamental open issue of science and engineering, and is also key issues in characterizing the mechanical behavior of a structural material. For a given material with an original cross-section area  $A$ , if the applied maximum tensile force is  $F_{\max}$ , the fracture strength can be calculated by  $\sigma_f = F_{\max}/A$  [487]. It is well known that the actual strengths of various metallic materials are significantly different due to the difference in their microstructures and processing in details [487]. Theoretically, the Young's modulus  $E$  correlates with fracture tensile strength,  $\sigma_f$  of a material as [488]:  $\sigma_f = \left(\frac{E E_s}{d}\right)^{1/2}$ , where  $E_s$  is the surface energy per unit area, and  $d$  is the spacing of parallel atomic planes. For normal solids,  $\sigma_f$  is estimated to be about  $E/5 \sim E/10$  [488–491]. Frenkel suggested that the ideal strength of a metal should be given approximately by  $G/5$  [492]. However, the practical fracture strength for crystalline metallic materials is much lower than the theoretical values. In most metals the actual strength is closer to  $E/500$ – $E/10,000$  or  $G/1000$  due to the motion of dislocations or other defects at much lower stresses. The factors determining fracture strength have no simple link with interatomic potentials, yet there is a rough correlation between  $E$  and  $\sigma_f$ :  $E/\sigma_f = 500 \sim 10000$ . The correlation provides evidences for the existence of defects such as dislocations in crystalline alloys and assists in understanding the relation between microstructure and mechanical properties [491]. One of most important characteristics of metallic glasses is their ultrahigh strength. Analogous to dislocation-free crystals, the strength and the shear strength of a metallic glass is expected to be close to the theoretical value ( $\sim E/10$  for fracture strength or  $\sim G/5$  for shear strength). However, the extensive experimental results show that the highest strength of metallic glasses is also about 3–4 times smaller than the theoretical strength. The deviation from the theoretical value is attributed to the existence of manufacture flaws or structural “defects” and unique deformation model and local shearing of the glasses [493–499], and a number of micro-scale mechanisms have been proposed to describe the spatially and temporally heterogeneous deformation. However, the physical process that governs the yielding and strength of glassy alloys still remains mysterious and has been the recent topic of intense discussions [29,45].

The study of relationship between fracture strength and Young's modulus in BMGs could provide insight on the issue. Primary analysis based on limited data from metallic glasses show that the strength normalized with respect to  $E$  [54,393]. However, there currently is very active development of new compositions for forming BMGs and the reported strength ranges widely from 300 MPa to more than 5000 MPa and the Young's modulus ranges from 25 GPa to 300 GPa [56]. The Co-based glassy alloy exhibits ultrahigh fracture strength (5.185 GPa) and high  $E$  (268 GPa) [175]. In particular, the newly developed Sr-, Ce-, Yb- and CaLi-based BMGs with low  $E$  value ( $< 30$  GPa, is comparable to those of polymers) [113–128,173] and low strengths (300–500 MPa) demonstrates that BMGs are not

necessarily “hard” but could be “soft” [113–128,173,500,501]. The plentiful data available on elastic moduli and mechanical properties permit a better assessment for metallic glasses by establishing links between strength and elastic moduli.

Table 12 lists relevant data on typical metallic glasses in the literatures (including almost all kinds of developed BMGs based on different elements with representative compositions). Even though the original data are obtained from different groups with various testing conditions, the data on these metallic glasses, plotted in Fig. 81, show clear good correlations between fracture strength  $\sigma_f$  and  $E$ :

$$E/\sigma_f \approx 50 \quad (9.1)$$

There may be some composition-dependent spread in the correlation, but it is remarkable that the spread is so small and certainly much less than for that of the crystalline materials. On the other hand, for these metallic glasses, the ratio of  $E/\sigma$  is 50, which approximately 10–200 times larger than those of their crystalline counterparts and is close to the theoretical strength (about  $E/5 - E/10$ ) [488]. This indicates the fundamental mechanical properties of the metallic glasses are significantly different from those of crystalline alloys. The correlation is remarkable good as that found when comparing different glasses, as can be seen when all the data on various metallic glasses prepared by different methods with marked different properties are combined. The glasses based on Ca, CaLi, Sr, La and Ce with the lowest values of  $E$ , the Co- and Fe-based BMGs with strength well in excess of 4000 MPa, and the recent report of tungsten-based glasses with extreme high  $E$  ( $=309$  GPa) and exceptionally stronger mechanical properties than those of any metallic glasses so far reported [424], all fit well on the same correlation. The existence of the positive correlation does not depend on the chemical composition of the BMGs but is mainly related to the intrinsic homogeneous glassy structure. Overall, it would appear that glassy alloys are more strength than their crystalline counterparts, and the high strength is intrinsic in BMGs and closely related to their elastic properties [56].

Data for room temperature shear stress at yielding  $\tau_Y$  and shear modulus  $G$  of BMGs reveals a similar relationship:  $\tau_Y = \gamma_c G$  [82]. Fig. 82 shows the experimental shear stress at yielding,  $\tau_Y$  ( $\approx \sigma_Y/2$ ) vs.  $G$  for BMGs [82]. A clear linear correlation with a best fit of  $\gamma_c = G/\tau_Y = 0.0267$  are obtained. Based on the correlation, a scaling relationship among the shear flow barrier, a universal critical yield strain  $\gamma_c$  and the isoconfigurational shear modulus,  $G$ , were constructed [82], which reveals that for a fixed glass

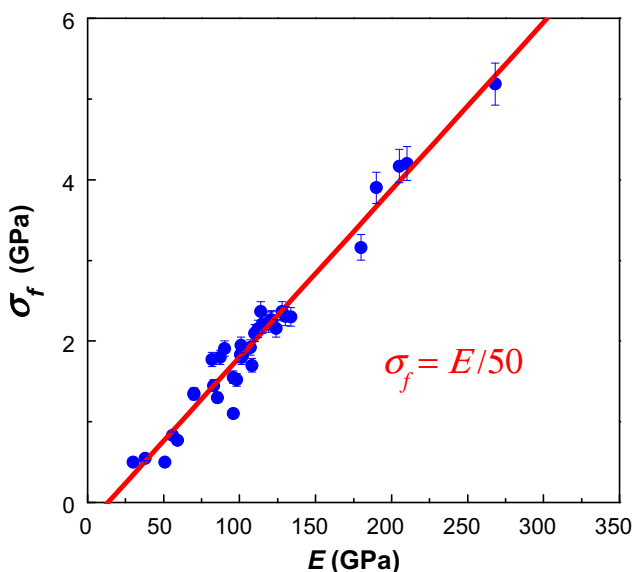


Fig. 81. The correlation of mechanical strength  $\sigma_f$  with elastic modulus  $E$  for all the metallic glasses (listed in Table 12) for which relevant data are available.

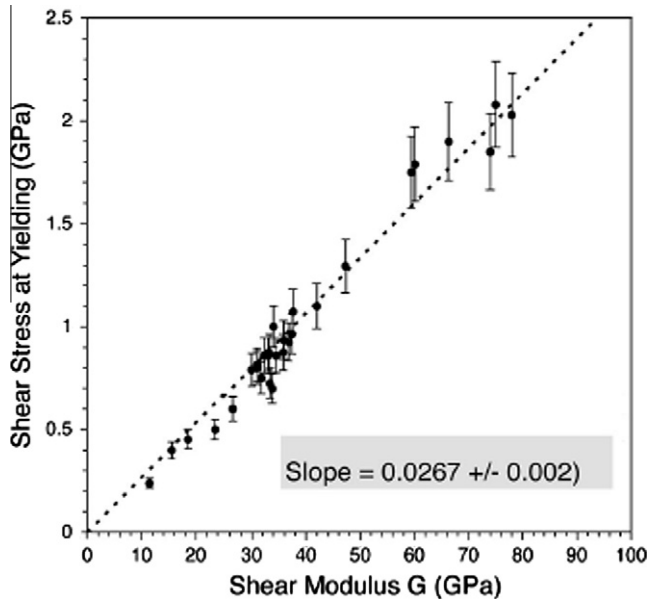


Fig. 82. Experimental shear stress at yielding,  $\tau_y$  vs. shear modulus  $G$  at room temperature for various BMGs [82].

configuration, the barrier height for shear flow is proportional to  $G$ . It is also found that  $G$  has a strong dependence on the specific configurational potential energy of the equilibrium liquid, and the temperature dependence of  $G$  in the liquid state is directly related to the fragility of the metallic glass-forming liquids. A rheology law of metallic glass-forming liquids has been proposed and validated in which  $G$  was identified to be the effective thermodynamic state variable controlling flow [82,493]. A lower  $G$  implies that the shear flow barrier for an unstressed shear cooperative zone is relatively small, which allows the atoms to get into a higher potential energy configuration and benefits the plastic yielding behavior.

The strength and the shear strength of a metallic glass are still about 3–4 times smaller than the theoretical strength. In conventional mechanical test, the metallic glasses usually fracture in brittle manner before macroscopic yielding occurs, which making it difficult to unambiguously determine their yield stress. The deviation from the theoretical value is attributed to the existence of manufacture flaws or structural “defects”, and unique deformation model and local shearing of the glasses [494,502]. In crystalline metallic materials, reducing sample size can lead to defect-free materials and the approach of the theoretical strength in crystalline materials [503]. Along this idea, Bei et al. determined the highest shear strength of BMGs by employing nanoindentation, the measured values are very close to the theoretical values [494]. The results suggest that the strength of BMGs is determined solely on the bonding force between the constitutive atoms. Recently, detectable sample size effect on strength was reported in the micro-compression experiments of metallic glasses, and about 9% increase over bulk values from the micro-pillars was measured [504]. This increase in strength is attributed to decreases in the flaw population in the microscale specimens demonstrating the sample size effect in shear band initiation in macroscopic samples and influence of flaws on the strength of the BMGs.

Both  $E$  and yielding strength show general linear correlation with  $T_g$ . By incorporating the term of molar volume  $V_m$ , the fracture strength of glassy alloys has been found to have a clearer linear relation with  $T_g$  [54,323,402]. A number of attempts have been made to explore the underlying physics of the linearity [323,505]. Recently, an inherent relationship of yield strength  $\tau_y$  with glass transition temperature  $T_g$  and molar volume  $V$  of metallic glasses in a universal scaling equation of  $\tau_y = 3R \cdot (T_g - RT)/V$  [506] (where  $\tau_y$  is yield shear stress and  $\tau_y \approx \sigma_y/2$ ) is derived from fundamental

thermodynamics and validated by various metallic glasses with well-defined yielding. As shown in Fig. 83a, the room temperature yield shear strengths (spanning from  $\sim 1.7$  GPa to  $\sim 4.0$  GPa) for typical BMGs (listed in Table 15) do show a distinct dependence on  $(T_g - RT)/V$  in a linear manner. The relationship between  $\tau_y$  and  $(T_g - RT)/V$  is plotted as the solid line, and equation derived from fundamental thermodynamics fits the experimental results well. It is interesting to note that the fitting slope is just equal to the Dulong–Petit limit  $3R$  while  $\gamma_0$  is equal to 1. In comparison with other empirical relations, the slope of 50 in other study [323] is actually the product of Dulong–Petit limit  $3R$  and the Schmid factor 2, both of which are invariable for BMGs. According to experimental observations and computer simulations, the yield point of BMGs corresponds to the destabilized propagation by the percolation of a large number of local shearing events with a critical shear strain,  $\gamma_0$  [486]. The transition from local shearing to macroscopic shear bands results from the dramatic increase of the atom mobility and softening along a shear plane motivated by the input of mechanical energy [507,508]. The linearity intrinsic correlation between  $\tau_y$  and  $T_g$  demonstrates the transition is akin

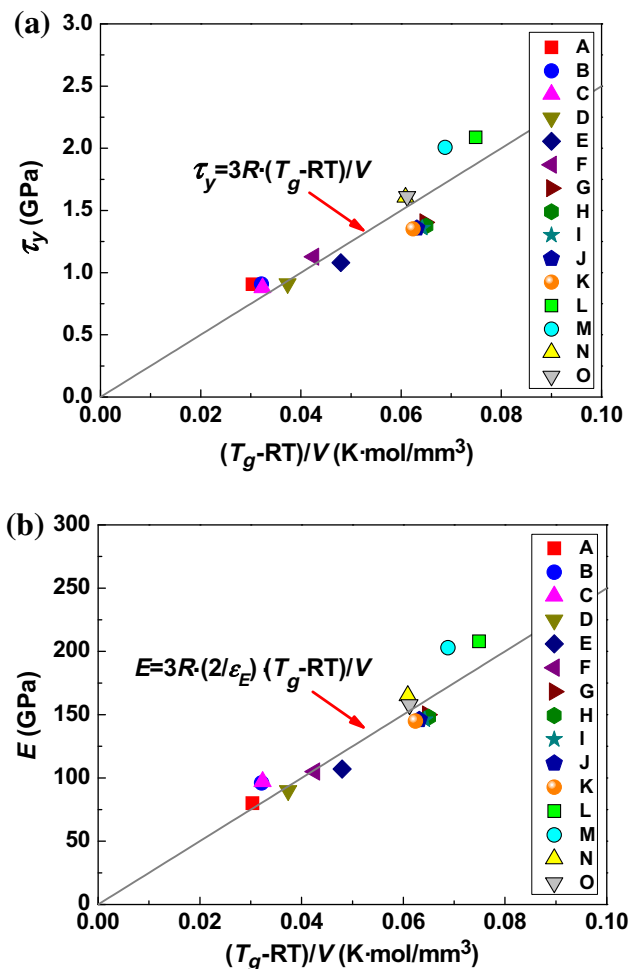


**Fig. 83.** (a) The relationship between yield shear stress  $\tau_y$  and glass transition temperature  $T_g$ . The solid line is the plot of Eq. (4),  $\tau_y = 3R \cdot (T_g - RT)/V$ , in which  $R$  is the gas constant. (b) The relationship among Young's modulus  $E$  and glass transition temperature  $T_g$ . The solid line is the plot of equation  $E = 3R \cdot (2/\epsilon_E) \cdot (T_g - RT)/V$ , in which  $R$  is the gas constant and  $\epsilon_E$  is the elastic limit in uniaxial compression [506].

**Table 15**

Summary of yield strength  $\sigma_y$ , Young's modulus  $E$ , glass transition temperatures  $T_g$ , and calculated molar volume  $V_m$  of 15 different BMGs from five alloy systems [506].

Label	BMG	$\sigma_y$ (GPa)	$E$ (GPa)	$T_g$ (K)	$T_m$ (K)	$V_m$ (mm <sup>3</sup> /mol)
A	Zr <sub>62</sub> Cu <sub>15.4</sub> Ni <sub>12.6</sub> Al <sub>10</sub>	1.812	80	652	–	11666
B	Zr <sub>59</sub> Ta <sub>5</sub> Cu <sub>18</sub> Ni <sub>8</sub> Al <sub>10</sub>	1.817	96	673	–	11,669
C	Zr <sub>41.2</sub> Ti <sub>13.8</sub> Cu <sub>12.5</sub> Ni <sub>10</sub> Be <sub>22.5</sub>	1.755	97	620	932	9949
D	(Cu <sub>0.5</sub> Zr <sub>0.5</sub> ) <sub>95</sub> Al <sub>5</sub>	1.824	90	693	–	10,570
E	Cu <sub>60</sub> Zr <sub>20</sub> Hf <sub>10</sub> Ti <sub>10</sub>	2.160	107	754	1128	9504
F	(Ti <sub>0.5</sub> Cu <sub>0.5</sub> ) <sub>84</sub> Ni <sub>7</sub> Hf <sub>5</sub> Zr <sub>3</sub> Si <sub>1</sub>	2.254	105	687	–	9136
G	Ni <sub>62.5</sub> Zr <sub>20</sub> Nb <sub>15</sub> Pd <sub>2.5</sub>	2.808	150	867	1368	8792
H	Ni <sub>60</sub> Zr <sub>20</sub> Nb <sub>15</sub> Pd <sub>5</sub>	2.752	148	873	1353	8850
I	Ni <sub>57.5</sub> Zr <sub>20</sub> Nb <sub>15</sub> Pd <sub>7.5</sub>	2.717	146	870	1351	8907
J	Ni <sub>55</sub> Zr <sub>20</sub> Nb <sub>15</sub> Pd <sub>10</sub>	2.714	146	864	1349	8965
K	Ni <sub>52.5</sub> Zr <sub>20</sub> Nb <sub>15</sub> Pd <sub>12.5</sub>	2.705	145	861	1352	9023
L	[(Fe <sub>0.8</sub> Co <sub>0.1</sub> Ni <sub>0.1</sub> ) <sub>0.75</sub> B <sub>0.2</sub> Si <sub>0.05</sub> ] <sub>96</sub> Nb <sub>4</sub>	4.177	208	818	–	6945
M	[(Fe <sub>0.6</sub> Ni <sub>0.4</sub> ) <sub>0.75</sub> B <sub>0.2</sub> Si <sub>0.05</sub> ] <sub>96</sub> Nb <sub>4</sub>	4.014	203	770	–	6864
N	Fe <sub>76</sub> Si <sub>9.6</sub> B <sub>8.4</sub> P <sub>6</sub>	3.212	165	783	1271	7964
O	(Fe <sub>0.76</sub> Si <sub>0.096</sub> B <sub>0.084</sub> P <sub>0.06</sub> ) <sub>99.9</sub> Cu <sub>0.1</sub>	3.225	158	785	–	7956

to a process of stress driven glass-to-liquid transition [506–508] and the yielding of BMGs can be rationally presumed as a critical point at which the accumulated internal energy by elastic deformation is high enough for the transition from a glass to a supercooled liquid. This contributes to the basic understanding of the strength and the thermodynamic origin of shear band formation and BMG yielding. The free-volume regions are the preferred regions to initiate the destabilization of glassy structure caused by either temperature (glass transition) or applied shear stresses (local shearing). The linear correlation between  $\tau_y$  and  $T_g$  evidently demonstrates that the strength of BMGs is controlled by a process of shear transformation, equivalent to glass transition (or localized glass transition), and thus the strength of BMGs is determined by the free volume or loosely atomic packing regions, and the elastic destabilization of metallic glasses driven by external forces is equivalent to the glass transition localized in shear bands induced by mechanical energy.

### 9.2. Correlation between elastic moduli and microhardness

Elastic modulus  $E$  and hardness  $H_v$  are two essential parameters of engineering materials, and their relationship is of keen interest. The indentation hardness,  $H_v$ , is the resistance of a material to a permanent indentation, conventionally defined as the average pressure under the indenter in fully developed plasticity, where the hardness  $H_v$ , given by the ratio of the applied load to the remnant contact area, of the plastic indentation. For traditional metallic crystalline materials, the relationship between  $H_v$  and elastic modulus was proposed by Tabor [509,510]. From statistical trend,  $E$  is usually considered to be a function of hardness for crystalline materials [511]. The summarized a number of measurements to show that for various crystalline materials hardness roughly scales with elastic modulus, while this rule neither has analytical support nor is generally obeyed.

For metallic glasses with homogenous structure relative to their corresponding crystal, it is interesting to know if there exist a general relationship between elastic moduli and hardness. Indentation tests including nanoindentation tests, which are quite easy to perform, have been widely used to measure the  $H_v$  of metallic glasses including BMGs and plentiful data are available. Table 12 lists relevant data of the Vicker microhardness  $H_v$  of typical metallic glasses which are able to be found in the literatures. As plotted in Fig. 84, there is a good correlation between  $H_v$  and  $E$ :

$$E/H_v \approx 20 \quad (9.2)$$

Even there is composition-dependent spread in the correlation, the spread is so small in various BMGs with markedly different mechanical properties. Due to the linear relationship between  $E$  and  $\sigma_f$  as shown above. The  $H_v$  and  $\sigma$ , as expected, show a remarkable good correlation as (as shown in Fig. 85):

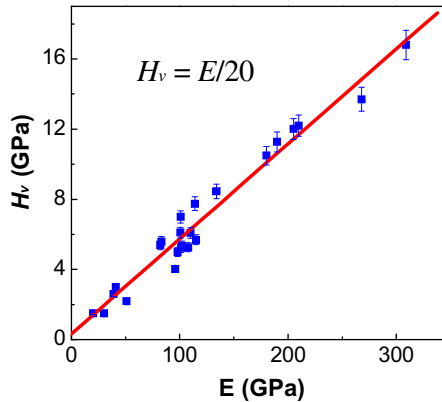


Fig. 84. The correlation of  $H_v$  and elastic modulus  $E$  for the metallic glasses (listed in Table 12) for which relevant data are available.

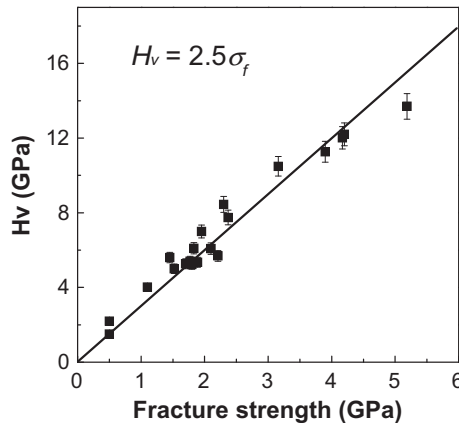


Fig. 85. The correlation of the  $H_v$  and mechanical strength  $\sigma_f$  for the available bulk metallic glasses.

$$H_v = 2.5\sigma_f \quad (9.3)$$

The ratio of  $H_v$  and  $\sigma$  is close to crystalline metallic materials, which gives a value of 2.7 [509]. Therefore, the microhardness can be characterized as a function of the elastic moduli in metallic glasses independent of the composition. The clear correlation is useful for hard or soft metallic glassy materials design and for BMG properties controlling.

### 9.3. Correlation between elastic moduli and toughness/plasticity

Whether a material shows plastic flow or brittle fracture on loading is of clear practical significance. In crystalline materials, the plastic deformation results from the motion of defects such as linear defect of dislocations, and the applied energy can be accommodated through many pathways including dislocation slip, twin, phase transformation, heat generation, etc. [512]. However, in metallic glasses, plastic deformation is not enabled to be accommodated by defects in crystalline materials such as dislocations. Some models such as free volume model and shear transformation zones model involving clusters of atoms that undergo cooperative shear displacements have been proposed [513,514] to understand the plastic flow in metallic glasses. Among these models, the STZ model is

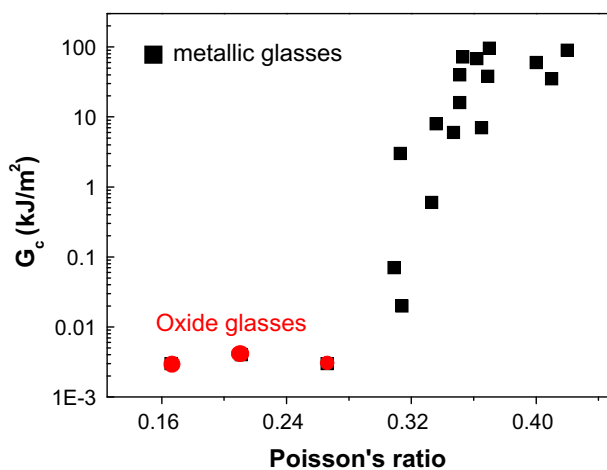
widely accepted. According to the STZ model, one STZ's operation creates a localized distortion of the surrounding material and triggers the autocatalytic formation of more STZs. The shear band is formed by a collective operation of many STZs due to the stress localization and local shear softening. The deformation in conventional metallic glasses occurs in thin shear bands with nano-scale thickness, and the shear softening in the deformation zones leads to inhomogeneous flow and shearing-off failure without macroscopic plasticity [370,390,513,514]. However, whereas most BMGs fail in this manner, some undergo surprisingly extensive plastic deformation in compression or bending, or under some confinements [85,377–394,515–530]. It is so far difficult to observe the changes in atomic structure during deformation and the exact nature of local atomic motion in deforming metallic glasses is not fully resolved. Atomic-scale simulations play an important role in the study of the deformation mechanism. Different explanations and models such as free volume model and STZ model have been given for understanding the intrinsic ductility of some BMGs. Egami [302–304,340] attempted to describe the deformation of metallic glasses through local atomic rearrangements that result in different coordination and leading eventually in local alteration of the elastic modulus of material. However, the exact mechanism of the deformation of metallic glasses is still unclear.

For crystalline metals, the plastic flow and the glide of dislocations on close-packed planes tested at low homologous temperature are controlled by  $G$ , and the brittle fracture which arises due to the dilatation cause by stress present near a crack/defect is controlled by  $K$ . It has long been known that in polycrystalline metals the ratio of  $G$  to  $K$ , correlates with mechanical behavior. That is, high  $G/K$  favors brittleness and vice versa [531–534]. The data on some polycrystalline pure metals provide a qualitative ranking from ductile (e.g. Ag, Au, Cd, Cu) to brittle (e.g. Be, Ir) behavior as  $G/K$  increases [532]. Similar studies on the relationship between Young's modulus and the shear modulus or Poisson's ratio for cracked brittle materials have also been reported. A relation between  $E$  and  $\nu$  as a function of crack density for materials containing large amount of cracks is derived [535,536]. The negative Poisson's ratio effects on natural layered ceramic have been investigated which show that the negative Poisson's ratio effect can yield very high energy absorption in a natural layered ceramics and increase the volume strain energy per unit volume by 1100% and, simultaneously, decrease the deformation strain energy per unit volume by about 44%. The negative Poisson's ratio effect effectively enhances the deformation capacity by about 1 order of magnitude in the tension of the natural layered ceramics [536].

Therefore, the correlations established between plastic deformation and elastic constants could assist in elucidating flow and fracture mechanisms, in understanding annealing-induced embrittlement in metallic glasses, and in guiding alloy design to alleviate brittleness. The flow and fracture of metallic glasses, in relation to elastic constants particularly  $G/K$  or Poisson's ratio  $\nu$ , have been widely studied because the Poisson's ratio has been known to vary with the strength of intermolecular forces and the chemical constituents of both a crystal and glass. Chen et al. first reported that ductile metallic glasses tended to have a large Poisson's ratio or lower  $G/K$  [111]. Recently, the remarkable relationship between toughness and  $G/K$  or  $\nu$  has been established in metallic glasses [56,319]. After then, the relationships between elastic moduli and toughness or compressive plasticity of metallic glass especially in BMGs have been extensively studied [56,85,113,161,272,319–321,334,335,352,537–539]. The available data of toughness and elastic moduli of  $G/K$  or Poisson's ratio for as-cast BMGs are collected in Table 16. Because the metallic glasses under comparison have such a wide range of Young's modulus  $E$ , it is better to quantify their mechanical behavior in terms of the energy of fracture  $G_c$ . This is the energy required to create two new fracture surfaces, and for ideally brittle materials is just  $2\gamma$ , where  $\gamma$  is the surface energy per unit area. Under plane strain,  $G_c = K_c^2/E(1 - \nu^2)$  [544], where  $K_c$  is the stress intensity ( $\text{MPa m}^{1/2}$ ) at fracture. Fig. 86 shows the relation between  $G/K$  and fracture energy  $G_c$  [319]. A clear correlation between  $G_c$  and  $G/K$  or  $\nu$  can be seen. With low values of  $G/K$ , the glasses based on Zr, Cu or Pt all have fracture energies in excess of  $1 \text{ kJ m}^{-2}$ , exhibit extensive shear banding, and have vein-pattern fracture surfaces. With high  $G/K$  the Mg- and Fe-based metallic glasses approach the ideal brittle behavior ( $G \approx 1 \text{ J m}^{-2}$ ) associated with oxide glasses. The results indicate that the ratio of  $G/K$ , correlates with mechanical behavior, e.g., the intrinsic plasticity or brittleness of metallic glasses correlates with the ratio of  $G$  to  $K$ : high  $G/K$  favors brittleness and vice versa, and when the ratio  $G/K$  exceeds a critical value, the metallic glass is brittle. The correlation is the same as that found when comparing different glasses, and the annealing-induced embrittlement also correlates with a critical

**Table 16**The data of  $E$ ,  $G/K$ , Poisson's ratio  $\nu$ , the stress intensity  $K_c$  (MPa m<sup>1/2</sup>), and the energy of fracture,  $G_c$  on available BMGs.

Glassy systems	$E$ (GPa)	$G/K$	$\nu$	$K_c$ (MPa m <sup>1/2</sup> )	$G_c$ (kJ/m <sup>2</sup> )	Refs.
Zr <sub>35</sub> Ti <sub>30</sub> Cu <sub>8.25</sub> Be <sub>26.75</sub>	86.9	0.285	0.37	85	96.1	[158]
Zr <sub>57</sub> Ti <sub>5</sub> Cu <sub>20</sub> Ni <sub>8</sub> Al <sub>10</sub>	82.0	0.303	0.362	80	68	[54,540]
Zr <sub>57</sub> Nb <sub>5</sub> Cu <sub>15.4</sub> Ni <sub>12.6</sub> Al <sub>10</sub>	87.3	0.297	0.365	27	7	[54,540]
Zr <sub>41</sub> Ti <sub>4</sub> Cu <sub>12.5</sub> Ni <sub>10</sub> Be <sub>22.5</sub>	101.3	0.324	0.353	86	72	[54,541]
Zr <sub>61</sub> Cu <sub>17.3</sub> Ni <sub>12.8</sub> Al <sub>7.9</sub> Sn <sub>1</sub>	77.4	0.274	0.374	46.2	44	This work
Zr <sub>61</sub> Cu <sub>16.3</sub> Ni <sub>12.8</sub> Al <sub>7.9</sub> Sn <sub>2</sub>	81.92	0.300	0.363	37.6	14.6	This work
Annealed 0.75 @ 623 K	101.6	0.329	0.351	68	40	[278,541]
Annealed 1.5 @ 623 K	101.6	0.329	0.351	42.5	16	[278,541]
Annealed 3 @ 623 K	107.5	0.339	0.347	27	6	[278,541]
Annealed 6 @ 623 K	111.4	0.368	0.336	32	8	[278,541]
Annealed 12 @ 623 K	113.3	0.376	0.333	9	0.6	[278,541]
Cu <sub>60</sub> Zr <sub>20</sub> Hf <sub>10</sub> Ti <sub>10</sub>	101.1	0.288	0.369	67	38	[54,542]
Ti <sub>40</sub> Zr <sub>25</sub> Cu <sub>12</sub> Ni <sub>3</sub> Be <sub>20</sub>	97.3	0.279	0.352	39.7	14.2	[545]
Ce <sub>70</sub> Al <sub>10</sub> Ni <sub>10</sub> Cu <sub>10</sub>	30.3	0.427	0.313	10	3	[54,319]
Dy <sub>40</sub> Y <sub>16</sub> Al <sub>24</sub> Co <sub>20</sub>		0.417	0.317		0.06	[506]
Mg <sub>65</sub> Cu <sub>25</sub> Tb <sub>10</sub>	51.3	0.439	0.309	2	0.07	[54,319]
Fe <sub>50</sub> Mn <sub>10</sub> Mo <sub>14</sub> Cr <sub>4</sub> C <sub>16</sub> B <sub>6</sub>	200.0	0.423	0.314	2	0.02	[320]
Fe <sub>48</sub> Cr <sub>15</sub> Mo <sub>14</sub> C <sub>15</sub> B <sub>6</sub> Er <sub>2</sub>	192	0.420	0.316	12.7	0.722	[320]
Pd <sub>77.5</sub> Cu <sub>6</sub> Si <sub>16.5</sub>	88.8	0.189	0.41	51	35	[54,543]
Fe <sub>80</sub> P <sub>13</sub> C <sub>7</sub>	137.3	0.214	0.4	77	60	[319,543]
Pt <sub>57.5</sub> Cu <sub>14.7</sub> Ni <sub>5.3</sub> P <sub>22.5</sub>	94.8	0.167	0.42	84	90	[113]
Pt <sub>74.7</sub> Cu <sub>1.5</sub> Ag <sub>0.3</sub> P <sub>18</sub> B <sub>4</sub> Si <sub>1.5</sub>		0.150	0.43	125		[113]
Pd <sub>79</sub> Ag <sub>3.5</sub> P <sub>6</sub> Si <sub>9.5</sub> Ge <sub>2</sub>		0.18	0.42	200		[671]
Fused silica	72.9	0.858	0.166	0.5	0.003	[54,319]
Window glass	67.2	0.716	0.211	0.2	0.004	[54,319]
Toughened glass	87.0	0.555	0.266	0.5	0.003	[54,319]

**Fig. 86.** The correlation of fracture energy  $G_c$  with ratio  $G/K$  for all the collected data on metallic glasses (as-cast and annealed), as well as for oxide glasses. The divide between the tough and brittle regimes is in the range  $\nu_{crit} \sim 0.32$  [319].

$G/K$  of 0.41–0.43 [319]. The correlation can also be expressed in terms of the Poisson's ratio  $\nu$ . Higher values of  $\nu$  give higher fracture energy, and the transition between brittle and tough regimes being for  $\nu_{crit} \sim 0.32$ . The larger the  $\nu$  is, the more ductile the BMGs become, and small variation of  $\nu$  will significantly change the ductility. The toughness and Poisson's ratio correlation is verified in more and more metallic glass systems [56,85,113,161,282,319–321,334,335,352,537,538,545]. The correlation, which is regarded as to be a reflection of the similarity in the deformation and fracture mechanisms

between the various metallic glasses with marked differences in toughness, assists in understanding the mechanisms of plastic flow and fracture in glassy systems.

The correlation between  $G/K$  (or  $\nu$ ) and fracture energy is interpreted in terms of a competition between plastic flow and fracture [319] or in terms of a competition between shear and dilatation [56,113]. A low value of  $G$  implies weak resistance to plastic deformation in shear, while a high value of  $K$  implies strong resistance to the dilatation required for mode I crack propagation. And this would make it more difficult to attain the critical shear displacement and thus explain the increased toughness. For crystalline metals, the relationship between  $G/K$  and fracture can be explained quantitatively in terms of plastic deformation processes near the crack tip [365], but no similar quantitative model has been developed for metallic glasses yet. Still, the idea that a low value of  $G/K$  favors extension of the shear bands over crack propagation has obvious intuitive appeal [370].

According to STZ model, the plastic flow of metallic glasses occurs through cooperative shearing of unstable STZs activated by shear stress [514]. Recently, it is found that the measured STZ volumes of the six BMG systems increase with Poisson's ratio and BMG ductility, suggesting an intrinsic correlation between ductility and the Poisson's ratio [546]. Because an elastic strain of  $\approx 2.0\%$  is required for the formation of an embryonic shear band in BMGs that consists of a local collection of STZs, a large STZ volume, when compared with a small one, enables a smaller number of STZs to be activated for the nucleation of a shear band in plastic yielding of metallic glasses. Hence, STZs with a large size reinforce the shear capability of the metallic glass and promote the formation of multiple shear bands (or increase the shear bands forming ability of a metallic glass), which concurs with the fact that a higher Poisson's ratio represents a higher possibility for the material to shear under applied stresses [546].

In metallic glasses, the nature of chemical bonds is linked with the Poisson ratio [302]. In particular, low  $\nu$  values have been associated with a covalent-like contribution to the chemical bond, as expected for metal–metallic glasses. Therefore, a more difficult movement among structural units and a “rough” energy surface in energy landscape model are expected, and the plastic flow becomes difficult and the material shows a brittle behavior [56,302]. On the other hand, a higher Poisson ratio is related to a more isotropic bonding behavior [302], so that plastic flow becomes easier and a more ‘flat’ energy landscape is expected.

Poon et al. [272] extended the toughness and Poisson's ratio correlation to individual Fe- and Ti-based BMGs via changes in alloy content which display crossover from brittle to ductile via controlling Poisson's ratio. They found that the compositional dependences of elastic moduli are anomalous considering the elastic moduli of the alloying elements, and the same critical value of  $\nu$  or  $G/K$  can be obtained which corresponds well to the crossover from brittle to ductile of these BMGs. The result lends support to the universal nature of the brittle-to-plastic transition for metallic glasses. The finding indicates that the crossover from brittle to ductile at a critical  $\nu$  or  $G/K$  in some BMGs can be realized by tuning their elastic properties. In Mg-based BMGs, a critical  $\nu$  is found to locate at the demarcation separating brittle and ductile BMGs [423]. The elastic constants and plasticity change tendency upon changing composition in  $(\text{Cu}_{50}\text{Zr}_{50})_{100-x}\text{Al}_x$  ( $x = 0-8$  at.%) BMGs have been studied [537] and the results show that the plasticity of the BMGs is sensitive to the change of Al content that can be well characterized by the Poisson's ratio. The  $\nu$  and plasticity have a homologous evolution with regard to the adjustment of composition in the alloy are shown in Fig. 87. The plastic deformations with regard to Al percentage composition in  $(\text{Cu}_{50}\text{Zr}_{50})_{100-x}\text{Al}_x$  BMGs exhibits marked different and a maximum plasticity of 16% is reached for  $(\text{Cu}_{50}\text{Zr}_{50})_{105}\text{Al}_5$ , while  $(\text{Cu}_{50}\text{Zr}_{50})_{92}\text{Al}_8$  only has a disappointing plasticity of less than 0.5% as shown in Fig. 87a. The distinct contrast implies the ductility of the BMGs is very sensitive to the composition. Meanwhile, the Al composition dependence of  $\nu$  or  $G/K$  shows anomalous considering the elastic moduli of the alloying elements as presented in Fig. 87b. It can be clearly seen that  $\nu$  has a maximum around the composition of  $(\text{Cu}_{50}\text{Zr}_{50})_{95}\text{Al}_5$ . Both Poisson's ratio and plastic strain have a similar change tendency upon the variation of Al content, and show the maximum peak around the same composition of  $(\text{Cu}_{50}\text{Zr}_{50})_{95}\text{Al}_5$ . The sample with the largest ductility of 16% plastic strain has the largest Poisson's ratio value of 0.372 in the BMGs. The similar variation tendency of plastic strain and Poisson's ratio to the change of Al content reveals that they are well correlated. The change of the Al content leads to dramatically microstructural change in certain composition of the CuZr-based BMGs, and furthermore, exquisitely adjusts the elastic properties of the BMGs. The

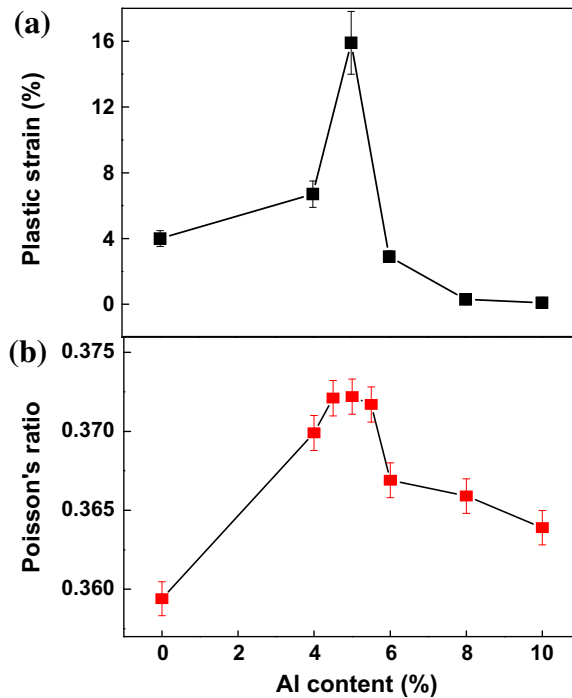


Fig. 87. The dependence of plastic strain (a) and Poisson's ratio (b) on Al content for the  $(\text{Cu}_{50}\text{Zr}_{50})_{100-x}\text{Al}_x$  BMGs [537].

phenomenon may be due to the intrinsic structural characteristics of BMGs consisting of packed atomic clusters [547–549].

The composition-related correlation between the Poisson's ratio and plasticity implies ductile BMGs could be obtained by appropriately adjustment of the compositions in known or unknown BMG-forming alloys [85,550,551]. The subtle changes of the compositional dependent structure and plasticity of the alloy has been found in ZrAlNiCu BMG-forming system [85]. Minor content deviation drastically changes the plasticity of the ZrAlNiCu BMGs. The plastic BMGs were synthesized on the basis of the appropriate choice of composition by controlling Poisson's ratio. The excellent plastic BMGs with relative high Poisson's ratio are found to possess microstructures composed of strongly bonded hard regions surrounded by weakly bonded soft region. Such unique microstructures bestow the BMGs ability to undergo true strain larger than 30% which could be obtained only at high temperature previously [85]. The Poisson's ratio is an indicator of the high concentration of the thermally unstable free volumes in soft regions of the BMGs, due to the fact that Poisson's ratio decreases with increasing annealing temperatures (annihilation of more fraction of free volume annealed at higher temperatures) [109]. Furthermore, it is self-evident that the concentrations of the free volumes play essential role responsible for how much plasticity could be obtained in BMGs, because reduction of them would decrease the plasticity and even induce severe embrittlement of BMGs [552]. On the other hand, the increase of the open-volume would enhance ductility [553–555]. The findings are in support of universal critical Poisson's ratio for plasticity in metallic glasses. The correlation between the Poisson's ratio and plasticity now has become a useful guideline for the development of plastic BMGs.

#### 9.4. Correlation between elastic moduli and fracture

Bulk metallic glasses with disordered structures and unique mechanical behaviors exhibit much different and intricate dynamic fracture corrugations. This diversity in patterns indicates that the

fundamental mechanism that underpins the fracture properties of metallic glasses is of particularity as compared with that of crystalline alloys [354,373–376]. Metallic glasses normally exhibit a macroscopic brittle fracture while plastic deformation ability only appears on the crack tip zone in micro or even nano-scale, and their fracture behavior is dominated by shear band forming and propagating, and the shear fracture along the shear band brings out an adiabatic heating generally resulting in viscous layer on the fracture surface, in which any tiny change of the local crack-tip stress field should more easily leave obvious markings on the fracture surface compared with brittle non-metallic glasses. In addition, comparing with non-metallic glasses, the fracture surface features of conducting brittle metallic glasses could be conveniently investigated on a nanometer scale by using high resolution scanning electron microscopy (HRSEM), providing more information at high spatial resolution about crack propagation, which is very important for understanding the mechanism of the dynamic fracture.

Recent experimental observations show that the fracture morphology of tough BMGs with high value of Poisson's ratio are rough and with a deep vein morphology (or dimple), whereas the brittle glasses with smaller Poisson's ratio have very shallow (nanometer scale) vein patterns [354,373–376]. SEM image of the fracture surface of BMGs with different values of toughness and Poisson's ratios shows the 'dimple' structure similar in shape but different in size as shown in Fig. 88. The brittle BMG such as Mg-based BMG has a nanometer-scale "dimple" structure, while the tough Ti-based BMG has dimple structure with size in micro scale [354]. From the available data, Fig. 89 exhibits a clear correlation between the fracture toughness  $K_c$  and dimple size (corresponding to the plastic process zone size) measured from fracture surface for various glasses with marked differences in toughness  $K_c$ . This can also express a correlation between measured plastic zone size and the plane strain fracture energy  $G_c$  [354]. The  $G_c$  is related to elastic moduli (Young's modulus and Poisson's ratio) of the BMGs and can be calculated in plane strain state as:  $G_c = \frac{K_c^2}{E(1-\nu)^2}$ . The important implication of the correlation is that the fracture even in brittle metallic glassy materials proceeds through the local softening mechanism (similar to the tough metallic glasses) but at different length scales. Such observation could help for understanding the plastic deformation mechanism and the correlation between the mechanical properties and elastic moduli.

The typical vein size on the fracture surface (corresponding to the size of the plastic zone) for a range of BMGs (the data are listed in Table 17) show a dependence of the Poisson ratio. From Fig. 90 one can see a clear correlation between the plastic zone size and Poisson's ratio and Dependence of fracture energy  $G_{IC}$  on typical vein size  $w$  on the same fracture surface for a range of BMGs. There is critical value of  $\nu = 0.33$  exists which divide the tough and brittle BMGs similar to that of toughness and Poisson's ratio correlation. This nanoscale plastic zone offers a natural "laboratory" for formation of metallic nanostructures. The extreme physical conditions inside the zone guarantee the glassy state of the formed nanostructures [556,557]. Since the dimensions of the nanostructures link to the size of the plastic zone  $w$ , and the value of  $w$  correlates to the Poisson's ratio, the correlations of  $w$ , mechanical behavior and  $\nu$  can assist in approximately controlling the size of the nanostructures spontaneously formed by fracture of appropriate BMG systems through the different sizes of the plastic zone.

The correlations of plastic zone size, mechanical behavior and  $\nu$  can also assist in understanding flow and fracture mechanisms, and in guiding alloy design to alleviate the macroscopic brittleness of metallic glasses. The observed effect of length scale could be especially important for  $\mu\text{m}$ - and  $\text{nm}$ -scale fabrication of metallic glass structures such as manufacturing metallic glass foams by modulating wall thickness and other glassy nanostructures [556,557].

It has been suggested that metallic glasses follow the Mohr–Coulomb criterion [494,558], so that the shear strength depends on a combination of tensile/compressive and shear stresses. In terms of the Mohr circle, the friction coefficient is the slope of the tangent to the circles corresponding to the tensile and compressive stresses. In addition, the friction coefficient has been suggested to be specific for each amorphous alloy [370]. The relationship between Poisson's ratio and Mohr–Coulomb friction coefficient in metallic glasses has been analyzed, and an increase of the friction coefficient with increasing Poisson ratio has been foreseen, if the ratio between elastic strain under uniaxial and shear stresses remains constant [559].

Recently, nanoscale periodic striped patterns have been reported on fracture surfaces of metallic glasses [373–376,557]. The formation of nanostripes is favored in brittle BMGs with low Poisson' ratio such as Mg-, Tb- and Fe-based BMGs, and their period value, ranging from  $\sim 30$  to  $\sim 120$  nm, depends strongly on the specific materials and appears to be a characteristic length in fracture process. The extremely uniform nanostripes over a large area of  $\sim \text{mm}^2$ , prepared by simply breaking BMGs at room temperature. It is found that the characteristic stripe period ( $d$ ) can be roughly estimated as:

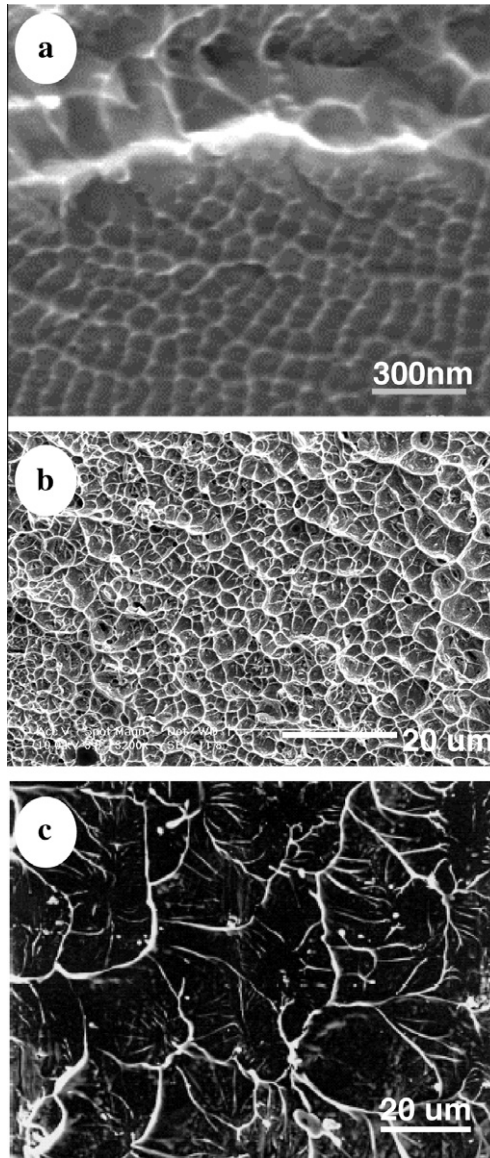


**Fig. 88.** High magnification SEM image of the fracture surface; (a) nanometer-scale “dimple” structure of the brittle Mg-based BMG. (b) Ce-based BMG, (c) tough Ti-based BMG [354].

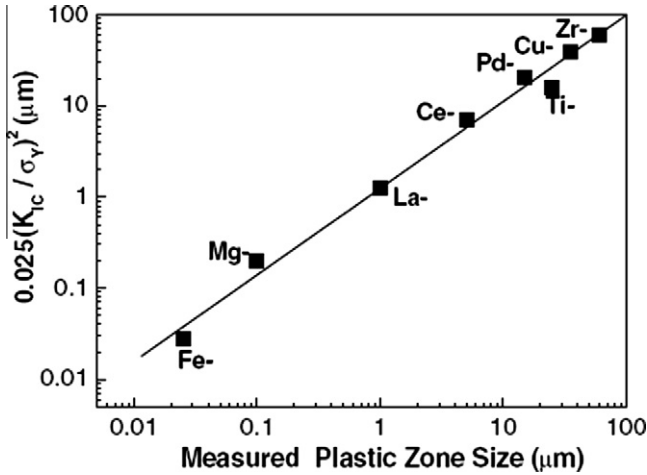


Fig. 89. Fracture toughness or strength response to the plastic process zone size [354].

Table 17

The parameters of vein size ( $w$ ) corresponding to the size of plastic zone, elastic modulus ratio ( $G/K$ ), Poisson ratio ( $\nu$ ) and fracture energy ( $G_{IC}$ ) of a variety of typical BMGs [506].

BMGs	$w$ ( $\mu\text{m}$ )	$G/K$	$\nu$	$G_{IC}$ ( $\text{kJ m}^{-2}$ )
Dy <sub>40</sub> Y <sub>16</sub> Al <sub>24</sub> Co <sub>20</sub>	0.08	0.417	0.317	0.06
Mg <sub>65</sub> Cu <sub>25</sub> Tb <sub>10</sub>	0.1	0.439	0.309	0.07
La <sub>55</sub> Al <sub>25</sub> Cu <sub>10</sub> Ni <sub>5</sub> Co <sub>5</sub>	1	0.354	0.342	0.7
Pr <sub>60</sub> Al <sub>10</sub> Ni <sub>10</sub> Cu <sub>20</sub>	5	0.302	0.363	–
Ce <sub>70</sub> Al <sub>10</sub> Cu <sub>10</sub> Ni <sub>10</sub>	5	0.427	0.313	3
Zr <sub>57</sub> Cu <sub>15.4</sub> Ni <sub>12.6</sub> Al <sub>10</sub> Nb <sub>5</sub>	6	0.297	0.365	7
Ti <sub>40</sub> Zr <sub>25</sub> Ni <sub>3</sub> Cu <sub>12</sub> Be <sub>20</sub>	15	0.324	0.354	22.74
Cu <sub>60</sub> Zr <sub>20</sub> Hf <sub>10</sub> Ti <sub>10</sub>	35	0.288	0.369	38
Zr <sub>41.2</sub> Ti <sub>13.8</sub> Cu <sub>12.5</sub> Ni <sub>10</sub> Be <sub>22.5</sub>	60	0.324	0.353	72

$$d = a \frac{\chi}{G} \quad (9.4)$$

where  $\chi$  represents the surface tension of viscous materials,  $a$  is constant, and  $a \approx 2000$ . Stripes period and features for Zr-, Cu-, Ni-, Mg-, Tb-, La- and Fe-based metallic glasses agree well with the theoretical predictions. From Eq. (9.4) one can see that the formation and the characteristic stripe period are mainly determined by two factors: surface tension of viscous liquid and shear modulus of the metallic glasses.

## 10. The summary for elastic correlations

It is becoming clear that some features and properties of metallic glasses are correlated with elastic moduli, and some correlations are remarkably well. These correlations can be simply illustrated in Fig. 91. With more and more data are collected in future in metallic glass field, more correlations could be established. The challenge now is to understand these correlations and experimental observations, which may have common structural and physical origins. The understanding of these correlations is helpful for developing new metallic glass compositions and new systems that combine desirable GFA with excellent mechanical and physical properties, and permits more widespread, cost-effective application of these paradigm-shifting materials in industries [560–564]. These correlations are also useful for establishing the models which permit deep understanding of the puzzles in metallic glasses.

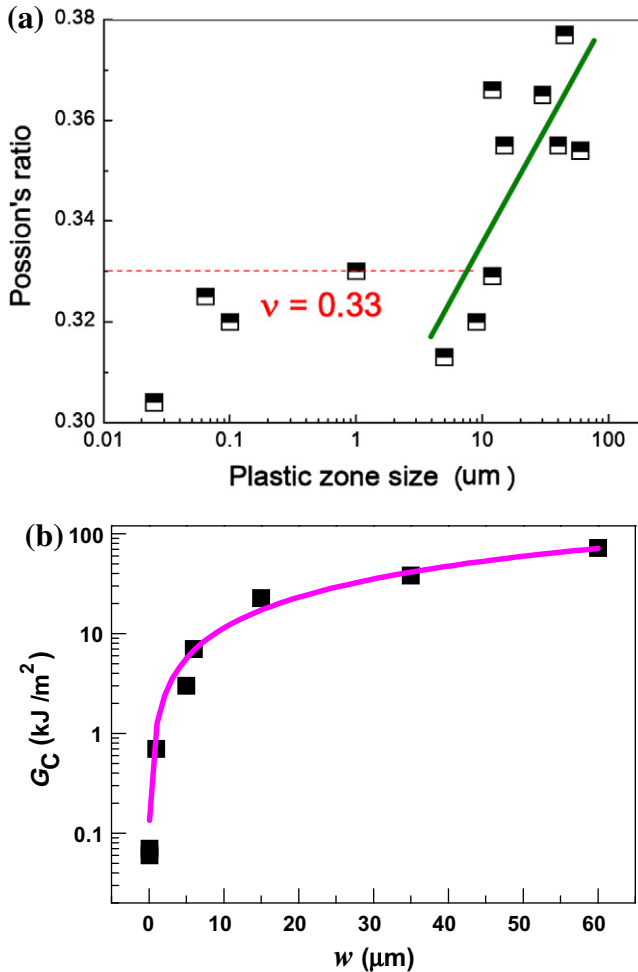


**Fig. 90.** (a) The correlation between the plastic zone size and Poisson's ratio for various BMGs. There is critical value of  $\nu = 0.33$  exists which divide the tough and brittle BMGs similar to that our toughness and Poisson's ratio correlation. (b) Dependence of fracture energy  $G_{IC}$  on typical vein size  $w$  on the same fracture surface for a range of BMGs.

## 11. Searching metallic glasses based on elastic moduli criterion

To explore new alloys or compositions with excellent glass-forming ability, GFA, in a simple and cheaper operation such as copper model casting is a major challenge in metallic glassy materials field [54]. Quite a number of criteria based on thermodynamic quantities, kinetic constraints on crystal nucleation and/or growth for the BMGs formation have been proposed to evaluate the GFA of alloys, and these criteria have played important role in the exploration of novel compositions and systems of metallic glasses. However, none of these criteria have been established to be sufficiently robust and predictive to be considered as necessary and sufficient for bulk glass formation, and none of them can be used to predict and control the properties of the formed metallic glasses, and the development of new metallic glass in practice has always been tedious trial-and-error task of synthesizing new metallic glasses whether the resulting glass has excellent GFA or would turn out to be excellent in some properties.

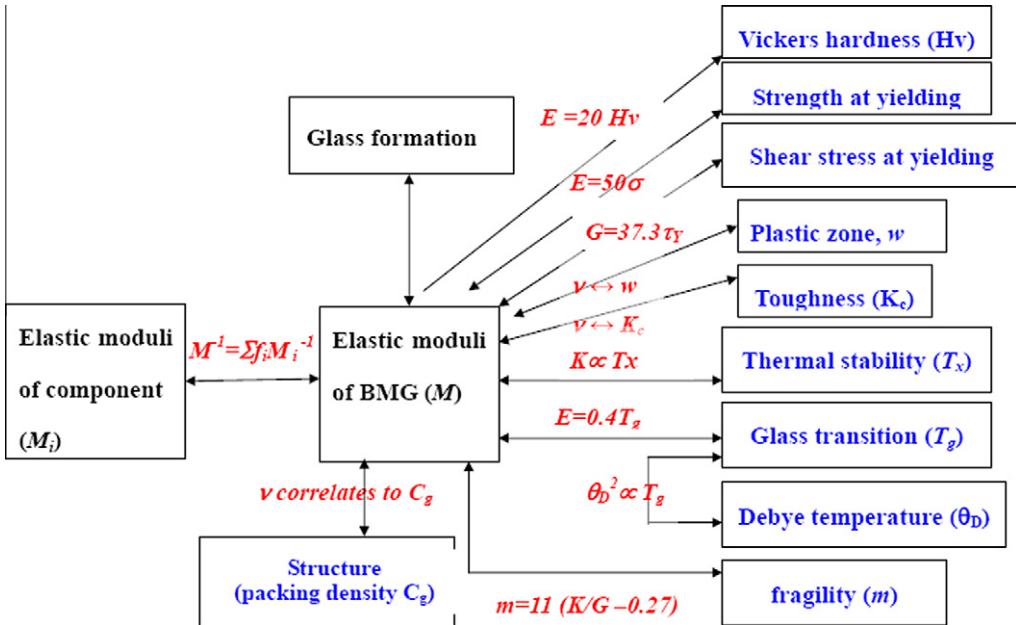


**Fig. 91.** Schematic diagram to show the correlations between the elastic moduli and glass formation, structure and properties of the metallic glasses

The striking systematic correlations among elastic constants, mechanical properties, GFA, and the glass transition of the metallic glasses open up the possibility of developing BMGs on the basis of their elastic moduli correlations. On the other hand, the elastic moduli of a BMG can be improved or tailored by proper selection of main components or adding minor elements with suitable elastic moduli, and the controlled elastic moduli of the alloy, in turn, can tailor the formation and properties of the BMGs.

The glass formation from solidification of liquid can be treated as the change of their different configurations or flow, or the markedly slow down of the flow. The flow can be modeled as activated hopping between their different configurations across energy barriers. The energy barriers of the flow or the viscosity of the metallic glass-forming liquids correlate well with instantaneous elastic moduli [36]. So, from physics point of view, on one hand, these correlations confirm that elastic moduli are the key physical quantity controlling the main properties of supercooled liquids and glasses; on the other hand, they indicate that it is reasonable to understand or predict glass formation based on the elastic moduli.

The elastic moduli criterion for metallic glass formation can be described as following: The elastic moduli  $M$  correlate with glass formation, thermal stability, and mechanical and some physical properties of metallic glasses. Furthermore, the  $M$  can be estimated from the elastic constants  $M_i$  of the constituent elements. This means that glass formation and some properties of a BMG depend strongly on the *elastic moduli* of its components especially the base component. Therefore, the glass formation and some features and properties such as mechanical properties of a glass-forming alloy can be predicted by its elastic moduli through selection of components with suitable elastic moduli. That is, the established elastic moduli and GFA correlations, since the moduli of glasses scale with those of their elemental components, provide guidelines for the development of BMGs with desirable properties by selection of components with suitable elastic moduli. As a compensative criterion to the existing empirical criteria [371], the elastic moduli criterion can efficiently improve the BMG searches especially for searching properties controllable BMGs rather than the trial-and-error method.

For example, to get a BMG with larger Poisson's ratio ( $E$  or  $G$  or  $K$ ), one can choose the main components with high Poisson's ratio ( $E$  or  $G$  or  $K$ ). Alternatively, one can increase the fraction of the

component with high Poisson's ratio ( $E$  or  $G$  or  $K$ ). For a give alloy system, lower Poisson's ratio could have higher GFA. Therefore, one can, combining the consideration of the thermodynamic BMG-forming criteria (such as  $T_{rg} = T_g/T_b$ , and large supercooled liquid region), improve the GFA of the alloy by decreasing the  $\nu$  of the alloy through addition or substitution of elements with low Poisson's ratio. These correlations are particularly useful for improving or tailoring the properties of the glass by proper selection of base element or adding component with suitable elastic moduli. For instance, to improve the plasticity in a BMG-forming system, one can increase  $\nu$  of the alloy by addition of elements with high Poisson's ratio. To search BMG with high strength, one can choose the base and main constitute components with high Young's modulus. Fig. 92 schematically illustrates the improvement and tailoring the formation and properties of the metallic glasses by proper selection or adding component with suitable elastic moduli.

A series of new rare-earth (RE) based BMGs with desirable properties is formed based on the elastic criterion [56,135,332,333]. This is case for the application of the elastic moduli criterion. The RE elements were chosen because of their chemical comparability, fantastic physical and chemical properties, which come from the unique configuration of unpaired  $4f$  and  $5f$  electrons, and well-regulated changing atomic size, density and elastic constants (as shown in Table 2). The RE-based BMGs show various GFA, and the size of the resultant glasses changes from thin ribbon to bulk form. Therefore, if a series of RE-based BMGs with the same or similar composition can be synthesized, they are a potential model system for investigating the relations between the GFA and some physical parameters and the relationship between the GFA and properties including thermal stability, fragility, elastic and mechanical properties. Based on the elastic moduli criteria, to develop RE-based BMG with higher thermal stability and elastic moduli, the BMGs based on Er, Sc, Tm, Yb and Lu were developed. In the RE family, Sc, Er, Tm, and Lu have higher elastic moduli (e.g. for Er:  $E = 70$  GPa,  $K = 44$  GPa, and  $G = 28$  GPa; For Tm:  $E = 74$  GPa,  $K = 45$  GPa, and  $G = 31$  GPa [565,566]). To fabricate the Er-based BMG with superior GFA for example, the Er–Co alloy is firstly prepared because of the large negative enthalpy of formation between them ( $\sim -40$  kJ/mole) [567,568]. With the addition of Al and Y (minor addition of some rare earth and transition metals have been found to be very effective for improving the GFA of the BMG-forming alloys [58]), the GFA of the Er–Co alloy can be greatly improved and the new family of Er-based BMGs has been developed. Using the similar way, the Sc-, Tm, and Lu-based BMGs with high elastic moduli, high thermal stability and strength and hardness have been developed

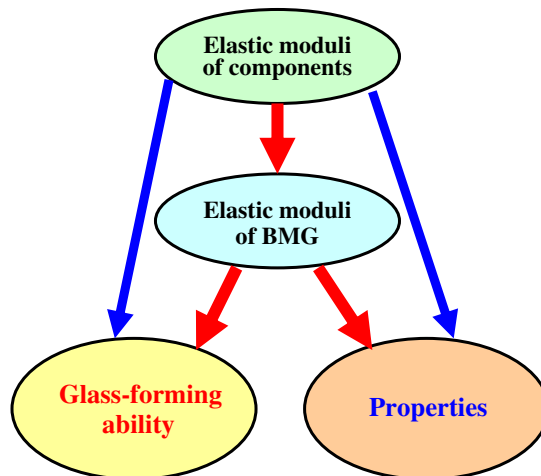


**Fig. 92.** Schematic show of the elastic moduli criterion for glass formation and properties controlling. The illustration shows how the formation and properties of the bulk metallic glasses can be improved or tailored by proper selection or adding component with suitable elastic moduli ( $M_i$ ). The choose of components with suitable elastic moduli can control the elastic moduli of a BMG and then control the GFA and some properties of BMG based on the correlation between elastic moduli and GFA and properties.

**Table 18**

The elastic constants,  $T_g$ ,  $T_x$ ,  $T_l$  and  $T_{rg} = T_g/T_l$  for the RE-based BMGs.  $d_c$  is critical dimension of the BMGs. (The thermal parameters were determined by DSC with a heating rate of 10 K/min.)

BMG	$T_g$ (K)	$T_x$ (K)	$T_l$ (K)	$T_{rg}$	$d_c$ (mm)	$E$ (GPa)	$G$ (GPa)	$K$ (GPa)	$\nu$
Sc <sub>36</sub> Al <sub>24</sub> Co <sub>20</sub> Y <sub>20</sub>	662	760	1048	0.63	3	85.2	32.3	77.5	0.317
Lu <sub>39</sub> Y <sub>16</sub> Al <sub>25</sub> Co <sub>20</sub>	687	769	1117	0.61	5	78.9	30.0	71.3	0.316
Tm <sub>39</sub> Y <sub>16</sub> Al <sub>25</sub> Co <sub>20</sub>	664	735	1140	0.58	3	75.0	29.4	55.3	0.274
Er <sub>50</sub> Al <sub>24</sub> Co <sub>20</sub> Y <sub>6</sub>	651	702	1079	0.60	8	71.1	27.0	65.1	0.318
Ho <sub>35</sub> Y <sub>21</sub> Al <sub>24</sub> Co <sub>20</sub>	644	696	1074	0.63	5	69.1	26.2	63.6	0.319
Dy <sub>46</sub> Al <sub>24</sub> Co <sub>18</sub> Fe <sub>2</sub> Y <sub>10</sub>	627	677	1023	0.63	5	64.2	24.4	58.5	0.317
Tb <sub>36</sub> Y <sub>20</sub> Al <sub>24</sub> Co <sub>20</sub>	619	686	1021	0.62	5	63.6	24.0	60.5	0.325
Gd <sub>36</sub> Al <sub>24</sub> Co <sub>20</sub> Y <sub>20</sub>	603	658	1048	0.60	3	62.2	23.6	57.4	0.319
Sm <sub>40</sub> Y <sub>15</sub> Al <sub>25</sub> Co <sub>20</sub>	590	657	950	0.66	3	57.1	21.5	54.7	0.326
Nd <sub>60</sub> Fe <sub>20</sub> Co <sub>10</sub> Al <sub>10</sub>	485	615	815	0.59	5	54.1	20.7	54.1	0.317
Pr <sub>60</sub> Al <sub>10</sub> Ni <sub>10</sub> Cu <sub>20</sub>	417	452	806	0.51	5	37.2	13.6	45.2	0.363
La <sub>66</sub> Al <sub>14</sub> Cu <sub>10</sub> Ni <sub>10</sub>	395	449	731	0.54	5	35.7	13.4	34.9	0.330
Yb <sub>62.5</sub> Zn <sub>15</sub> Mg <sub>17.5</sub> Cu <sub>5</sub>	381	401	645	0.59	4	26.5	10.4	19.8	0.276
Ce <sub>68</sub> Al <sub>10</sub> Cu <sub>20</sub> Fe <sub>2</sub>	352	423	708	0.50	5	30.8	11.8	31.0	0.313

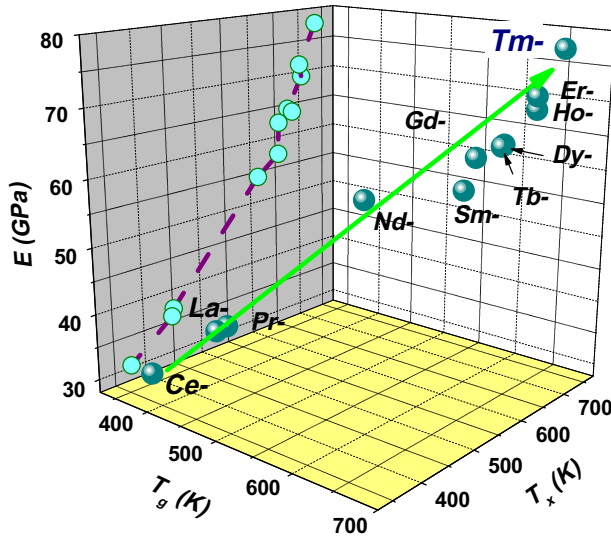


**Fig. 93.** The dependence of  $E$  on  $T_g$  and  $T_x$  for typical RE-based BMGs [118].

[56,118,119,135,332,333,569,570]. Table 18 lists the thermal parameters and elastic properties of a series of RE-based BMGs (RE = La, Ce, Pr, Nd, Sm, Gd, Tb, Dy, Ho, Er, Tm, Yb, Lu and Sc). Fig. 93 exhibits the comparison of  $E$ ,  $T_g$  and  $T_x$  of the BMGs based on RE in lanthanide family (except main component, the other compositions are different slightly). These RE-based BMGs show clear correlations between the  $T_g$  (or  $T_x$ ) and elastic moduli, and the Tm and Lu-based BMGs have largest elastic moduli among the RE-based BMGs. Fig. 94a and b shows the correlation between  $T_g$  and  $T_x$  with moduli of  $K$ ,  $G$  and  $E$  of these RE-based BMGs [135]. The BMGs with heavy RE (have high moduli) have much higher  $T_g$ ,  $T_x$ , and  $T_l$  compared to those of the light RE-based BMGs. The Ce-based BMG has the lowest  $T_g$ , and  $T_x$  (359 and 377 K, respectively), yet Sc-based BMG exhibits the highest  $T_g$ , and  $T_x$  (662 and 760 K) as well as the largest supercooled liquid region  $\Delta T = 98$  K. The linearly increase trend of  $T_g$  and  $T_x$  with increasing elastic moduli indicating a clear correlations between the thermal stability of the BMG with their elastic moduli, and the RE-based BMGs formation and properties could be tailorable through selecting proper main component with suitable elastic constants. Interestingly, it is found that RE<sub>55</sub>Al<sub>25</sub>Co<sub>20</sub>

(RE = Y, Ce, La, Pr, Nd, Sm, Gd, Tb, Dy, Ho, Er, Tm, and Lu) with same composition can be cast into BMG. These BMGs show regularly increasing of thermal stability, with the increase of elastic constants of the base RE elements [332]. As shown in Table 19, the RE<sub>55</sub>Al<sub>25</sub>Co<sub>20</sub> BMGs, with the broad values of  $T_g$  ranging from low temperature [La<sub>55</sub>Al<sub>25</sub>Co<sub>20</sub> alloy has the lowest  $T_g$  (477 K), which is close to room temperature] to high temperature (Lu<sub>55</sub>Al<sub>25</sub>Co<sub>20</sub> has the highest  $T_g$  (701 K), which is close to those of Zr- and Fe-based BMGs [52]). The value of  $T_g$  increases gradually with the increasing of elastic moduli of the RE element. In addition, the  $T_x$ , and  $T_l$  have also similar changing trend in these BMGs. The thermal stability of the RE<sub>55</sub>Al<sub>25</sub>Co<sub>20</sub> BMGs can be tailored via the substitution of the base RE constituent with different elastic moduli. The values of  $\rho$ ,  $E$ ,  $G$ ,  $K$ , and  $\theta_D$  of the BMGs also increase with increasing atomic number of RE element (or the increasing elastic moduli of the RE element) and there are exist the correlation between  $T_g$  and elastic constants and  $\theta_D$  as shown in Figs. 95 and 96 [138]. For the RE<sub>55</sub>Al<sub>25</sub>Co<sub>20</sub> BMGs, the values of  $1000 T_g / A\theta_D^2$  are between 0.130 and 0.153 further confirming the correlation between  $T_g$  and  $\theta_D$ .

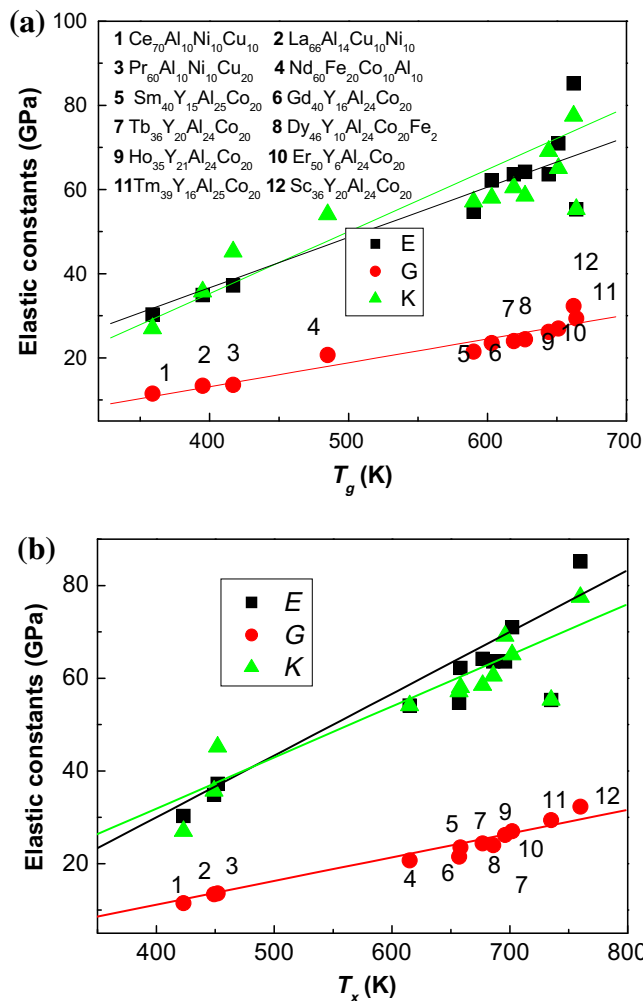


**Fig. 94.** (a) The relationship between the  $T_g$  and  $E$ ,  $G$ ,  $K$  of various RE-based BMGs. (b) The relationship between the  $T_x$  and  $E$ ,  $G$ ,  $K$  of the RE-based BMGs.

**Table 19**

The composition of  $\text{RE}_{55}\text{Al}_{25}\text{Co}_{20}$  BMGs, their  $T_g$  and  $T_x$ , liquidus temperature  $T_l$ , and glass-forming ability represented by a reduced glass transition temperature  $T_{rg}$ ,  $\Delta T = T_x - T_g$ , critical diameter  $d_c$  (the thermal parameters were obtained by DSC with a heating rate: 10 K/min), and their density  $\rho$ , elastic constants ( $E$ ,  $G$ , Poisson ratio and  $K$ ) [138,332].

Composition	$d_c$ (mm)	$T_g$ (K)	$T_x$ (K)	$T_l$ (K)	$\Delta T$ (K)	$T_{rg}$ (K)	$\rho$ (g/cm <sup>3</sup> )	$E$ (GPa)	$G$ (GPa)	$K$ (GPa)	$\nu$
$\text{Y}_{55}\text{Al}_{25}\text{Co}_{20}$	2	633	694	1060	61	0.597	4.683	–	–	–	–
$\text{La}_{55}\text{Al}_{25}\text{Co}_{20}$	5	477	540	771	63	0.619	5.802	40.90	15.42	39.34	0.327
$\text{Ce}_{55}\text{Al}_{25}\text{Co}_{20}$	1	–	538	800	–	–	–	–	–	–	–
$\text{Pr}_{55}\text{Al}_{25}\text{Co}_{20}$	5	509	585	826	76	0.616	6.373	45.90	17.35	43.48	0.324
$\text{Nd}_{55}\text{Al}_{25}\text{Co}_{22}$	2	525	593	859	68	0.611	6.584	–	–	–	–
$\text{Sm}_{55}\text{Al}_{25}\text{Co}_{20}$	1	529	555	885	26	0.598	6.584	–	–	–	–
$\text{Gd}_{55}\text{Al}_{25}\text{Co}_{20}$	2	585	657	971	72	0.602	7.343	–	–	–	–
$\text{Tb}_{55}\text{Al}_{25}\text{Co}_{20}$	3	612	674	1001	62	0.611	7.488	59.53	22.85	50.19	0.302
$\text{Dy}_{55}\text{Al}_{25}\text{Co}_{20}$	3	635	708	1031	73	0.616	7.560	61.36	23.52	52.22	0.304
$\text{Ho}_{55}\text{Al}_{25}\text{Co}_{20}$	3	649	707	1055	58	0.615	7.888	66.64	25.42	58.81	0.311
$\text{Er}_{55}\text{Al}_{25}\text{Co}_{20}$	5	663	722	1079	59	0.628	8.157	70.72	27.08	60.70	0.306
$\text{Tm}_{55}\text{Al}_{25}\text{Co}_{20}$	3	678	733	1180	55	0.574	8.274	72.2	27.6	62.0	0.306
$\text{Lu}_{55}\text{Al}_{25}\text{Co}_{20}$	3	701	781	1167	80	0.608	8.694	80.0	30.6	69.2	0.307

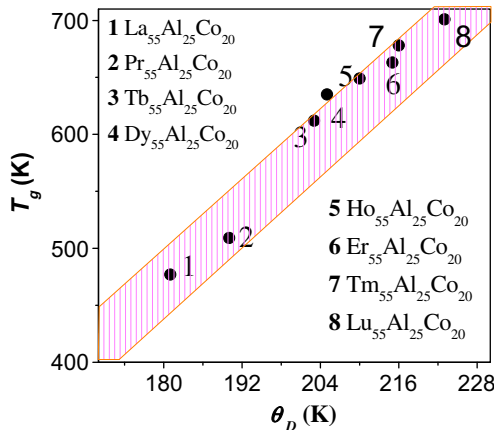


**Fig. 95.** The correlation between  $T_g$  and Debye temperature  $\theta_D$  for  $\text{RE}_{55}\text{Al}_{25}\text{Co}_{20}$  BMGs [138].

The correlation between plasticity and Poisson's ratio has been used as a guideline for the development of plastic BMGs by appropriate choice of composition with  $\nu$  control strategy [85,113,537]. Acoustic measurements show that some BMGs such as  $\text{Zr}_{61.88}\text{Cu}_{18}\text{Ni}_{10.12}\text{Al}_{10}$ ,  $\text{Zr}_{64.13}\text{Cu}_{15.75}\text{Ni}_{10.12}\text{Al}_{10}$  and  $\text{Zr}_{62}\text{Cu}_{15.5}\text{Ni}_{12.5}\text{Al}_{10}$  among a class of quaternary ZrCuNiAl BMGs exhibit larger Poisson's ratio relative to that of other BMGs, and exhibit super large plasticity [85]. As results of such heavily deformation, the BMG rods were compressed into flakes without fracture, implying high flowability of the BMGs. Moreover, the BMGs could be bended into desired shapes as could be done with familiar flexible metals such as aluminum and copper. The maximum bended angle approaches  $90^\circ$  in both rods and plates. The extended plasticity of the BMGs is susceptible to the composition. Minor content deviation ( $<1$  at.%) can drastically change the plasticity of the BMGs. The results indicate that even in the reported BMG systems, extraordinarily plastic BMGs are highly possible to be obtained by appropriate choice of the composition utilizing the correlation between Poisson's ratio and plasticity. The strategy would provide useful guidelines for the development of plastic BMGs as high-performance structural materials in other known or unknown BMG-forming alloys, and open up a research area of both fundamental and applied importance [85].

Based on the correlation between  $T_g$  and elastic moduli, a new class of CaLiMgZn metallic glasses in bulk form which combine multiple superior properties and high stability at room temperature and polymer-like thermoplastic formability and manufacturability near ambient temperature (such as

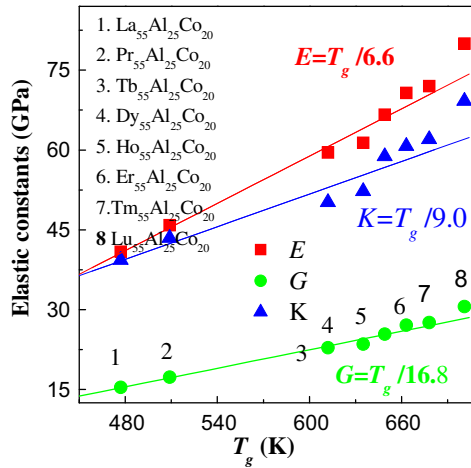


Fig. 96. The correlation between  $T_g$  and elastic constants of  $\text{RE}_{55}\text{Al}_{25}\text{Co}_{20}$  BMGs [138].

in hot water) was developed [237]. The CaLi-based BMGs consist of the cheaper main components of Ca, Mg and Li, and simultaneously offer the excellent glass-forming ability, exceptionally low glass transition temperature ( $\sim 35\text{--}60^\circ\text{C}$ ) approaching room temperature, the ultralow elastic moduli ( $\sim 23$  GPa) comparable to that of human bones, high elasticity (2%) and strength, ultralow density ( $< 2$  g/cm<sup>3</sup>), exceptional thermodynamic and kinetic stability, strong liquid fragility similar to that of oxide glasses, ultrahigh specific strength and lower electrical resistivity at room temperature, and superplasticity and polymer-like thermoplastic formability near room temperature. The highly unusual metallic glasses could have potential in structural and functional applications and facilitate studies of the nature of glasses [237]. The desirable and unusual properties combination of the CaLi-based BMGs are attributed to that Li element has the lowest elastic moduli (4.9 GPa) and density (0.525 g/cm<sup>3</sup>) among the metal elements according to elastic moduli correlations. The Li element content can effectively modulate the properties of CaLi-BMGs. The  $T_g$  decreases monotonically with the increase of the content of Li element, and the other properties of CaLi-based BMGs, such as elastic moduli and density, can also be controlled by Li content. The work is another example for the designing new metallic glasses with good combinations of properties by selection of components with suitable elastic moduli according to the elastic moduli correlations. A series of BMGs such as Sr-, Ta-, Zn-based BMGs have also been developed based on the elastic criterion [173,333].

## 12. Elastic models of supercooled liquids and metallic glasses

In order to describe and understand the liquids and glasses, the choice of the key concepts or parameters that connect atomic structure with the properties is critical. The striking systematic correlations between linear elastic constants and various properties and features of metallic glasses imply that the metallic glasses may exhibit universal behaviors based on several measurable parameters of elastic constants. The elastic moduli could be key parameters for prediction of physically relevant features of metallic glasses and could also assist in the possibly definition of a common concept and model for the long-standing issues of glass formation and nature. The next two sections will introduce the elastic models for the glass-forming liquids and metallic glasses, and suggest elastic moduli perspectives of the metallic glasses based on these observed experimental correlations, observations and elastic models.

Glasses are liquids that have become frozen in time and space, and the molecules or atoms in a glass are arranged much like those in liquid but are more tightly and densely packed. The transition of a liquid into a glass by lowering temperature or by applying stress may appear conceptually simple.

In some cases, a flowing state can be restored by exceeding a threshold of external force, such a force seemingly creates a glass (jamming) [571,572], and the glass formation is not just rapid cool any more. However, some simple phenomenon and questions, such as where and why the liquid end and glass begin, and the physical principles governing these various frozen fluids, has turned out to be one of most difficult and controversial problems [573–576]. Therefore, the nature of glass and the formation mechanism of the glass were listed as one of 125 future important scientific issues by special selection of Science [576]. The central problems in glass physics is to explain the dramatic temperature dependent relaxation time of liquid or dramatic viscosity increases when the liquid approaches  $T_g$ , and the flow mechanism of glasses when temperature or stress are applied to them [79,437]. To understand the glassy nature and glass formation, it is necessary to study supercooled liquid because glasses are formed from viscous liquids and then the properties and features of glasses inherited from liquids.

As early as 1867, Maxwell suggested that on a sufficiently short time scale any liquid is elastic and behaves like a solid [577], and the liquid is solidlike on time scale much shorter than relaxation time  $\tau_R$ . Maxwell is the first to correlate the elastic modulus to liquid, and he proposed a relation between the relaxation time and viscosity  $\eta$  of a liquid as:

$$\tau_R = \eta/G_\infty \quad (12.1)$$

The Maxwell relation also provides the implication to understand the glass and glass transition. The value of  $G_\infty$  is in the range of 1–10 GPa,  $\eta \sim 10^{13}$  Pa s around  $T_g$ , so the Maxwell relaxation time (or  $\alpha$  relaxation time),  $\tau_R$ , is of order 100–1000 s. The  $\tau_R$  and  $\eta$  are roughly proportional since  $G_\infty$  is much less temperature dependent than  $\tau_R$  and  $\eta$ .

The glass-former liquids exhibit universal features which relate to the temperature dependence of the viscosity. When the glass transition happens the molecular or atom motion virtually ceases and the viscosity of liquid becomes extremely large ( $\sim 10^{13}$  Pa s). The so-called “Angell plot” [437,578] exhibits the logarithm of the viscosity for a variety of viscous liquids (including non-metallic and metallic glasses) as a function of inverse temperature normalized to unity at  $T_g$ , which can describe the universal features which relate to the temperature dependence of the viscosity. Because it would be easy to understand a viscosity with Arrhenius temperature dependence, it is generally assumed that dynamics is dominated by barriers to be overcome by thermal fluctuations, and the  $T$  dependence of  $\eta$  can be expressed as [579]:

$$\eta = \eta_0 \left( \frac{\Delta E}{k_B T} \right) \quad (12.2)$$

where  $\eta_0 \sim 10^{-3}$  Pa s is prefactor. This is referred to as Arrhenius temperature dependence by reference to rate theory which discovered that chemical reaction times usually follow this law [580]. It is found that vast majority of viscous liquids show a stronger than the Arrhenius increase of the viscosity upon cooling toward the glass transition, and only few liquids, e.g. pure silica  $\text{SiO}_2$  and  $\text{GeO}_2$ , follow the Arrhenius law. Therefore, the activation energy in the Arrhenius expression must be temperature dependent:

$$\eta = \eta_0 \left( \frac{\Delta E(T)}{k_B T} \right) \quad (12.3)$$

The non-Arrhenius temperature dependence of the Maxwell relaxation time or viscosity can be characterized by the concept of fragility  $m$  [240,581–584]. If the glass transition temperature is defined by  $\tau(T_g) = 10^3$  s, from Eq. (12.3), the Arrhenius behavior is then characterized by  $m = 16$ .

Many models have been proposed to understand why glass-forming liquids are non-Arrhenius [79]. The well-known models are the free volume model [585–587], the Adam–Gibbs entropy model [588,589], the energy landscape approach [35,295], the mode-coupling theory [590,591], and the elastic models. A successful model of viscous liquids must explain why the activation energy has such strong temperature dependence and can correlate the activation energy to simple and readily measurable parameters. The free volume model and the Adam–Gibbs entropy model link the activation energy to a macroscopic observable of volume and entropy. While the elastic models link the activation energy to the readily measurable instantaneous elastic moduli [79,592–595].

### 12.1. Elastic models for glass-forming supercooled liquids

The difference between solids and fluids can be defined by a nondimensional number of  $D$ , which is the so-called Deborah number (named after the Biblical prophetess of Deborah, who said that the mountains flow before the lord) [596]:

$$D = t_r/t_o \quad (12.4)$$

where  $t_r$  is the time of relaxation, and  $t_o$  is the time of observation. If your observation time is very large, or conversely, if the  $t_r$  is very small, you see the material flowing. On the other hand, if  $t_r$  of a material is much larger than your  $t_o$ , the material, for practical purposes, is a solid. The elastic model is based on the assumption that a viscous liquids can be viewed as “solid which flow” in enough short time scale. That is: Viscous liquid  $\approx$  solid which flow [79]. This means that any liquid is solidlike when it is probed on a sufficiently short time scale, and its short time elastic properties are characterized by the instantaneous elastic moduli of  $G_\infty$ ,  $E_\infty$ , and  $K_\infty$ . Actually, a glass is different from a liquid by virtue of its ability to support shear stress, and a forced solid flows by sudden, rare and localized atomic or molecular rearrangements. The barrier transition for a “flow event” or the height of the activation energy for flow (an atomic or molecular rearrangement) can be determined by short-time elastic properties which characterized by instantaneous moduli. In other words, the dramatically increase of the viscosity is due to the increase of the range of elastic interaction between local relaxation events in glass-forming liquids. All the present elastic models are set up along this idea [79].

Tobolsky, Powell, and Eyring are the first to suggest that the flow activation energy of supercooled liquids be determined by the instantaneous elastic properties [594]. They proposed, based on the harmonic approximation, that the activation energy can be expressed as [597]:

$$\Delta E \propto k_B T \left( \frac{a^2}{\langle x^2 \rangle} \right) \quad (12.5)$$

where  $\langle x^2 \rangle$  is the vibrational mean-square displacement depending on temperature, and for a harmonic system,  $\langle x^2 \rangle \propto T$ ,  $a$  is the average intermolecular distance. From Eq. (12.5), one can see that  $\Delta E$  is temperature independent. However, for most glass-forming liquids  $\langle x^2 \rangle$  decreases faster than temperature upon cooling, resulting in the increase of  $\Delta E$  upon cooling. They then further reasoned that the relevant potential is that resisting shear deformation, indicating that  $\Delta E \propto G_\infty$  [594], and the final relation is obtained:

$$\Delta E = \lambda a^3 G_\infty \quad (12.6)$$

where  $\lambda (\sim 1)$  is constant.  $G_\infty$  is much more temperature dependent in viscous liquids than in glasses.

Mooney [598] and Bueche [599] assumed that a “liquid flow” comes about when thermal fluctuations generate a local expansion exceeding a certain critical values, and the probability of this happening is determined by the short-time elastic properties of the liquid, and their calculation leads to

$$\Delta E = \lambda M v_l^2 \quad (12.7)$$

where  $\lambda (\sim 1)$  is constant and  $M$  the molecular mass,  $v_l$  is the longitudinal sound velocity.

Based on the Maxwell relation, Nemilov derived the relation between  $\Delta E$  and  $G_\infty$  as [600]:

$$\Delta E = \lambda a^3 G_\infty \quad (12.8)$$

where  $\lambda (\sim 1)$  and  $a$  are constant.

Dyre proposed a so-called shoving model based on following three assumptions [79,601–603]: (1) The activation energy  $\Delta E$  for flow is mainly elastic energy and is determined by the work done to shove aside the surrounding; (2) The elastic energy is mainly located in the surroundings of the flow event; and (3) The elastic energy is mainly shear elastic energy. The basic picture of the model is the same as that of the free volume model, namely that extra volume is needed for a flow event to occur. The instantaneous shear modulus  $G_\infty$  determines the shoving work, and the final expression for the temperature dependent activation energy is [79]:

$$\Delta E = V_c G_\infty(T) \quad (12.9)$$

where  $V_c$  is a characteristic microscopic volume which is temperature independent.  $G_\infty(T)$  in glass-forming liquid is much more temperature-dependent than in glasses. The elastic models offer a simple and effective scenario for explaining the phenomena in glass transition and glass formation, and the correlations between elastic moduli and properties.

## 12.2. Elastic models for metallic glasses

The forced flow by sudden, rare and localized atomic rearrangements in metallic glass is different from the flow of its liquid, and it is localized, non-Newtonian inhomogeneous flow [513,514]. While the activation energy barrier for a “flow event” (an atomic or molecular rearrangement) is also a key for understanding the deformation and mechanical properties of the metallic glasses. Several phenomenological models have been proposed to explain inhomogeneous flow or non-Newtonian flow in metallic glasses, and most of them are based on two hypothetical flow mechanisms: dilatation [513] and cooperative shear [514]. The related models can be classified into two categories: free volume model [513,604,605] and shear transformation zone model, STZ [514,606–610]. By drawing an analogy between glassy and granular materials, the free volume proposes that the deformation of metallic glasses is accommodated by the creation of microstructural free volume via flow-induced dilatation [513]. There are some evidences of deformation-induced dilatation provided by experimental assessment of excess molar volume by positron annihilation spectroscopy and X-ray synchrotron radiation [610,611] and simulation [612]. The model has been widely and successfully used in metallic glass studies to effectively replicate and simulate their flow characteristics. However, it has not been possible to quantitatively link measurable free volume to flow as predicted from free volume models. This is due to the lack of a fundamental definition of free volume, leading to constitutive models that possibly lack thermodynamic consistency [82,223,558,613–616]. The cooperative shear theory or the concept of STZs proposed that the deformation of metallic glasses is accommodated by plastic rearrangements of atomic regions that involve tens of atoms [516]. Experimental evidence [82,220,613,614] shows that the STZ hypothesis is consistent with the classical thermodynamic theories of liquids and glasses based on the concept of potential energy landscapes, PEL. A theory for aging of metallic glasses based on  $\Delta E \propto G$  had ever been proposed to explain the observation that during aging the effective glass viscosity increases as a linear function of time [584].

According to the framework of the PEL theory [33–35,295], the energetic landscape of a glass-forming liquid system comprises a population of inherent states associated with local minima (basins) corresponding to the stable configurational states are separated by saddle points (or energy barriers). The liquid alloy is supposed to locate at local minima (or inherent state) in PEL, and the flow event or the configurational hopping is the process that the system escapes from one local minimum to another or the disappearance of barrier between neighbor local minima. Johnson and Samwer [82] regarded the flow in metallic glass as an activated hopping between inherent states across energy barrier  $\Delta E$ , and merged the PEL picture with STZ concept. By assuming the average potential energy vs. shear strain in the vicinity of a basin to be a sinusoid, as employed by Frenkel [615] to calculate the theoretical shear strength of a dislocation-free crystal, Johnson and Samwer set up the cooperative shear model (CSM) [82,223], which gives rise to a relation between viscosity and isocfigurational shear moduli. The model together with others work [606–609,614] provides effective interpretation of plastic flow in metallic glasses well below  $T_g$ .

For various BMGs, the yielding at room temperature can be described by a critical shear strain  $\gamma_c$  ( $\gamma_c = 0.0267$ ) [82]. The yield shear stress  $\tau_y = \gamma_c G$ , and the yield stress  $\sigma_y = 0.02E$  [56] and  $\tau_y = \sigma_y/2$  [82]. The Johnson and Samwer model based on the assumption that the energetics within an individual STZ under applied shear stress can be described by PEL. Following Frenkel theory, the elastic energy of an STZ can be described by a periodic elastic energy density  $\phi$  to the shear strain coordinate  $\gamma$  and assume that the  $\phi$  vs.  $\gamma$  in the vicinity of a basin to be a sinusoid [615]:

$$\phi(\gamma) = \phi_0 \sin^2(\pi\gamma/4\gamma_c) \quad (12.10)$$

where  $\phi_0$  is a total barrier energy density and  $4\gamma_c$  is the average configurational spacing. The shear modulus  $G$  of a STZ is:

$$G = d^2 \phi / d\gamma^2 |_{\gamma=0} = \frac{\pi^2 \phi_0}{8\gamma_c^2} \quad (12.11)$$

This leads to the linear relationship between  $G$  and barrier energy density as

$$\phi_0 = \frac{8}{\pi^2} \gamma_c^2 G \quad (12.12)$$

For an effective STZ with volume  $\Omega$ , the total energy barrier for configurational hopping between inherent states or the activation barrier for shear flow can be expressed as [82]:

$$\Delta E = \frac{8}{\pi^2} \gamma_c^2 G \Omega \quad (12.13)$$

The barrier at finite  $\tau$  approaches zero as  $\tau \rightarrow \tau_c$ . That is, the activation energy goes to zero at a critical stress  $\tau_c$ , or  $\tau_c = \phi' |_{\max} = \pi \phi_0 / 4\gamma_c$ . Eq. (12.3) then can be rewritten as:  $\Delta E \propto G (\tau - \tau_c)^{3/2}$ . This is the Johnson–Samwer elastic model for plastic yielding or flow of metallic glasses where the activation energy for a STZ depends on the shear modulus. The results confirm that the basic idea of the activation energy is proportional to an elastic modulus can also be applied to describe glasses below  $T_g$ .

The Johnson–Samwer model predicts the yield criterion and its dependence on temperature in the BMGs, and leads to natural expressions for the Newtonian and Non-Newtonian viscosity law for the BMGs, as well as the fragility of the BMG-forming liquids [223]. For example, it is verified that the viscosity has a unique functional relationship and a one to one correspondence with the shear modulus over a broad range of rheological behavior even in glassy state. That is, the variation in viscosity can be correlated uniquely to variations in  $G$  as:

$$\frac{G}{G_0} = \left[ \frac{kT}{\Delta E_0} \ln \left( \frac{\eta}{\eta_\infty} \right) \right]^q \quad (12.14)$$

where  $\Delta E_0 = \frac{8}{\pi^2} \gamma_c^2 G_0 \Omega_0$ .  $q$  is indices quantifying the contributions of  $G$  and  $\Omega$  to the change of activation energy. This  $\eta$  and  $G$  relationship indicates that the flow in metallic glass induced by either thermal excitation (e.g. by varying temperature) or mechanical deformation (by varying strain rate) is governed by the dependence of isoconfigurational shear modulus on configurational potential energy of corresponding the inherent state. The model is found to be in agreement with a variety of experimental observations [56,82,223].

### 12.3. Extended elastic model for flow in metallic glass-forming liquids and glasses

The extended elastic model of metallic glasses and metallic glass-forming liquids based on several assumptions [616,617]:

- (1) Metallic glasses are frozen liquids and their atoms or clusters are arranged much like those in their melt but are more tightly, densely packed and much more viscous; It is well accepted that even below the conventional elastic limit, the metallic glasses show nonelastic rheological response under constant load. In accordance with the properties, the metallic glasses can be characterized as highly viscous.
- (2) On the other hand, a viscous metallic liquid can be viewed as solid which flow in enough short time scale. That is any liquid is solid-like when probed on a sufficiently short time scale, and its short time elastic properties can be characterized by the instantaneous elastic moduli of  $G_\infty$ ,  $E_\infty$ , and  $K_\infty$ ;
- (3) For the metallic glasses, the glass formation, glass transition, relaxation, and plastic deformation can be regarded as different elementary flow events activated by different processes such as thermal process or mechanical process, and the flow event is governed by the activation energy; The barrier transition for a “flow event” or the height of the activation energy for flow (atomic or molecular rearrangement) is due to the increase of the elastic interaction in local relaxation events in glass-forming liquids. The MG-forming liquids can be characterized by the instantaneous elastic moduli of  $G_\infty$ ,  $E_\infty$ , and  $K_\infty$ . In the perspective of the potential energy landscape

(PEL) theory, the flow event or the configurational hopping in BMGs or BMG-forming liquids is the process that the system escapes from one local minimum to another (an activated hopping between inherent states across energy barrier  $\Delta E$ ) or the disappearance of barrier between neighbor local minima. Fig. 97 schematically illustrates the flow based on the concept of PEL. There are two flow modes: the  $\beta$ -mode is the stochastically and reversible activated hopping events across “subbasins” confined within the inherent “megabasin” (intrabasin hopping) and the  $\alpha$ -mode is irreversible hopping events extending across different megabasins (interbasin hopping).

- (4) Extensive experimental evidence show that the flow viscosity of metallic glass-forming liquids follows the general Arrhenius equation:  $\eta(T) = \eta_0 \left( \frac{\Delta E(T)}{k_B T} \right)$ . The activation energy  $\Delta E$  for the flow events both in liquid state and glass is temperature dependent. According to the definition of glass transition temperature, at  $T_g$ ,  $\eta(T_g) = 10^{13}$  Pa s. We note that the definition  $\eta(T_g) = 10^{13}$  poise is widely accepted in this community and have been confirmed by experiments (for review see: [79,437,477]). For metallic glasses, it is a constant with minor and neglectable variations. From  $\eta(T_g) = \eta_0 \left( \frac{\Delta E(T_g)}{k_B T_g} \right) = 10^{13}$  Pa s, one can see that  $\Delta E(T_g)/k_B T_g$  is a universal constant at  $T_g$  for all metallic glasses.

We define the activation energy of a unit volume as the activation energy density ( $\rho_E$ ) [616–618]:

$$\rho_E = \frac{\Delta E}{V_m} \quad (12.15)$$

The definition of activation energy density can rule out the vague characteristic volume involved in both homogeneous and inhomogeneous flow and directly relates the flow activation event to the elastic moduli [600,616–618].

We estimate the energy barrier between two potential energy minima from the curvature around the minima [617,618]. Consider the one-dimensional PEL with two minima separated the distance  $2\gamma_0$  as shown in Fig. 98. The two thin curves give the potential estimated by second-order expansions around the minima, and the barrier height is estimated by extrapolating from the minima. The estimated barriers are clearly larger than the actual barriers as shown in Fig. 98, but the estimated and actual barriers are proportional. The activation energy  $\Delta E$  for flow in BMGs or in MG-forming liquids is assumed to be mainly elastic energy. Then, in the energy landscape perspective, the activation energy density of flow can be expressed in a harmonic form  $\rho_E = \frac{1}{2} M \gamma^2$  using second order Taylor expansion around the minima [619], where  $M$  is the elastic moduli, and  $\gamma$  is the elastic strain. According to the equipartition law of statistical mechanics:  $\frac{1}{2} M \langle \gamma^2 \rangle \propto \frac{1}{2} k_B T / V_m$ , suggesting  $\langle \gamma^2 \rangle \propto k_B T / M V_m$ .

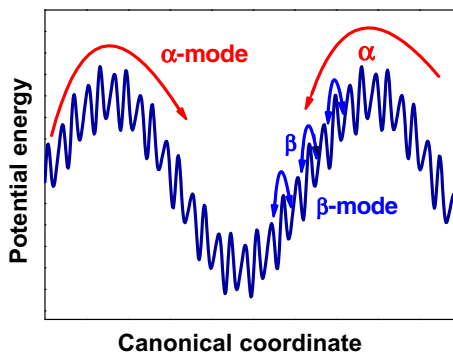


**Fig. 97.** A schematically illustration of flow and its corresponding origination of potential energy landscapes. There are two kinds of flow modes: the  $\beta$ -mode is the stochastically and reversible activated hopping events across “subbasins” confined within the inherent “megabasin” (intrabasin hopping) and the  $\alpha$  mode is irreversible hopping events extending across different landscape megabasins (interbasin hopping).

Assuming the distance  $r_0$  between the minima is constant, then,  $\rho_E = \frac{1}{2}M\gamma_0^2 = \frac{1}{2} \frac{k_B T}{\langle \gamma^2 \rangle V_m} \gamma_0^2$ , or  $\rho_E \propto \frac{k_B T_m / V_m}{\langle \gamma^2 \rangle}$ . Because the atoms release three degrees of freedom around glass transition in BMGs, one gets  $\langle \gamma^2 \rangle = \frac{k_B T}{V_m M_x} + \frac{k_B T}{V_m M_y} + \frac{k_B T}{V_m M_z}$ , where  $x, y, z$  represent the three directions in Cartesian coordinate, and  $M_x, M_y,$  and  $M_z$  are the corresponding elastic moduli. For isotropic metallic glasses, they represent two shear modulus and one longitudinal modulus, as  $M_x = M_y = \rho v_s^2$  and  $M_z = \rho v_l^2 = K + 4G/3$ , where  $\rho$  is the mass density, and  $v_s$  and  $v_l$  are the shear and longitudinal sound velocities, respectively. Then, one gets,

$$\langle \gamma^2 \rangle \propto \frac{2k_B T / V_m}{\rho v_s^2} + \frac{k_B T / V_m}{\rho v_l^2} = \frac{2k_B T / V_m}{G} + \frac{k_B T / V_m}{K + 4G/3} \tag{12.16}$$

And then, one obtains:

$$\rho_E \propto \frac{G(K + 4G/3)}{2K + 11G/3} \tag{12.17}$$

The linear contribution of  $G$  and  $K$  can be estimated by defining the temperature dependency of  $\rho_E$ ,  $I = \frac{d \ln \rho_E(T)}{d \ln T}$  [619]. That is:

$$I = \left( 1 - \frac{KG}{2K^2 + \frac{19}{3}KG + \frac{44}{9}G^2} \right) \cdot I_G + \frac{KG}{2K^2 + \frac{19}{3}KG + \frac{44}{9}G^2} \cdot I_K \tag{12.18}$$

alternatively,  $I = (1 - \alpha) \cdot I_G + \alpha \cdot I_K$ , where  $I_G$  and  $I_K$  are temperature indices, respectively. And

$$\alpha = \frac{KG}{2K^2 + \frac{19}{3}KG + \frac{44}{9}G^2} \tag{12.19}$$

For metallic glasses,  $G/K$  varies from 0.2 to 0.5 [see Table 1], and gives the partition coefficient of  $\alpha = 0.07 \pm 0.01$ . The partition coefficient for  $G$  and  $K$  suggests that both the volume-conservative shearing (corresponding to  $G$ ) and volume-nonconservative dilatation (corresponding to  $K$ ) contribute to the flow, and dilatation contributes around 7% to the activation energy density for creating the room for atoms rearrangement, which has been observed both by simulation and experiments [616–618].

To determine exact contribution of  $K$  and  $G$  to the  $\rho_E$  for flow, the acoustic velocities change during glass transition has been studied. The  $T$ -dependent transversal and longitudinal velocities change differently during the glass transition process [232], and the ratio of the relative changes of the two velocities is about  $\frac{\Delta v_s}{v_s} : \frac{\Delta v_l}{v_l} \approx 2 : 1$  [232]. From  $\rho v_s^2 = G$  and  $\rho v_l^2 = \frac{4}{3}G + K$ , we obtain the relative changes of  $G$  and  $K$ ,  $\frac{\Delta G}{G} : \frac{\Delta K}{K} \approx 5 : 1$ . In 3D space, there are two shear modes (corresponding to  $G$ ) and one radial mode (dilatation mode corresponding to  $K$ ) when atoms move. Thus, the contribution of

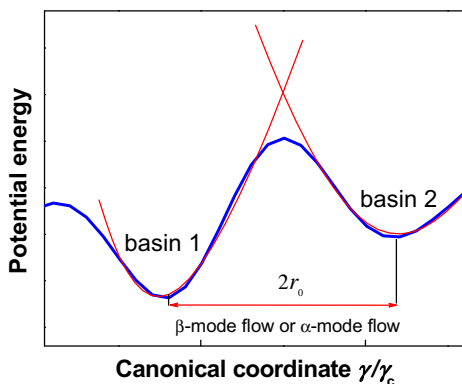


Fig. 98. The schematic map of potential energy density landscape with the distance  $2\gamma_0$  between the minima. The thin curve gives the estimation by second order Taylor expansions around the minima. The barrier height estimated by extrapolating from the minima. The estimated and actual barriers are proportional [619].

$G$  should be doubled, and the ratio of the contribution of  $G$  and  $K$  in  $\rho_E$  should be about 10:1 (Refs. [616,617]), that is

$$\rho_E = \Delta E/V_m = (10G + K)/11 \quad (12.20)$$

This indicates  $\alpha = 1/11 = 9\%$ , which is consistent with the above result.

The extended elastic model shows that  $\rho_E$  is determined by both  $G$  and  $K$  in a way of  $\rho_E(10G + K)/11$ , which is different from most other elastic models for flow in glasses and supercooled liquids, which consider the case of simple shear and involve only shear modulus. The extended elastic model suggests that the both homogeneous and inhomogeneous flow is shearing process combining free volume generation, and demonstrates that both shear and free volume are important for flow, and provides an intuitional picture of the flow of the atoms or atomic groups in glass or liquid. In fact, the shear induced dilatation has been widely observed. Both experimental evidence [312,322,323,402] and the jamming model of granular systems [620] show that shear as well as dilatation movements are involved in the flow during glass transition and deformation. We justify that the flow activation energy density  $\rho_E$  relates not to  $G$  or  $K$  but relate to both shearing transformation (corresponding to volume-preserving  $G$ ) and dilatation (corresponding to volume-nonpreserving  $K$ ).

The elastic model is further experimentally verified. We check the correlations between  $T_g$  and the elastic moduli for various metallic glasses. The flow viscosity of MG-forming liquids follows:  $\eta(T) = \eta_0 \ln\left(\frac{\Delta E(T)}{k_B T}\right)$ . According to the definition of glass transition temperature, at  $T_g$ , for BMGs,  $\eta(T_g) = 10^{13}$  Pa s. From  $\eta(T_g) = \eta_0 \left(\frac{\Delta E(T)}{k_B T}\right) = 10^{13}$  Pa s, or  $\frac{\Delta E(T)}{k_B T}|_{T=T_g} \equiv \text{constant}$ . One can see that  $\Delta E(T_g)/k_B T_g$  is a constant at  $T_g$  for all metallic glasses. According to our model,  $\frac{\rho_E V_m}{k_B T_g} = (10G + K)V_m/11RT_g = \text{constant}$ . Fig. 99a shows the data of  $(10G + K)V_m/11RT_g$  vs. various kinds of metallic glasses listed in Table 20. These BMGs cover many typical systems including Zr-, Cu-, Ca-, Mg-, Ni-, Fe-, and rare earth elements based BMGs, and their thermal, mechanical and physical properties are markedly different (see Tables 1 and 20). Their values of  $T_g$ ,  $E$  and Poisson's ratio span from 317 K to 930 K, 23 GPa to 195 GPa, 0.276–0.41, respectively. One can see that these data can be well fitted by a constant 0.075. The data of  $(10G + K)V_m/11RT_g$  for various metallic glasses vs. other parameters such as density and Poisson's ratio are shown in Fig. 99b. The metallic glasses are independent with these parameters and can also be well fitted by the constant of 0.075. The experimental comparison further testifies the above model. As a comparison, Fig. 99c and d also shows the plots of  $kV_m/T_g$  and  $GV_m/T_g$  vs. Poisson's ratio. Fitting to the data yields  $kV_m/T_g \propto 8.78\nu$  and  $GV_m/T_g \propto -0.86\nu$ , which indicating that the sole  $K$  or  $G$  cannot characterize the activation energy density well. Similar correlations have been found in different forms in different groups [92,323,506,621], which also support that volume factor must be considered to make the ratio of activation energies and  $T_g$  be a constant. The elastic moduli scaled with  $V_m$  are widely found to show better correlations with the thermal and mechanical properties for metallic glasses [312,322,323,402].

The elastic model is further experimentally confirmed by creep experiment in elastic regime of BMG at RT [622]. The attempt was made to amplify the measurable dilatation effects of homogeneous deformation by performing tests at RT to suppress structural relaxation. According to the elastic model, it is expected that plastic deformation induces dilatation of the glassy structure. In inhomogeneously deformed samples, the shear bands show clear structural changes resulting from the very high local shear, and possibly also linked to local heating and rapid cooling. The  $Zr_{46.75}Ti_{8.25}Cu_{7.5}Ni_{10}Be_{27.5}$  (Vit4,  $T_g = 625$  K) is chosen to perform tests below its yielding strength at RT to suppress structural relaxation. Ultrasonic measurements have been exploited to measure the subtle changes in the moduli of the MG uniaxially loaded with a strain rate of  $1 \times 10^{-4} \text{ s}^{-1}$  at 80% of the MG yield strength ( $\sigma_y \approx 1.9$  GPa) for periods of hours at RT. After 38 h of pre-compression, detectable permanent deformation after the load is removed is found. No shear bands are observed indicating the homogeneous deformation [622].

The evolution of density and elastic moduli with pre-compression time within the apparently elastic region indicates that the pre-compression induces dilatation [622]. The relative variations of elastic moduli show that the  $E$  and  $G$  decrease by similar small amounts, while the  $K$  decreases slightly more [622]. Loading for 38 h, the viscous strain is  $\sim 2 \times 10^{-4}$ , associated with a fractional density decrease of

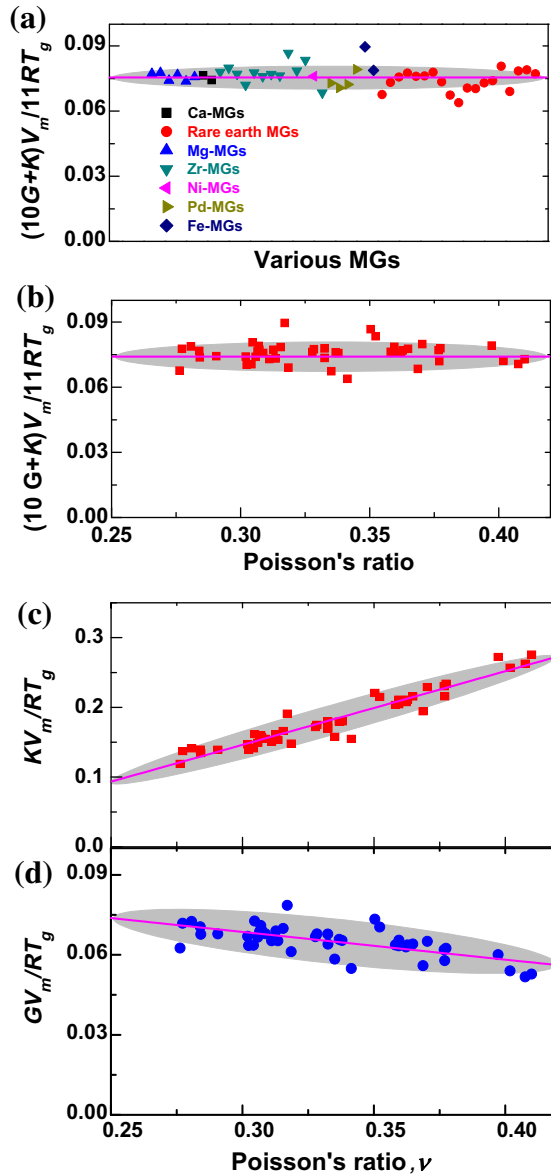


**Fig. 99.** (a) The experiment data of  $(10G + K)V_m/11RT_g$  vs. various MGs. (b) The  $(10G + K)V_m/11RT_g$  vs.  $\nu$ . The  $(10G + K)V_m/11RT_g$  is independent of MGs and can be well fitted by a constant. (c) The  $kV_m/RT_g$  and (d)  $GV_m/RT_g$  vs.  $\nu$  for the same MGs. The fit result show they have clear dependence on  $\nu$  [619,620].

$\sim 2 \times 10^{-3}$ . The density change though large, 10 times the viscous strain, is broadly consistent with the observed fractional decreases in elastic moduli of  $(5-7) \times 10^{-3}$ . The decreases in  $K$  therefore appear entirely consistent with the dilatation induced by pre-compression. It is noted that the elastic moduli and density increase during relaxation, and the increases are greater under hydrostatic pressure. Therefore, the changes in elastic moduli and density in our case are not consistent with structural relaxation. Also, on annealing-induced relaxation, the changes in  $K$  are much smaller than the changes

**Table 20**

The compositions, average molar volume  $V_m$ ,  $K$ ,  $E$ ,  $G$ ,  $\nu$ , and the combined parameters  $\text{moduli} \cdot V_m/T_g$  of 46 different kinds of BMGs [56,333].

Compositions	$T_g$ (K)	$V_m$ ( $\text{cm}^3/\text{mol}$ )	$K$ (GPa)	$E$ (GPa)	$G$ (GPa)	$\nu$	$GV_m/T_g$	$KV_m/T_g$	$(0.91G + 0.09K)/V_mT_g$
$\text{Ca}_{65}\text{Mg}_{8.54}\text{Li}_{9.96}\text{Zn}_{16.5}$	317	20.25	20.15	23.4	8.95	0.307	0.572	1.287	0.636
$\text{Ca}_{65}\text{Mg}_{8.31}\text{Li}_{9.69}\text{Zn}_{17}$	320	20.10	18.45	23.2	8.98	0.291	0.564	1.159	0.618
$\text{Yb}_{62.5}\text{Zn}_{15}\text{Mg}_{17.5}\text{Cu}_5$	385	19.24	19.78	26.5	10.4	0.276	0.520	0.989	0.562
$\text{Ce}_{70}\text{Al}_{10}\text{Ni}_{10}\text{Cu}_{10}$	359	16.94	27.00	30.3	11.5	0.314	0.543	1.274	0.609
$(\text{Ce}_{20}\text{La}_{80})_{68}\text{Al}_{10}\text{Cu}_{20}\text{Co}_2$	366	16.78	32.63	31.8	11.9	0.338	0.544	1.496	0.629
$\text{Ce}_{68}\text{Al}_{10}\text{Cu}_{20}\text{Nb}_2$	345	16.70	30.06	31.0	11.7	0.328	0.564	1.455	0.644
$(\text{Ce}_{80}\text{La}_{20})_{68}\text{Al}_{10}\text{Cu}_{20}\text{Co}_2$	355	16.69	31.79	31.1	11.6	0.337	0.547	1.494	0.632
$\text{Ce}_{68}\text{Al}_{10}\text{Cu}_{20}\text{Co}_2$	352	16.57	30.33	31.3	11.8	0.328	0.555	1.428	0.634
$\text{Ce}_{68}\text{Al}_{10}\text{Cu}_{20}\text{Ni}_2$	352	16.57	31.77	31.9	12.0	0.333	0.564	1.495	0.648
$\text{Ce}_{68}\text{Al}_{10}\text{Cu}_{20}\text{Co}_2$	351	16.44	30.13	30.3	11.46	0.333	0.532	1.411	0.611
$\text{La}_{60}\text{Al}_{20}\text{Co}_{20}$	477	15.96	39.17	38.7	14.5	0.335	0.486	1.311	0.560
$\text{Pr}_{55}\text{Al}_{25}\text{Co}_{20}$	509	15.07	43.48	45.9	15.4	0.341	0.456	1.287	0.531
$\text{Dy}_{55}\text{Al}_{25}\text{Co}_{20}$	635	14.27	52.22	61.4	23.5	0.304	0.529	1.174	0.587
$\text{Tb}_{55}\text{Al}_{25}\text{Co}_{20}$	612	14.15	50.19	59.5	22.9	0.302	0.528	1.160	0.585
$\text{Ho}_{55}\text{Al}_{25}\text{Co}_{20}$	649	13.85	58.81	66.6	25.4	0.311	0.542	1.255	0.607
$\text{Er}_{55}\text{Al}_{25}\text{Co}_{20}$	663	13.55	60.70	70.7	27.1	0.306	0.553	1.241	0.615
$\text{Tm}_{39}\text{Y}_{16}\text{Al}_{25}\text{Co}_{20}$	664	13.51	66.10	77.5	29.7	0.305	0.604	1.345	0.671
$\text{Tm}_{55}\text{Al}_{25}\text{Co}_{20}$	678	13.47	62.00	72.2	25.6	0.319	0.509	1.232	0.574
$\text{Lu}_{39}\text{Y}_{16}\text{Al}_{25}\text{Co}_{20}$	687	13.30	71.30	78.9	30.0	0.316	0.581	1.380	0.653
$\text{Lu}_{45}\text{Y}_{10}\text{Al}_{25}\text{Co}_{20}$	698	13.25	70.20	79.1	31.1	0.307	0.590	1.332	0.657
$\text{Lu}_{55}\text{Al}_{25}\text{Co}_{20}$	701	13.20	69.20	80.0	30.6	0.307	0.576	1.303	0.642
$\text{Mg}_{65}\text{Cu}_{25}\text{Gd}_{10}$	421	12.51	45.10	50.6	19.3	0.313	0.573	1.340	0.642
$\text{Mg}_{65}\text{Cu}_{25}\text{Y}_9\text{Gd}_1$	423	12.37	39.05	52.2	20.4	0.277	0.597	1.142	0.646
$\text{Mg}_{65}\text{Cu}_{25}\text{Y}_{10}$	419	12.36	41.36	49.1	18.9	0.302	0.556	1.220	0.616
$\text{Mg}_{65}\text{Cu}_{25}\text{Y}_8\text{Gd}_2$	420	12.23	39.85	51.7	20.1	0.284	0.586	1.161	0.638
$\text{Mg}_{65}\text{Cu}_{25}\text{Y}_5\text{Gd}_5$	422	12.05	39.10	50.6	19.7	0.284	0.563	1.117	0.613
$\text{Mg}_{65}\text{Cu}_{25}\text{Tb}_{10}$	415	11.95	44.70	51.3	19.6	0.309	0.565	1.288	0.630
$\text{Zr}_{64.13}\text{Cu}_{15.75}\text{Ni}_{10.12}\text{Al}_{10}$	640	11.68	106.63	78.4	28.5	0.377	0.519	1.946	0.648
$\text{Zr}_{65}\text{Cu}_{15}\text{Ni}_{10}\text{Al}_{10}$	652	11.65	106.65	83.0	30.3	0.37	0.541	1.906	0.664
$\text{Zr}_{61.88}\text{Cu}_{18}\text{Ni}_{10.12}\text{Al}_{10}$	651	11.51	108.33	80.1	29.1	0.377	0.514	1.915	0.640
$\text{Zr}_{55}\text{Al}_{19}\text{Co}_{19}\text{Cu}_7$	733	11.44	114.90	101.7	30.8	0.377	0.481	1.794	0.599
$\text{Zr}_{57}\text{Nb}_{5}\text{Cu}_{15.4}\text{Ni}_{12.6}\text{Al}_{10}$	687	11.44	107.70	87.3	32.0	0.365	0.533	1.793	0.646
$\text{Zr}_{57}\text{Ti}_5\text{Cu}_{20}\text{Ni}_8\text{Al}_{10}$	657	11.43	99.20	82.0	30.1	0.362	0.523	1.725	0.632
$(\text{Zr}_{55}\text{Ti}_6\text{Cu}_{22}\text{Ni}_{13})_{85.7}\text{Al}_{14.3}$	689	10.74	112.60	92.7	34.0	0.363	0.530	1.755	0.640
$\text{Cu}_{45}\text{Zr}_{45}\text{Al}_7\text{Gd}_3$	670	10.71	105.86	90.1	33.2	0.358	0.530	1.692	0.635
$\text{Zr}_{46.75}\text{Ti}_{8.25}\text{Cu}_{10.15}\text{Ni}_{10}\text{Be}_{27.25}$	622	10.21	111.90	100	37.2	0.35	0.610	1.836	0.721
$\text{Zr}_{48}\text{Nb}_8\text{Cu}_{12}\text{Fe}_8\text{Be}_{24}$	658	10.17	113.60	95.7	35.2	0.36	0.544	1.756	0.653
$\text{Zr}_{41}\text{Ti}_{14}\text{Cu}_{12.5}\text{Ni}_{10}\text{Be}_{22.5}$	625	9.79	114.10	101	37.4	0.352	0.586	1.787	0.694
$\text{Ni}_{45}\text{Ti}_{20}\text{Zr}_{25}\text{Al}_{10}$	733	9.61	129.60	109	40.2	0.359	0.527	1.699	0.632
$\text{Cu}_{60}\text{Zr}_{20}\text{Hf}_{10}\text{Ti}_{10}$	754	9.50	128.20	101	36.9	0.369	0.465	1.616	0.569
$\text{Pd}_{77.5}\text{Cu}_6\text{Si}_{16.5}$	633	8.74	166.00	89.7	31.8	0.41	0.439	2.293	0.606
$\text{Pd}_{64}\text{Ni}_{16}\text{P}_{20}$	630	8.29	166.00	91.9	32.7	0.408	0.430	2.183	0.588
$\text{Pd}_{40}\text{Cu}_{40}\text{P}_{20}$	590	7.98	158.00	93.0	33.2	0.402	0.449	2.136	0.601
$\text{Pd}_{39}\text{Ni}_{10}\text{Cu}_{30}\text{P}_{21}$	560	7.97	159.10	98.2	35.1	0.397	0.500	2.264	0.658
$\text{Fe}_{53}\text{Cr}_{15}\text{Mo}_{14}\text{Er}_1\text{C}_{15}\text{B}_6$	900	7.94	180.00	195	75.0	0.317	0.610	1.588	0.698
$\text{Fe}_{61}\text{Mn}_{10}\text{Cr}_4\text{Mo}_6\text{Er}_1\text{C}_{15}\text{B}_6$	930	7.48	146.00	193	75.0	0.281	0.603	1.174	0.654

in  $G$  or  $E$ , in contrast to the relative magnitudes in our case. The found clear dilatation effect in the viscous flow in the apparently elastic regime of the glass reveals that the large volume increase associated with the local shearing events'. This also indicates that the role of bulk modulus during flow. The results as well as others further confirm the proposed elastic model.

Shear-induced dilatation has also been reported in the inhomogeneous deformation of BMGs [623–625]. It was reported that the cold rolling of  $\text{Pd}_{77.5}\text{Cu}_6\text{Si}_{16.5}$  BMG to reductions of 30–40% in thickness gives a density decrease of 0.15% [623]. The authors attempt to estimate the change of free volume in the shear bands, and find that the free-volume increase in the shear bands would be 30–50%! This forces them to conclude that not all of the free volume generated by deformation can be in the bands and a significant fraction must be in the matrix between the bands.

The shear elastic energy density  $\phi$  of a flow unit can be expressed as  $\phi(\gamma) = \phi_0 \sin^2(\pi\gamma/4\gamma_c)$  [82], where  $\phi$  is the total barrier energy density and  $\gamma$  is the shear strain. The  $G$  can be reduced from the shear elastic energy density  $\phi$  not the shear elastic energy, in a way of  $G = \phi''|_{\gamma=0} = \frac{\phi_0}{8\gamma_c^2/\pi^2}$  [82]. This indicates that  $G$  is related to the barrier energy density. The  $K$  can be expressed as  $K = V_0 \left. \frac{\partial^2 U}{\partial V^2} \right|_{V=V_0} = \partial^2(U/V_0)/\partial(V/V_0)^2|_{V=V_0}$ , where  $U$  is the atomic potential energy,  $V_0$  is the atomic equilibrium volume,  $U/V_0$  is the energy density, and  $V/V_0$  correlates with elastic strain. In harmonic approximation around  $V_0$ , the  $U$  can be expressed in a parabolic form as  $U = U_0(1 - \alpha V/V_0)^2$  [79], where  $\alpha$  is constant depending on the atomic bonding nature. This gives  $K = 2\alpha^2 U_0/V_0$ , which correlates with the potential energy density at equilibrium state. Thus, both  $G$  and  $K$  are proportional to their corresponding deformation energy density. Therefore, it is reasonable for  $\rho_E$  rather than the activation energy shows direct correlation with the combined moduli of  $K$  and  $G$ .

### 13. The elastic perspectives on metallic glasses

In conventional crystalline alloys, their properties and characteristics can be understood in microstructure including the crystal structure, the degree of order, and the contents and distributions of defects such as vacancies, interstitials, dislocations, twins and grain boundaries [51]. The metallic glasses have no such “microstructure” to speak of, and their ‘many-body’ random structural nature is extremely difficult to be described or detected accurately like their crystalline counterpart [626–628]. And the glass is even thought to be an unsuitable basis for understanding the relation of structure and properties. It is therefore a major challenge to describe the metallic glasses, to understand their formation and features, and to establish their structure–properties or structure–features relationship. The systematical elastic property studies indicate that elastic moduli can be used as key parameters for modeling, understanding and describing the most fundamental issues in metallic glasses. The elastic property studies draw several important conclusions, which lead to the elastic models and elastic perspectives on the metallic glasses. These conclusions are summarized as following:

- (1) The subtle local atomic-scale structural changes induced by tuning composition, temperature, pressure, aging and internal or external stress can be effectively characterized by the easy measurable parameter of elastic moduli. There are close links between the microstructural change and properties/features of the glasses through the medium of elastic constants.
- (2) There are exist clear correlations even in macroscopic and empirical levels among the elastic moduli, the glass formation and transition, the properties and features, and the strong/fragile characteristics of metallic glasses. These correlations provide predictability and help one to get insight into the properties–structure relationship and then the common origin of the unique properties and features of the disordered systems [56,305–383,629]. These correlations between elastic constants and properties (or features) also have clues for searching new glass compositions that combine desirable glass-forming ability with good mechanical properties.
- (3) The glass formation, glass transition, relaxation, and homogeneous and inhomogeneous deformation in metallic glasses are all closely related to flow events controlled by activation energy barrier.
- (4) For the flow both in glasses and supercooled liquids, its energy barrier is determined by their elastic moduli. The elastic model offers a simple scenario for explaining and understanding the nature of metallic glasses and correlations in metallic glasses.

Based on above experimental observations and conclusions, and on the assumptions of that the metallic glasses are frozen liquids and they can be characterized as highly viscous, the elastic perspective of the metallic glasses is suggested as that:

The glass formation from solidification of liquid, the mechanical plastic deformation, relaxations, glass transition and formation, and the aging of glasses can be treated as flow phenomenon or the change of their different configurations driven by different processes. The flow can be modeled as activated hopping between inherent states across energy barrier in the potential energy landscape

induced by different processes such as thermal or mechanical process [33–35]. The flow viscosity of metallic glass-forming liquids follows the general Arrhenius equation:  $\eta(T) = \eta_0 \left( \frac{\Delta E(T)}{k_B T} \right)$ , and the flow event is governed by the activation energy,  $\Delta E(T)$ . The energy barrier of the flow of both newtonian and nonnewtonian metallic glass-forming liquids over a broad range of rheological behavior is found to be determined by the instantaneous elastic moduli scaled with volume, and the variation in the configurational change or the flow events in glass or liquid induced either by thermal excitation or mechanical deformation can be then correlated to the variations in elastic modulus. That is, the elastic moduli, i.e. the high-frequency shear modulus  $G_\infty$  accompanying  $K_\infty$  as well as the volume factor, are the key physical quantity controlling the main thermodynamic and kinetic, mechanical and dynamic properties, and even glass-forming ability of supercooled liquids and glasses. The  $K$  and volume have to be considered since a flow event requires a local volume increase. The elastic perspective can be schematically illustrated in Fig. 100. According to the elastic moduli perspectives, many complex issues in glasses and supercooled liquids can be simply treated and understood based on several ready measurable parameters of elastic constants.

In the following, we will show that many important issues and experimental observations on metallic glasses can be understood and explained via the elastic perspectives. The elastic moduli correlation, elastic model and elastic moduli perspectives provide different points of view on some important fundamental issues of metallic glasses.

The first example is about slow down: when cooling from the melting point  $T_m$  to the glass transition temperature  $T_g$ , the temperature dependence of the viscosity  $\eta$  of glass-forming liquids slows down and follows a general Arrhenius equation. One of the well-known theories to understand the non-Arrhenius behavior is the Adam–Gibbs model [588], in which an idea of cooperatively rearrangement regions (CRR) was proposed to explain the non-Arrhenius behavior by the temperature dependence of configurational entropy  $S_{conf}$ . However, this conventional wisdom has recently been challenged [36,253]. For example, the experiments invariably find the length scales of the heterogeneity are of a few nanometers only [36,253], and this is clearly inconsistent with the assumption of the CRRs which is largely unaffected by its surroundings. While according to the elastic perspectives, the CRRs arisen from Adam–Gibbs model are not necessary to explain the non-Arrhenius. On the contrary, high viscosity is related directly to the high barrier (or high instantaneous elastic moduli) for atoms and molecules to be overcome in the system. In the dynamic point of view, upon cooling from  $T_m$  to  $T_g$  the increasing barrier energy makes the relaxation time longer. As the relaxation time of the liquids reaches the order of 100 s which is the order of the usual experimental time scale, glass is formed.

The yielding and fracture of metallic glasses are generally attributed to the formation of principal shear bands. The issue of formation mechanism of shear bands, as a case, can be understood in terms of elastic perspectives. Contradictory mechanisms of dramatic temperature rise [516] or stress induced dilatation (formation of free volumes) [617] both supported by experimental evidence has been proposed for the shear bands nucleation and formation. According to elastic perspectives on the metallic glasses, the nucleation and formation of shear band is a localized flow in metallic glasses which is controlled by elastic moduli. The localized destabilization of glassy structure (or activation

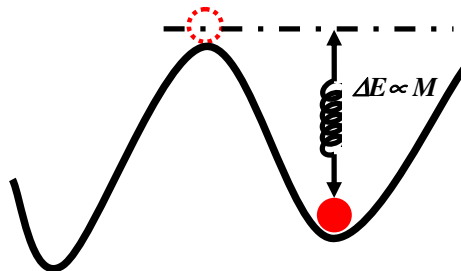


**Fig. 100.** Schematic illustration of the flow events both for homogenous flow in supercooled liquids and inhomogeneous flow in glasses controlled by elastic moduli  $M$ : The activation of flow events requires of energies of  $\Delta E$  related to  $M$ . External stress (in glass) or thermal fluctuation in liquids can soften  $M$  and induce the occurrence of flows.

of shear transformation zones and their self-organized into embryo of shear band) is a kind of elastic moduli softening corresponding to collision of saddle point between inherent structures in potential energy landscape. In other words, the elastic destabilization or softening and the flow events in shear bands driven by external forces is equivalent to the glass transition induced by mechanical energy or free volume increase [506]. Shear banding is a kind of localized glass transition in nano-scale thin layers. Therefore, the controversial issue of formation mechanism of shear bands actually is the elastic moduli softening process, and the shear bands nucleation and formation then can be caused equivalently by temperature rise induced by mechanical energy (shear stress) or by free volume increase (dilatation) or by combination of the temperature rise and free volume increase effects. The plastic deformation of BMGs occurs upon reaching to a critical energy threshold, at which the accumulated internal energy from elastic deformation is sufficiently high for the transition from glass to a supercooled liquid with high atom mobility. Mechanical stress, equivalent to thermal activation energy, can significantly enhance the atomic mobility by inducing a glass to supercooled liquid transition in shear bands, which is a key factor responsible radically for the deformation of BMGs. The mechanical work, analogous to thermal activation energy, drive the glass-to-supercooled-liquid transition in shear bands which is usually attainable at a temperature above the  $T_g$  with enhanced atomic mobility. The shear banding in BMGs can be regarded as a stress induced localized glass-to-supercooled-liquid transition.

The plastic mechanism for the large plastic bulk metallic glasses found recently can be explained according to the elastic perspectives. These plastic BMGs usually have low  $G$  and larger Poisson's ratio due to their inhomogeneous structure, which indicates that the activation barrier  $\Delta E$  is relatively smaller for operation of the STZs (the fundamental unit of plasticity of metallic glass [488]) in these metallic glasses because the energy barrier for operation a plastic unit or STZ is mainly correlated to  $G$  according to the elastic perspective. One STZ's operation creates a localized distortion of the surrounding material and triggers the autocatalytic formation of more STZs, and these STZs self-organized into the embryo of shear bands. On the other hand, the STZ volumes of plastic flow of BMGs are also found to increase with  $v$ . This means that a larger STZ compared with small one enables a smaller number of STZs to be activated for nucleation of a shear band, and reinforce the shear capability of the metallic glass and promote the formation of multiple shear bands [546]. So, according to the elastic perspective, to decrease the activation barrier  $\Delta E$  or the decrease shear modulus, one can enhance the plasticity of a metallic glass. This is agreement with the fact that a higher Poisson's ratio represents a higher possibility for a BMG to have better plasticity and toughness.

The static inhomogeneous microstructure (or the inhomogeneous distribution of the free volumes) and the stress fluctuation of metallic glasses, which has close relationship with their mechanical properties and structural relaxations, can be well characterized by the local elastic modulus fluctuation [85,376–378,382,383,630–635]. A link between structure and dynamic heterogeneity was also recently suggested on the basis of numerical simulation and experimental observations [630–635]. The structural and dynamic heterogeneities can be characterized by the elastic modulus [634], and the local fluctuations in the elastic modulus in metallic glasses can provide insight on the relaxations, plastic deformation mechanism [634]. The elastic–plastic transition is given by the percolation of 'soft spots' within the distribution of elastic moduli. The local fluctuations in the elastic modulus, which corresponds to the inhomogeneous microstructure or the stress fluctuation, can also explain the composition dependent mechanical properties in metallic glass systems.

The structural and bonding inhomogeneous microstructure would induce the local fluctuations in the shear modulus in a metallic glass, which can be characterized by  $G^{\#}/\langle G \rangle$ , where the  $G^{\#}$  and  $\langle G \rangle$  are local and the global shear modulus, respectively [382]. Different glassy alloy systems have different characteristic  $G^{\#}/\langle G \rangle$ . The elastic moduli fluctuations can be attributed to the local topological and chemical fluctuations in the metallic glasses. The local shear modulus  $G^{\#}$  of the metallic glass in the region with high density of free volumes or lower density of free volumes (with 10–20 atom flow units) must be lower or higher than the global shear modulus  $\langle G \rangle$  measured, which has been confirmed by simulation and experimental observations [634,636]. This leads to the so-called soft and hard regions in some plastic bulk metallic glasses with larger plasticity [85]. Ichutsubo et al. [226,257,637] found that the elastic inhomogeneity with a certain correlation length exists in dense metallic glasses and the correlation length value can reflect the characteristic domain size in glasses,

and the static structural heterogeneity correlates with Poisson's ratio and fragility. Since shear deformation (STZs and their self-organization) occurs preferentially in the soft regions with high density of free volumes and low shear resistance in metallic glass, if there is a sufficiently large population of flow unit of STZs with low  $G^\#$  value, then a network of multiple shear bands can form easily to shield potential brittle damage and plasticity ensues. This explain some monolithic glassy alloys with structural or bonding heterogeneity on length scales ranging from nanometer to submicrometer can lead to superior large plasticity. The glassy alloy with larger different characteristic  $G^\#/\langle G \rangle$  has larger plasticity. The elastic inhomogeneity also explains the structural origin of the correlation between plasticity and Poisson's ratio [56].

The  $\beta$ -relaxation or Johari–Goldstein relaxation [248–250] has been proved being an intrinsic and universal feature of metallic glasses [97,130,242–244,246–248,638–640], while the physical and structural origin is not clear yet. It usually is related to some kinds of localized motions with cooperative nature, a reminiscent of STZs in metallic glasses [248–250]. It is found that the activation of STZs and slow  $\beta$ -relaxations in metallic glasses are directly related through elastic moduli [641]. The results have implications on the origins of the  $\beta$ -relaxation and the flow resistances of STZs as well as its relationship with the intrinsic plasticity and the scenario of inhomogeneous atomic structure of unrelaxed metallic glasses. From the perspective of elastic model and potential energy landscape theory, the  $\beta$ -relaxations are identified as hopping events across the energy barrier related to elastic moduli within an inherent megabasin, while the  $\alpha$ -relaxations entail escape from one megabasin and eventually jump into another by overcoming the energy barrier [641]. Experimentally, the activation energy of the  $\beta$ -relaxations of BMGs,  $E_\beta$ , can be determined by various methods such as differential scanning calorimeter or dynamic mechanical spectroscopy (DMA) [97,130,242–244,246–248,636,641–643]. The activation of isolated STZ confined within elastic matrix is regarded to associate with the  $\beta$ -relaxation process [82], and the percolation of STZs would result in the plastic yielding of BMGs, associated with  $\alpha$ -relaxation. However, the validity of the correlation between the activation of STZ and the  $\beta$ -relaxation remains unclear, mainly due to the unclearness of the nature and the origin of the  $\beta$ -relaxation and how the events of STZs relate to the  $\beta$ -relaxations.

Fig. 101a shows the  $E''$  of a typical  $\text{La}_{55}\text{Al}_{15}\text{Ni}_{10}\text{Cu}_{10}\text{Co}_{10}$  bulk metallic glass between 300 K and 500 K with testing frequencies varied from 0.1 Hz to 8 Hz [641]. The broad humps around 320–400 K were identified as the slow  $\beta$ -relaxations [242–244], and the  $E_\beta$  was estimated by plotting  $\log(f)$  vs.  $1000/T_p$ , where  $T_p$  is the peak temperature of the hump as shown in the inset of Fig. 101a. For  $\text{La}_{55}\text{Al}_{15}\text{Ni}_{10}\text{Cu}_{10}\text{Co}_{10}$  metallic glass, its activation energy  $E_\beta$  is about  $89 \pm 6$  kJ/mol. Table 21 summarizes the values of  $E_\beta$  and  $T_g$  determined from DMS measurements for various BMGs. Fig. 101b shows the plot of  $E_\beta$  vs.  $RT_g$  of the data listed in Table 21. An approximately linear relationship of  $E_\beta \approx 26(\pm 2)RT_g$  can be obtained ( $R$  is the gas constant) [641]. The similar empirical relationship between  $E_\beta$  and  $T_g$  in the form of  $E_\beta \approx 24RT_g$  has also been found to exist in nonmetallic glasses [641,644], which agrees well with that in metallic glasses. The results indicate that  $E_\beta$  scales with  $T_g$ , the characteristic temperature of  $\beta$ -relaxation or glass transition, and this confirms that the “ $\beta$ -relaxation to  $\alpha$ -relaxation” is a self-similar organization.

The energy barrier of STZs can be estimated using the cooperative shear model [82]. Assuming  $n$  atoms take part in an isolated STZ event, let  $\Omega = nC_fV_a$  where  $V_a = M/(\rho N_0)$  is the atomic volume,  $N_0$  Avogadro's number,  $\rho$  density and  $M$  molar mass,  $C_f \geq 1$  is a free volume parameter. The molar potential energy barrier for an unsheared STZ is thus  $W_{STZ} = N_0W = (8/\pi^2)nG\gamma_c^2C_fV_m$ , here  $V_m = N_0V_a$  is molar volume. Taking account  $C_f = 1.12$ ,  $n = 200$ , one gets  $W_{STZ} \approx 0.397GV_m$ . The relevant data of  $G$ ,  $V_a$ , and  $GV_m$  and estimated  $W_{STZ}$  for more than 40 different BMGs are collected in Table 22. Fig. 102 shows a plot of the molar potential energy barrier  $W_{STZ}$  for an unsheared STZ vs. the  $E_\beta$  (estimated as  $E_\beta \approx 26RT_g$ ) for the BMGs listed in Table 22. The plot reveals nearly a one-to-one correspondence between  $E_\beta$  and  $W_{STZ}$  that extends over a broad range, suggesting a clear correlation between  $W_{STZ}$  and  $E_\beta$ , or  $E_\beta \approx W_{STZ}$ . This linear relationship is further checked to well stand in individual systems of BMGs based on such as Zr-, Cu-, Fe-, and rare-earth based BMGs [641]. The results confirm that the potential STZs and the  $\beta$ -relaxations are directly correlated through elastic moduli. Fig. 103 plots the  $GV_m$  (correlated to  $W_{STZ} \approx 0.397GV_m$ ) against  $RT_g$  ( $E_\beta \approx 26RT_g$ ) for BMGs listed in Table 22. It can be seen that the  $GV_m$  and  $RT_g$  are correlated for various BMGs, and the generalized correlation in essence is a manifestation of the relationship between activation of STZs and  $\beta$ -relaxation. As  $GV_m$  is a measurement of the

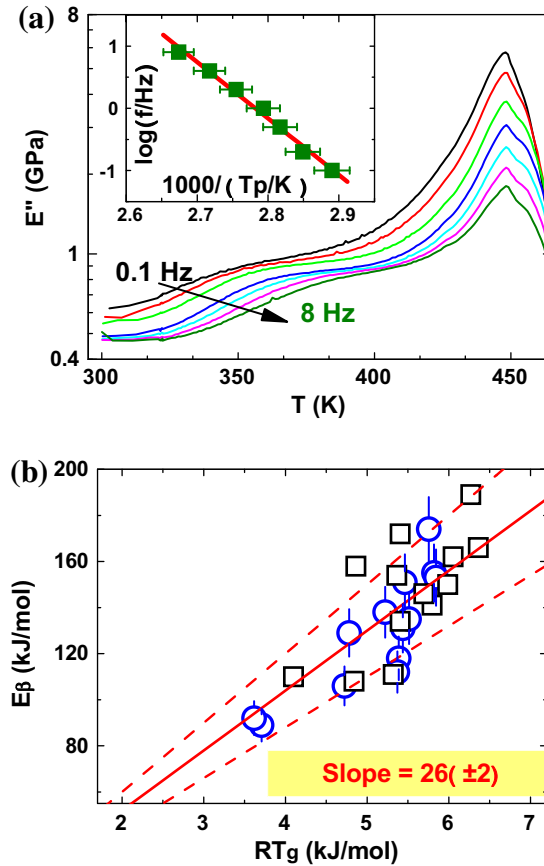


**Fig. 101.** (a) The temperature dependence of the loss modulus  $E''$  for a  $\text{La}_{55}\text{Al}_{15}\text{Ni}_{10}\text{Cu}_{10}\text{Co}_{10}$  BMG, measured with frequencies  $f$  (from top to bottom, indicated by the arrow) 0.1, 0.2, 0.5, 1, 2, 4, and 8 Hz, at the heating rate of 2 K/min. The inset plots  $\log(f)$  versus  $1000/T_p$ , where  $T_p$  is the peak temperature of the  $\beta$  relaxation hump around 320–400 K. (b) Relationship between activation energy of  $\beta$ -relaxation  $E_\beta$  and  $RT_g$  for metallic glasses listed in Table 21. The open squares and circles denote measurements from DSC and DMS respectively [641].

energy barrier of STZs and  $RT_g$  measures activation energy of the  $\beta$ -relaxation, one can readily use  $GV_m$  and  $RT_g$ , which can be easily measured, to characterize the events of STZs and the  $\beta$ -relaxations in BMGs. In other words, the two fundamental issues of plastic deformation and relaxations in metallic glasses are correlated through elastic moduli, which have been verified by simulation [645,646].

The  $\beta$ -relaxation relates to the dynamical heterogeneity in glasses, whereas its structural origin is rather vague. On the other hand, there is general consensus that the potential STZs are nucleated around the sites of free volumes, where the atomic packing is relative loose. This picture is validated by the experimental observations that some BMGs consist of the weakly bonded regions (or soft regions) and strongly bonded regions (or hard regions) and the heterogeneous structure benefit the plastic deformation of the metallic glasses [85,393,529,645–651]. Based on the correlation between STZ and  $\beta$ -relaxation in activation energy, the origin of  $\beta$ -relaxation could be understood from the microstructural characteristic of metallic glasses. A schematic 2-D plot of such a structure is shown in Fig. 104a and b for fragile and strong metallic glass, respectively. The microstructure of BMGs is inhomogeneous in the atomic scale and comprises closely packed and loosely packed regions. The  $\beta$ -relaxations, similar to the events of potential STZs, take place in the loosely packed regions as indicated in Fig. 104, where the local translational atomic motions can be readily activated, compared with that in

**Table 21**

Activation energy of  $\beta$ -relaxation  $E_\beta$ , glass transition temperature  $T_g$ , of different metallic glasses. In DMA, the  $T_g$  was determined at the testing frequency of 1 Hz.

Metallic glass	$E_\beta$ (kJ/mol)	$T_g$ (K)	Method	Refs.
La <sub>55</sub> Al <sub>15</sub> Ni <sub>10</sub> Cu <sub>10</sub> Co <sub>10</sub>	89	446	DMS	[641]
Cu <sub>47</sub> Zr <sub>47</sub> Al <sub>6</sub>	155	700	DMS	[641]
Cu <sub>45</sub> Zr <sub>45</sub> Al <sub>10</sub>	153	703	DMS	[641]
Zr <sub>46.75</sub> Ti <sub>18.25</sub> Cu <sub>7.5</sub> Ni <sub>10</sub> Be <sub>27.5</sub>	118	648	DMS	[641]
Zr <sub>64.13</sub> Cu <sub>15.75</sub> Ni <sub>10.12</sub> Al <sub>10</sub>	112	646	DMS	[641]
Zr <sub>57</sub> Cu <sub>15.4</sub> Ni <sub>12.6</sub> Al <sub>10</sub> Nb <sub>5</sub>	135	663	DMS	[641]
Tm <sub>39</sub> Y <sub>16</sub> Al <sub>25</sub> Co <sub>20</sub>	151	657	DMS	[641]
La <sub>55</sub> Al <sub>25</sub> Ni <sub>20</sub>	110	493	DSC	[243]
Pd <sub>40</sub> Ni <sub>10</sub> Cu <sub>30</sub> P <sub>20</sub>	129	575	DMS	[243]
Zr <sub>46.75</sub> Ti <sub>18.25</sub> Cu <sub>7.5</sub> Ni <sub>10</sub> Be <sub>27.5</sub>	138	628	DMS	[243]
Zr <sub>65</sub> Cu <sub>15</sub> Ni <sub>10</sub> Al <sub>10</sub>	131	654	DMS	[243]
(Cu <sub>50</sub> Zr <sub>50</sub> ) <sub>92</sub> Al <sub>8</sub>	174	692	DMS	[243]
La <sub>57.5</sub> (Cu <sub>50</sub> Ni <sub>50</sub> ) <sub>25</sub> Al <sub>17.5</sub>	92	435	DMS	[243]
(Fe <sub>85</sub> Ni <sub>15</sub> ) <sub>83</sub> P <sub>17</sub>	134	650	DSC	[641]
(Fe <sub>85</sub> Cr <sub>15</sub> ) <sub>83</sub> P <sub>17</sub>	150	720	DSC	[641]
(Fe <sub>85</sub> V <sub>15</sub> ) <sub>83</sub> P <sub>17</sub>	162	728	DSC	[641]
(Fe <sub>85</sub> Mo <sub>15</sub> ) <sub>83</sub> P <sub>17</sub>	189	754	DSC	[641]
(Fe <sub>75</sub> Ni <sub>25</sub> ) <sub>83</sub> P <sub>17</sub>	111	640	DSC	[641]
(Fe <sub>75</sub> Co <sub>25</sub> ) <sub>83</sub> P <sub>17</sub>	146	685	DSC	[641]
(Fe <sub>75</sub> Mn <sub>25</sub> ) <sub>83</sub> P <sub>17</sub>	141	697	DSC	[641]
(Fe <sub>75</sub> Cr <sub>25</sub> ) <sub>83</sub> P <sub>17</sub>	166	765	DSC	[641]
(Fe <sub>50</sub> Ni <sub>50</sub> ) <sub>83</sub> B <sub>17</sub>	172	650	DSC	[641]
(Fe <sub>5</sub> Ni <sub>5</sub> ) <sub>83</sub> P <sub>17</sub>	154	645	DSC	[641]
Pd <sub>48</sub> Ni <sub>32</sub> P <sub>20</sub>	92	582	DSC	[641]
Al <sub>82</sub> Ni <sub>10</sub> Ce <sub>8</sub>	158	585	DSC	[641]
Pd <sub>43</sub> Ni <sub>10</sub> Cu <sub>27</sub> P <sub>20</sub>	106	568	DMS	[243]

closely packed regions. We speculate that the structural heterogeneity is the common structural origin of events of STZs and the  $\beta$ -relaxations. The  $\beta$ -relaxation in BMGs then corresponds to a process involving “thermal driven events of STZs”, i.e., a group of atoms within loosely packed regions undergo an inelastic distortion from one configuration to another, crossing an energy barrier, and consequently,  $E_\beta \approx W_{STZ}$ . For  $\beta$ -relaxation, the driven force is essentially obtained from the thermal fluctuations, and there is no directional flow and the process is reversible due to the confinements of the surrounding closely packed regions. In contrast, the directional flow events of STZs induced by external shear stress.

The connection of events of STZs and the slow  $\beta$ -relaxations in BMGs could help us to understand the deformation mechanisms and plasticity of BMGs. For a fragile system with larger fragility and Poisson's ratio,  $\nu$ , it shows marked structural heterogeneity, depicted in Fig. 104a, which comprises more loosely packed regions for triggering the  $\beta$ -relaxations and the activation of STZs. This means lowering  $E_\beta$  or  $W_{STZ}$  compared with that of strong BMGs [with smaller fragility and  $\nu$  as shown in Fig. 104b]. According to the correlations of Poisson ratio with structural heterogeneity, fragility and plasticity, the fragile BMG is expected to have lower  $W_{STZ}$  and  $E_\beta$  and better plasticity [652,653].

In a broad class of polymer glasses there is similar connection between mechanical prosperities and  $\beta$ -relaxation [654–659]. For instance, in many polymer glasses the transition from ductile to brittle occurs at the characteristic temperature of the  $\beta$ -relaxations [654,655], and transitions of impact toughness yield strength and failure modes were also often correlated with  $\beta$ -relaxations [656]. Moreover, polymers with pronounced  $\beta$ -relaxations often possess good ductility and vice versa. Some theories such as Eyring's model have been proposed to relate molecular motions to mechanical properties. However, these models are unable to account for all the experiments results, and the correlation between mechanical properties to  $\beta$ -relaxation is still an open question. This might due to the complicated structures (which consisting primarily of chains units) and dynamics of glassy polymers, and the modes of molecular motions responsible for  $\beta$ -relaxations could vary from one type of polymer glass to another [654].

**Table 22**

Summary of data on BMG compositions and density  $\rho$ , Young's modulus  $E$ , shear modulus  $G$ , Poisson ratio  $\nu$ , glass transition temperature  $T_g$ , and  $GV_m$ . The molar energy barrier of STZs,  $W_{STZ} \approx 0.397GV_m$ , taking  $n = 200$ ,  $\gamma_c = 0.027$ ,  $\zeta = 3$ ,  $C_f = 1.12$  (see the text).

BMG	$\rho$ (g/cm <sup>3</sup> )	$E$ (GPa)	$G$ (GPa)	$GV_m$ (kJ/mol)	$\nu$	$T_g$ (K)	$W_{STZ}$ (kJ/mol)
Au <sub>49</sub> Ag <sub>5.5</sub> Pd <sub>2.3</sub> Cu <sub>26.9</sub> Si <sub>16.3</sub>	11.60	74.4	26.5	291.4	0.406	405	115.7
Au <sub>55</sub> Cu <sub>25</sub> Si <sub>20</sub>	12.20	69.8	24.6	261.8	0.417	348	103.9
Ca <sub>65</sub> Li <sub>9.96</sub> Mg <sub>8.54</sub> Zn <sub>16.5</sub>	1.96	23.4	9.0	180.9	0.307	333	71.8
Ce <sub>68</sub> Al <sub>10</sub> Cu <sub>20</sub> Co <sub>2</sub>	6.81	30.3	11.4	186.6	0.333	351	74.1
Ce <sub>70</sub> Al <sub>10</sub> Cu <sub>20</sub>	6.70	29.9	11.3	190.6	0.329	342	75.7
Ce <sub>70</sub> Al <sub>10</sub> Ni <sub>10</sub> Cu <sub>10</sub>	6.67	30.3	11.5	194.8	0.313	359	77.3
Cu <sub>46</sub> Zr <sub>42</sub> Al <sub>7</sub> Y <sub>5</sub>	7.23	84.6	31.0	316.8	0.364	713	125.8
Cu <sub>46</sub> Zr <sub>46</sub> Al <sub>8</sub>	7.08	93.7	34.3	355.4	0.366	701	141.1
Cu <sub>46</sub> Zr <sub>54</sub>	7.62	83.5	30.0	309.0	0.391	696	122.7
Cu <sub>47</sub> Zr <sub>47</sub> Al <sub>6</sub>	7.13	92.4	33.8	352.5	0.367	701	139.9
Cu <sub>48</sub> Zr <sub>48</sub> Al <sub>4</sub>	7.22	88.7	32.4	338.2	0.370	689	134.3
Cu <sub>50</sub> Hf <sub>43</sub> Al <sub>7</sub>	11.00	113.0	42.0	421.6	0.358	774	167.4
Cu <sub>50</sub> Zr <sub>50</sub>	7.40	87.0	32.0	334.7	0.360	670	132.9
Cu <sub>57.5</sub> Hf <sub>27.5</sub> Ti <sub>15</sub>	9.91	103.0	37.3	349.3	0.356	729	138.7
Dy <sub>55</sub> Al <sub>25</sub> Co <sub>20</sub>	7.56	61.4	23.5	335.7	0.304	635	133.3
Er <sub>55</sub> Al <sub>25</sub> Co <sub>20</sub>	8.16	70.7	27.1	366.8	0.306	663	145.6
Fe <sub>53</sub> Cr <sub>15</sub> Mo <sub>14</sub> Er <sub>1</sub> C <sub>15</sub> B <sub>6</sub>	6.92	195.0	75.0	595.6	0.320	860	236.5
Fe <sub>61</sub> Mn <sub>10</sub> Cr <sub>4</sub> Mo <sub>6</sub> Er <sub>1</sub> C <sub>15</sub> B <sub>6</sub>	6.89	193.0	75.0	560.8	0.280	870	222.6
Fe <sub>68</sub> Mo <sub>5</sub> Ni <sub>5</sub> Cr <sub>2</sub> P <sub>12.5</sub> C <sub>5</sub> B <sub>2.5</sub>	7.50	152.7	57.9	397.8	0.329	699	157.9
Fe <sub>70</sub> Mo <sub>5</sub> Ni <sub>5</sub> P <sub>12.5</sub> C <sub>5</sub> B <sub>2.5</sub>	7.48	152.5	57.3	395.1	0.331	696	156.9
Fe <sub>74.5</sub> Mo <sub>5.5</sub> P <sub>12.5</sub> C <sub>5</sub> B <sub>2.5</sub>	7.54	151.1	56.9	389.9	0.326	702	154.8
Ho <sub>55</sub> Al <sub>25</sub> Co <sub>20</sub>	7.89	66.6	25.4	351.7	0.311	649	139.6
La <sub>55</sub> Al <sub>25</sub> Cu <sub>10</sub> Ni <sub>5</sub> Co <sub>5</sub>	6.00	41.9	15.6	248.0	0.342	430	98.5
Lu <sub>39</sub> Y <sub>16</sub> Al <sub>25</sub> Co <sub>20</sub>	7.59	78.9	30.0	399.2	0.316	687	158.5
Lu <sub>55</sub> Al <sub>25</sub> Co <sub>20</sub>	8.69	80.0	30.6	404.1	0.307	701	160.4
Mg <sub>65</sub> Cu <sub>25</sub> Gd <sub>10</sub>	3.79	50.6	19.3	241.4	0.313	425	95.8
Mg <sub>65</sub> Cu <sub>25</sub> Y <sub>10</sub>	3.28	50.1	18.9	233.8	0.329	425	92.8
Pd <sub>40</sub> Cu <sub>30</sub> Ni <sub>10</sub> P <sub>20</sub>	9.28	92.0	34.5	274.0	0.399	593	108.8
Pd <sub>40</sub> Cu <sub>40</sub> P <sub>20</sub>	9.30	93.0	33.2	264.8	0.402	548	105.1
Pd <sub>60</sub> Cu <sub>20</sub> P <sub>20</sub>	9.78	91.0	32.3	273.3	0.409	604	108.5
Pd <sub>64</sub> Ni <sub>16</sub> P <sub>20</sub>	10.10	91.9	32.7	271.0	0.405	452	107.6
Pd <sub>77.5</sub> Cu <sub>6</sub> Si <sub>16.5</sub>	10.40	89.7	31.8	278.0	0.409	550	110.4
Pr <sub>60</sub> Al <sub>10</sub> Ni <sub>10</sub> Cu <sub>20</sub>	6.88	36.9	13.5	207.6	0.300	409	82.4
Pt <sub>57.5</sub> Cu <sub>14.7</sub> Ni <sub>5</sub> P <sub>22.8</sub>	15.20	95.7	33.4	289.0	0.434	490	114.7
Pt <sub>60</sub> Ni <sub>15</sub> P <sub>25</sub>	15.70	96.1	33.8	287.6	0.420	488	114.2
Tm <sub>39</sub> Y <sub>16</sub> Al <sub>25</sub> Co <sub>20</sub>	7.30	77.5	29.7	401.3	0.304	664	159.3
Tm <sub>55</sub> Al <sub>25</sub> Co <sub>20</sub>	8.27	72.2	27.6	371.9	0.306	678	147.6
Yb <sub>62.5</sub> Zn <sub>15</sub> Mg <sub>17.5</sub> Cu <sub>5</sub>	6.52	26.5	10.4	200.0	0.276	381	79.4
Zr <sub>41.2</sub> Ti <sub>13.8</sub> Ni <sub>10</sub> Cu <sub>12.5</sub> Be <sub>22.5</sub>	5.90	95.0	34.1	347.0	0.352	618	137.8
Zr <sub>46.75</sub> Ti <sub>8.25</sub> Cu <sub>7.5</sub> Ni <sub>10</sub> Be <sub>27.5</sub>	6.00	95.6	35.3	351.3	0.355	621	139.5
Zr <sub>48</sub> Nb <sub>8</sub> Ni <sub>12</sub> Cu <sub>14</sub> Be <sub>18</sub>	6.70	93.9	34.3	352.1	0.367	620	139.8
Zr <sub>53.1</sub> Ti <sub>5.4</sub> Cu <sub>19.8</sub> Ni <sub>11.7</sub> Al <sub>10</sub>	6.75	86.0	31.3	339.3	0.370	657	134.7
Zr <sub>62</sub> Cu <sub>15.5</sub> Ni <sub>12.5</sub> Al <sub>10</sub>	6.62	79.7	28.9	333.6	0.378	643	132.4
Zr <sub>64.13</sub> Cu <sub>13.5</sub> Ni <sub>12.37</sub> Al <sub>10</sub>	6.65	79.7	28.9	332.7	0.377	652	132.1

By identifying the equivalence between the activation energy of steady state homogeneous deformation and the effective activation energy of  $\alpha$ -relaxation at  $T_g$  of metallic glasses, it is found that the  $\alpha$ -relaxation and plastic deformation in metallic glasses are closely correlated [620]. The correlation indicates that the plastic deformation in metallic glasses, analogous to thermal induced glass transition, can be regarded as a stress driven glass-to-supercooled-liquid transition which is usually attainable at a temperature above  $T_g$  with enhanced atomic mobility. The correlation has also implications for understanding the found correlation between  $\nu$  and  $m$  in metallic glasses. Very recently, we developed a new BMG which has very low  $T_g$  and elastic modulus ( $G = 6$  GPa). Due to the low flow activation energy of the glass, the glass transition or homogenous flow in the BMG can be realized by applied stress at RT, which also confirms the similarity of plastic flow and glass transition in BMGs [660].

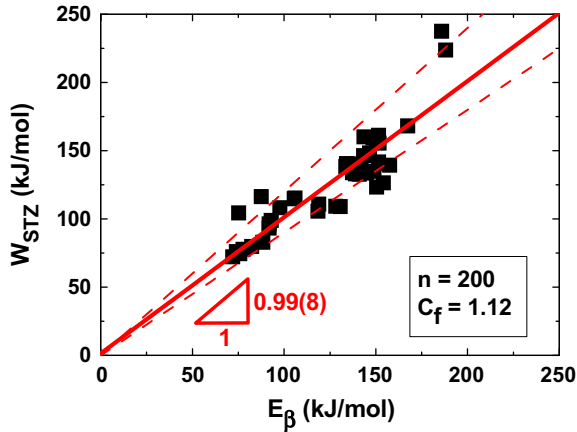


**Fig. 102.** Relationship between activation energy of  $\beta$  relaxation  $E_\beta$  and energy barriers of STZs  $W_{STZ}$ . Assuming  $n \sim 200$  atoms take part in one STZ events, and free volume parameter  $C_f \sim 1.12$ . The solid line corresponds to a least square linear fit in the form  $y = kx + b$  [641].

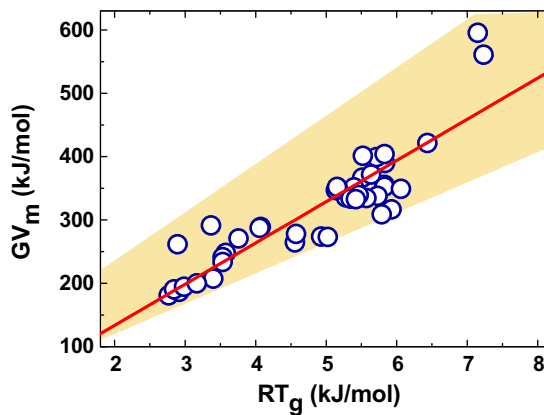


**Fig. 103.** Dependence of  $RT_g$  on  $GV_m$  of BMGs listed in Table 22 [641].

Through computer simulation of steady-state flow in a  $Zr_{50}Cu_{40}Al_{10}$  metallic glass using a set of realistic potentials, Guan et al. find a simple scaling relationship between temperature and stress as they affect viscosity [661]. The results suggest that the plastic flow and mechanical failure in metallic glasses are consequences of stress-induced glass transition.

Born [26] derived the general conditions for stability of crystal lattices and suggested that at the melting point, the shear modulus should vanish, i.e.,  $G = 0$ . Further investigations found that the  $G$  does not vanish at the melting temperature. Based on the Lindemann melting criterion, Varshni [225] suggested that melting occurs when  $G$  is reduced to a value given by  $G(T) = f_m G(0 \text{ K})$ , where  $f_m$  is a factor that would depend on the crystal structure and the nature of binding. For pure crystalline metals,  $f_m$  is proposed to be 0.55. Because of the similarity between melting and the glass transition, especially the existence of a Lindemann-type criterion for glass transition, the glass transition can be assumed to occur when  $G$  is reduced to a value defined by  $G(T) = f_g G(0 \text{ K})$ . For metallic glasses, it is found that  $G(T_g) = 0.85G(0 \text{ K})$  [446]. In general, it can be expressed as:  $G$  (glass transition point) = 0.85 $G(0 \text{ K})$ . This suggests that the glass transition occurs when the shear modulus decreases to 85% of the shear

modulus at 0 K. Since the flow in supercooled liquid approaching  $T_g$  is controlled by elastic moduli, the glass transition can be regarded as a kind of dramatic elastic moduli change which can be caused by either temperature (glass transition) or densification (like jamming) or load (high pressure). These factors play similar role in glass transition through rapidly change the elastic moduli of the glass-forming system at glass transition point, which is schematically illustrated in Fig. 105. In glass-forming liquids, when the temperature is rapidly cooled to  $T_g$  or the increase of the density of the liquid to a critical high value, the elastic moduli will rapidly reach the elastic moduli softening line as indicated in Fig. 105 and the liquid is frozen into glass. One can also unfreeze the glass or yield the glass or make flow in glass either by raising temperature or by applying shear stress to reach the elastic moduli softening line. The plastic deformation in metallic glasses can also regarded as the glass to supercooled liquid transition (confined in shear bands) which occurs upon reaching to a critical energy threshold or elastic modulus threshold by applied heating or stress to sufficiently high internal energy for the transition.

The various correlations found in metallic glasses can be understood via the elastic perspective. For example, the correlation of  $T_g$  and moduli  $E$  or  $G$  can be understood on the elastic perspective. The liquid structure freezes at  $T_g$ , and the moduli  $M$  of the liquid is approximately  $M_\infty(T_g)$ . According to the framework of the elastic model, the  $\Delta E(T_g)/k_B T_g$  is a universal constant at  $T_g$  for different metallic glasses and the flow average barrier  $\Delta E$  between local minima is related to  $M$ :  $\Delta E \propto M$  [600–602]. Therefore,  $M/T_g$  should be a universal constant. That is, for various metallic glasses  $T_g$  is closely related to the elastic modulus  $G$  or  $E$ . From the construction of the fragility plot, all viscosity or relaxation time curves intersect at  $T_g$  [where  $\log \eta = \log \eta(T_g) = \log(10^{13} \text{ Poise}) = 13$ ] and at very high temperatures,  $T_g/T \rightarrow 0$ , where all liquids have  $\log \eta = \log \eta_0 = -4$  [662]. This means that if a liquid has a steeper slope of  $\log \eta$  near  $T_g$ , it inevitably has a smaller slope of  $\log \eta$  at high temperature. At high temperatures,

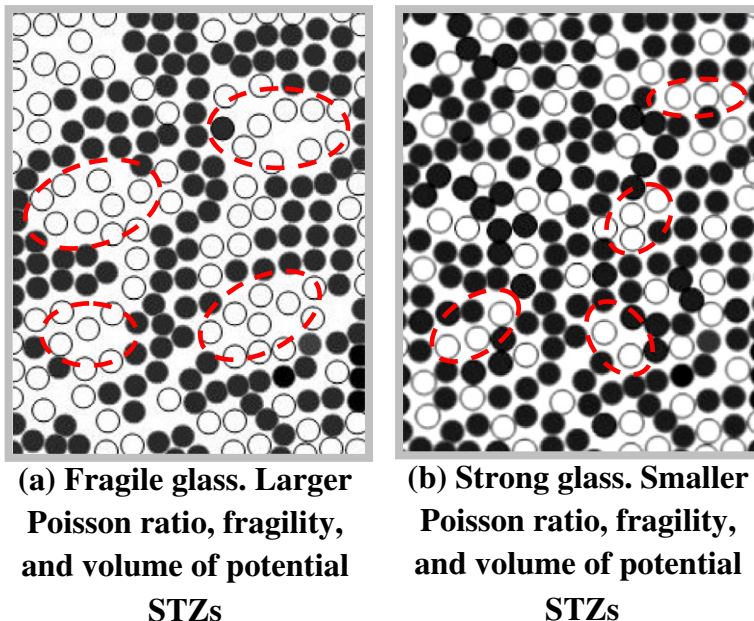


**Fig. 104.** Schematic plots of microstructures of (a) fragile and (b) strong BMGs. Atoms in closely packed regions and loosely packed regions are indicated by small filled (black) and open (white) circles, nucleation sites of potential STZs and  $\beta$ -relaxations are indicated by large dash circles. The  $\beta$ -relaxation is regarded as “thermal driven events of STZs”. Atoms in closely packed regions form stiff “cages” that encapsulate the atoms in loosely packed regions. The inelastic movements of the atoms in loosely packed regions can be driven by thermal fluctuation. Because of the confinements of the surrounding stiff “cages”, the atoms within loosely packed regions cannot escape from the cages but rearrange themselves cooperatively, similar some what to the activation of STZs. If the thermal or mechanical drive is large enough to break the “cages”,  $\alpha$ -relaxation emerges.

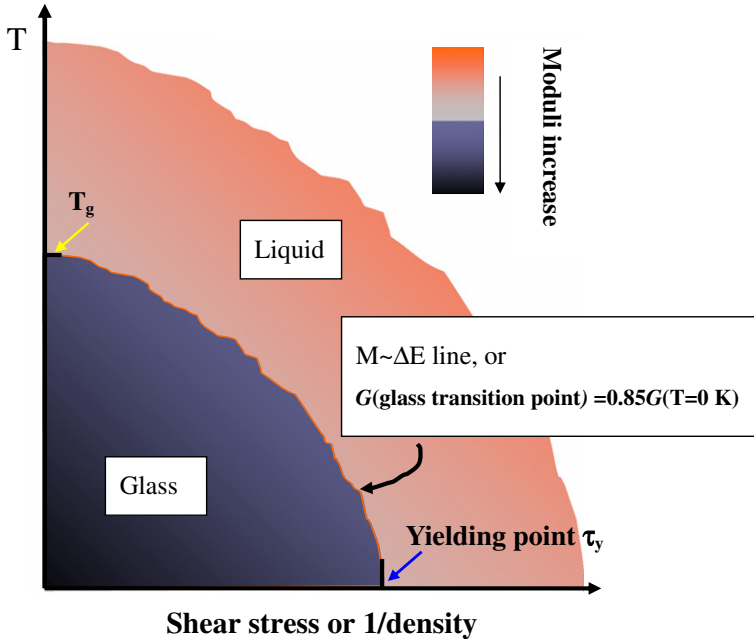


**Fig. 105.** A possible diagram for flow in glass.  $M$  is elastic moduli,  $\Delta E$  is activation energy for flow. The line ( $M \sim \Delta E$ ) in the temperature and applied shear stress plane is speculative and indicates how the temperature and shear stress equivalently induce the flow in glasses. The elastic moduli change is represented by the color change indicated in the figure. For metallic glasses, it is found that  $G(\text{glass transition point}) = 0.85G(T = 0 \text{ K})$ .

relaxation in most of the liquids shows Arrhenius temperature dependence:  $\eta = \eta_0 \exp(\Delta E/T)$ . Thus, the high- $T$  slope of  $\log \eta$  in the fragility plot,  $\Delta E/T_g$ , can also be a measure of fragility. Experimental data show that  $\Delta E/T_g$  indeed roughly correlates with fragility  $m$  in various glasses [81]:  $\frac{T_g}{\Delta E} \propto m$ . According to elastic model, both  $\Delta E$  and  $T_g$  correlate with elastic moduli. Therefore, the  $m$  should correlate with ratio of the elastic moduli for metallic glasses.

According to the elastic perspectives, the elastic moduli have relationship with glass-forming ability of an alloy. The correlation between fragility and GFA has been found in many BMG-forming systems [307,316]. On the other hand, the fragility correlates with the Poisson's ratio in various glasses including metallic glasses [56,309]. Therefore, the Poisson's ratio can be regarded as an indicator of the GFA of an alloy. Because the average barrier for flow,  $\Delta E$ , is mainly related to  $G$  [79], for the BMG-forming systems with low  $G$  or larger Poisson's ratio, their  $\Delta E$  is easy to be surmounted via small strain energy. While surmounting the large energy barrier (small value of Poisson's ratio) will take some finite time and large energy, in order for the system to track the changes in the PEL through structural rearrangements. For example, in Fe-based BMGs, there is tendency suggests that GFA is enhanced by increasing of energy barrier [174]. Therefore, an alloy development strategy relies on dramatically increasing flow activation energy, or increasing  $GV_m$  or decreasing Poisson's ratio, which can result in high GFA in an alloy system.

The correlations between  $T_g$  and  $\theta_D^2$ , and  $T_g$  and  $G$  in metallic glasses mean that the glass transition of the bulk glass-forming alloys has the characteristics of melting [56]. The elastic moduli perspective offers a simple scenario for explaining the found glass transition Lindemann criterion [56,57]. Assuming that the vibration in metallic glasses is modeled harmonically by having a single force constant written as  $M\omega_0^2$  ( $\omega_0$  is characteristic frequency), Eqs. (12.5)–(12.8) are equivalent in their temperature variations:

$$\frac{\Delta E}{k_B T} \propto \frac{M v_l}{k_B T} \propto \frac{a^3 G_\infty}{k_B T} \propto \frac{a^2}{\langle x^2 \rangle} \quad (13.1)$$

The equation explains the observed Lindermann criterion for the glass transition in various metallic glasses [56,57]. Due to the  $\Delta E$  relative to  $T_g$  is a universal constant, the ratio  $a^2/\langle x^2 \rangle$  is then universal at  $T_g$ . That is,  $M\theta_D/T_g \propto a^2/\langle x^2 \rangle$  is universal for various metallic glasses, which is the Lindermann-like criterion for glass transition in metallic glasses [56]. Accumulating evidences have also convinced that amorphization is a disorder-driven melting process, and a unified approach can be found for melting and amorphization [147]. The glass transition, approaching from the solid and inducing the transition of the glass state to supercooled liquid state, may be regarded as a “melting” process (alternatively

**Table 23**

The compositions,  $T_g/\rho$ , molar mass  $M$ , Debye temperature  $\theta_D$ ,  $E$ ,  $G$ ,  $K$ , and  $\rho$  of typical 48 different kinds of metallic glasses.

Composition	$T_g/\rho$ K cm <sup>3</sup> /g	$M$ (g/mol)	$\theta_D$ (K)	$E$ (GPa)	$G$ (GPa)	$K$ (GPa)	$\rho$ (g/cm <sup>3</sup> )
Cu <sub>60</sub> Zr <sub>20</sub> Hf <sub>10</sub> Ti <sub>10</sub>	90.56	79.01	282.0	101.1	36.9	128.2	8.304
Zr <sub>41</sub> Ti <sub>14</sub> Cu <sub>12.5</sub> Ni <sub>10</sub> Be <sub>22.5</sub>	100.62	59.94	320.0	97.8	36.1	113.0	6.162
Ti <sub>40</sub> Zr <sub>25</sub> Ni <sub>3</sub> Cu <sub>12</sub> Be <sub>20</sub>	120.84	53.15	338.0	96.2	35.5	109.6	5.445
Zr <sub>48</sub> Nb <sub>8</sub> Cu <sub>12</sub> Fe <sub>8</sub> Be <sub>24</sub>	102.07	65.47	306.0	96.0	35.3	113.7	6.447
(Zr <sub>0.59</sub> Ti <sub>0.06</sub> Cu <sub>0.22</sub> Ni <sub>0.13</sub> ) <sub>84</sub> Al <sub>16</sub>	106.49	70.09	294.0	95.1	35.2	106.7	6.545
Zr <sub>40</sub> Ti <sub>15</sub> Cu <sub>11</sub> Ni <sub>11</sub> Be <sub>21.5</sub> Mg <sub>0.5</sub> Y <sub>1</sub>	103.40	60.06	315.0	94.2	34.7	109.8	6.044
Zr <sub>48</sub> Nb <sub>8</sub> Cu <sub>14</sub> Ni <sub>12</sub> Be <sub>18</sub>	97.68	68.78	295.0	93.9	34.3	118.8	9.190
(Zr <sub>0.59</sub> Ti <sub>0.06</sub> Cu <sub>0.22</sub> Ni <sub>0.13</sub> ) <sub>85.7</sub> Al <sub>14.3</sub>	104.64	70.97	291.0	92.4	33.9	112.3	6.585
(Cu <sub>50</sub> Zr <sub>50</sub> ) <sub>94</sub> Al <sub>6</sub>	94.96	74.36	282.4	92.4	33.8	113.8	7.129
(Zr <sub>55</sub> Al <sub>15</sub> Cu <sub>20</sub> Ni <sub>10</sub> ) <sub>98</sub> Y <sub>2</sub>	107.02	73.12	286.0	92.0	33.8	110.5	6.559
Zr <sub>41</sub> Ti <sub>14</sub> Cu <sub>12.5</sub> Ni <sub>2</sub> Be <sub>22.5</sub> Fe <sub>8</sub>	104.51	59.72	314.0	91.6	34.0	99.6	5.932
(Zr <sub>0.59</sub> Ti <sub>0.06</sub> Cu <sub>0.22</sub> Ni <sub>0.13</sub> ) <sub>88</sub> Al <sub>12</sub>	101.58	72.15	288.0	91.1	33.4	111.5	6.704
(Cu <sub>50</sub> Zr <sub>50</sub> ) <sub>90</sub> Al <sub>7</sub> Gd <sub>3</sub>	90.56	76.25	277.1	90.1	33.2	105.8	7.122
Zr <sub>57</sub> Nb <sub>5</sub> Cu <sub>15.4</sub> Ni <sub>12.6</sub> Al <sub>10</sub>	100.94	76.52	274.0	87.0	31.9	106.7	6.806
(Zr <sub>0.59</sub> Ti <sub>0.06</sub> Cu <sub>0.22</sub> Ni <sub>0.13</sub> ) <sub>90</sub> Al <sub>10</sub>	97.48	73.17	279.0	85.9	31.3	112.1	6.740
(Zr <sub>55</sub> Al <sub>15</sub> Cu <sub>20</sub> Ni <sub>10</sub> ) <sub>96</sub> Y <sub>4</sub>	106.25	73.44	278.0	85.9	31.5	104.8	6.438
Zr <sub>65</sub> Al <sub>10</sub> Ni <sub>10</sub> Cu <sub>15</sub>	98.16	77.39	266.9	83.0	30.3	106.7	6.642
Zr <sub>57</sub> Nb <sub>5</sub> Cu <sub>15.4</sub> Ni <sub>12.6</sub> B <sub>1</sub> Al <sub>10</sub>	99.50	76.63	266.0	82.4	30.0	108.2	6.764
Tm <sub>55</sub> Al <sub>25</sub> Co <sub>20</sub>	81.94	111.45	216.0	72.2	25.6	62.0	8.274
Er <sub>50</sub> Y <sub>6</sub> Al <sub>24</sub> Co <sub>20</sub>	83.62	107.23	218.0	71.0	27.0	65.1	7.785
Er <sub>55</sub> Al <sub>25</sub> Co <sub>20</sub>	81.28	110.53	215.0	70.7	27.1	60.7	8.157
Ho <sub>55</sub> Al <sub>25</sub> Co <sub>20</sub>	82.28	109.24	210.0	66.6	25.4	58.8	7.888
Dy <sub>46</sub> Y <sub>10</sub> Al <sub>24</sub> Co <sub>20</sub> Fe <sub>2</sub>	88.99	103.02	214.0	64.2	24.4	58.5	7.046
Tb <sub>36</sub> Y <sub>20</sub> Al <sub>24</sub> Co <sub>20</sub>	95.44	93.26	222.0	63.6	24.0	60.5	6.583
Gd <sub>40</sub> Y <sub>16</sub> Al <sub>24</sub> Co <sub>20</sub>	90.84	95.39	218.0	62.2	23.5	58.0	6.486
Dy <sub>55</sub> Al <sub>25</sub> Co <sub>20</sub>	83.99	107.91	205.0	61.4	23.5	52.2	7.560
Tb <sub>55</sub> Al <sub>25</sub> Co <sub>20</sub>	81.73	105.94	203.0	59.5	22.9	50.2	7.488
(Mg <sub>65</sub> Cu <sub>25</sub> Gd <sub>10</sub> ) <sub>99</sub> Ti <sub>1</sub>	107.87	47.00	275.7	52.3	19.9	47.8	3.940
Mg <sub>60</sub> Cu <sub>25</sub> Gd <sub>15</sub>	98.82	54.06	261.0	52.2	19.9	46.6	4.220
Nd <sub>60</sub> Al <sub>10</sub> Fe <sub>20</sub> Co <sub>10</sub>	69.11	106.30	190.8	51.7	19.8	44.3	7.018
Pr <sub>55</sub> Al <sub>25</sub> Co <sub>20</sub>	79.87	96.03	190.0	45.9	17.4	43.5	6.373
La <sub>55</sub> Al <sub>25</sub> Cu <sub>10</sub> Ni <sub>5</sub> Co <sub>5</sub>	79.85	95.38	183.0	41.9	15.6	44.2	5.836
Pr <sub>60</sub> Al <sub>10</sub> Ni <sub>10</sub> Cu <sub>20</sub>	59.49	105.82	160.0	37.2	13.6	45.2	6.875
Pr <sub>60</sub> Cu <sub>20</sub> Ni <sub>10</sub> Al <sub>10</sub>	59.28	105.82	160.0	37.2	13.6	45.2	6.900
Ce <sub>68</sub> Al <sub>10</sub> Cu <sub>20</sub> Co <sub>2</sub>	52.13	111.87	146.1	31.3	11.8	30.3	6.752
Ce <sub>70</sub> Al <sub>10</sub> Ni <sub>10</sub> Cu <sub>10</sub>	53.82	113.01	144.0	30.3	11.5	27.0	6.670
Yb <sub>62.5</sub> Zn <sub>15</sub> Mg <sub>17.5</sub> Cu <sub>5</sub>	58.32	125.39	131.0	26.5	10.4	19.8	6.516
<i>Metalloid elements alloyed BMGs</i>							
Zr <sub>41</sub> Ti <sub>14</sub> Cu <sub>12.5</sub> Ni <sub>9</sub> Be <sub>22.5</sub> C <sub>1</sub>	100.96	59.48	335.0	105.6	39.5	107.8	6.171
Pd <sub>40</sub> Ni <sub>10</sub> Cu <sub>30</sub> P <sub>20</sub>	63.29	73.70	279.4	99.8	35.5	172.6	9.259
Pd <sub>40</sub> Ni <sub>40</sub> P <sub>20</sub>	61.93	72.24	292.0	108.3	38.6	185.1	9.413
Pd <sub>64</sub> Fe <sub>16</sub> P <sub>20</sub>	62.77	83.24	256.0	93.0	33.1	161.8	10.037
Ni <sub>80</sub> P <sub>20</sub>	75.98	53.15	324.0	102.8	36.9	159.0	8.133
Pd <sub>39</sub> Ni <sub>10</sub> Cu <sub>30</sub> P <sub>21</sub>	61.29	72.94	280.0	98.1	35.1	158.5	9.137
Pd <sub>77.5</sub> Si <sub>16.5</sub> Cu <sub>6</sub>	58.46	90.92	250.0	98.1	34.8	181.6	10.777
(Fe <sub>60</sub> Cr <sub>10</sub> Mo <sub>9</sub> C <sub>13</sub> B <sub>6</sub> Er <sub>2</sub> ) <sub>95</sub> Cu <sub>5</sub>	103.65	53.43	451.4	191.3	72.8	171.4	7.921
Fe <sub>60</sub> Cr <sub>10</sub> Mo <sub>9</sub> C <sub>13</sub> B <sub>6</sub> Er <sub>2</sub>	104.85	52.90	471.0	205.5	79.2	169.1	7.916
Pd <sub>32</sub> Ni <sub>48</sub> P <sub>20</sub>	63.98	68.42	295.0	104.9	37.5	173.4	6.715
Fe <sub>48</sub> Cr <sub>15</sub> Mo <sub>14</sub> C <sub>15</sub> B <sub>6</sub> Er <sub>2</sub>	108.42	53.83	483.0	218.9	83.6	191.0	7.849

softening in elastic moduli) of metallic glass. In fact, the typical  $Zr_{41.2}Ti_{13.8}Cu_{12.5}Ni_{10}Be_{22.5}$  BMG can be directly transformed to melt state by glass transition, and the crystallization process can be prevented when the heating rate is above 200 K/s [663]. For lower heating rate, the crystallization intervenes in the melting process of metallic glasses, and they cannot be directly transformed into melt state, the melting process actually is the melt of crystallized phases. The elastic model explains the found Lindemann-like criterion for metallic glasses [664,665].

The elastic moduli correlations can distinguish bonding characteristic in metallic glasses [363]. The bonding nature, which is of vital importance in determining the properties of condensed matter including metallic glasses [666–670,675], depends mainly on the atomic packing structures and varies for different systems especially for the systems that contain metalloid elements. By statistically analysis of 48 different kinds of typical metallic glasses (listed in Table 23), clear correlations between the dimensionless ratio of glass transition temperature/Debye temperature ( $T_g/\theta_D$ ) and density ( $\rho$ ), and between Young's modulus or shear modulus and  $T_g/\rho$ . The other 10 metallic glasses alloyed with metalloid elements, however, deviate markedly from the correlations as shown in Fig. 106. Both the two characteristic temperatures of  $T_g$  and  $\theta_D$  reflect the nature of the atomic bonding [56]. The alloying of metalloid elements results in bigger density and larger  $\theta_D$  in the metallic glasses and obvious deviation from the correlation. The  $G$  and  $E$  of the 37 kinds of metallic glasses consisting of metallic elements also show clear linear relationship with  $T_g/\rho$  as shown in Fig. 107a and b. And the metalloid-alloyed metallic glasses also markedly deviate from the correlations and their elastic moduli tend to be larger.

The alloying of metalloid elements would induce some covalent-like bonds between the metalloid and metallic elements which strengthens and shortens the atomic bonding. The metalloid and metallic elements usually have large negative mixing heat which favors the formation of strong atomic bonding [100]. Some of the small metalloid elements can also act as interstitial atom to cause the dense structure. The density of an alloy also has close relation with its bonding characteristics such as bonding length and angle. Thus, the density of the metallic glasses should differ from the weighted average density of the component elements due to the atomic bonding in the glass, and the density change reflects the bonding characteristics. Fig. 108 shows the difference between the measuring density  $\rho_{ex}$  and the weighted average value  $\rho_{av}$  in the form of  $(\rho_{ex} - \rho_{av})/\rho_{av}$  vs.  $V_{mol}$  ( $V_{mol} = M/\rho_{ex}$ ,  $M$  is the average molar mass). The  $\rho_{av}$  is calculated according to:  $\rho_{av}^{-1} = \sum f_i \rho_i^{-1}$  ( $\rho_i$  is the density of the  $i$ th crystalline compositional element;  $f_i$  is the atomic concentration of the  $i$ th composition element). The data of density of metallic glasses is from Table 23. The density variation of the BMGs with only metal components is less than 8%. While the metalloid-alloyed systems show larger density variation deriving from the large negative heat mixing between metalloid and metallic atoms. The alloying of white phosphorus ( $\rho = 1.823 \text{ g/cm}^3$ ) induces the largest density variation of about 17 ~ 27%. [If use violet phosphorus ( $\rho = 2.340 \text{ g/cm}^3$ ), the change decreases to around 7 ~ 15%.] This is due to the strength

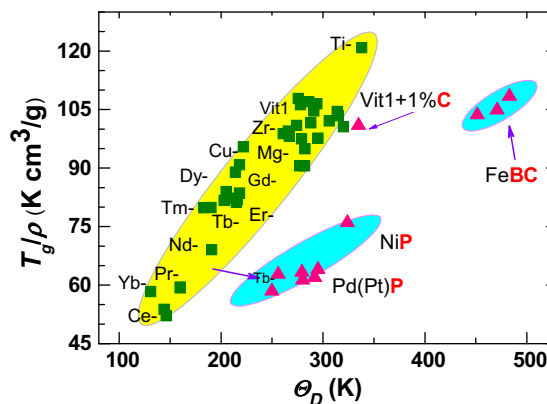


**Fig. 106.** The  $T_g$  when scaled with density shows clear correlation with  $\theta_D$  for the 37 metallic glasses consisting of only metal elements. The 10 metalloid-alloyed metallic glasses markedly deviate from the correlation.

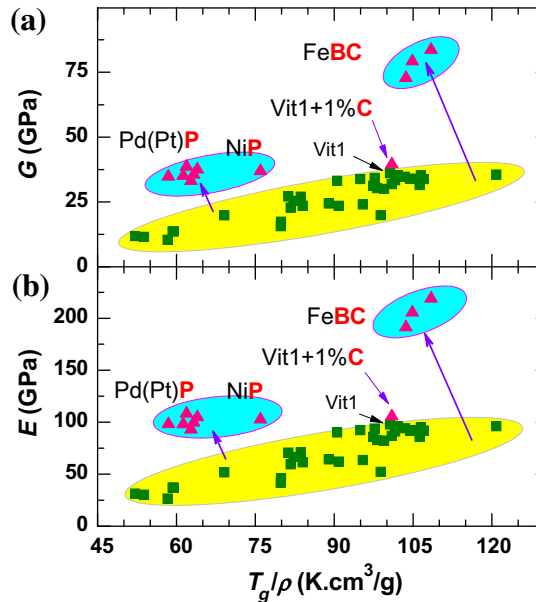


**Fig. 107.** The elastic moduli, (a)  $G$  and (b)  $E$ , show good correlation with  $T_g/\rho$  for the metallic glasses consisting of only metal elements, and metalloid-alloyed metallic glasses markedly deviate from the correlation [363].

of the covalent bonds in the P alloyed metallic glasses is much stronger than the van der Waals' force in the white P crystal. Carbon, boron and silicon have strong bonds with the metallic elements, and the length of the bonds would decrease when they are alloyed with metal elements, which is certified by the increased of density. Even 1 at.% alloying of carbon in Zr-based BMG increases the density because the small carbon atoms perform as interstitial atoms and would tighten the amorphous structure [100]. Thus, the alloying of metalloid elements would tighten the amorphous structure by strengthening and shortening the atomic bonds, and increase the local packing density. Therefore, the different bonding characteristics in metallic glasses can be explained and distinguished well via elastic moduli perspectives.

#### 14. Summary and outlook

The paper presents a comprehensive review of the elastic properties, elastic models and elastic perspectives of the metallic glasses, and would like to emphasize the key roles of elastic moduli in understanding the formation, glass transition and natures, structural characteristics, physical and mechanical properties of metallic glasses, and in exploring novel metallic glasses.

Since the elastic moduli in isotropic metallic glasses are relatively easily measurable parameters using various acoustic measurements, the elastic moduli and their composition, aging, pressure and temperature dependence of metallic glasses are systematically investigated by using the various ultrasonic methods. Plentiful data of transverse and longitudinal acoustic velocities, density, elastic constants, Debye temperature, Grueneisen constant as well as their composition, pressure and temperature dependence of various metallic glasses and some typical non-metallic glasses have been compiled, classified and compared.

A survey of the density, thermodynamic and kinetic, mechanical and physical properties, glass formation, fragility, stability, relaxation, melting and crystallization of various metallic glasses available are also presented for establishing the possible correlations among them and elastic moduli. It is found that the static structural heterogeneity, anisotropy and subtle local atomic-scale structural change in-

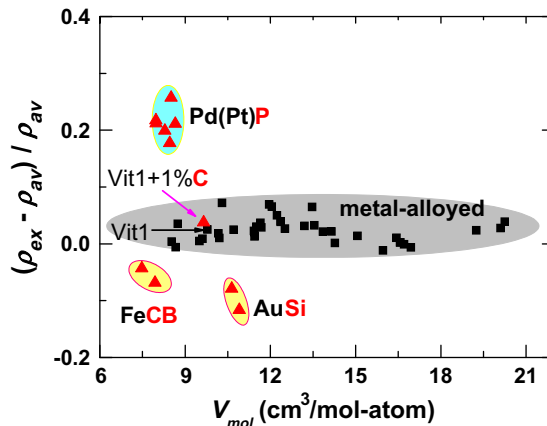


Fig. 108. The relative changes of density after amorphization vs. molar volume [363].

duced by composition variation, relaxations, pressure, temperature, and internal or external stress can be effectively characterized by the readily measurable parameter of elastic moduli. The elastic moduli such as Poisson's ratio or shear modulus or bulk modulus show clear correlation with the atomic structure of various metallic glasses, which indicates that the elastic moduli can be used as a probe for detecting the microstructural characteristics and changes of the metallic glasses. The pressure dependence of elastic moduli provides information of equation of state and anharmonic effects of the metallic glasses, and the temperature dependence of elastic properties verifies that the viscosity has a unique functional relationship with the isoconfigurational shear modulus which is related to fragility of glass-forming liquids. The static structural inhomogeneous in metallic glasses and the stress fluctuation can be well reflected by the local elastic modulus fluctuation. These indicate that even though the microstructure of metallic glasses cannot be well characterized like crystalline alloys, the elastic moduli are useful parameters for reflecting the microstructural change of the metallic glasses induced by temperature, pressure, aging and mechanical deformation. This makes possible establish the links between the microstructural change and physical and mechanical properties of the metallic glasses. The correlation, to some extent, is useful for understanding the structure–property relationship and allows getting insight into microstructure of the metallic glasses. The close links between microstructure and elastic moduli can be applied to control many features and properties of the metallic glasses through the controlling of the microstructure and composition.

It is found that a lot of features and properties of metallic glasses correlate remarkably well with elastic moduli. Furthermore, the elastic moduli are closely correlated with the strong/fragile characteristics of the glass-forming liquid, possibly also with glass-forming ability, and with the toughness/brittleness of the metallic glasses. On the other hand, the elastic constants of BMGs show a correlation with a weighted average of the elastic constants of the constituent elements. These correlations go beyond simple chance results and, instead, their basis lies within the amorphous nature of metallic glasses. Although the theoretical and physical reasons for these correlations are to be further clarified, these close links between the thermodynamic, kinetic, elastic, and plastic properties of metallic glasses appear to provide predictability for these apparently disordered systems at a level that far exceeds that for their ordered crystalline cousins. The elastic moduli then can be regarded as an indicator for predicting new bulk metallic glasses with controlled physical and mechanical properties and assist in selecting alloying components for controlling the properties and glass-forming ability, and thus can guide new metallic glasses design. The feasibility for making metallic glasses with specific elastic properties opens new realms of possibilities for fabrication of high precision tools (such as surgery equipments, potential bone graft substitute and optic parts) and for hard disk drives rotating at very high speeds and micro- and even nano-scale manufactures. We present the understanding

the found correlations for the metallic glasses, which would benefit improved structural simulation based on *ab initio* and molecular dynamic calculations.

We introduce several phenomenological elastic models explaining the flow in glass-forming liquids and metallic glasses. Based on the statistics studies of many different kinds of metallic glasses, we find that average molar volume  $V_m$  of the metallic glasses is another critical parameter involved in both homogeneous and inhomogeneous flows in glass. The flow activation energy of various glasses when scaled with  $V_m$ , which is defined as flow activation energy density  $\rho_E = \Delta E/V_m$ , shows much better correlation with the shear modulus  $G$  and bulk modulus  $K$ , and the  $\rho_E$  of viscosity can be simply and quantitatively expressed as:  $E(10G + K)/11$ . The proposed new extended elastic model for the flow in glasses and supercooled liquids fits the experimental observations well and the physical origin of the model is discussed. The model is suggestive for understanding the glass transition and deformation in metallic glass and may offer a simple scenario for explaining the some found correlations and fundamental issues in metallic glasses.

We find that the activation of STZs and slow  $\beta$ -relaxations in metallic glasses are directly related through elastic moduli, which indicates that many issues in metallic glasses such as the mechanical deformation, relaxations and stability of glasses can be treated as flow or the change of their different configurations. The plastic deformation or shear banding in metallic glasses can be regarded as a localized glass to supercooled liquid transition induced by external stress. The flow can be modeled as activated hopping between inherent states across energy barrier in the potential energy landscape. The energy barriers of the flow of both Newtonian and nonnewtonian metallic glass-forming liquids over a broad range of rheological behavior are determined by the instantaneous elastic moduli scaled with volume, and the variation in the configurational change or the flow events in glass or liquid induced either by thermal excitation or mechanical deformation can be correlated to the variations in elastic modulus. The  $K$  and volume have to be considered since a flow event requires a local volume increase.

To understand the liquids and glasses, the choice of the key concepts or parameters that connect atomic structure with the properties is critical. The glass transition is the key phenomenon determining properties for glassy materials. It is usually described in terms of transport (e.g., viscosity) and/or thermodynamic quantities. Based on a series of work and found correlations and elastic models, we conclude that the elastic moduli, which can be readily measured by experiments such as acoustic method and determined from interatomic potentials or directly from first principle, are key parameters for developing, characterizing, toughening and understanding the metallic glasses. That is, they are the key physical quantity controlling the main thermodynamic and kinetic, intrinsic static structural heterogeneity, mechanical and dynamic properties, and even glass-forming ability of supercooled liquids and glasses and bring about predictive capability. The elastic perspectives, which consider all metallic glasses exhibit universal behavior based on a small number of readily measurable parameters of elastic moduli, would provide insight into the understanding of the metallic glass and help for designing new metallic glasses.

As a frontier of materials science and condensed matter physics, the metallic glass field is progressing at a very fast pace. This presents a lot of unresolved issues and challenges and offers great opportunities for future study. It is too early to tell whether or not the elastic model and the elastic perspectives can provide basically correct explanation of the glass formation, relaxation, deformation mechanism of metallic glass. These ideas that calls for more careful and accurate experimental validation. The elastic property study and the understanding of metallic glasses based on the elastic perspectives are likely to remain an active branch in this field for many years. It is believed that the metallic glasses field is on the threshold of significant further advances that can transform our understanding of the glassy state.

## Acknowledgments

The author, particularly, want to thank R.J. Wang who, patiently, spent more than 10 years to systematically measure the acoustic data of various glasses. I would appreciate the long-standing support and encouragement from Prof. Y.D. Dong, Prof. W.K. Wang, Prof. D.S. Jin and Prof. C. W. Che. The experimental assistances, cooperation and discussions from M.X. Pan, D.Q. Zhao, H.Y. Bai, F.Y. Li, D.W. Ding, Y.X. Zhuang, Y. Zhang, B.C. Wei, Z. Zhang, Z. Bian, L.M. Wang, P. Wen, Z.X. Wang, L. Xia, X.K. Xi, Y.H.

Zhao, Y.X. Wei, B. Zhang, S. Li, M.B. Tang, G. Wang, Z.F. Zhao, Y.H. Liu, Y. Li, Y.T. Wang, P. Yu, Q. Luo, L.L. Li, X.F. Liu, J.Q. Wang, J.G. Wang, J.F. Li, B.A. Sun, H.B. Yu, X.X. Xia, K. Zhao, H.L. Peng, H.B. Ke, J. Yi, W. Jiao, Z. Wang, L.S. Huo, C.C. Yuan, D. Meng, J.T. Huo, B. Huang, J. Ma, S.T. Liu and M. Gao are greatly appreciated.

The author is indebted to Prof. A.L. Greer, Prof. K. Samwer, Prof. T. Egami, Prof. J. Dyre, Prof. C.T. Liu, Prof. Y. Wu, Prof. J. Eckert, Prof. T.G. Nieh, Prof. J.J. Lewandowski, Prof. M.W. Chen, and Dr. X.L. Wang for valuable discussions and their comments and advices.

This article is dedicated to my mother, Man Ping DAI.

The author is grateful to the financial support of the National Natural Science Foundation of China (Grant Nrs. 50321101, 50621061, 50921091 and 50731008), the State Key Project of Fundamental Research of Ministry of Science and Technology of China (MOST 973) (Grant Nrs. 2007CB613904 and 2010CB731603), and the Chinese Academy of Sciences.

## References

- [1] Byrne CJ, Eldrup M. Bulk metallic glasses. *Science* 2008;321:502.
- [2] Cheng YT, Johnson WL. Disordered materials: a survey of amorphous solids. *Science* 1987;235:997.
- [3] Spaepen F. The art and science of microstructural control. *Science* 1987;235:1010.
- [4] Dyre J. Mysteries of the glass transition. *Phys Today* 2008;61:15.
- [5] Hodge I. Mysteries of the glass transition. *Phys Today* 2008;61:15.
- [6] Hoffmann HJ. Mysteries of the glass transition. *Phys Today* 2008;61:16.
- [7] Fecht HJ, Johnson WL. Entropy and enthalpy catastrophe as a stability limit for crystalline material. *Nature* 1988;334:50.
- [8] He Y, Poon SJ, Sheflet GJ. Synthesis and properties of metallic glasses that contain aluminium. *Science* 1988;241:1640.
- [9] Angell CA. Insights into phases of liquid water from study of its unusual glass-forming properties. *Science* 2008;319:582.
- [10] Lu X, Mochrie SGJ, Narayanan S, Sandy AR, Sprung M. How a liquid becomes a glass both on cooling and on heating. *Phys Rev Lett* 2008;100:045701.
- [11] Greer AL. Confusion by design. *Nature* 1993;366:303.
- [12] Cahn RW, Greer AL. Metastable states of alloys. In: Cahn RW, Haasen P, editors. *Physical metallurgy*. Elsevier Science BV; 1996 [chapter 19].
- [13] Schroers J, Paton N. Amorphous metal alloys form like plastics. *Adv Mater Process* 2006;61:164.
- [14] Löffler JF. Bulk metallic glasses. *Intermetallics* 2003;11:529.
- [15] Launeya ME, Hofmann DC, Johnson WL, Ritchie RO. Solution to the problem of the poor cyclic fatigue resistance of bulk metallic glasses. *PNAS* 2009;106:4986.
- [16] Wang R. Short-range structure for amorphous intertransition metal alloys. *Nature* 1979;278:700.
- [17] Highmore RJ, Greer AL. Eutectics and the formation of amorphous alloys. *Nature* 1989;339:363.
- [18] Fecht HJ. Defect-induced melting and solid-state amorphization. *Nature* 1992;356:133.
- [19] Liu BX, Lai WS, Zhang Q. Irradiation induced amorphization in metallic multilayers and calculation of glass-forming ability from atomistic potential in the binary metal systems. *Mater Sci Eng R* 2000;29:1.
- [20] Angell CA. Insights into phases of liquid water from study of its unusual glass-forming properties. *Science* 2008;319:582.
- [21] Chen H, He Y, Shiflet GJ, Poon SJ. Deformation-induced nanocrystal formation in shear bands of amorphous alloys. *Science* 1994;367:541.
- [22] Eastgate LO, Langer JS, Pechenik L. Dynamics of large-scale plastic deformation and the necking instability in amorphous solids. *Phys Rev Lett* 2003;90:045506.
- [23] Schall P, Weitz DA, Spaepen F. Structural rearrangements that govern flow in colloidal glasses. *Science* 2007;318:1895.
- [24] Weita DA. Unjamming a polymer glass. *Science* 2009;323:214.
- [25] Landau LD, Lifshitz EM. *Theory of elasticity*. 3rd ed. Oxford: Reed Educational and Professional Publishing Ltd.; 1999.
- [26] Born M, Huang K. *Dynamical theory of crystal lattices*. Oxford: Clarendon Press; 1968.
- [27] Testardi LR, Krause JT, Chen HS. Large anharmonicity of amorphous and crystalline phases of a Pd–Si alloy. *Phys Rev B* 1973;8:4464.
- [28] Girifalco LA. *Statistical physical of materials*. New York: Wiley; 1973. p. 78.
- [29] Wen P, Johari GP, Wang RJ, Wang WH. Change in the vibrational properties of bulk metal glass with time. *Phys Rev B* 2006;73:224203.
- [30] Zener C. *Elasticity and anelasticity of metals*. Chicago, Illinois: The Univ. of Chicago press; 1948.
- [31] Ke TS. *The theory of internal friction in solids*. Beijing: China Scientific Press; 2000 [in Chinese].
- [32] Courtney TH. *Mechanical behavior of materials*. 2nd ed. McGraw-Hill Companies, Inc.; 2000.
- [33] Goldstein M. Viscous liquids and the glass transition. V. Sources of the excess specific heat of the liquid. *J Chem Phys* 1976;64:4767.
- [34] Wales DJ. *Energy landscapes*. Cambridge (UK): Cambridge University Press; 2003.
- [35] Stillinger FH. A topographic view of supercooled liquids and glass formation. *Science* 1995;267:1935.
- [36] Dyre JC, Olsen NB. Landscape equivalent of the shoving model. *Phys Rev E* 2004;69:042501.
- [37] Stillinger F, Weber T. Hidden structure in liquids. *Phys Rev A* 1982;25:978.
- [38] Angell CA. Structural instability and relaxation in liquid and glassy phases near the fragile liquid limit. *J Non-Cryst Solids* 1988;102:205.
- [39] Mayr SG. Activation energy of shear transformation zones: a key for understanding rheology of glasses and liquids. *Phys Rev Lett* 2006;97:195501.
- [40] Frenkel J. *Kinetic theory of liquids*. New York: Dover; 1955.

- [41] Zwanzig R, Mountain RD. High-frequency elastic moduli of simple fluids. *J Chem Phys* 1965;43:4464.
- [42] Krüger JK, Baller J, Britz T, le Coutre A, Peter R, Bactavatchalou R, et al. Cauchy-like relation between elastic constants in amorphous materials. *Phys Rev B* 2001;66:012206.
- [43] Glasstone S, Laidler KJ, Eyring H. The theory of rate processes. New York: McGraw-Hill; 1941.
- [44] Born M. Thermodynamics of crystals and melting. *J Chem Phys* 1939;7:591.
- [45] Nemilov SV. Interrelation between shear modulus and the molecular parameters of viscous flow for glass forming liquids. *J Non-Cryst Solids* 2006;352:2715.
- [46] Knuyt G, De Schepper L, Stals LM. Calculation of some metallic glass properties, based on the use of a Gaussian distribution for the nearest-neighbour distance. *Philos Mag B* 1990;61:965.
- [47] Grimvall G. In: Wohlfarth EP, editor. Thermophysical properties of materials (selected topics in solid state physics), vol. 18. Amsterdam: North-Holland; 1986.
- [48] Krüger JK, Britz T, le Coutre A, Baller J, Possart W, Alnot P, et al. as indicated by a violation of the generalized Cauchy relation. *New J Phys* 2003;5:80.1.
- [49] Pineda E. Theoretical approach to Poisson ratio behavior during structural changes in metallic glasses. *Phys Rev B* 2006;73:104109.
- [50] Schreiber D. In: Elastic constants and their measurement. New York: McGraw-Hill; 1973. p. 35–81 [chapter 3].
- [51] Kittel C. Introduction to solid state physics. 6th ed. New York: John Wiley & Sons Inc.; 1986.
- [52] Papadakis EP. Ultrasonic attenuation and velocity in three transformation products in steel. *J Appl Phys* 1964;35:1474.
- [53] Pugh SF. Relations between the elastic moduli and the plastic properties of polycrystalline pure metals. *Philos Mag* 1954;45:823.
- [54] Wang WH, Dong C, Shek CH. Bulk metallic glasses. *Mater Sci Eng R* 2004;44:45.
- [55] Wang WH, Wang RJ, Zhao DQ. Elastic constants and their pressure dependence of  $Zr_{41}Ti_{14}Cu_{12.5}Ni_9Be_{22.5}C_1$  bulk metallic glass. *Appl Phys Lett* 1999;74:1803.
- [56] Wang WH. Correlation between elastic moduli and properties in bulk metallic glasses. *J Appl Phys* 2006;99:093506.
- [57] Wang WH, Wen P. Relation between glass transition temperature and Debye temperature in bulk metallic glasses. *J Mater Res* 2003;18:2747.
- [58] Wang WH. Roles of minor additions in formation and properties of bulk metallic glasses. *Prog Mater Sci* 2007;52:540.
- [59] Duan G, Lind ML, Blauwe K, Wiest A, Johnson WL. Thermal and elastic properties of Cu–Zr–Be bulk metallic glass forming alloys. *Appl Phys Lett* 2007;90:211901.
- [60] Wang RJ, Li FY, Xu J, Xie HS. Ultrasonic study of silicate glasses. *J High Press Phys* 1994;8:177 [in Chinese].
- [61] Harms U, Jin O, Schwarz RB. Effects of plastic deformation on the elastic modulus and density of bulk amorphous  $Pd_{40}Ni_{10}Cu_{30}P_{20}$ . *J Non-Cryst Solids* 2003;317:200.
- [62] Xu J, Zhang Y, Hou W, Xu H, Guo J, Wang Z, et al. Measurements of ultrasonic wave velocities at high temperature and high pressure for window glass, pyrophyllite, and kimberlite up to 1400 C and 5.5 GPa. *High Temp High Pressure* 1994;26:375.
- [63] Wang JQ, Wang WH, Bai HY. Soft ytterbium-based bulk metallic glasses with strong liquid characteristic by design. *Appl Phys Lett* 2009;94:041910.
- [64] Migliori A, Sarrao JL. Resonant ultrasound spectroscopy: applications to physics, materials measurements and nondestructive evaluation. New York: Wiley; 1997.
- [65] Migliori A, Sarrao JL, Visscher WM, Bell TM, Lei M, Fisk Z, et al. Resonant ultrasound spectroscopic techniques for measurement of the elastic moduli of solids. *Physica B* 1993;183:1.
- [66] Leisure RG, Willis FA. Resonant ultrasound spectroscopy. *J Phys: Condens Matter* 1997;9:6001.
- [67] Hiraoo M, Ogi H. EMATs for science and industry. Boston: Kluwer; 2003.
- [68] Dmarest Jr HH. Cube-resonance method to determine the elastic constants of solids. *J Acoust Soc Am* 1971;49:768.
- [69] Bossuyt S, Giménez S, Schroers J. Resonant vibration analysis for temperature dependence of elastic properties of bulk metallic glass. *J Mater Res* 2007;22:533.
- [70] Papadakis EP. Ultrasonic phase velocity by the pulse-echo-overlape method incorporating diffraction phase correlations. *J Acoust Soc Am* 1967;42:1045.
- [71] Cook RK. Variation of elastic constants and static strains with hydrostatic pressure: a method for calculation from ultrasonic measurements. *J Acoust Soc Am* 1957;29:445.
- [72] Purdom RC, Prohovsky EW. Ultrasonic attenuation in quartz at low temperatures. *Phys Rev B* 1970;2:551.
- [73] Paul A, Chattopadhyay AK, Basu C. Ultrasonic investigations of  $PbO-V_2O_5-P_2O_5$  glass. *J Appl Phys* 1998;84:2513.
- [74] Grimsditch M, Gray KE, Bhadra R, Kampwirth RT, Rehn LE. Brillouin scattering study of lattice-stiffness changes due to ion irradiation: dramatic softening in  $Nb_3Ir$ . *Phys Rev B* 1987;35:883.
- [75] Barrett HH, Holland MG. Critique of current theories of Akhiezer damping in solids. *Phys Rev B* 1970;1:2538.
- [76] Mendelev MI, Rehbein DK, Ott RT, Kramer MJ, Sordelet DJ. Computer simulation and experimental study of elastic properties of amorphous Cu–Zr alloys. *J Appl Phys* 2007;102:093518.
- [77] Cahn RW, Haasen P, Kramer EJ. Materials science and technology. In: Zarzycki J, editor. Glasses and amorphous materials, vol. 9. Weimheim (Germany): VCH Verlagsgesellschaft mbH; 1993.
- [78] Ashby MF, Greer AL. Metallic glasses as structural materials. *Scripta Mater* 2006;54:321.
- [79] Dyre JC. Colloquium: the glass transition and elastic models of glass-forming liquids. *Rev Mod Phys* 2006;78:953.
- [80] Rouxel T. Elastic properties of glasses: a multiscale approach. *CR Mecanique* 2007;334:743.
- [81] Novikov VN, Sokolov AP. Poisson's ratio and the fragility of glass-forming liquids. *Nature* 2004;432:961.
- [82] Johnson WL, Samwer K. A universal criterion for plastic yielding of metallic glasses with  $(t/T_g)^{2/3}$  temperature dependence. *Phys Rev Lett* 2005;95:195501.
- [83] Hachenberg J, Bedorf D, Samwer K, Richert R, Kahl A, Demetriou MD, et al. Merging of the  $\alpha$  and  $\beta$  relaxations and aging via the Johari–Goldstein modes in rapidly quenched metallic glasses. *Appl Phys Lett* 2008;92:131911.
- [84] Zink M, Samwer K, Johnson WL, Mayr SG. Validity of temperature and time equivalence in metallic glasses during shear deformation. *Phys Rev B* 2006;74:012201.

- [85] Liu YH, Wang G, Wang RJ, Zhao DQ, Pan MX, Wang WH. Super plastic bulk metallic glasses at room temperature. *Science* 2007;315:1385.
- [86] Fefferman AD, Pohl RO, Zehnder AT, Parpia JM. Acoustic properties of amorphous silica between 1 and 500 mK. *Phys Rev Lett* 2008;100:195501.
- [87] Wang WH. Elastic moduli and behaviors of metallic glasses. *J Non-Cryst Solids* 2005;351:1481.
- [88] Greer AL. Metallic glasses. *Science* 1995;267:1947.
- [89] Miracle DB. A structural model for metallic glasses. *Nature Mater* 2004;3:697.
- [90] Sheng HW, Luo WK, Alamgir FM, Bai JM, Ma E. Atomic packing and short-to-medium range order in metallic glasses. *Nature* 2006;439:419.
- [91] Kui HW, Greer AL, Turnbull D. Formation of bulk metallic glass by fluxing. *Appl Phys Lett* 1984;45:615.
- [92] Inoue A, Yamaguchi H, Zhang T, Masumoto T. Al–La–Cu amorphous alloys with a wide supercooled liquid region. *Mater Trans JIM* 1990;31:104.
- [93] Peker A, Johnson WL. A highly processable metallic glass:  $Zr_{41.2}Ti_{13.8}Cu_{12.5}Ni_{10.0}Be_{22.5}$ . *Appl Phys Lett* 1993;63:2342.
- [94] Debenedetti PG. *Metastable liquids*. Princeton: Princeton Univ. Press; 1996.
- [95] Khonik SV, Granato AV, Joncich DM, Pompe A, Khonik VA. Evidence of distributed interstitialcy-like relaxation of the shear modulus due to structural relaxation of metallic glasses. *Phys Rev Lett* 2008;100:065501.
- [96] Conner RD, Dandliker RB, Johnson WL. Mechanical properties of tungsten and steel fiber reinforced  $Zr_{41.25}Ti_{13.75}Cu_{12.5}Ni_{10.0}Be_{22.5}$  metallic glass matrix composites. *Acta Mater* 1998;46:6089.
- [97] Liu XF, Zhang B, Wen P, Ma XM, Wang WH. Excess wing in Ce-based bulk metallic glass-forming supercooled liquid. *J Non-Cryst Solids* 2006;352:4013.
- [98] Wei BC, Zhang TH, Li WH, Xing DM, Zhang LC, Wang YR. Indentation creep behavior in Ce-based bulk metallic glasses at room temperature. *Mater Trans* 2005;46:2959.
- [99] Wang WH, Bao ZX, Eckert J. Equation of state of  $ZrTiCuNiBe$  bulk amorphous alloy. *Phys Rev B* 2000;61:3166.
- [100] Wang WH, Macht MP, Wollenberger H. Enhanced thermal stability and microhardness in metallic glass  $ZrTiCuNiBe$  alloys by carbon addition. *Appl Phys Lett* 1997;71:58.
- [101] Zhang Y, Ji YF, Zhao DQ, Zhuang YX, Wang RJ, Pan MX, et al. Glass forming ability and properties of Zr/Nb-based bulk metallic glasses. *Scripta Mater* 2001;44:1107.
- [102] Wen P, Wang RJ, Pan MX, Zhao DQ, Wang WH. Characteristics of microstructure and glass transition of  $(Zr_{0.59}Ti_{0.08}Cu_{0.22}Ni_{0.13})_{100-x}Al_x$  bulk metallic glasses. *J Appl Phys* 2003;93:759.
- [103] Bian Z, Wang RJ, Pan MX, Zhao DQ, Wang WH. Excellent wave absorption ability of Zr-based bulk metallic glass composites containing carbon nanotubes. *Adv Mater* 2003;15:616.
- [104] Dong YD, Wang WH, Xiao KQ, Liu L, Tong SH, He YZ. Structural investigation of mechanically alloyed Al–Fe system. *Mater Sci Eng A* 1991;134:867.
- [105] Zhang Y, Zhao DQ, Wang RJ, Pan MX, Wang WH. Glass forming ability and properties of Zr/Nb-based bulk metallic glasses. *Mater Trans* 2000;41:1423.
- [106] Wang WH, Fan GJ, Wang RJ, Eckert J. Formation and properties of Zr–(Ti,Nb)–Cu–Ni–Al bulk metallic glasses. *Mater Trans* 2001;42:587.
- [107] Zhang Y, Zhao D Q, Wang R J, Pan M X, Wang WH. Formation  $ZrNiCuAl$  bulk metallic glasses with low purity elements. *Mater Trans* 2000;41:1410.
- [108] Wang WH, Lewandowski JJ, Greer AL. Understanding the glass-forming ability of  $Cu_{50}Zr_{50}$  alloys in terms of a metastable eutectic. *J Mater Res* 2005;20:2307.
- [109] Wang LM, Wang WH, Wang RJ, Zhan ZJ, Dai DY, Sun LL, et al. Ultrasonic investigation of  $Pd_{39}Ni_{10}Cu_{30}P_{21}$  bulk metallic glass upon crystallization. *Appl Phys Lett* 2000;77:1147.
- [110] Wang LM, Sun LL, Wang WH, Wang WK. Elastic constants of  $PdNiCuP$  bulk metallic glass under high pressure. *Appl Phys Lett* 2000;77:3734.
- [111] Chen HS, Krause JT, Coleman E. Elastic constants, hardness and their implications to flow properties of metallic glasses. *J Non-Cryst Solids* 1975;18:157.
- [112] Lambson EF, Lambson WA, Macdonald JE, Gibbs MRJ, Saunders GA, Turnbull D. Elastic behavior and vibrational anharmonicity of a bulk  $Pd_{40}Ni_{40}P_{20}$  metallic glass. *Phys Rev B* 1986;33:2380.
- [113] Schroers J, Johnson WL. Ductile bulk metallic glass. *Phys Rev Lett* 2004;93:255506.
- [114] Schroers J, Lohwongwatana B, Johnson WL, Peker A. Gold based bulk metallic glass. *Appl Phys Lett* 2005;87:061912.
- [115] Yu P, Bai HY, Wang WH. Superior glass-forming ability of metallic alloys from microalloying. *J Mater Res* 2006;21:1674.
- [116] Wang ZX, Li FY, Pan MX, Zhao DQ, Wang WH. Effects of high pressure on the nucleation of  $Cu_{60}Zr_{20}Hf_{10}Ti_{10}$  bulk metallic glass. *J Alloys Compd* 2005;388:262.
- [117] Xi XK, Zhao DQ, Pan MX, Wang WH. Glass-forming Mg–Cu–RE (RE = Gd, Pr, Nd, Tb, Y and Dy) alloys with strong oxygen resistance in manufacturability. *J Non-Cryst Solids* 2004;344:105.
- [118] Yu HB, Yu P, Wang WH, Bai HY. Thulium based bulk metallic glass. *Appl Phys Lett* 2008;92:141906.
- [119] Yu HB, Yu P, Bai HY. Lutetium based bulk metallic glass. *J Non-Cryst Solids* 2008;354:4539.
- [120] Li ZG, Hui X, Zhang CM, Chen GL. Formation of Mg-based bulk metallic glasses. *J Alloy Compd* 2007;454:168.
- [121] Zhang Q, Ma H, Ma E, Xu J. Mg–Cu–(Y,Nd) pseudo-ternary bulk metallic glasses: the effects of Nd on glass-forming ability and plasticity. *Scripta Mater* 2006;55:541.
- [122] Xi XK, Li S, Wang RJ, Zhao DQ, Pan MX, Wang WH. Bulk scandium based metallic glasses. *J Mater Res* 2005;20:2243.
- [123] Zhang B, Pan MX, Zhao DQ, Wang WH. “Soft” bulk metallic glasses based on cerium. *Appl Phys Lett* 2004;85:61.
- [124] Zhang B, Wang RJ, Pan MX, Zhao DQ, Wang WH. Properties of Ce-based bulk metallic glass-forming alloys. *Phys Rev B* 2004;70:224208.
- [125] Zhang B, Zhao DQ, Pan MX, Wang WH, Greer AL. An amorphous metallic thermoplastic. *Phys Rev Lett* 2005;94:205502.
- [126] Zhang B, Wang RJ, Zhao DQ, Pan MX, Wang WH. Superior glass-forming ability through microalloying in cerium-based alloys. *Phys Rev B* 2006;73:092201.
- [127] Zhang B, Zhao DQ, Pan MX, Wang RJ, Wang WH. Formation of cerium based bulk metallic glasses. *Acta Mater* 2006;54:3025.

- [128] Zhang B, Zhao DQ, Pan MX, Wang RJ, Wang WH. Metallic plastics based on misch metals. *J Non-Cryst Solids* 2006;352:5687.
- [129] Li Z, Bai HY, Wang WL, Wang WH. Formation, properties, thermal characteristics and crystallization of hard magnetic Pr–Al–Fe–Cu bulk metallic glasses. *J Mater Res* 2003;18:2208.
- [130] Zhao ZF, Zhang Z, Wen P, Pan MX, Zhao DQ, Zhang Z, et al. Highly glass forming alloy with very low glass transition temperature. *Appl Phys Lett* 2003;82:4699.
- [131] Zhao ZF, Wen P, Wang RJ, Zhao DQ, Pan MX, Wang WH. The formation and properties of Pr-based bulk metallic glasses. *J Mater Res* 2006;21:369.
- [132] Wang YT, Pang ZY, Wang RJ, Zhao DQ, Pan MX, Han BS, et al. Doping-induced formation of bulk nanocrystalline alloys with controllable microstructure and properties. *J Non-Cryst Solids* 2006;352:444.
- [133] Li S, Zhao DQ, Pan MX, Wang WH. A bulk metallic glass based on heavy rare earth gadolinium. *J Non-Cryst Solids* 2005;351:2568.
- [134] Li S, Wang J, Pan MX, Zhao DQ, Wang WH. Bulk metallic glasses based on heavy rare earth dysprosium. *Scripta Mater* 2005;53:1489.
- [135] Li S, Xi XK, Wei YX, Luo Q, Wang WH. Formation and properties of new heavy rare-earth-based bulk metallic glasses. *Sci Technol Adv Mater* 2005;6:823.
- [136] Li S, Wang RJ, Pan MX, Zhao DQ, Wang WH. Heavy rare earth based bulk metallic glasses with high thermal stability. *Intermetallics* 2006;14:592.
- [137] Li S, Wang RJ, Wang WH. Bulk metallic glasses based on rare-earth elements in lanthanum series. *J Non-Cryst Solids* 2006;352:3942–6.
- [138] Li S, Wang RJ, Pan MX, Zhao DQ, Wang WH. Formation and properties of RE<sub>55</sub>Al<sub>25</sub>Co<sub>20</sub> (RE = Y, Ce, La, Pr, Nd, Gd, Tb, Dy, Ho, and Er) bulk metallic glasses. *J Non-Cryst Solids* 2008;354:1080.
- [139] Wei YX, Zhang B, Wang RJ, Zhao DQ, Pan MX, Wang WH. Erbium and cerium based bulk metallic glasses. *Scripta Mater* 2006;54:599–602.
- [140] Luo Q, Zhao DQ, Pan MX, Wang RJ, Wang WH. Hard and fragile rare earth holmium based bulk metallic glasses. *Appl Phys Lett* 2006;88:181909.
- [141] Luo Q, Zhao DQ, Pan MX, Wang WH. Magnetocaloric effect in Gd-based bulk metallic glasses. *Appl Phys Lett* 2006;89:081914.
- [142] Luo Q, Zhao DQ, Pan MX, Wang WH. Magnetocaloric effect of Ho-, Dy- and Er-based bulk metallic glasses in helium and hydrogen liquefaction temperature range. *Appl Phys Lett* 2007;90:211903.
- [143] Liu XF, Wang RJ, Zhao DQ, Pan MX, Wang WH. Bulk metallic glasses based on binary cerium and lanthanum elements. *Appl Phys Lett* 2007;91:041901.
- [144] Wang RJ, Li FY, Wang JF, Wang WH. Responses of glassy structure and properties to pressure and diversification. *Appl Phys Lett* 2003;83:2814.
- [145] Buchnau U, Wischnewski A. Fragility and compressibility at the glass transition. *Phys Rev B* 2004;70:092201.
- [146] Annapurna K, Tarafder A, Phani KK. Compositional dependence of ultrasonic velocities in glasses. *J Appl Phys* 2007;102:083542.
- [147] Okamoto PR, Lam NQ, Rehn LE. In: Ehrenrein H, Spaepen F, editors. *Solid state physics*, vol. 52. San Diego: Academic press; 1999. p. 1–135.
- [148] Wang WH, Wei Q, Friedrich S. Microstructure and decomposition and crystallization in metallic glass ZrTiCuNiBe alloy. *Phys Rev B* 1998;57:8211.
- [149] Wang WH, Wei Q, Macht MP, Wollenberger H. Structural studies of metallic glass ZrTiCuNiBe alloy by electron diffraction intensity analysis. *Appl Phys Lett* 1997;71:1053.
- [150] Anderson OL. *Physical acoustics*, vol. IIIB. New York: Academic; 1965.
- [151] Wang WH, Bai HY, Luo JL, Wang RJ, Jin D. Supersoftening phonon in ZrTiCuNiBe bulk metallic glass. *Phys Rev B* 2000;62:25.
- [152] Zhang Z, Keppens V, Senkov ON, Miracle DB. Elastic properties of Ca-based bulk metallic glasses studied by resonant ultrasound spectroscopy. *Mater Sci Eng A* 2007;471:151.
- [153] Yu P, Bai HY, Tang MB, Wang WL. Excellent glass-forming ability in simple Cu<sub>50</sub>Zr<sub>50</sub>-based alloys. *J Non-Cryst Solids* 2005;351:1328.
- [154] Tang MB, Zhao DQ, Pan MX, Wang WH. Binary Cu–Zr bulk metallic glasses. *Chin Phys Lett* 2004;21:901.
- [155] Wei BC, Löser W, Xia L, Roth S, Pan MX, Wang WH, et al. Anomalous thermal stability of Nd–Fe–Al–Co bulk metallic glass. *Acta Mater* 2002;50:4357.
- [156] Wei BC, Zhang Y, Zhuang YX, Zhao DQ, Pan MX, Wang WH. Nd<sub>65</sub>Al<sub>10</sub>Fe<sub>25–x</sub>Co<sub>x</sub> (x = 0, 5, 10) bulk metallic glasses with wide supercooled liquid regions. *J Appl Phys* 2001;89:3529.
- [157] Duan G, Wiest A, Lind MA, Kahl A, Johnson WL. Lightweight Ti-based bulk metallic glasses excluding late transition metals. *Scripta Mater* 2008;58:465.
- [158] Duan G, Wiest A, Lind MA, Li J, Rhim WK, Johnson WL. Bulk metallic glass with benchmark thermoplastic processability. *Adv Mater* 2007;19:4272.
- [159] Fabian J, Allen P. Theory of sound attenuation in glasses: the role of thermal vibrations. *Phys Rev Lett* 1999;82:1478.
- [160] Yu P, Bai HY, Wang WH. Formation of amorphous sulfur by rapid compression. *Appl Phys Lett* 2009;94:011910.
- [161] Gu XJ, Poon SJ, Shiflet GJ, Widom M. Mechanical properties, glass transition temperature, and bond enthalpy trends of high metalloid Fe-based bulk metallic glasses. *Appl Phys Lett* 2008;92:161910.
- [162] Bian Z, Wang RJ, Wang WH, Zhang T, Inoue A. Carbon nanotube reinforced Zr-based bulk metallic glass composites and their properties. *Adv Funct Mater* 2004;14:55.
- [163] Bian Z, Wang RJ, Zhao DQ, Pan MX, Wang ZX, Wang WH. Excellent ultrasonic absorption ability of carbon-nanotube-reinforced bulk metallic glass composites. *Appl Phys Lett* 2003;82:2790.
- [164] Bian Z, Pan MX, Zhang Y, Wang WH. Carbon nanotube reinforced Zr<sub>52.5</sub>Cu<sub>17.9</sub>Ni<sub>14.6</sub>Al<sub>10</sub>Ti<sub>5</sub> bulk metallic glass composites. *Appl Phys Lett* 2002;81:4739.

- [165] Kozhevnikov VF, Payne WB, Olson JK, Allen A, Taylor PC. Sound velocity in liquid and glassy selenium. *J Non-Cryst Solids* 2007;353:3254.
- [166] Wang WH, Li FY, Pan MX, Zhao DQ, Wang RJ. Elastic property and its response to pressure in a typical bulk metallic glass. *Acta Mater* 2004;52:715.
- [167] Wang WH, Wen P, Zhang Y, Pan MX, Wang RJ. Equation of state of bulk metallic glass studied by ultrasonic method. *Appl Phys Lett* 2001;79:3947.
- [168] Wang ZX, Wang RJ, Wang WH. Elastic properties of  $\text{Cu}_{60}\text{Zr}_{20}\text{Hf}_{10}\text{Ti}_{10}$  bulk metallic glass under high pressure. *Mater Lett* 2006;60:831.
- [169] Zhang B, Wang RJ, Wang WH. Unusual responses of acoustic and elastic properties to pressure and crystallization of Ce-based bulk metallic glass. *Phys Rev B* 2005;72:104205.
- [170] Zhang Z, Wang RJ, Xia L, Wei BC, Zhao DQ, Pan MX, et al. Elastic behavior and microstructural characteristic of  $\text{Nd}_{60}\text{Al}_{10}\text{Fe}_{20}\text{Co}_{10}$  bulk metallic glass investigated by ultrasonic measurement under pressure. *J Phys C* 2003;15:4503.
- [171] Wang LM, Wang RJ, Sun LL, Wang WH, Wang WK. Pressure dependence of the elastic constants and vibrational anharmonicity of  $\text{Pd}_{39}\text{Ni}_{10}\text{Cu}_{30}\text{P}_{21}$  bulk metallic glass. *J Phys C* 2003;15:101.
- [172] Rouxel T. Elastic properties and short to medium range order in glasses. *J Am Ceram Soc* 2007;90:3019.
- [173] Zhao K, Wang WH. Sr based bulk metallic glasses. *Scripta Mater* 2009;61:1091.
- [174] Memetriou MD, Kaltenboeck G, Suh JY, Garrett G, Floyd M, Crewdson C, et al. Glassy steel optimized for glass-forming ability and toughness. *Appl Phys Lett* 2009;95:041907.
- [175] Inoue A, Shen B, Kato H, Yavari AR. Co-based bulk glassy alloy with ultrahigh strength and soft magnetic properties. *Nat Mater* 2003;2:661.
- [176] Ohtsuki M, Tamura R, Yoda S, Ohmura T. Hard metallic glass of tungsten-based alloy. *Appl Phys Lett* 2004;84:4911.
- [177] Poisson SD. *Traite de Mecanique*, I, II. Paris: Courcier Pub.; 1811.
- [178] Dyre JC. Heir of liquid treasure. *Nat Mater* 2004;3:749.
- [179] Hao YL, Li SJ, Sun BB, Si ML, Yang R. Ductile titanium alloy with low Poisson's ratio. *Phys Rev Lett* 2007;98:216405.
- [180] Gschneidner Jr K, Russell A, Pecharsky A, Morris J, Zhang Z, Lograsso T, et al. A family of ductile intermetallic compounds. *Nat Mater* 2003;2:587.
- [181] Hecker SS, Rohr DL, Stein DF. Brittle fracture in iridium. *Metall Trans A* 1978;9:481.
- [182] Lakes RS. No contractile obligations. *Nature* 1992;358:713.
- [183] Keskar NR, Chelikowsky JR. Negative poisson's ratios in crystalline  $\text{SiO}_2$  from first principle calculations. *Nature* 1992;358:222.
- [184] Baughman RH, Dantas SO, Stafstrom S, Zakhidov AA, Mitchell TB, Dubin DHE. Negative poisson's ratios for extreme states of matter. *Science* 2000;288:2018.
- [185] Zallen R. *The physics of amorphous solids*. New York: Wiley Interscience Publication; 1983.
- [186] Saunder GA, Ball D, Cankurtaran M, Wang Q, Amscheidt E, Jacobs C, et al. Ultrasonic study of the temperature and pressure dependences of the elastic properties of fcc Co–Mn alloy single crystals. *Phys Rev B* 1997;55:11181.
- [187] Anderson OL. Some remarks on the volume dependence of the Grüneisen parameter. *J Geophys Res* 1968;73:5187.
- [188] Mallinder FP, Proctor BA. Elastic constants of fused silica as a function of large tensile strain. *Phys Chem Glass* 1964;5:91.
- [189] Powell BE, Skove MJ. Measurement of higher-order elastic constants, using finite deformations. *Phys Rev* 1968;174:977.
- [190] Barrett HH, Holland MG. Critique of current theories of akhieser damping in solids. *Phys Rev B* 1970;1:2538.
- [191] Wang RJ, Wang WH, Li FY, Wang LM, Zhang Y, Wen P. The Grüneisen arameter for bulk amorphous materials. *J Phys C* 2003;15:603.
- [192] Wang WH, Li LL, Pan MX, Wang RJ. Characteristics of glass transition and supercooled liquid state of  $\text{ZrTiCuNiBe}$  bulk metallic glass. *Phys Rev B* 2001;63:052204.
- [193] Rehn LE, Okamoto PR, Pearson J, Bhadra R, Grimsdith M. Solid-state amorphization of  $\text{Zr}_3\text{Al}$ : evidence of an elastic instability and first-order phase transformation. *Phys Rev Lett* 1987;59:2987.
- [194] Golding B, Bagley BG, Hsu FS. Soft transverse phonons in a metallic glass. *Phys Rev Lett* 1972;29:68.
- [195] Murnaghan FD. The compressibility of media under extreme pressures. *Proc Natl Acad Sci USA* 1944;30:244.
- [196] Bridgman PW. *The physics of high pressure*. London: Bell and Sons; 1958.
- [197] Sheng HW, Liu HZ, Cheng YQ, Wen J, Lee PL, Luo WK, et al. Polymorphism in metallic glasses. *Nat Mater* 2007;6:192.
- [198] Yavari AR. Change the face of disorder. *Nat Mater* 2007;6:181.
- [199] Zeng QS, Li YC, Feng CM, Liermann P, Somayazulu M, Shen GY, et al. Anomalous compression behavior in lanthanum/ cerium-based metallic glass under high pressure. *Proc Natl Acad Sci USA* 2007;104:13565.
- [200] Tang MB, Bai HY, Wang WH, Bogdanov D, Winzer K, Samwer K, et al. Heavy-fermion behavior in cerium based metallic glasses. *Phys Rev B* 2007;75:172201.
- [201] Lambson EF, Saunders GA, Bridge B, El-Mallawany RA. The elastic behaviour of  $\text{TeO}_2$  glass under uniaxial and hydrostatic pressure. *J Non-Cryst Solids* 1984;69:117.
- [202] Wei YX, Wang RJ, Wang WH. Soft phonons and phase transition in amorphous carbon. *Phys Rev B* 2005;72:012202.
- [203] Mansour AN, Wong CP, Brizzolara RA. Atomic structure of amorphous  $\text{Al}_{100-2x}\text{Co}_x\text{Ce}_x$  ( $x = 8, 9, \text{ and } 10$ ) and  $\text{Al}_{80}\text{Fe}_{10}\text{Ce}_{10}$  alloys: an XAFS study. *Phys Rev B* 1994;50:12401.
- [204] Cahn RW. *Glasses and amorphous materials*. Weinheim: VCH Press; 1991.
- [205] Kurkjian CR, Krause JT, McSkimmin HJ, Andreatch P, Bateman TB. In: Douglas RW, Ellis B, editors. Pressure dependence of elastic constants and Grueneisen parameters in fused  $\text{SiO}_2$ ,  $\text{GeO}_2$ ,  $\text{BeF}_2$  and  $\text{B}_2\text{O}_3$ . *Amorphous materials*. London: Wiley Interscience; 1970. p. 45.
- [206] Kondo K, Ito S, Sawaoka A. Nonlinear pressure dependence of the elastic moduli of fused quartz up to 3 GPa. *J Appl Phys* 1981;52:2826.
- [207] Rouxel T, Ji H, Hammouda T, Moreac A. Poisson's ratio and the densification of glass under high pressure. *Phys Rev Lett* 2008;100:255501.
- [208] Graham LJ, Chen R. Temperature and pressure dependence of the elastic properties of  $\text{RbAg}_4\text{I}_5$ . *J Appl Phys* 1975;46:2433.
- [209] Alers GA. In: Mason WP, editor. *Physical acoustics: Part A, vol. IV*. New York: Academic Press; 1966 [chapter 7].

- [210] Bernstein BT. Electron contribution to the temperature dependence of the elastic constants of cubic metals. I. Normal metals. *Phys Rev B* 1963;132:50–3.
- [211] Nowick AS, Berry BS. Anelastic relaxation in crystalline solids. New York: Academic Press; 1972.
- [212] Fukuhara M, Matsui AH, Takeshima M. Low-temperature elastic anomalies in an anthracene single crystal. *Chem Phys* 2000;97:258.
- [213] Nagel C, Ratzke K, Schmidtke E, Wolff J, Geyer U, Fraupel F. Free-volume changes in the bulk metallic glass  $Zr_{46.7}Ti_{8.3}Cu_{7.5}Ni_{10}Be_{27.5}$  and the undercooled liquid. *Phys Rev B* 1998;57:10224.
- [214] Wang WH, Bai HY, Zhang M, Zhao JH, Zhang XY, Wang WK. Interdiffusion phenomena in multilayers investigated by *in situ* low angle X-ray diffraction method. *Phys Rev B* 1999;59:10811.
- [215] Angell CA. Glass-formers and viscous liquid slowdown since David Turnbull: enduring puzzles and new twists. *MRS Bull* 2008;33:1.
- [216] Yu HB, Wang WH, Bai HY, in press.
- [217] Busch R, Johnson WL. Thermodynamics and kinetics of the undercooled liquid and the glass transition of the  $Zr_{41.2}Ti_{13.8}Cu_{12.5}Ni_{10}Be_{22.5}$  alloy. *J Appl Phys* 1995;77:4039.
- [218] Zhuang YX, Wang WH, Zhang Y, Pan MX, Zhao DQ. Glass transition and crystallization kinetics of  $ZrTiCuNiBe$  bulk metallic glasses. *Appl Phys Lett* 1999;75:2392.
- [219] Wang WH, Zhuang YX, Pan MX, Yao YS, behavior Glass transition, crystallization kinetic and microstructure change of  $ZrTiCuNiBe$  BMG under high pressure. *J Appl Phys* 2000;88:3914.
- [220] Lind ML, Duan G, Johnson WL. Isoconfigurational elastic constants and liquid fragility of a bulk metallic glass-forming alloy. *Phys Rev Lett* 2006;97:015501.
- [221] Harmon JS, Demetriou MD, Johnson WL. Deformation of glass forming metallic liquids: configurational changes and their relation to elastic softening. *Appl Phys Lett* 2007;90:131912.
- [222] Harmon JS, Demetriou MD, Johnson WL. Rheology and ultrasonic properties of  $PtNiCuP$  liquid. *Appl Phys Lett* 2007;90:171923.
- [223] Johnson WL, Demetriou MD, Harmon JS, Lind ML, Samwer K. Rheology and ultrasonic properties of metallic glass-forming liquids: a potential energy landscape perspective. *MRS Bull* 2007;32:644.
- [224] Duan G, Lind ML, Demetriou MD, Johnson WL, Goddard III WA, Samwer K. Strong configurational dependence of elastic properties for a binary model metallic glass. *Appl Phys Lett* 2006;89:151901.
- [225] Varshni YP. Temperature dependence of the elastic constants. *Phys Rev B* 1970;2:3952.
- [226] Tanak K, Ichitsubo T, Matsubar E. Elasticity and anelasticity of metallic glass near the glass transition temperature. *Mater Sci Eng A* 2006;442:278.
- [227] Schroter K, Wilde G, Willnecker R, Weiss M, Samwer K, Donth E. Shear modulus and compliance in the range of the dynamic glass transition for metallic glasses. *Eur Phys J B* 1998;5:1.
- [228] Grimsditch M, Bhadra R. Shear waves through the glass–liquid transformation. *Phys Rev Lett* 1989;62:2616.
- [229] Tamura S, Fukuhara M, Inoue A. Changes in mechanical properties of Zr-based bulk metallic glass under linear heating and cooling. *J Appl Phys* 2007;101:073520.
- [230] Fukuhara M, Inoue A, Nishiyama N. Rubberlike entropy elasticity of a glassy alloy. *Appl Phys Lett* 2006;89:101903.
- [231] Safarik DJ, Schwarz RB. Elastic constants of amorphous and single-crystal  $Pd_{40}Cu_{40}P_{20}$ . *Acad Mater* 2007;55:5736.
- [232] Zhang B, Bai HY, Wang RJ, Wu Y, Wang WH. Shear modulus as a dominant parameter in glass transitions: ultrasonic measurement of the temperature dependence of elastic properties of glasses. *Phys Rev B* 2007;76:012201.
- [233] Fan GJ, Freels M, Choo H, Liaw PK, Rhim WK, Johnson WL, et al. Thermophysical and elastic properties of  $Cu_{50}Zr_{50}$  and  $(Cu_{50}Zr_{50})_{95}Al_5$  bulk metallic glass forming alloys. *Appl Phys Lett* 2006;89:241917.
- [234] Louzguine-Luzgin DV, Yavari AR, Fukuhara M, Ota K, Xie G, Vaughan G, et al. Free volume and elastic properties changes in  $Cu-Zr-Ti-Pd$  bulk glassy alloy on heating. *J Alloy Compd* 2007;431:136.
- [235] Sivkov G, Yagodin D, Kofanov S, Gornov O, Volodin S, Bykov V, et al. Physical properties of the liquid  $Pd$  18 at.% Si alloy. *J Non-Cryst Solids* 2007;353:3274.
- [236] Abrosimova GE, Kobelev NP, Kolyvanov EL, Khonik VA. The influence of heat treatment on the ultrasonic velocity and elastic moduli of a  $Zr-Cu-Ni-Al-Ti$  bulk metallic glass. *Phys Solid State* 2004;46:1859.
- [237] Khonik VA, Mitrofanov YP, Lyakhov SA, Khoviv DA, Konchakov RA. Recovery of structural relaxation in aged metallic glass as determined by high-precision *in situ* shear modulus measurements. *J Appl Phys S* 2009;105:123521.
- [238] Li JF, Zhao DQ, Zhang ML, Wang WH. CaLi based bulk metallic glasses with multiple superior properties. *Appl Phys Lett* 2008;93:171907.
- [239] Zhao K, Liu KS, Li JF, Wang WH, Jiang L. Superamphiphobic CaLi-based bulk metallic glasses. *Scripta Mater* 2009;60:225.
- [240] Böhmer R, Ngai KL, Angell CA, Plazek DJ. Nonexponential relaxations in strong and fragile glass formers. *J Chem Phys* 1993;99:4201.
- [241] Mansfield ML. Model of the glass transition. *J Chem Phys* 1995;103:8124.
- [242] Wen P, Zhao DQ, Pan MX, Wang WH, Huang YP, Guo ML. Relaxation of metallic  $Zr_{46.25}Ti_{8.25}Cu_{7.5}Ni_{10}Be_{27.5}$  bulk glass-forming supercooled liquid. *Appl Phys Lett* 2004;84:2790.
- [243] Zhao ZF, Wen P, Shek CH, Wang WH. Measurements of slow  $\beta$ -relaxations in metallic glasses and supercooled liquids. *Phys Rev B* 2007;75:174201.
- [244] Wen P, Zhao ZF, Wang WH. Physical aging in  $Zr_{46.75}Ti_{8.25}Cu_{7.5}Ni_{10}Be_{27.5}$  typical bulk metallic glass manifested as enthalpy relaxation. *Sci China G* 2008;51:356.
- [245] Wang LM, Liu RP, Wang WH. Relaxation time dispersion in glass-forming metallic liquids and glasses. *J Chem Phys* 2008;128:164503.
- [246] Zhao ZF, Wen P, Wang WH, Shek CH. The observation of secondary relaxation in a fragile  $Pd_{40}Ni_{10}Cu_{30}P_{20}$  bulk metallic glass. *Appl Phys Lett* 2006;89:071920.
- [247] Wang WH, Wen P, Liu XF. Excess wing in bulk metallic glasses forming supercooled liquids. *J Non-Cryst Solids* 2006;352:5103.
- [248] Ngai KL. Johari–Goldstein relaxation as the origin of the excess wing observed in metallic glasses. *J Non-Cryst Solids* 2006;352:404.

- [249] Lunkenheimer P, Schneider U, Brand R, Loidl A. Glassy dynamics. *Contem Phys* 2000;41:15.
- [250] Johari GP, Goldstein M. Viscous liquids and the glass transition. II. Secondary relaxations in glasses of rigid molecules. *J Chem Phys* 1970;53:2372.
- [251] Ngai KL. Universality of low frequency fluctuation, dissipation and relaxation properties of condensed matter. *Comments Solid State Phys* 1979;9:127.
- [252] Johari GP. Localized molecular motions of  $\beta$ -relaxation and its energy landscape. *J Non-Cryst Solids* 2002;307–310:317.
- [253] Donth E. The glass transition. Berlin Heidelberg: Springer-Verlag; 2001.
- [254] Nielsen LE. Mechanical properties of polymers. New York: Reinhold; 1962 [chapter 7].
- [255] Bakke E, Busch R, Johnson WL. The viscosity of the  $Zr_{46.75}Ti_{8.25}Cu_{7.5}Ni_{10}Be_{27.5}$  bulk metallic glass forming alloy in the supercooled liquid. *Appl Phys Lett* 1995;67:3260.
- [256] Yu P, Wang RJ, Zhao DQ, Bai HY. Temperature dependence of elastic moduli of bulk metallic glasses down to liquid nitrogen temperature. *Appl Phys Lett* 2007;90:251904.
- [257] Tarumi R, Hirao M, Ichitsuho T, Matsubara E, Saida J, Kato H. Low-temperature acoustic properties and quasi-harmonic analysis for Cu-based bulk metallic glass. *Phys Rev B* 2007;76:104206.
- [258] Zhang Z, Keppens V, Liaw PK, Yokoyama Y, Inoue A. Elastic properties of Zr-based bulk metallic glasses studied by resonant ultrasound spectroscopy. *J Mater Res* 2007;22:364.
- [259] Yu P, Wang RJ, Zhao DQ, Bai HY. Anomalous temperature dependence of elastic moduli of Ce-based bulk metallic glasses at low temperature. *Appl Phys Lett* 2007;91:201911.
- [260] Fukuhara M, Wada T, Inoue A, Yin F. Low-temperature dependence of elastic moduli and internal friction for glassy  $Pd_{42.5}Ni_{7.5}Cu_{30}P_{20}$ . *Philos Mag Lett* 2008;88:335.
- [261] Fukuhara M, Wang X, Inoue A, Yin F. Low temperature dependence of elastic moduli and internal friction for the glassy alloy  $Zr_{55}Cu_{30}Al_{10}Ni_{5}$ . *Phys Status Solidi* 2007;1:220.
- [262] Augereau F, Laux D, Allais L, Mottot M, Caes C. Ultrasonic measurement of anisotropy and temperature dependence of elastic parameters by a dry coupling method applied to a 6061-T6 alloy. *Ultrasonics* 2007;46:34.
- [263] Ledbetter H. Materials at low temperature. Metals Park: Am. Soc. for Met.; 1983.
- [264] Ledbetter H. Relationship between bulk-modulus temperature dependence and thermal expansivity. *Phys Status Solidi (b)* 1994;181:81.
- [265] Murrell JN, Kettle SF. The chemical bond. New York: Wiley; 1985.
- [266] Li WH, Shin K, Lee CG, Wei BC, Zhang TH. Simple phenomenological determination of contact stiffness and elastic modulus of Ce-based bulk metallic glasses through nanoindentation. *Appl Phys Lett* 2007;90:171928.
- [267] Xi XK, Li LL, Zhang B, Wang WH, Wu Y. Correlation of atomic cluster symmetry and glass-forming ability of metallic glass. *Phys Rev Lett* 2007;99:095501.
- [268] Koskenmaki DC, Gschneidner Jr KA. Handbook on the physics and chemistry of rare earths, vol. 1. Amsterdam: North-Holland; 1978. p. 337.
- [269] Lawrence JM, Riseborough PS, Rarks RD. Valence fluctuation phenomena. *Rep Prog Phys* 1981;44:1.
- [270] Bustingorry S, Jagla EA, Lorenzana J. Thermodynamics of volume-collapse transitions in cerium and related compounds. *Acta Mater* 2005;53:5183.
- [271] Li HQ, Fan C, Tao KX, Choo H, Liaw PK. Compressive behavior of a Zr-based metallic glass at cryogenic temperatures. *Adv Mater* 2006;18:752.
- [272] Gu XJ, McDermott AG, Poon SJ, Shiflet GJ. Critical Poisson's ratio for plasticity in Fe–Mo–C–B–Ln bulk amorphous steel. *Appl Phys Lett* 2006;88:211905.
- [273] Yao JH, Wang JQ, Li Y. Ductile FeNbB bulk metallic glass with ultrahigh strength. *Appl Phys Lett* 2008;92:251906.
- [274] Fukuhara M, Wang X, Inoue A. Thermal elasticity in glassy alloys based on topology of metallic clusters. *Appl Phys Lett* 2007;91:171908.
- [275] Fukuhara M, Yagi M, Matsuo A. Temperature dependence of elastic parameters and internal frictions for TiNi alloy. *Phys Rev B* 2002;65:224210.
- [276] McGrum NG, Read RE, Williams G. Anelastic and dielectric effects in polymeric solids. New York (London): Wiley; 1967. p. 1.
- [277] Wang WH, Bai HY. Role of small atoms in the formation and properties of Zr–Ti–Cu–Ni–Be bulk amorphous alloys. *J Appl Phys* 1998;84:5961.
- [278] Wang WH, Wang RJ, Yang WT, Wei BC, Wen P, Zhao DQ, et al. Stability of supercooled liquid state of ZrTiCuNiBe bulk metallic glass forming alloy. *J Mater Res* 2002;17:1385.
- [279] Wang WH, Wang RJ, Pan MX, Yao YS. Microstructural transformation in  $Zr_{41}Ti_{14}Cu_{12.5}Ni_{10}Be_{22.5}$  bulk metallic glass under high pressure. *Phys Rev B* 2000;62:11292.
- [280] Bothe K, Neuhaeuser H. Study of structural relaxation in metallic glasses by modulus measurements. *Scripa Metall* 1982;16:1053.
- [281] Primak W. Kinetics of processes distributed in activation energy. *Phys Rev* 1955;100:1677.
- [282] Gibbs MRJ, Evetts JE, Leake JA. Activation energy spectra and relaxation in amorphous materials. *J Mater Sci* 1983;18:278.
- [283] Khonik VA. The kinetics of irreversible structural relaxation and homogeneous plastic flow of metallic glasses. *Phys State Sol (a)* 2000;177:173.
- [284] Hodge IM. Enthalpy relaxation and recovery in amorphous materials. *J Non-Cryst Solids* 1994;169:211.
- [285] Scherer GW. Relaxation in glass and composites. New York: Wiley; 1986.
- [286] Davies RO, Jones GO. Thermodynamic and kinetic properties of glasses. *Adv Phys* 1953;2:370.
- [287] Olsen NB, Dyre JC, Christensen T. Violations of conservation laws in viscous liquid dynamics. *Phys Rev Lett* 1998;81:1031.
- [288] Granato AV. The specific heat of simple liquids. *J Non-Cryst Solids* 2002;307–310:376.
- [289] Busch R, Johnson WL. The kinetic glass transition of the  $Zr_{46.75}Ti_{8.25}Cu_{7.5}Ni_{10}Be_{27.5}$  bulk metallic glass former-supercooled liquids on a long time scale. *Appl Phys Lett* 1998;72:2695.
- [290] Nemilov SV. Structural aspect of possible interrelation between fragility (length) of glass forming melts and Poisson's ratio of glasses. *J Non-Cryst Solids* 2007;353:4613.

- [291] Johari GP, Shim JG. Enthalpy recovery on thermal cycling within the non-equilibrium state of a glass. *J Non-Cryst Solids* 2000;261:52.
- [292] Gillod J. Le module d'élasticité et le tat structural des verres. *Verres Refract* 1946;1:26.
- [293] Concustell A, Alcalá G, Mato S, Woodcock TG, Gebert A, Eckert J, et al. Effect of relaxation and primary nanocrystallization on the mechanical properties of  $\text{Cu}_{60}\text{Zr}_{22}\text{Ti}_{18}$  bulk metallic glass. *Intermetallics* 2005;13:1214.
- [294] Goldstein M. Viscous liquids and the glass transition: sources of the excess heat capacity. *J Chem Phys* 1969;51:3728.
- [295] Debenedetti PG, Stillinger FH. Supercooled liquids and glass transition. *Nature* 2001;410:259.
- [296] Dyre JC. Solidity of viscous liquids. *Phys Rev E* 1999;59:2458.
- [297] Langer J. The mysterious glass transition. *Phys Today* 2007;60:8.
- [298] Anderson PW. Through a glass lightly. *Science* 1995;267:1615.
- [299] Turnbull D, Cohen MH. Free-volume model of the amorphous phase: glass transition. *J Chem Phys* 1961;34:120.
- [300] Turnbull D, Cohen MH. On the free-volume model of the liquid–glass transition. *J Chem Phys* 1970;52:3038.
- [301] Macedo PB, Litovitz TA. On the relative roles of free volume and activation energy in the viscosity of liquids. *J Chem Phys* 1965;42:245–56.
- [302] Egami T. Formation and deformation of metallic glasses: atomistic theory. *Intermetallics* 2006;14:882.
- [303] Egami T. Universal criterion for metallic glass formation. *Mater Sci Eng A* 1997;226–228:261.
- [304] Egami T. Nano-glass mechanism of bulk metallic glass formation. *Mater Trans* 2002;43:510.
- [305] Scorpigno T, Ruocco G, Sette F, Monaco G. Is the fragility of a liquid embedded in the properties of its glass? *Science* 2003;302:849.
- [306] Johari GP. On Poisson's ratio of glass and liquid vitrification characteristics. *Philos Mag* 2006;86:1567.
- [307] Senkov ON. Correlation between fragility and glass-forming ability of metallic alloys. *Phys Rev B* 2007;76:104202.
- [308] Novikov VN, Ding Y, Sokolov AP. Correlation of fragility of supercooled liquids with elastic properties of glasses. *Phys Rev E* 2005;71:061501.
- [309] Novikov VN, Sokolov AP. Correlation of fragility and Poisson's ratio: difference between metallic and nonmetallic glass formers. *Phys Rev B* 2006;74:064203.
- [310] Sokolov AP, Novikov VN, Kisliuk A. Fragility and mechanical moduli: do they really correlate? *Philos Mag* 2007;87:613.
- [311] Johari GP. Poisson's ratio and liquid's fragility. *Nature* 2006;42:E7.
- [312] Jiang M, Dai LH. Intrinsic correlation between fragility and bulk modulus in metallic glasses. *Phys Rev B* 2007;76:054204.
- [313] Qin Q, McKenna GB. Correlation between dynamic fragility and glass transition temperature for different classes of glass-forming liquids. *J Non-Cryst Solids* 2006;352:2977.
- [314] Battezzati L. Is there a link between melt fragility and elastic properties of metallic glasses? *Mater Trans* 2005;46:2915.
- [315] Park ES, Na JH, Kim DH. Correlation between fragility and glass-forming ability/plasticity in metallic glass-forming alloys. *Appl Phys Lett* 2007;91:031907.
- [316] Meng QG, Zhang SG, Xia MX, Li JG, Zhou JK. Supercooled liquid fragility and thermodynamic refinement for evaluation of metallic glass-forming ability. *Appl Phys Lett* 2007;90:031910.
- [317] Sastry S. The relationship between fragility, configurational entropy and the potential energy landscape of glass-forming liquids. *Nature (London)* 2001;409:164.
- [318] Speedy JR. Relation between a liquid and its glass. *J Phys Chem B* 1999;103:4060.
- [319] Lewandowski JJ, Wang WH, Greer AL. Intrinsic plasticity or brittleness of metallic glasses. *Philos Mag Lett* 2005;85:77.
- [320] Lewandowski JJ, Gu XJ, Shamimi A, Poon SJ, Shiflet GJ. Tough Fe-based bulk metallic glasses. *Appl Phys Lett* 2008;92:091918.
- [321] Li Y, Bai HY, Wang WH, Samwer K. Low-temperature specific-heat anomaly and boson peak in fragile and strong bulk metallic glasses. *Phys Rev B* 2006;74:052201.
- [322] Egami T, Poon SJ, Zhang Z, Keppens V. Glass transition in metallic glasses: a microscopic model of topological fluctuations in the bonding network. *Phys Rev B* 2007;76:024203.
- [323] Yang B, Liu CT, Nieh TG. Unified equation for the strength of bulk metallic glasses. *Appl Phys Lett* 2006;88:221911.
- [324] Zhang HW, Subhash G, Jing XN, Kecskes LJ, Dowding RJ. Evolution of hardness–yield strength relationships for bulk metallic glasses. *Philos Mag Lett* 2006;86:333.
- [325] Zhu D, Chen H. Low temperature specific heat and fragility of glasses. *J Non-Cryst Solids* 1998;224:97.
- [326] Kato H, Chen HS, Inoue A. Relationship between thermal expansion coefficient and glass transition temperature in metallic glasses. *Scripta Mater* 2008;58:1106.
- [327] Tanaka H. Relationship among glass-forming ability, fragility, and short-range band ordering of liquids. *J Non-Cryst Solids* 2005;351:678.
- [328] Tanaka H. Relation between thermodynamics and kinetics of glass-forming liquids. *Phys Rev Lett* 2003;90:055701.
- [329] Ito K, Moynihan CT, Angell CA. Thermodynamic determination of fragility-to-strong liquid transition in water. *Nature* 1999;398:492.
- [330] Ngai KL, Sokolov A, Steffen W. Correlation between boson peak strength and characteristics of local segmental relaxation in polymer. *J Chem Phys* 1997;107:5268.
- [331] Sokolov AP, Calemczuk R, salce B, Kisliuk A, Quitmann D, Duval E. Low-temperature anomalies in strong and fragile glass formers. *Phys Rev Lett* 1997;78:2405.
- [332] Wang WH. Bulk metallic glasses with functional physical properties. *Adv Mater* 2009;21:4524–44.
- [333] Luo Q, Wang WH. Rare earth based bulk metallic glasses. *J Non-Cryst Solids* 2009;355:759.
- [334] Gu XJ, Poon SJ, Shiflet GJ, Widom M. Ductility improvement of amorphous steels: roles of shear modulus and electronic structure. *Acta Mater* 2008;56:88.
- [335] Gu XJ, Poon SJ, Shiflet GJ. Mechanical properties of iron-based bulk metallic glasses. *J Mater Res* 2007;22:344.
- [336] Hu L, Bian X, Qin X, Yue Y, Zhao Y, Wang C. Thermodynamic basis for cluster kinetics: prediction of the fragility of marginal metallic glass-forming liquids. *J Phys Chem B* 2006;110:21950.
- [337] Chen HS, Krause JT. Correlation between Young's modulus and thermal properties of metallic glasses. *Scripta Metall* 1977;11:761.

- [338] Bordat P, Affouard F, Ngai KL. Does the interaction potential determine both the fragility of a liquid and the vibrational properties of its glassy state? *Phys Rev Lett* 2004;93:105502.
- [339] Ao ZM, Li S, Jiang Q. The determination of Young's modulus in noble metal nanowires. *Appl Phys Lett* 2008;93:081905.
- [340] Egami T. Magnetic amorphous alloys: physics and technological applications. *Rep Prog Phys* 1984;47:1601.
- [341] Rouxel T. Elastic properties and short- to medium-range order in glasses. *J Am Ceram Soc* 2007;90:3019.
- [342] Kováčik J. Correlation between elastic modulus, shear modulus, Poisson's ratio and porosity in porous materials. *Adv Eng Mater* 2008;10:250.
- [343] Zhang JL, Wu WH, Zhou HW, Guo XZ, Huang YN. Obtaining the glass transition temperature by measuring the crack healing process of glassformers. *Appl Phys Lett* 2008;92:131906.
- [344] Pedersen UR, Bailey NP, Schrøder TB, Dyre JC. Strong pressure-energy correlations in van der Waals liquids. *Phys Rev Lett* 2008;100:015701.
- [345] Park ES, Kim DH. Correlation between volumetric change and glass-forming ability of metallic glass-forming alloys. *Appl Phys Lett* 2008;92:091915.
- [346] Ristic R, Stubicarz M, Bbasic E. Correlation between mechanical, thermal and electronic properties in Zr–Ni–Cu amorphous alloys. *Philos Mag* 2007;87:5629.
- [347] Larini L, Ottochian A, De Michele C, Leporini D. Universal scaling between structural relaxation and vibrational dynamics in glass-forming liquids and polymers. *Nat Phys* 2008;4:42.
- [348] Chang YC, Huang JC, Cheng YT, Lee CJ, Du XH, Nieh TG. On the fragility and thermomechanical properties of Mg–Cu–Gd–B bulk metallic glasses. *J Appl Phys* 2008;103:103521.
- [349] Xia X, Wolynes PG. Fragilities of liquids predicted from the random 1st order transition theory of glasses. *PNAS* 2000;97:2990.
- [350] Louzguine-Luzgin DV, Saito T, Saida J, Inoue A. Thermal conductivity of metallic glassy alloys and its relationship to the glass forming ability and the observed cooling rates. *J Mater Res* 2008;23:2238.
- [351] Guo J, Bian XF, Li XL, Wang CD. Correlation between supercooled liquid fragility and potential energy landscape in Gd- and Pr-based glass-forming alloys. *Sci China G* 2008;51:387.
- [352] Poon SJ, Zhu A, Shiflet GJ. Poisson's ratio and intrinsic plasticity of metallic glasses. *Appl Phys Lett* 2008;92:261902.
- [353] Zhang Y, Zhao DQ, Pan MX, Wang WH. Glass-forming properties of Zr-based bulk metallic glasses. *J Non-Cryst Solids* 2003;315:206.
- [354] Xi XK, Zhao DQ, Pan MX, Wang WH, Wu Y, Lewandowski JJ. Fracture of brittle metallic glasses: brittleness or plasticity. *Phys Rev Lett* 2005;94:125510.
- [355] Xia XX, Wang YT, Wang WH, Greer AL. Plastic zone at crack tip: a nanolab for formation and study of metallic glassy nanostructures. *J Mater Res* 2009;24:2986.
- [356] Tandaiya P, Ramamurty U, Ravichandran G, Narasimhan R. Effect of Poisson's ratio on crack tip fields and fracture behavior of metallic glasses. *Acta Mater* 2008;56:6077.
- [357] Liu Y, Wu H, Liu CT, Zhang Z, Keppens V. Physical factors controlling the ductility of bulk metallic glasses. *Appl Phys Lett* 2008;93:151915.
- [358] Li Y, Guo Q, Kalb JA, Thompson CV. Matching glass-forming ability with the density of the amorphous phase. *Science* 2008;322:1816.
- [359] Baricco M, Baser TA, Das J, Eckert J. Correlation between Poisson's ratio and Mohr–Coulomb coefficient in metallic glasses. *J Alloy Compd* 2009;483:125.
- [360] Yokoyama Y, Ishikawa T, Okada JT, Yasuhiro, Watanabe, Nanao S, et al. Volume and viscosity of Zr–Cu–Al glass-forming liquid alloys. *J Non-Cryst Solids* 2009;351:317.
- [361] Torchinsky DH, Johnson JA, Nelson K. A direct test of the correlation between elastic parameters and fragility of ten glass formers and their relationship to elastic models of the glass transition. *J Chem Phys* 2009;130:064502.
- [362] Lu Z, Li J, Shao H, Gleiter H, Ni X. The correlation between shear elastic modulus and glass transition temperature of bulk metallic glasses. *Appl Phys Lett* 2009;94:091907.
- [363] Wang JQ, Wang WH, Bai HY. Distinguish bonding characteristic in metallic glasses by correlations. *J Non-Cryst Solids* 2011;357:220.
- [364] Alexander S. Amorphous solid: their structure, lattice dynamics and elasticity. *Phys Rep* 1998;296:65.
- [365] Kelly A. Strong solids. 2nd ed. Oxford: Clarendon Press; 1973.
- [366] Knuyt G, Stals LM. Calculation of some metallic-glass properties, based on the use of a Gaussian distribution for the nearest-neighbour distance: III. Elastic constants. *Philos Mag B* 1991;64:299.
- [367] Ashby MF. Materials selection in mechanical design. 3rd ed. Oxford: Butterworth-Heinemann; 2005.
- [368] Greer AL, Ma E. Bulk metallic glasses: at the cutting edge of metals research. *MRS Bull* 2007;32:611.
- [369] Johnson WL. Bulk amorphous metal – an emerging engineering material. *JOM* 2002;54:40.
- [370] Schuh CA, Hufnagel TC, Ramamurty U. Mechanical behavior of amorphous alloys. *Acta Mater* 2007;55:4067.
- [371] Inoue A. Stabilization of metallic supercooled liquid and bulk amorphous alloys. *Acta Mater* 2000;48:279.
- [372] Chen MW. Mechanical behavior of metallic glasses: microscopic understanding of strength and ductility. *Annu Rev Mater Res* 2008;38:445.
- [373] Wang G, Zhao DQ, Bai HY, Pan MX, Xia AL, Han BS, et al. Nanoscale periodic morphologies on fracture surface of brittle metallic glasses. *Phys Rev Lett* 2007;98:235501.
- [374] Wang G, Wang YT, Liu YH, Pan MX, Zhao DQ, Wang WH. The evolution of nanoscale morphology on fracture surface of brittle metallic glass. *Appl Phys Lett* 2006;89:121909.
- [375] Xi XK, Zhao DQ, Pan MX, Wang WH, Wu Y, Lewandowski JJ. Periodic corrugation on dynamics fracture surface in brittle bulk metallic glass. *Appl Phys Lett* 2006;89:181911.
- [376] Wang G, Han YN, Xu XH, Ke FJ, Han BS, Wang WH. Ductile to brittle transition in dynamic fracture of a brittle bulk metallic glass. *J Appl Phys* 2008;103:093520.
- [377] Wang G, Liu YH, Yu P, Zhao DQ, Pan MX, Wang WH. Structural evolution of shear bands in work hardenable ductile bulk metallic glass. *Appl Phys Lett* 2006;89:251909.

- [378] Das J, Tang MB, Kim KB, Theissmann R, Baier F, Wang WH, et al. "Work-hardenable" ductile bulk metallic glass. *Phys Rev Lett* 2005;94:205501.
- [379] Zhang Y, Wang WH, Greer AL. Making metallic glasses plastic by control of residual stress. *Nat Mater* 2006;5:857.
- [380] Wang JG, Zhao DQ, Pan MX, Wang WH. Iron based alloy with hierarchical structure and superior mechanical performance. *Adv Eng Mater* 2008;10:46.
- [381] Liu YH, Wang G, Pan MX, Yu P, Zhao DQ, Wang WH. Deformation behaviors and mechanism of NiCoNbTa bulk metallic glasses with high strength and plasticity. *J Mater Res* 2007;22:869.
- [382] Chen MW, Inoue A, Zhang W, Sakurai T. Extraordinary plasticity of ductile bulk metallic glasses. *Phys Rev Lett* 2006;96:245502.
- [383] Yao KF, Ruan F, Yang YQ, Chen N. Ductile bulk metallic glass. *Appl Phys Lett* 2006;88:122106.
- [384] Cao QP, Li JF, Zhou YH, Horsewell A, Jiang JZ. Effect of rolling deformation on the microstructure of bulk  $\text{Cu}_{60}\text{Zr}_{20}\text{Ti}_{20}$  metallic glass and its crystallization. *Acta Mater* 2006;54:4373.
- [385] Cao QP, Li JF, Zhou Y. Mechanically driven phase separation and corresponding microhardness change in  $\text{Cu}_{60}\text{Zr}_{20}\text{Ti}_{20}$  bulk metallic glass. *Appl Phys Lett* 2005;86:081913.
- [386] Du XH, Huang JC, Hsieh KC, Lai YH, Chen HM, Jang JSC, et al. Two-glassy-phase bulk metallic glass with remarkable plasticity. *Appl Phys Lett* 2007;91:131901.
- [387] Tao PJ, Yang YZ, Bai XJ, Xie ZW, Chen XC, Dong ZJ, et al. Zr-based bulk metallic glass with super-plasticity under uniaxial compression at room temperature. *J Non-Cryst Solids* 2008;354:3742.
- [388] Bae DH, Lee SW, Kwon JW, Yi S, Park JS. Deformation behavior of ZrAlCuNiSn metallic glasses. *J Mater Res* 2006;21:1305.
- [389] Guo H, Yan PF, Wang YB, Tan J, Zhang ZF, Sui ML, et al. Tensile ductility and necking of metallic glass. *Nat Mater* 2007;6:735–9.
- [390] Yavari AR, Lewandowski JJ, Eckert J. Mechanical properties of bulk metallic glasses. *MRS Bull* 2007;32:635.
- [391] Yao JH, Wang JQ, Li Y. Ductile Fe–Nb–B bulk metallic glass with ultrahigh strength. *Appl Phys Lett* 2008;92:251906.
- [392] Sharma P, Yubuta K, Kimura H, Inoue A. Brittle metallic glass deforms plastically at room temperature in glassy multilayers. *Phys Rev B* 2009;80:024106.
- [393] Wang JG, Zhao DQ, Pan MX, Wang WH. Mechanical heterogeneity and mechanism of plasticity of metallic glasses. *Appl Phys Lett* 2009;94:031904.
- [394] Lee CM, Park KW, Lee JC. Plasticity improvement of a bulk amorphous alloy based on its viscoelastic nature. *Scripta Mater* 2008;59:802.
- [395] Busch R, Schroers J, Wang WH. Thermodynamics and kinetics of bulk metallic glasses. *MRS Bull* 2007;32:620.
- [396] Fornell J, Suriñach S, Baróand MD, Sort J. Unconventional elastic properties, deformation behavior and fracture characteristics of newly developed rare earth bulk metallic glasses. *Intermetallics* 2009;17:1090.
- [397] Gruenisen E. *Handb. d. Phys.*, vol. 10.1. Berlin: Springer; 1926.
- [398] Nemilov SV. Thermodynamic and kinetic aspects of the vitreous state. Boca Raton: CRC Press; 1995.
- [399] Miracle DB, Egami T, Flores KM, Kelton KF. Structural aspects of metallic glasses. *MRS Bull* 2007;32:629.
- [400] Park KW, Lee CM, Lee MR, Fleury E, Falk ML, Lee JC. Paradoxical phenomena between the homogeneous and inhomogeneous deformations of metallic glasses. *Appl Phys Lett* 2009;94:021907.
- [401] Ashby MF. Materials—a brief history. *Philos Mag Lett* 2008;88:749.
- [402] Wang JQ, Wang WH, Yu HB, Bai HY. Correlation between molar volume and elastic moduli in metallic glasses. *Appl Phys Lett* 2009;94:121904.
- [403] Luo Q, Zhang B, Wang RJ, Wang WH. Aging and stability of Ce-based bulk metallic glass with glass transition temperature near room temperature. *Appl Phys Lett* 2006;88:151915.
- [404] K Xi X, Sandor MT, Liu YH, Wang WH, Wu Y. Structural changes induced by microalloying in  $\text{Cu}_{46}\text{Zr}_{47-x}\text{Al}_7\text{Gd}_x$  metallic glasses. *Scripta Mater* 2009;61:967–9.
- [405] Sakaguchi RL, Wiltbank BD, Murchison CF. Prediction of composite elastic modulus and polymerization shrinkage by computational micromechanics. *Dent Mater* 2004;20:397.
- [406] Jacquet E, Trivauday F, Varchon D. Calculation of the transverse modulus of a unidirectional composite material and of the modulus of an aggregate: application of the rule of mixtures. *Compos Sci Technol* 2000;60:345.
- [407] Liu GR. A SBS method of rule-mixture of fiber and particle reinforced composite materials. *Compos Struct* 1998;40:313.
- [408] Zhang Y, Greer AL. Correlations for predicting plasticity or brittleness of metallic glasses. *J Alloys Comp.* 2007;434–435:2.
- [409] Turnbull D. Under what conditions can a glass be formed? *Contemp Phys* 1969;10:473.
- [410] Egami T, Waseda Y. Atomic size effect on the formability of metallic glasses. *J Non-Cryst Solids* 1984;64:114.
- [411] Cai AH, Chen H, An WK, Tan JY, Zhou Y. Relationship between melting enthalpy  $\Delta H_m$  and critical cooling rate  $R_c$  for bulk metallic glasses. *Mater Sci Eng A* 2007;457:6.
- [412] Jiang Q, Chi BQ, Li JC. A valence electron concentration criterion for glass-formation ability of metallic liquids. *Appl Phys Lett* 2003;82:2984.
- [413] Xia L, Fang SS, Wang Q, Dong YD, Liu CT. Thermodynamic modeling of glass formation in metallic glasses. *Appl Phys Lett* 2006;88:171905.
- [414] Wang YM, Shek CH, Wong CH, Wang Q, Zhang XF, Dong C. The  $e/a$  criterion for the largest glass-forming abilities of the Zr–Al–Ni(Co) alloys. *Mater Trans, JIM* 2004;45:1180.
- [415] Xia M, Zhang S, Li J, Ma C. Thermal stability and its prediction of bulk metallic glass systems. *Appl Phys Lett* 2006;88:261913.
- [416] Lin XH, Johnson WL. Formation of Ti–Zr–Cu–Ni bulk metallic glasses. *J Appl Phys* 1995;78:6514.
- [417] Cohen MH, Turnbull D. Composition requirements for glass formation in metallic and ionic systems. *Nature (London)* 1961;189:131.
- [418] Lu ZP, Shen J, Sun JF, Liu CT. Binary eutectic clusters and glass formation in ideal glass-forming liquids. *Appl Phys Lett* 2006;89:071910.
- [419] Nagel SR, Tauc J. Nearly-free-electron approach to the theory of metallic glass alloys. *Phys Rev Lett* 1975;35:380.
- [420] Zheng Q, Xu J, Ma E. High glass-forming ability correlated with fragility of MgCuGaGd alloys. *J Appl Phys* 2007;102:113519.

- [421] Maloney CE, Lemaître A. Amorphous systems in athermal, quasistatic shear. *Phys Rev E* 2006;74:016118.
- [422] Gagnon G, Patton J, Lacks DJ. Energy landscape view of fracture and avalanches in disordered materials. *Phys Rev E* 2001;64:051508.
- [423] Zheng Q, Ma H, Ma E, Xu J. MgCu(Y,Nd) pseudo-ternary bulk metallic glasses: the effects of Nd on glass-forming ability and plasticity. *Scripta Mater* 2006;55:541.
- [424] Ohtsuki M, Tamura R, Yoda S, Ohmura T. Hard metallic glass of tungsten-based alloy. *Appl Phys Lett* 2004;84:4911.
- [425] Xu DH, Duan G, Johnson WL, Garland C. Formation and properties of new Ni-based amorphous alloys with critical casting thickness up to 5 mm. *Acta Mater* 2004;52:3493.
- [426] Amiya K, Inoue A. Formation, thermal stability and mechanical properties of Ca-based bulk amorphous alloys. *Mater Trans JIM* 2002;43:81.
- [427] Inoue A, Shen BL, Chang CT. Super-high strength of over 4000 MPa for Fe-based bulk glassy alloys in  $[(\text{Fe}_{1-x}\text{Co}_x)_{0.75}\text{B}_{0.2}\text{Si}_{0.05}]_{96}\text{Nb}_4$  system. *Acta Mater* 2004;52:4093.
- [428] Lambson EF, Lambson WA, Turnbull D. Elastic behavior and vibrational anharmonicity of a bulk  $\text{Pd}_{40}\text{Ni}_{40}\text{P}_{20}$  metallic glass. *Phys Rev B* 1986;33:2380.
- [429] Chen HS. Alloying effect on the viscous flow in metallic glasses. *J Non-Cryst Solids* 1978;29:223.
- [430] Chen HS, Turnbull D. Thermal evidence of a glass transition in Au–SiGe alloy. *Appl Phys Lett* 1967;10:284.
- [431] Zhang W, Guo H, Chen MW, Saotome Y, Qin CL, Inoue A. New Au-based bulk glassy alloys with ultralow glass transition temperature. *Scripta Mater* 2009;61:744.
- [432] Nemilov SV. Viscous flow of glasses correlated with their structure: application of the rate theory. *Sov J Glass Phys Chem* 1992;18:1.
- [433] Tallon JL. The thermodynamics of elastic deformation-I, equation of state for solids. *J Phys Chem Solids* 1980;41:837.
- [434] Johnson WL. Thermodynamic and kinetic aspects of crystal to glass transformation in metallic materials. *Prog Mater Sci* 1986;30:81.
- [435] Bai HY, Luo JL, Wang WH. Low temperature specific heat of bulk glassy and crystalline  $\text{Zr}_{41}\text{Ti}_{14}\text{Cu}_{12.5}\text{Ni}_{10}\text{Be}_{22.5}$  alloys. *Appl Phys Lett* 2001;78:2697.
- [436] Chen Q, Sundman B. Calculation of Debye temperature for crystalline structures: a case study on Ti, Zr and Hf. *Acta Mater* 2001;49:947.
- [437] Angell CA, Ngai KL, McKenna GB, McMillian PF, Martin SW. Relaxation in glass-forming liquids and amorphous solids. *J Appl Phys* 2000;88:3113.
- [438] Angell CA. Oxide glasses in light of the 'ideal glass' concept: I. Ideal and nonideal transitions, and departures from ideality. *J Am Ceram Soc* 1968;51:117.
- [439] Schnaus UE, Moynihan CT, Gammon RW, Macedo PB. The relation of the glass transition temperature to vibrational characteristics of network glasses. *Phys Chem Glasses* 1970;11:213.
- [440] Lindemann A. Ueber die Berechnung molekularer Eigenfrequenzen. *Z Phys* 1910;11:609.
- [441] Yamanaka S, Maekawa T, Muta H, Matsuda T, Kobayashi S, Kurosaki K. Thermal and mechanical properties of  $\text{SrHfO}_3$ . *J Alloys Compd* 2003;381:295.
- [442] Malinovsky VK, Novikov VN. The nature of the glass transition and the excess low-energy density of vibrational states in glasses. *J Phys: Condens Matter* 1992;4:L139.
- [443] Novikov VN, Rossler ER, Surovtsev NV. Strong and fragile liquids in percolation approach to the glass transition. *Europhys Lett* 1996;35:289.
- [444] Granato AV. Interstitialcy model for condensed matter state of fcc metals. *Phys Rev Lett* 1992;68:974.
- [445] Jiang Q, Shi HX, Li JC. Finite size effect on glass transition temperatures. *Thin Solid Films* 1999;354:283.
- [446] Lu Z, Li J. Correlation between average melting temperature and glass transition temperature in metallic glasses. *Appl Phys Lett* 2009;94:061913.
- [447] Angell CA. Formation of glasses from liquids and biopolymers. *Science* 1995;267:1924.
- [448] Zschimmer E. *Chemische Technologie des Glases*. Spamerschen Buchdruckerei, Leipzig; 1913, p. 445.
- [449] Priya M, Das SP. Fragility and elastic behavior of a supercooled liquid. *Phys Rev E* 2007;76:061501.
- [450] Hodge IM. Comment on the fragility of liquids—a brief critique. *J Non-Cryst Solids* 1997;202:164.
- [451] Battezzati L, Castellero A, Rizzi P. On the glass transition in metallic melts. *J Non-Cryst Solids* 2007;353:3318.
- [452] Johari G, Hallbrucker A, Mayer E. The glass–liquid transition of hyperquenched water. *Nature* 1987;330:552.
- [453] Na JH, Park ES, Kim YC, Fleury E, Kim WT, Kim DH. Poisson ratio and fragility of bulk metallic glasses. *J Mater Res* 2008;23:523.
- [454] Wang LM, Velikov V, Angell CA. Direct determination of kinetic fragility indices of glassforming liquids by differential scanning calorimetry: kinetic versus thermodynamic fragilities. *J Chem Phys* 2002;117:10184.
- [455] Bruning R, Samwer K. Glass transition on long time scales. *Phys Rev B* 1992;46:11318.
- [456] Busch R, Bakke E, Johnson WL. Viscosity of the supercooled liquid and relaxation at the glass transition of the  $\text{ZrTiCuNiBe}$  bulk metallic glass forming alloy. *Acta Mater* 1998;46:4725.
- [457] Shadovskaya L, Busch R. On the fragility of Nb–Ni-based and Zr-based bulk metallic glasses. *Appl Phys Lett* 2004;85:2508.
- [458] Perera DN. Compilation of fragility parameters for metallic glasses. *J Phys: Condens Matter* 1999;11:3807.
- [459] Borrego JM, Conde A, Roth S, Eckert J. Glass-Forming Ability and Soft Magnetic Properties of  $\text{FeCoSiAlGaPCB}$  Amorphous Alloys. *J Appl Phys* 2002;92:2073.
- [460] Xi XK, Zhao DQ, Pan MX, Wang WH. Highly processable  $\text{Mg}_{65}\text{Cu}_{25}\text{Tb}_{10}$  bulk metallic glass. *J. Non-cryst. Solids* 2004;344:189.
- [461] Sun BA, Pan MX, Zhao DQ, Wang WH, Xi XK, Wu Y. Al-rich bulk metallic glasses. *Scripta Mater* 2008;59:1159.
- [462] Wang WH, Pan MX, Zhao DQ, Hu Y, Bai HY. Enhance soft magnetic properties of  $\text{FeCoZrMoWB}$  bulk metallic glass by microalloying. *J. Phys. Condens Matter*. 2004;16:3719.
- [463] Chen HS, Turnbull D. Evidence of a glass–liquid transition in a gold–germanium–silicon alloy. *J Chem. Phys.* 1968;48:2560.

- [464] Close HG, Fecht HJ. Vitrification close to the Kauzmann point of eutectic Au–Pb–Sb alloys. *Mater. Sci. Eng. A* 1994;179/180:77.
- [465] Tool AQ. Relation between inelastic deformability and thermal expansion of glass in its annealing range. *J. Amer. Ceram. Soc.* 1946;29:240.
- [466] Ritland HN. Density phenomena in the transformation range of a borosilicate crown glass. *J. Amer. Ceram. Soc.* 1954;37:370.
- [467] Narayanaswamy OS. A model of structural relaxation in glass. *J. Am. Ceram. Soc.* 1971;54:491.
- [468] Pohl RO, Liu X. Low-temperature thermal conductivity and acoustic attenuation in amorphous solids. *Rev of Mod. Phys.* 2002;74:991.
- [469] Sette F, Krisch MH, Masciovecchio C, Ruocco G, Monaco G. Dynamics of glasses and glass-forming liquids studied by inelastic X-ray scattering. *Science* 1998;280:1550.
- [470] Buchenau U, Nucker N, Dianoux AJ. Neutron scattering study of the low-frequency vibrations in vitreous silica. *Phys Rev Lett* 1984;53:2316.
- [471] Grigera TS, Martin-Mayer V, Parisl G, Verrocchio P. Phonon interpretation of the boson peak in supercooled liquids. *Nature* 2003;422:289.
- [472] Parisl G. On the origin of the boson peak. *J Phys: Condens Matter* 2003;15:S765.
- [473] Tang MB. Doctoral thesis, Properties at low temperature in Cu–Zr based bulk metallic glasses. Institute of Physics, Chinese Academy of Sciences; 2006.
- [474] Li Y, Yu B, Bai HY. Boson peak in bulk metallic glasses. *J Appl Phys* 2008;104:013520.
- [475] Li Y. Doctoral thesis, Boson Peak in Bulk Metallic Glasses. Institute of Physics, Chinese Academy of Sciences; 2007.
- [476] Tang MB, Bai HY, Pan MX, Zhao DQ, Wang WH. Einstein oscillator in highly random packed bulk metallic glass. *Appl Phys Lett* 2005;86:021910.
- [477] Tang MB, Bai HY, Wang WH. Tunneling states and localized mode in binary bulk metallic glass. *Phys Rev B* 2005;72:012202.
- [478] Zhou Z, Uher C, Xu DH, Johnson WL, Gannon W, Aronson MC. On the existence of Einstein oscillators and thermal conductivity in bulk metallic glass. *Appl Phys Lett* 2006;89:031924.
- [479] Keppens V, Senkov ON, Miracle D. Localized Einstein modes in Ca-based bulk metallic glasses. *Philos Mag.* 2007;87:503.
- [480] Tian Y, Li Zi Q, Jiang EY. Low temperature specific heat and thermal conductivity of bulk metallic glass (Cu<sub>50</sub>Zr<sub>50</sub>)<sub>94</sub>Al<sub>6</sub>. *Solid State Commun* 2009;14:1527.
- [481] Phillips WA. *Amorphous Solids: Low temperature properties*. Berlin: Springer-Verlag; 1981.
- [482] Keppens V, Mandrus D, Sales BC, Chakoumakos BC, Dai P, Coldea R, et al. Localized vibrational modes in metallic solids. *Nature* 1998;395:876.
- [483] Hermann RP, Jin R, Schweika W, Grandjean F, Mandrus D, Sales BC, et al. Einstein oscillators in thallium filled antimony skutterudites. *Phys Rev Lett* 2003;90:135505.
- [484] Wang JQ, Bai HY. High pressure behaviors of Yb-based bulk metallic glass. *Scripta Mater* 2009;61:453.
- [485] Liu XF, Wang WH. Poisson's ratio of metallic glasses under pressure and low temperature. *Scripta Mater* 2010;62:254.
- [486] Shi Y, Falk ML. Strain localization and percolation of state structure in amorphous solids. *Phys Rev Lett* 2005;95:095502.
- [487] Mayers MA, Chawla KK. *Mech. Behavior of Mater*. Upper Saddle River, New Jersey: Prentice Hall; 1999.
- [488] Lawn B. *Fracture of brittle solids*. Cambridge: Univ. Cambridge; 1993.
- [489] Li T, Morris JW, Nagasako JN, Kuramoto S, Chrzan DC. "ideal" engineering alloys. *Phys Rev Lett* 2007;98:105503.
- [490] Chen MW, Ma E, Hemker KJ, Sheng HW, Wang YM, Cheng XM. Deformation twinning in nanocrystalline Al. *Science* 2003;300:1275.
- [491] Devincere B, Hoc T, Kubin L. Dislocation mean free paths and strain hardening of crystals. *Science* 2008;320:1745.
- [492] Frenkel J. Zur theorie der elastizitätsgrenze und der festigkeit kristallinischer körper. *Z. Phys.* 1926;37:572.
- [493] Demetriou MD, Harmon JS, Tao M, Duan G, Samwer K, Johnson WL. Cooperative shear model for the rheology of glass-forming metallic liquids. *Phys Rev Lett* 2006;97:065502.
- [494] Bei H, Lu ZP, George EP. Theoretical strength and the onset of plasticity in bulk metallic glasses investigated by nanoindentation with a spherical indenter. *Phys Rev Lett* 2004;93:125504.
- [495] Huang YJ, Shen J, Sun JF. Formation, thermal stability and mechanical properties of TiZrCuNiSn bulk metallic glass. *Sci. in China G* 2008;51:372.
- [496] Chen N, Yao KF. Pd–Si binary bulk metallic glass. *Sci. in China G* 2008;51:414.
- [497] Volkert CA, Donohue A, Spaepen F. Effect of sample size on deformation in amorphous metals. *J Appl Phys* 2008;103:083539.
- [498] Delogu F. Atomic mobility and strain localization in amorphous metals. *Phys Rev Lett* 2008;100:075901.
- [499] Zhang ZF, Eckert J. Unified tensile fracture criterion. *Phys Rev Lett* 2005;94:094301.
- [500] Senkov ON, Miracle DB. Composition range and glass forming ability of ternary Ca–Mg–Cu bulk metallic glasses. *J Alloy Compd* 2006;424:394.
- [501] Senkov ON, Miracle DB, Keppens V, Liaw PK. Development and characterization of low-density Ca-based bulk metallic glasses: an overview. *Metall Mater Trans A* 2008;39:1888.
- [502] Packard CE, Schuh CA. Initiation of shear bands near a stress concentration in metallic glass. *Acta Mater* 2007;55:5348.
- [503] Shan ZW, Mishra RK, Syedatif SA, Warren OL, Minor AM. Mechanical annealing and source-limited deformation in submicrometre diameter. *Nat Mater* 2008;7:115.
- [504] Schuster BE, Wei Q, Ervin MH, Hruszkewycz SO, Miller MK, Hufnagel TC, et al. Bulk and microscale compressive properties of a Pd-based metallic glass. *Scripta Mater* 2007;57:517–20.
- [505] Battezzati L, Baldissin D. Quantitative evaluation of lengthscales for temperature rise in shear bands and for failure of metallic glasses. *Scripta Mater* 2008;59:223.
- [506] Liu YH, Liu CT, Wang WH, Inoue A, Sakurai T, Chen MW. Thermodynamic origin of shear band formation and universal scaling law of metallic glass strength. *Phys Rev Lett* 2009;103:065504.
- [507] Lee HN, Paeng K, Swallen SF, Ediger MD. Direct measurement of molecular mobility in actively deformed polymer glasses. *Science* 2009;323:231.

- [508] Liu AJ, Nagel SR. Jamming is not just cool any more. *Nature* 1998;396:21.
- [509] Tabor D. The hardness of metals. Oxford University Press; 1951.
- [510] Bao YW, Wang W, Zhou YC. Investigation of the relationship between elastic modulus and hardness based on depth-sensing indentation measurements. *Acta Mater* 2004;52:5397.
- [511] Prasad SLA, Mayuram MM, Krishnamurthy R. Response of plasma-sprayed alumina–titania composites to static indentation process. *Mater Lett* 1999;41:234.
- [512] Friedel J. Dislocations. Oxford: Pergamon; 1967.
- [513] Spaepen F. A microscopic mechanism for steady state inhomogeneous flow in metallic glasses. *Acta Mater* 1977;25:407.
- [514] Argon AS. Plastic deformation in metallic glasses. *Acta Mater* 1979;27:47.
- [515] Lowhaphandu P, Lewandowski JJ. Fracture toughness and notched toughness of bulk amorphous alloy: ZrTiNiCuBe. *Scripta Mater* 1998;38:1811.
- [516] Lewandowski JJ, Greer AL. Temperature rise at shear bands in metallic glasses. *Nat Mater* 2006;5:15.
- [517] Wang YM, Li J, Harza AV, Barbee TW. Ductile crystalline-amorphous nanolaminates. *PNAS* 2007;104:1155.
- [518] Park ES, Chang HJ, Kim DH. Effect of addition of Be on glass-forming ability, plasticity and structural change in Cu–Zr bulk metallic glasses. *Acta Mater* 2008;56:3120.
- [519] Jiang JB, Zhang W, Xie GQ, Inoue A. Unusual room temperature ductility of a Zr-based bulk metallic glasses containing nanoparticles. *Appl Phys Lett* 2007;90:231907.
- [520] Yu P, Bai HY, Zhao JG, Jin CQ, Wang WH. Pressure effects on mechanical properties of bulk metallic glass. *Appl Phys Lett* 2007;90:051906.
- [521] Yu P, Liu YH, Wang G, Bai HY, Wang WH. Enhance plasticity of bulk metallic glasses by geometric confinement. *J Mater Res* 2007;22:2384.
- [522] Kim KB, Das J, Baier F, Tang MB, Wang WH, Eckert J. Heterogeneity of a  $\text{Cu}_{47.5}\text{Zr}_{47.5}\text{Al}_5$  bulk metallic glass. *Appl Phys Lett* 2006;88:051911.
- [523] Hofmann DC, Suh J, Wiest A, Duan G, Lind ML, Demetriou MD, et al. Designing metallic glass matrix composites with high toughness and ductile ductility. *Nature* 2008;451:1085.
- [524] Das J, Bostrom M, Mattern N, Kvicik A, Yavari AR, Greer AL, et al. Plasticity in bulk metallic glasses investigated via the strain distribution. *Phys Rev B* 2007;76:092203.
- [525] Schuh CA, Lund AC. Atomistic basis for the plastic yield criterion of metallic glasses. *Nat Mater* 2003;2:449.
- [526] Wang K, Fujita T, Zeng YQ, Nishiyama N, Inoue A, Chen MW. Micromechanism of serrated flow in a ductile NiPdP bulk metallic glasses. *Acta Mater* 2008;56:2834.
- [527] Park KW, Lee C, Lee M, Fleury E, Falk ML, Lee J. Paradoxical phenomenon between homogenous and inhomogeneous deformation in metallic glasses. *Appl Phys Lett* 2009;94:021907.
- [528] Delogu F. Effects of compression cycles on the atomic mobility in metallic glasses. *Phys Rev* 2009;B79:064205.
- [529] Yu HB, Hu J, Xia XX, Sun BA, Li XX, Wang WH, et al. Stress induced structural inhomogeneity and plasticity of bulk metallic glasses. *Scripta Mater* 2009;61:640.
- [530] Yu HB, Wang WH, Zhang JL, Shek CH, Bai HY. Statistic analysis on mechanical behavior in bulk metallic glasses. *Adv Eng Mater* 2009;11:370.
- [531] Hecker SS, Rohr DL, Stein DF. Brittle fracture in iridium. *Metall Trans A* 1978;9:481.
- [532] Pugh SF. Relations between the elastic moduli and the plastic properties of polycrystalline pure metals. *Philos Mag* 1950;45:823.
- [533] Kelly A, Tyson WR, Cottrell AH. Ductile and brittle crystals. *Philos Mag* 1967;15:567.
- [534] Rice JR, Thomson R. Ductile versus brittle behaviour of crystals. *Philos Mag* 1974;29:73.
- [535] Phani KK, Sanyal D. The relations between the shear modulus, the bulk modulus and Young's modulus for porous isotropic ceramic materials. *Mater Sci Eng A* 2008;490:305.
- [536] Song F, Zhou J, Xu X, Xu Y, Bai Y. Effect of a negative Poisson ratio in the tension of ceramics. *Phys Rev Lett* 2008;100:245502.
- [537] Yu P, Bai HY. Anomalous compositional dependence of Poisson's ratio and plasticity in CuZrAl bulk metallic glasses. *Mater Sci Eng A* 2008;485:1.
- [538] Castellero A, Uhlenhaut DI, Moser B, Löffler J. Critical Poisson ratio for room-temperature embrittlement of amorphous  $\text{Mg}_{85}\text{Cu}_5\text{Y}_{10}$ . *Philos Mag Lett* 2007;87:383.
- [539] Poon SJ, Shiflet GJ, Ponnambalam V. Supercooled liquids, glass transition and bulk metallic glasses. *Mater Res Soc Symp Proc* 2003;754:167.
- [540] Lewandowski JJ, Thurston AK, Lowhaphandu P. Fracture toughness of amorphous metals and composites. *Mater Res Soc Symp Proc* 2003;754:307.
- [541] Lewandowski JJ. Effects of annealing and changes in stress state on fracture toughness of bulk metallic glass. *Mater Trans JIM* 2001;42:633.
- [542] Wesseling P, Nieh TG, Wang WH, Lewandowski JJ. Preliminary assessment of flow, notch toughness, and high temperature behavior of  $\text{Cu}_{60}\text{Zr}_{20}\text{Hf}_{10}\text{Ti}_{10}$  bulk metallic glass. *Scripta Mater* 2004;51:151.
- [543] Davis LA. Fracture toughness of metallic glasses. *Metall Trans A* 1975;10:235.
- [544] Irwin GR. Analysis of stresses and strains near the end of a crack traversing a plate. *J Appl Mech* 1957;24:361.
- [545] Gu XJ, Poon SJ, Shiflet GJ, Lewandowski JJ. Ductile-to-brittle transition in a Ti-based bulk metallic glass. *Scripta Mater* 2009;60:1027–30.
- [546] Pan D, Inoue A, Sakurai T, Chen MW. Experimental characterization of shear transformation zones for plastic flow of bulk metallic glasses. *PNAS* 2008;105:14769.
- [547] Lekka Ch E, Ibenskas A, Yavari AR, Evangelakis GA. Tensile deformation accommodation in microscopic metallic glasses via subnanocluster reconstructions. *Appl Phys Lett* 2007;91:214103.
- [548] Williams SR, Royall CP, Bryant G. Crystallization of dense binary hard-sphere mixtures with marginal size ratio. *Phys Rev Lett* 2008;100:225502.
- [549] Royall CP, Williams SR, Ohtsuka T, Tanaka H. Direct observation of local structural mechanism for dynamic arrest. *Nat Mater* 2008;7:556.

- [550] Caron A, Wunderlich R, Louzguine-Luzgin DV, Xie G, Inoue A, Fecht H-J. Influence of minor aluminum concentration changes in zirconium-based bulk metallic glasses on the elastic, anelastic, and plastic properties. *Acta Mater* 2010;58:2004.
- [551] Gu XJ, Poon SJ, Shiflet GJ, Lewandowski JJ. Compressive plasticity and toughness of a Ti-based bulk metallic glass. *Acta Mater* 2010;58:1708.
- [552] Murali P, Ramamurty U. Embrittlement of a bulk metallic glass due to sub-T<sub>g</sub> annealing. *Acta Mater* 2005;53:1467.
- [553] Kramer EA, Johnson WL, Cline C. The effects of neutron irradiation on a superconducting metallic glass. *Appl Phys Lett* 1979;35:815.
- [554] Ye F, Sprengel W, Wunderlich RK, Fecht H-J, Schaefer H-E. Reversible atomic processes as basic mechanisms of the glass transition. *PNAS* 2008;104:12962.
- [555] De Hey P, Sietsma J, Van Den Beukel A. Structural disordering in amorphous Pd<sub>40</sub>Ni<sub>40</sub>P<sub>20</sub> induced by high temperature deformation. *Acta Mater* 1998;46:5873.
- [556] Conner RD, Johnson WL, Paton NE, Nix WD. Shear bands and cracking of metallic glass plates in bending. *J Appl Phys* 2003;94:904.
- [557] Xia XX, Wang WH, Greer AL. Plastic zone at crack tip: a nanolab for formation and study of metallic glassy nanostructures. *J Mater Res* 2009;24:2986.
- [558] Donovan PE. A yield criterion for Pd<sub>40</sub>Ni<sub>40</sub>P<sub>20</sub> metallic glass. *Acta Metall* 1989;37:445.
- [559] Baricco M, Baser TA, Das J, Eckert J. Correlation between Poisson ratio and Mohr–Coulomb coefficient in metallic glasses. *J Alloy Compd* 2009;483:125.
- [560] Zink M, Samwer K, Johnson WL, Mayr SG. Validity of temperature and time equivalence in metallic glasses during shear deformation. *Phys Rev B* 2006;74:012201.
- [561] Wang YT, Bai HY, Pan MX, Zhao DQ, Wang WH. Giant enhancement of magnetocaloric effect in metallic glass and matrix composites. *Sci China G* 2008;51:337.
- [562] Li Y, Poon SJ, Shiflet GJ, Xu J, Kim DH, Loeffler JF. Formation of bulk metallic glasses and their composites. *MRS Bull* 2007;32:624.
- [563] Telford M. The case for bulk metallic glass. *Mater Today* 2004;7:36.
- [564] Yavari AR. A new order for metallic glasses. *Nature* 2006;439:405.
- [565] American Institute of Physics Handbook. Mc Graw-Hill; 1972
- [566] <http://www.webelements.com>.
- [567] de Boer FR, Miedema AR, Niessen AK. Cohesion in metals. North-Holland: Amsterdam; 1988.
- [568] Li JH, Dai XD, Liang SH, Tai KP, Kong Y, Liu BX. Interatomic potentials of the binary transition metal systems and some applications in materials physics. *Phys Rep* 2008;455:1.
- [569] Liu Y, Zhang J, Wang Y, Zhu Y, Yang Z, Chen J, et al. Weak exchange effect and large refrigeration capacity of in bulk metallic glass Gd<sub>0.32</sub>Tb<sub>0.26</sub>Co<sub>0.20</sub>Al<sub>0.22</sub>. *Appl Phys Lett* 2009;94:112507.
- [570] Zhao K, Luo Q, Wang WH. Binary rare earth based bulk metallic glasses. *J Non-Cryst Solids* 2009;355:1001.
- [571] Stanley HE. Freezing by heating. *Nature* 2000;404:718.
- [572] Liu AJ, Nagel SR. Nonlinear dynamics: jamming is not just cool any more. *Nature* 1998;396:21.
- [573] Furukawa A, Tanaka H. Violation of the incompressibility of liquid by simple shear flow. *Nature* 2006;443:434.
- [574] Goyon J, Colin A, Ovarlez G, Ajdari A, Bocquet L. Spatial cooperativity in soft glassy flows. *Nature* 2008;454:84.
- [575] Anderson PW. Lectures on amorphous systems. In: Balian R, Maynard R, Toulouse G, editors. III-condensed matter. North-Holland, Amsterdam.
- [576] For details see: Special selection. *Science* 2005;309:83.
- [577] Lamb J. Viscoelasticity and lubrication: a review of liquid properties. *J Rheol* 1978;22:317.
- [578] Angell CA. Strong and fragile liquids. In: Ngai KL, Wright GB, editors. Relaxations in complex systems. Washington (DC): US GPO; 1985. p. 3–11.
- [579] Brush SG. Theories of liquid viscosity. *Chem Rev* Washington, DC 1962;62:513–48.
- [580] Arrhenius S. Über die Reaktionsgeschwindigkeit bei der Inversion von Rohrzucker durch Säuren. *Z Phys Chem* 1889;4:226.
- [581] Plazek DJ, Ngai KL. Correlation of polymer segmental chain dynamics with temperature-dependent timescale shifts. *Macromolecules* 1991;24:1222.
- [582] Ruocco G, Sciortino F, Zamponi F, De Michele C, Scopigno T. Landscapes and fragilities. *J Chem Phys* 2004;120:10666.
- [583] Schug KU, King HE, Böhmer R. Fragility under pressure: diamond anvil cell viscometry of orthoterphenyl and salol. *J Chem Phys* 1998;109:1472.
- [584] Granato AV, Khonik VA. An interstitialcy theory of structural relaxation and related viscous flow of glasses. *Phys Rev Lett* 2004;93:155502.
- [585] Roseveare WE, Powell RE, Eyring H. The structure and dynamics of liquids. *J Appl Phys* 1941;12:669.
- [586] Doolittle AK. Studies in Newtonian flow. II. The dependence of the viscosity of liquids on free-space. *J Appl Phys* 1951;22:1471.
- [587] Cohen MH, Turnbull D. Molecular transport in liquids and glasses. *J Chem Phys* 1959;31:1164.
- [588] Adam G, Gibbs JH. On the temperature dependence of cooperative relaxation properties in glass-forming liquids. *J Chem Phys* 1965;43:139.
- [589] Gibbs JH, DiMarzio EA. Nature of the glass transition and the glassy state. *J Chem Phys* 1958;28:373.
- [590] Götze W, Sjögren L. Relaxation processes in supercooled liquids. *Rep Prog Phys* 1992;55:241.
- [591] Das SP. Mode-coupling theory and the glass transition in supercooled liquids. *Rev Mod Phys* 2004;76:785.
- [592] Dyre JC. Solidity of viscous liquids. III. Alfa relaxation descape equivalent of the shoving model. *Phys Rev E* 2005;72:011501.
- [593] Dyre JC. Solidity of viscous liquids. IV. Density fluctuations. *Phys Rev E* 2006;74:021502.
- [594] Tobolsky A, Powell RE, Eyring H. Elasticviscous properties of matter. In: Burk RE, Grummit O, editors. *Frontiers in chemistry*, vol. 1. New York: Interscience; 1943. p. 125–90.

- [595] Trachenko K. The Vogel–Fulcher–Tammann law in the elastic theory of glass transition. *J Non-Cryst Solids* 2008;354:3903.
- [596] Reiner M. The Deborah number. *Phys Today* 1964;17:62.
- [597] Roland CM, Ngai KL. The anomalous Debye–Waller factor and the fragility of glasses. *J Chem Phys* 1996;104:2967.
- [598] Mooney M. A theory of the viscosity of a Maxwellian elastic liquid. *Trans Soc Rheol* 1957;1:63.
- [599] Bueche F. Mobility of molecules in liquids near the glass temperature. *J Chem Phys* 1959;30:748.
- [600] Nemilov SV. Kinetics of elementary processes in the condensed state. II. Shear relaxation and the equation of state for solids. *Russ J Phys Chem* 1968;42:726.
- [601] Dyre JC. Energy master equation: a low temperature approximation to Bässler's random-walk model. *Phys Rev B* 1995;51:12276.
- [602] Bailey NP, Schroder TB, Dyre JC. Exponential distributions of collective flow-event properties in viscous liquid dynamics. *Phys Rev Lett* 2009;102:055701.
- [603] Dyre JC, Olsen NB, Christensen T. Local elastic expansion model for viscous-flow activation energies of glass-forming molecular liquids. *Phys Rev B* 1996;53:2171.
- [604] Wilde G, Goerler GP, Willnecker R. Calorimetric thermodynamical, and rheological characterizations of bulk glass-forming PdNiP. *J Appl Phys* 2000;87:1141.
- [605] Beukel AVD, Sietsma J. On the nature of the glass transition in metallic glasses. *Philos Mag B* 1990;61:539.
- [606] Falk ML, Langer JS. Dynamics of viscoplastic deformation in amorphous solids. *Phys Rev E* 1998;57:7192.
- [607] Langer JS. Dynamic of shear-transformation zones in amorphous plasticity: formulation in terms of an effective disorder temperature. *Phys Rev E* 2004;70:041502.
- [608] Langer JS, Lemaître A. Dynamic model of super-Arrhenius relaxation rates in glassy materials. *Phys Rev Lett* 2005;94:175701.
- [609] Mayr SG. Activation energy of shear transformation zones: a key for understanding rheology of glasses and liquids. *Phys Rev Lett* 2006;97:195501.
- [610] Hajlaoui K, Benameur T, Vaughan G, Yavari AR. Thermal expansion and indentation-induced free volume in Zr-based metallic glasses measured by real-time diffraction using synchrotron radiation. *Scripta Mater* 2004;51:843.
- [611] Flores KM, Suh D, Dauskardt RH, Asoka-Kumar P, Sterne PA, Howell RH. Characterization of free volume in a bulk metallic glass using positron annihilation spectroscopy. *J Mater Res* 2002;17:1153.
- [612] Falk ML. The flow of glass. *Science* 2007;318:1880.
- [613] Chathoth SM, Damaschke B, Koza MM, Samwer K. Dynamic singularity in multicomponent glass-forming metallic liquids. *Phys Rev Lett* 2008;101:037801.
- [614] Stevenson JD, Schmalian J, Wolynes PG. The shapes of cooperatively rearranging regions in glass-forming liquids. *Nat Phys* 2006;2:268.
- [615] Frenkel J. Zur Theorie der Elastizitätsgrenze und der Festigkeit Kristallinischer Körper. *Z Phys* 1926;37:572.
- [616] Wang JQ, Wang WH, Bai HY. Extended elastic model for flow in metallic glass-forming liquids and glasses. *J Non-Cryst Solids* 2011;357:223.
- [617] Wang JQ, Wang WH, Liu YH, Bai HY. Characterization of activation energy for flow in metallic glasses. *Phys Rev* 2011;B83:012201.
- [618] Wang WH. Correlation between relaxations and plastic deformation, and elastic model of flow in metallic glasses and glass-forming liquids. *J Appl Phys*, in press.
- [619] Dyre JC, Olsen NB. Landscape equivalent of the shoving model. *Phys Rev E* 2004;69:042501.
- [620] Spaepen F. Metallic glasses: must shear bands be hot? *Nat Mater* 2006;5:7.
- [621] Egami T, Poon SJ, Zhang Z, Keppens V. Glass transition in metallic glasses: a microscopic model of topological fluctuations in the bonding network. *Phys Rev B* 2007;76:024203.
- [622] Ke HB, Wen P, Wang WH, Greer AL. Homogeneous deformation of metallic glass at room temperature reveals large dilatation. *Scripta Mater* 2011;64:966–9.
- [623] Liu YH, Wang K, Inoue A, Sakurai T, Chen MW. Energetic criterion on intrinsic ductility of bulk metallic glasses. *Scripta Mater* 2010;62:586.
- [624] Cahn RW, Pratten NA, Scott MG, Sinning HR, Leonardsson L. Studies of relaxation of metallic glasses by dilatometry and density measurements. *Mater Res Soc Symp Proc* 1984;28:241.
- [625] Méar FO, Lenk B, Zhang Y, Greer AL. Structural relaxation in a heavily cold-worked metallic glass. *Scripta Mater* 2008;59:1243.
- [626] Greer AL. Metallic glasses ... on the threshold. *Mater Today* 2009;12:14.
- [627] Garrahan JP, Chandler D. Coarse-grained microscopic model of glass formers. *PNAS* 2003;100:9710–4.
- [628] Billinge SJL, Levin I. The problem with determining atomic structure at the nanoscale. *Science* 2007;316:561.
- [629] Cheng YQ, Shen HW, Ma E. Relationship between structure, dynamics, and mechanical properties in metallic glass-forming alloys. *Phys Rev B* 2008;78:014207.
- [630] Tanaka H, Kawasaki T, Shintani H, Watanabe K. Critical-like behavior of glass-forming liquids. *Nat Mater* 2010;9:324.
- [631] Widmer-Cooper A, Perry H, Harrowell P, Reichman D. Irreversible reorganization in a supercooled liquid originates from localized soft modes. *Nat Phys* 2008;4:711.
- [632] Fujita T, Guan PF, Sheng HW, Inoue A, Sakurai T, Chen MW. Coupling between chemical and dynamic heterogeneities in a multicomponent bulk metallic glass. *Phys Rev B* 2010;81:142204(R).
- [633] Caprion D, Matsui J, Schober HR. Dynamic heterogeneity of relaxations in glasses and liquids. *Phys Rev Lett*. 2000;85:4293.
- [634] Wagner H, Bedorf D, Küchemann S, Schwabe M, Zhang B, Arnold W, et al. Local elastic properties of a metallic glass. *Nat Mater* 2011;10:439.
- [635] Liu YH, Wang D, Nakajima K, Zhang W, Hirata A, Nishi T, et al. Characterization of nanoscale mechanical heterogeneity in a metallic glass by dynamic force microscopy. *Phys Rev Lett* 2011;106:125504.
- [636] Ye JC, Lu J, Liu CT, Wang Q, Yang Y. Atomistic free-volume zones and inelastic deformation of metallic glasses. *Nat Mater* 2010;9:619.

- [637] Ichitsubo T, Itaka W, Matsubara E, Kato H, Biwa S, Hosokawa S, et al. Elastic inhomogeneity and acoustic phonons in Pd-, Pt-, and Zr-based metallic glasses. *Phys Rev B* 2010;81:172201.
- [638] Hu LN, Yue YZ. Secondary relaxation in metallic glass formers: its correlation with the genuine Johari–Goldstein relaxation. *J Phys Chem C* 2009;113:15001.
- [639] Harmon JS, Demetriou MD, Johnson WL, Samwer K. Anelastic to plastic transition in metallic glass-forming liquids. *Phys Rev Lett* 2007;99:1355502.
- [640] Wang Z, Yu HB, Wen P, Bai HY, Wang WH. Pronounced slow  $\beta$ -relaxation in La-based bulk metallic glasses. *J Phys: Condens Matter* 2011;23:142202.
- [641] Yu HB, Wang WH, Bai HY, Wu Y, Chen MW. Relating activation of shear transformation zones to  $\beta$ -relaxations in metallic glasses. *Phys Rev B* 2010;81:220201(R).
- [642] Ke HB, Wen P, Zhao DQ, Wang WH. Correlation between dynamic flow and thermodynamic glass transition in metallic glasses. *Appl Phys Lett* 2010;96:251902.
- [643] Sun BA, Yu HB, Jiao W, Bai HY, Zhao DQ, Wang WH. The plasticity of ductile metallic glasses: a self-organized critical state. *Phys Rev Lett* 2010;105:035501.
- [644] Kudlic A, Tschirwitz C, Benkhof S, Blochowicz T, Rossler E. Slow secondary relaxation process in supercooled liquids. *Europhys Lett* 1997;40:649.
- [645] Rodney D, Schuh C. Distribution of thermally activated plastic events in a flowing glass. *Phys Rev Lett* 2009;102:235503.
- [646] Homer ER, Rodney D, Schuh CA. Kinetic Monte carlo study of activated state and correlated shear-transformation-zone activity during the deformation of an amorphous metal. *Phys Rev B* 2010;81:064204.
- [647] Pauly S, Liu G, Wang G, Kühn U, Mattern N, Eckert J. Microstructural heterogeneities governing the deformation of  $\text{Cu}_{47.5}\text{Zr}_{47.5}\text{Al}_5$  bulk metallic glass composites. *Acta Mater* 2009;57:5445.
- [648] Lee MH, Lee JK, Kim KT, Thomas J, Das J, Kühn U, et al. Deformation-induced microstructural heterogeneity in monolithic  $\text{Zr}_{44}\text{Ti}_{11}\text{Cu}_{9.8}\text{Ni}_{10.2}\text{Be}_{2.5}$  bulk metallic glass. *Phys Status Solidi* 2009;3:46.
- [649] Lee MH, Lee KS, Das J, Thomas J, Kühn U, Eckert J. Improved plasticity of bulk metallic glasses upon cold rolling. *Scripta Mater* 2010;62:678.
- [650] Sharma P, Yubuta K, Kimura H, Inoue A. Brittle metallic glass deforms plastically at room temperature in glassy multilayers. *Phys Rev B* 2009;80:024106.
- [651] Zhang JL, Yu HB, Lu JX, Bai HY, Shek CH. Enhancing plasticity of  $\text{Zr}_{46.75}\text{Ti}_{8.25}\text{Cu}_{7.5}\text{Ni}_{10}\text{Be}_{27.5}$  bulk metallic glass by precompression. *Appl Phys Lett* 2009;95:071906.
- [652] Ichitsubo T, Matsubara E, Yamamoto T, Nishiyama N, Saida J, Anazawa K. Microstructural of fragile metallic glasses inferred from ultrasound accelerated crystallization in Pd-based metallic glasses. *Phys Rev Lett* 2005;95:245501.
- [653] Ichitsubo T, Matsubara E, Hosokawa S. Low temperature elastic moduli of a Pd-based metallic glasses showing positive phonon dispersion. *Phys Rev B* 2008;78:052202.
- [654] Xiao CD, Jho JY, Yee AF. Correlation between the shear yielding behavior and secondary relaxations of bisphenol A polycarbonate and related copolymers. *Macromolecules* 1994;27:2761.
- [655] Tsui NT, Yang Y, Mulliken AD, Torun L, Boyce MC, Swager TM. Enhancement to the rate-dependent mechanical behavior of polycarbonate by incorporation of triptycenes. *Polymer* 2008;49:4703.
- [656] Chen LP, Yee AF, Moskala EJ. The molecular basis for the properties of a series of polyester copolymer glasses. *Macromolecules* 1999;32:5944.
- [657] Eyring H, Hirschfelder J. The theory of the liquid state. *J Chem Phys* 1937;41:249.
- [658] Boyce MC, Parks DM, Argon AS. Large inelastic deformation of glassy-polymers. 1: Rate dependent constitutive model. *Mech Mater* 1988;7:15.
- [659] Lee H-N, Paeng K, Swallen SF, Ediger MD. Direct measurement of molecular mobility in actively deformed polymer glasses. *Science* 2009;323:231.
- [660] Zhao K, Xia XX, Bai HY, Zhao DQ, Wang WH. Room temperature homogeneous flow in a bulk metallic glass with low glass transition temperature. *Appl Phys Lett* 2011;98:141913.
- [661] Guan P, Chen MW, Egami T. Stress–temperature scaling for steady-state flow in metallic glasses. *Phys Rev Lett* 2010;104:205701.
- [662] Barrer MR. The viscosity of pure liquids. I. Non-polymerised fluids. *Trans Faraday Soc* 1943;39:48.
- [663] Schroers J, Masuhr A, Johnson WL, Busch R. Pronounced asymmetry in the crystallization behavior during constant heating and cooling of a bulk metallic glass-forming liquid. *Phys Rev B* 1999;60:11855.
- [664] Zhang L, Shi L, Xu J. Hf–Cu–Ni–Al bulk metallic glasses: optimization of glass-forming ability and plasticity. *J Non-cryst Solids* 2009;355:1005.
- [665] Wang JG, Zhao DQ, Pan MX, Wang WH, Song SX, Nieh TG. Correlation between onset of yielding and free volume in metallic glasses. *Scripta Mater* 2010;62:477.
- [666] Wang WH. Bulk metallic glasses with functional physical properties. *Adv Mater* 2009;21:4524.
- [667] Peng HL, Li MZ, Wang WH. Structural signature of plastic deformation in metallic glasses. *Phys Rev Lett* 2011;106:135503.
- [668] Ma D, Stoica AD, Wang X-L. Power-law scaling and fractal nature of medium-range order in metallic glasses. *Nat Mater* 2009;8:30.
- [669] Trexler MM, Thadhani NN. Mechanical properties of bulk metallic glasses. *Prog Mater Sci* 2010;55:759.
- [670] Cheng YQ, Ma E. Atomic-level structure and structure–property relationship in metallic glasses. *Prog Mater Sci* 2011;56:379.
- [671] Demetriou MD, Laubey ME, Garrett G, Schramm JP, Hofmann DC, Johnson WL, et al. A damage-tolerant glass. *Nat Mater* 2011;10:123.
- [672] Wang J, Li R, Hua N, Zhang T. Co-based ternary bulk metallic glasses with ultrahigh strength and plasticity. *J Mater Res* 2011.
- [673] Meng D, Yi J, Zhao DQ, Ding DW, Bai HY, Pan MX, et al. Tantalum based bulk metallic glasses. *J Non-Cryst Solids* 2011;357:1787.

- [674] Shi LL, Xu J. Mg based bulk metallic glasses: glass transition temperature and elastic properties versus toughness. *J Non-Cryst Solids* 2011;357:2926.
- [675] Egami T. Atomic level stress. *Prog Mater Sci* 2011;56:637.